PEOPLE'S DEMOCRATIC REPUBLIC OF ALGERIA

MINISTRY OF HIGHER EDUCATION AND SCIENTIFIC RESEARCH

UNIVERSITY OF ECHAHID HAMMA LAKHDAR EL-OUED

Faculty of Technology

Department of Electrical Engineering

Thesis

Submitted in partial fulfillment of the requirements for Doctorate degree

Option: Telecommunications Networks

Presented by **KHENNOUFA FAICAL**

Thesis Title:

PHY Transceiver Design Based on Cooperative NOMA

Jury Members:

President	Ajgou Riadh	Professor	University of El-Oued
Examiner	Chaa Mourad	Professor	University of Ouargla
Examiner	Mekimah Boualem	MCA	University of Ouargla
Examiner	Hima Abdelkader	MCA	University of El-Oued
Supervisor	Khelil Abdellatif	Professor	University of El-Oued

June 2024

بسم الله الرحمن الرحيم

Acknowledgements

First, I thank my God for helping me with this success in my research.

I would like to thank my supervisor **Prof. Khelil Abdellaitf** for his guidance, advice, encouragement, and support during my PhD study. He has provided me with significant flexibility and autonomy in my research endeavors. Under his guidance, I acquired academic knowledge, honed research skills, and developed proficient writing abilities. His passion for work, meticulous approach to study, clear thinking, and professional integrity have left a lasting impression on me. Being one of his students and conducting research under his supervision has been a great honor for me.

I extend my sincere appreciation to **Prof. Fred Kara** from Zonguldak Bülent Ecevit University, Turkey, for his significant contributions and unwavering support throughout this research project. Prof. Kara has been a role model and an exceptionally competent international collaborator for me, and I gained a wealth of experience from him during this period. His extensive experience, detailed feedback, insightful comments, and tremendous efforts in editing and improving my work have been instrumental in publishing high-quality research in prestigious venues. His insights and perspectives have influenced the scope of my work, and his steadfast support has been pivotal to my achievements in scientific research. I am very proud to have gained invaluable experience from him.

I would like to extend my sincere gratitude and special thanks to **Prof. Khaled Rabie** from Manchester Metropolitan University, UK for his unwavering support and guidance. His extensive experience, detailed feedback, insightful comments, and tremendous efforts in editing and improving my work have been instrumental in publishing high-quality research in prestigious venues. His perspectives and experience have helped improve the quality of my work, and his steadfast support has been crucial to my achievements. I am deeply grateful for the invaluable experience gained under his supervision and the knowledge acquired from him, which I am proud to have learned.

I would like to thank **Prof. Halim Yanikomeroglu** for his support and guidance during my visit to Carleton University, Canada under the Study in Canada Scholarship (SICS) program. I gained substantial knowledge from him and his wealth of experience. His forward-thinking perspective on cutting-edge future projects was particularly enlightening for me. I am grateful for his invaluable support and guidance. His vast experience, detailed feedback, insightful comments, and tremendous efforts have been pivotal in improving my work and disseminating high-quality research. His mentorship has made a lasting impact on my academic journey. Having the opportunity to be a student under his mentorship and conducting research with his guidance has been a source of great pride for me.

I would like to thank **Dr. Taissir Y. Elganimi** from the University of Tripoli, Libya for his support, collaboration, and help during my research.

I would like to thank all collaborators for their support and help during my research.

I extend my sincere thanks to the members of the jury who graciously agreed to be a part of this humble endeavor. I am indebted to certain individuals and friends who provided unwavering support, enabling us to navigate obstacles optimistically. To all of you, my heartfelt gratitude.

This thesis is dedicated to my father, mother, brothers, and sister, who can take pride in seeing the culmination of years of sacrifices and hardships that have helped me progress in life.

Finally, I want to convey my thanks to my friends and colleagues at the University of Echahid Hamma Lakhdar, El-Oued, and everyone who has been a pillar of support throughout this period. Your camaraderie and encouragement have meant a great deal to me.

Dedication

Dedicated to my parents, brothers, sister, and family

Your unwavering support and love have been my inspiration throughout this journey. This thesis is a tribute to your boundless encouragement and belief in my potential.

To all my friends and those who have helped and continuously encouraged me, I extend my best wishes for continued success.

Thanks

KHENNOUFA FAICAL

Abstract

The upcoming next generation of wireless networks is expected to offer ultra-reliable and low-latency communication, and other features due to the unprecedently high growth of timely mobile data traffic and stringent quality-of-service (QoS) requirements. These features will make a range of applications possible, including multiple access strategies (e.g., non-orthogonal multiple access (NOMA)), cooperative communications, energy harvesting (EH), reconfigurable intelligent surfaces (RISs), and unmanned aerial vehicle (UAV). NOMA is one of the most exciting approaches to improve spectrum efficiency in the next generations of wireless networks. Cooperative communication is integrated with NOMA (CNOMA) to offer an effective approach to mitigate challenges in channel conditions, extend the coverage area, and enhance spectral efficiency. Moreover, to enhance energy efficiency and prolong battery life for devices, CNOMA is empowered with EH. Furthermore, RIS enhances wireless communication by controlling radio propagation with low-cost passive elements, adjusting reflection coefficients for altered electromagnetic wave propagation. NOMA has been integrated with RIS to effectively provide efficient transmission in next-generation networks. Besides, UAV communication is a beneficial option for maintaining connectivity during brief events and after natural disasters. The UAV is adapted with RIS (UAV-RIS) and can serve as a reflective layer between ground base stations and devices, enhancing wireless communication. This thesis aims to investigate the interplay of NOMA with cooperative communication to improve the performance and extend the coverage area. To this end, we use several technologies for the CNOMA system, such as cooperative with and without direct links, multiple relays (multi-hop relay), EH, and UAV-RISs.

First, we investigate the downlink CNOMA without direct links (WDL). We derive the closed-form ergodic capacity (EC), outage probability (OP), and bit error rate (BER) over the Rayleigh fading channel. We evaluate the power allocation factor and helper user distance. We compare our scheme with traditional cooperative orthogonal multiple access (COMA) WDL. Then, we investigate the downlink CNOMA with DL. We derive the OP and BER with imperfect successive interference cancellation (ISIC) and channel state information (ICSI) over the Rayleigh fading channel. We assess the power allocation factor and the helper user distance. Thereafter, we investigate the multi-hop CNOMA with two schemes WDLs and DLs under the ICSI and ISIC. We derive the end-to-end (e2e) OP and BER expressions for the considered systems under ICSI and ISIC. We discuss the influence of power allocation, the number of relays, ICSI, and SIC on the performance of the systems. We compare our findings with single relay CNOMA. Moreover, we investigated two CNOMA with EH schemes: Firstly, we obtained the BER of CNOMA with time switching (TS) and power splitting (PS) protocols over the Rayleigh fading channel with ICSI, ISIC, and ICI. We explore the impact of ISIC and CSI on BER performance within the parameters of EH. Secondly, we obtained the OP and BER of CNOMA with three EH protocols (TS, PS, and hybrid) over the Nakagami-m fading channel. We discuss optimal values for EH parameters and the power allocation coefficient. Besides, we examine the performance of the wireless-powered cooperative communication network with linear/non-linear EH in the presence of in-phase and quadrature-phase imbalance (IQI) and SIC imperfections over the Rayleigh fading channel in terms of OP, EC, and throughput. We assess the impact of IQI and SIC imperfections on the proposed scheme using various WPCCN parameters. We compare our system to conventional UL NOMA without EH. Finally, we examine the BER and energy efficiency (EE) of UAV-RIS NOMA in the presence of practical constraints. We compare our results with two schemes: UAV without RIS and conventional UAV-RIS OMA. We validate our numerical derivations through simulation results.

The results show the following. The best relay location is between the base station and users to achieve higher performance. Increasing the number of relays reduces the OP and BER. Multi-hop NOMA achieves high-performance gain compared to single relay schemes. The ICSI and ISIC decrease the system performance at the high signal-to-noise ratio (SNR). The EH schemes achieve higher performance compared to those without EH and the hybrid protocol is superior to all benchmarks, which are in the range of 1–3 dB and 0.5–1.5 dB for OP and BER performances, respectively. The non-linear EH limits system performance in high SNR regions and is significantly impacted by IQI and SIC imperfections. IQI negatively affects RF impairment, highlighting the necessity of IQI mitigation to maximize system capabilities. Finally, HWI, ICI, and ISIC degrade performance at high SNR, however, increasing the number of RIS reflecting elements at low SNR achieves satisfactory results. The UAV-RIS system outperforms UAVs without it, and OMA performs better than NOMA due to no inter-user interference IUI issues.

Keywords: BER, cooperative, EH, EC, NOMA, OP, and UAV-RIS.

Résumé

La prochaine génération de réseaux sans fil devrait offrir une communication ultra fiable et à faible latence, ainsi que d'autres fonctionnalités en raison de la croissance sans précédent du trafic de données mobiles en temps opportun et des exigences strictes en matière de qualité de service (QoS). Ces fonctionnalités rendront possible toute une gamme d'applications, notamment plusieurs stratégies d'accès (par exemple, l'accès multiple non orthogonal (NOMA)), les communications coopératives et la récupération d'énergie (EH), les surfaces intelligentes reconfigurables (RIS) et les véhicules aériens sans pilote (UAV). NOMA est l'une des approches les plus excitantes pour améliorer l'efficacité spectrale dans les prochaines générations de réseaux sans fil. La communication coopérative est intégrée à NOMA (CNOMA) pour offrir une approche efficace pour atténuer les défis liés aux conditions du canal, étendre la zone de couverture et améliorer l'efficacité spectrale. De plus, pour améliorer l'efficacité énergétique et prolonger la durée de vie de la batterie des appareils, CNOMA est renforcée par EH. En outre, RIS améliore la communication sans fil en contrôlant la propagation radio avec des éléments passifs peu coûteux, en ajustant les coefficients de réflexion pour une propagation d'ondes électromagnétiques modifiée. NOMA a été intégré à RIS pour fournir efficacement une transmission efficace dans les réseaux de prochaine génération. En outre, la communication UAV est une option bénéfique pour maintenir la connectivité pendant de brefs événements et après des catastrophes naturelles. L'UAV est adapté avec RIS (UAV-RIS) et peut servir de couche réfléchissante entre les stations de base au sol et les appareils, améliorant ainsi la communication sans fil. Cette thèse vise à étudier l'interaction de NOMA avec la communication coopérative pour améliorer les performances et étendre la zone de couverture. À cette fin, nous utilisons plusieurs technologies pour le système CNOMA, telles que la coopération avec et sans liens directs, plusieurs relais (relais multi-sauts), EH et UAV-RIS.

Tout d'abord, nous étudions le CNOMA en liaison descendante sans liens directs (WDL). Nous dérivons la capacité ergodique (EC), la probabilité de panne (OP) et le taux d'erreur binaire (BER) sous canal de fading de Rayleigh. Nous évaluons le facteur d'allocation de puissance et la distance de l'utilisateur assistant. Nous comparons notre schéma avec le COMA coopératif traditionnel en liaison descendante avec DL. Ensuite, nous étudions le CNOMA en liaison descendante avec DL. Nous dérivons le OP et le BER avec annulation successive d'interférence imparfaite (ISIC) et information d'état de canal (ICSI) sous canal de fading de Rayleigh. Nous évaluons le facteur d'allocation de puissance et la distance de l'utilisateur assistant. Ensuite, nous étudions le CNOMA multi-sauts avec deux schémas

WDLs et DLs sous ICSI et ISIC. Nous dérivons les expressions de panne (e2e) OP et BER pour les systèmes considérés sous ICSI et ISIC. Nous discutons de l'influence de allocation de puissance, du nombre de relais, d'ICSI et de SIC sur les performances des systèmes. Nous comparons nos résultats avec le CNOMA à un seul relais. De plus, nous avons étudié deux schémas CNOMA avec EH : Premièrement, nous avons obtenu le BER de CNOMA avec les protocoles de commutation temporelle (TS) et de fractionnement de puissance (PS) sur le canal de fading de Rayleigh avec ICSI, ISIC et ICI. Nous explorons l'impact de ISIC et de CSI sur les performances de BER dans les paramètres de EH. Deuxièmement, nous avons obtenu le OP et le BER de CNOMA avec trois protocoles EH (TS, PS et hybride) sur le canal de fading de Nakagami-m. Nous discutons des valeurs optimales pour les paramètres EH et le coefficient d'allocation de puissance. De plus, nous examinons les performances du réseau de communication coopérative alimenté par le sans-fil avec EH linéaire/non linéaire en présence de déséquilibre de phase en phase et en quadrature (IQI) et d'imperfections SIC sur le canal de fading de Rayleigh en termes de OP, EC et débit. Nous évaluons l'impact des imperfections IQI et SIC sur le schéma proposé en utilisant divers paramètres WPCCN. Nous comparons notre système au NOMA UL conventionnel sans EH. Enfin, nous examinons le BER et l'efficacité énergétique (EE) de UAV-RIS NOMA en présence de contraintes pratiques. Nous comparons nos résultats avec deux schémas : UAV sans RIS et UAV-RIS OMA conventionnel. Nous validons nos dérivations numériques par des résultats de simulation.

Les résultats montrent ce qui suit. Le meilleur emplacement du relais se situe entre la station de base et les utilisateurs pour obtenir de meilleures performances. L'augmentation du nombre de relais réduit le OP et le BER et NOMA multi-sauts atteint un gain de performance élevé par rapport aux schémas à un seul relais. L'ICSI et l'ISIC diminuent les performances des systèmes au rapport signal/bruit (SNR) élevé. Les schémas EH atteignent de meilleures performances par rapport à sans EH et le protocole hybride est supérieur à tous les benchmarks, qui se situent dans la plage de 1 à 3 dB et 0,5 à 1,5 dB pour les performances de OP et BER. L'EH non linéaire limite les performances du système dans les régions à SNR élevé et est significativement impacté par les imperfections IQI et SIC. L'IQI affecte négativement l'impairment RF, mettant en évidence la nécessité de la mitigation de l'IQI pour maximiser les capacités du système. Enfin, HWI, ICI et ISIC dégradent les performances à SNR élevé, cependant, l'augmentation du nombre d'éléments RIS réflecteurs à SNR faible atteint des résultats satisfaisants. Le système UAV-RIS surpasse les UAV sans celui-ci, et OMA est meilleur que NOMA en raison de l'absence de problèmes d'interférence inter-utilisateur (IUI).

Keywords : BER, coopérative, EH, EC, NOMA, OP, and UAV-RIS.

ملخص

من المتوقع أن يوفر الجيل التالي من الشبكات اللاسلكية اتصالات موثوقة للغاية وذات زمن وصول منخفض، وميزات أخرى بسبب النمو المرتفع غير المسبوق لحركة البيانات المتنقلة في الوقت المناسب والمتطلبات الصارمة لجودة الخدمة (QoS). ستجعل هذه الميزات مجموعة من التطبيقات ممكنة، بما في ذلك استراتيجيات الوصول المتعددة (على سبيل المثال، الوصول المتعدد غير المتعامد (NOMA)) والاتصالات التعاونية وحصاد الطاقة (EH)، والأسطح الذكية القابلة لإعادة التشكيل (RISs)، والمركبات الجوية بدون طيار (UAV)). يعد NOMA أحد الأساليب الأكثر إثارة لتحسين كفاءة الطيف في الأجيال القادمة من الشبكات اللاسلكية. تم دمج الاتصال التعاوني مع NOMA (CNOMA) لتقديم نهج فعال للتخفيف من تحديات في ظروف القناة، وتوسيع منطقة التغطية، و تحسين الكفاءة الطيفية. من ناحية اخرى، لتعزيز كفاءة الطاقة وإطالة عمر بطارية الأجهزة، تم تمكين CNOMA باستخدام EH. في المقابل يعمل نظام RIS على تعزيز الاتصال اللاسلكي عن طريق التحكم في انتشار الراديو باستخدام عناصر خامله منخفضة التكلفة، وضبط معاملات الانعكاس للتغييرات في انتشار الموجات الكهرومغناطيسية. تم دمج NOMA مع RIS لتوفير نقل فعال في شبكات الجيل التالي. في الجهة المقابلة، يعد الاتصال بالطائرات بدون طيار خياراً مفيداً للحفاظ على الاتصال أثناء الأحداث القصيرة للانقطاع وبعد الكوارث الطبيعية. تم دمج الطائرة بدون طيار مع RIS (UAV-RIS) ويمكن أن تكون بمثابة طبقة عاكسة بين محطات الارسال والأجهزة الأرضية، مما يعزز الاتصال اللاسلكي. تهدف هذه الأطروحة إلى دراسة جمع NOMA مع التواصل التعاوني لتحسين الأداء وتوسيع منطقة التغطية. ولتحقيق هذه الغاية، نستخدم العديد من التقنيات لنظام CNOMA، مثل التعاون مع الروابط المباشرة و غير المباشرة، والمرحلات المتعددة (مرحل متعدد القفزات)، وزس، وUAV-RISs.

بناءا علي هذا يتم دراسة أهداف الاطروحه علي النحو التالي. أولاً، نقوم بدراسة الوصلة الهابطة CNOMA بدون روابط مباشرة (WDL). نشتق الشكل التقريبي للسعة (EC)، واحتمال الانقطاع (OP)، ومعدل خطأ البتات (BER) عبر قناة خبو رايلي. بعد ذلك، نقيم عامل توزيع الطاقة ومسافة المستخدم المساعد. نقارن أيضا مخططنا مع المخطط التعاوني التقليدي للوصول المتعدد المتعامد (COMA) WDL. في الخطوة التالية، نقوم بدراسة الوصلة الهابطة CNOMA مع DL. نشتق OP وBER في ظل ضروف إلغاء التداخل المتتالي غير الكامل (ISIC) ومعلومات حالة القناة (ICSI) عبر قناة خبو Rayleigh. نفحص عامل توزيع الطاقة ومسافة المستخدم المساعد. عقب ذلك، ندرس CNOMA متعدد القفزات باستخدام مخططين WDLs وDLs في وجود ICSI وISIC. نستخرج تعبيرات OP وBER من طرف إلى طرف (e2e)

للأنظمة المقترحة في وجود ICSI وISIC. نستعرض تأثير توزيع الطاقة، وعدد المرحلات، وICSI، وSIC على أداء الأنظمة. نجري أيضا مقارنة نتائجنا التي توصلنا إليها مع CNOMA للمرحل الفردي التقليدي. إضافة إلى ما سبق، نعمل على دراسة اثنين من مخططات CNOMA مع EH: أولاً، نحصل على معدل BER لـ CNOMA مع بروتوكول تبديل الوقت (TS) وتقسيم الطاقة (PS) عبر قناة خبو Rayleigh في وجود ICSI وISIC وICI. نقوم ايضا باجراء تحقيق لاستكشاف تأثير ISIC وCSI على أداء BER ضمن معايير EH. ثانياً، نحصل على OP وBER لـ CNOMA مع ثلاثة بروتوكولات EH (TS وPS و hybrid) عبر قناة الخبو Nakagami-m. نناقش القيم المثلى لمعاملات EH ومعامل توزيع الطاقة. وبالإضافة هذا، نفحص أداء شبكة الاتصالات التعاونية التي تعمل بالطاقة اللاسلكية مع EH الخطي \ غير الخطي في ظل وجود خلل في الطور والطور التربيعي (IQI) وعيوب SIC على قناة خبو رايلي من حيث OP وEC ، والإنتاجية. نناقش كذلك تأثير عيوب IQI وSIC على المخطط المقترح باستخدام معاملات WPCCN المختلفة. نقارن المخطط المقترح مع UL NOMA التقليدي بدون EH. أخيراً، نفحص معدل الخطأ في البتات (BER) وكفاءة استخدام الطاقة (EE) لـ UAV-RIS NOMA في ظل وجود قيود عملية. نقارن ايضا نتائجنا مع مخططين: الطائرات بدون طيار بدون RIS والطائرات بدون طيار التقليدية UAV-RIS OMA. يثتم التحقق من صحة اشتقاقاتنا العددية من خلال نتائج المحاكاة.

تظهر النتائج ما يلي. أفضل موقع للترحيل هو بين محطة الارسال والمستخدمين لتحقيق أداء أعلى. تؤدي زيادة عدد المرحلات إلى تقليل OP وBER وتحقق NOMA متعددة القفزات مكاسب عالية في الأداء مقارنة بأنظمة المرحل الفردي. يعمل ICSI وISIC على تقليل أداء الأنظمة عند نسبة الإشارة إلى الضوضاء العالية (SNR). تحقق مخططات EH أداءً أعلى مقارنةً بدون EH ويتفوق البروتوكول hybrid على جميع المعايير، والتي تقع في نطاق ١–٣ ديسيبل و٠.٥–٠.١ ديسيبل لأداء OP وBER. يحد EH غير الخطي من أداء النظام في المناطق ذات نسبة الإشارة إلى الضوضاء (SNR) العالية ويتأثر بشكل كبير بعيوب IQI وSIC. يؤثر IQI سلباًا على ضعف التردد اللاسلكي، مما يسلط الضوء على ضرورة تخفيف IQI لزيادة قدرات النظام إلى أقصى حد. أخيراً، يؤدي كل من HWI وICI وISIC إلى تدهور الأداء عند نسبة SNR عالية، ومع ذلك، فإن زيادة عدد عناصر (RIS) العاكسة عند نسبة SNR منخفضة يحقق نتائج مرضية. يتفوق نظام UAV-RIS على الطائرات بدون طيار بدون RIS، و OMA اداء أفضل من NOMA بسبب عدم وجود مشكلات في التداخل بين المستخدمين (IUI).

الكلمات المفتاحية: BER، التعاون، EH، EC، NOMA، OP، و RIS.

Research Publications

Authored Paper- Published

- Faical Khennoufa, Khelil Abdellatif, Halim Yanikomeroglu, Safwan Alfattani, Metin Ozturk, and Ferdi Kara. «Two-Tier High Altitude Platform Stations (HAPS) for Exploring Wireless Energy Harvesting». submitted to IEEE Transactions on Wireless Communications, 2024.

- Faical Khennoufa, Khelil Abdellatif, Ferdi Kara, Halim Yanikomeroglu, Khaled Rabie, Taissir Y. Elganimi, and Safia Beddiaf.«Error performance analysis of UAV-mounted RIS for NOMA systems with practical constraints». IEEE Communications Letters, 2024.

- Faical Khennoufa, Abdellatif Khelil, Safia Beddiaf, Ferdi Kara, Khaled Rabie, Hakan Kaya, Ahmet Emir, Salama Ikki, and Halim Yanikomeroglu.«Wireless powered cooperative communication network for dual-hop uplink NOMA with IQI and SIC imperfections». IEEE Access, 2023.

- Faical Khennoufa, Abdellatif Khelil, Khaled Rabie, Hakan Kaya, and Xingwang Li.«An efficient hybrid energy harvesting protocol for cooperative NOMA systems: Error and outage performance». Physical Communication. 2023.

- Faical Khennoufa and Khelil Abdellatif.« BER Performance of Co-operative Relay NOMA-assisted PS Protocol with Imperfect SIC and CSI». International Journal of Sensors Wireless Communications and Control. 2023. 101952.

- Faical Khennoufa, Khelil Abdellatif, and Ferdi Kara. « Bit error rate evaluation of relay-aided cooperative NOMA with energy harvesting under imperfect SIC and CSI».Physical Communication. 2022.

- Faical Khennoufa, Khelil Abdellatif, and Ferdi Kara. « Bit error rate and outage probability analysis for multi-hop decode-and-forward relay-aided NOMA with imperfect SIC and imperfect CSI».AEU-International Journal of Electronics and Communications. 2022.

Co-Authored Paper- Published

- Safia Beddiaf, Abdellatif Khelil, Faical Khennoufa, Ferdi Kara, Khaled Rabie, Xingwang Li, Hakan Kaya, Ahmet Emir, and Halim Yanikomeroglu.Impact of hardware impairment on the uplink SIMO Cooperative NOMA with selection relay under imperfect CSI» IEEE Access, 2023.

- Safia Beddiaf, Abdellatif Khelil, Faical Khennoufa, and Khaled Rabie.« On the impact of IQI on cooperative NOMA with direct links in the presence of imperfect CSI». Physical Communication, 2023.

- Safia Beddiaf, Abdellatif Khelil, Faical Khennoufa, Ferdi Kara, Hakan Kaya, Xingwang Li, Khaled Rabie, and Halim Yanikomeroglu.«A Unified Performance Analysis of Cooperative NOMA With Practical Constraints: Hardware Impairment, Imperfect SIC and CSI». IEEE Access. 2022.

Conference Paper- Published

- Faical Khennoufa, Khelil Abdellatif, Halim Yanikomeroglu, Metin Ozturk, Taissir Elganimi, Ferdi Kara. «Multi-Layer Network Formation through HAPS Base Station and Transmissive RIS-Equipped UAV». submitted to IEEE Global Communications Conference (GLOBECOM), 2024.

- Faical Khennoufa, Abdellatif Khelil, and Elhadi Kenane. «BER and Outage Performance for Multi-hop User-Relays NOMA with Imperfect SIC and CSI ». In International Conference of Advanced Technology in Electronic and Electrical Engineering (ICATEEE). 2021.

- Faical Khennoufa and Abdellatif Khelil. «Exact bit error rate of cooperative NOMA without diversity combining ». In International Conference on Artificial Intelligence for Cyber Security Systems and Privacy (AI-CSP). 2021

- Faical Khennoufa and Abdellatif Khelil. «Capacity performance comparison of cooperative NOMA and OMA systems in DF and AF» The International Conference on Advances in Communication Technology, Computing and Engineering, Morocco, 2021.

Contents

List of Figures XVIII

List of Abbreviations XXII

General introduction 1

1 Fundamental Concepts of Wireless Communications 8
1.1 Introduction 8
1.2 Wireless Communications Channel Models 8
1.2.1 Rayleigh Fading Channel Model 8
1.2.2 Nakagami-m Fading Channel Model 9
1.3 Imperfect channel State Information 9
1.4 Wireless Communications Performance Metrics 9
1.4.1 Ergodic Capacity 9
1.4.2 Outage Probability 10
1.4.3 Bit Error Rate 10
1.5 NOMA Power Domain 10
1.5.1 Downlink NOMA 10
1.5.2 Uplink NOMA 12
1.6 Cooperative NOMA 12
1.6.1 Downlink Cooperative NOMA 13
1.6.2 Uplink Cooperative NOMA 14
1.7 Energy Harvesting 14
1.7.1 Power Splitting 15
1.7.2 Time Switching 16
1.7.3 Non-Linear Energy Harvesting 17
1.8 Uncrewed Aerial Vehicle 17
1.9 Reconfigurable Intelligent Surfaces 19
1.10 Conclusion 21

2 Cooperative NOMA Without Direct Link **23**
2.1 Introduction . . . 23
2.1.1 Related Works . . . 23
2.1.2 Motivation and Contributions . . . 24
2.2 System Model . . . 24
2.3 Performance Analysis . . . 26
2.3.1 Ergodic Capacity . . . 26
2.3.2 Outage Probability . . . 27
2.3.3 Bit Error Rate . . . 27
2.4 Numerical Results . . . 29
2.5 Conclusion . . . 37

3 Cooperative NOMA with Direct Link **38**
3.1 Introduction . . . 38
3.1.1 Related Works . . . 38
3.1.2 Motivation and Contributions . . . 39
3.2 System Model . . . 39
3.3 Performance Analysis . . . 40
3.3.1 Outage Probability . . . 41
3.3.1.1 Outage Probability of Downlink NOMA . . . 41
3.3.1.2 Outage Probability of CNOMA with DL . . . 41
3.3.1.3 Asymptotic Outage Probability . . . 42
3.3.2 Bit Error Rate . . . 42
3.3.2.1 BER of Downlink NOMA . . . 42
3.3.2.2 BER of CNOMA with DL . . . 43
3.4 Numerical Results . . . 45
3.5 Conclusion . . . 50

4 Cooperative NOMA with Multiple Relays **52**
4.1 Introduction . . . 52
4.1.1 Related Works . . . 52
4.1.2 Motivation and Contributions . . . 53
4.2 Cooperative NOMA assisted Multiple Relays Without Direct Links . . . 55
4.2.1 System Model . . . 55
4.2.2 Performance Analysis . . . 56
4.2.2.1 Outage Probablity . . . 56
4.2.2.2 Bit Error Rate . . . 58
4.3 Cooperative NOMA assisted Multiple Relays with Direct Links . . . 60

4.3.1 System Model 60
4.3.2 Performance Analysis 62
4.3.2.1 Outage Probability 62
4.3.2.2 Bit Error Rate 63
4.4 Numerical Results 64
4.4.1 Cooperative NOMA assisted Multiple Relays Without Direct Links 64
4.4.2 Cooperative NOMA Assisted Multiple Relay with Direct Links 72
4.5 Conclusion 77

5 Cooperative NOMA with Wireless Energy Harvesting 79
5.1 Introduction 79
5.1.1 Related Works 79
5.1.2 Motivation and Contributions 81
5.2 Cooperative NOMA with EH over Rayleigh Fading Channel 82
5.2.1 System Model 82
5.2.2 Performance Analysis 84
5.3 Cooperative NOMA with EH over Nagakamai-m Fading Channel 86
5.3.1 System Model 86
5.3.2 Performance Analysis 88
5.3.2.1 Outage Probablity 88
5.3.2.2 Bit Error Rate 89
5.4 Numerical Results 92
5.4.1 Cooperative NOMA with EH over Rayleigh Fading Channel 92
5.4.2 Cooperative NOMA with EH over Nagakamai-m Fading Channel 96
5.5 Conclusion 103

6 Wireless-Powered Cooperative Communication Network for Dual-Hop Uplink NOMA 105
6.1 Introduction 105
6.1.1 Related Works 105
6.1.2 Motivation and Contributions 106
6.2 System Model 107
6.3 Performance analysis 112
6.3.1 Outage Probability 112
6.3.1.1 Linear EH 112
6.3.1.2 Non-Linear EH 114
6.3.2 Ergodic Capacity 117
6.3.2.1 Linear EH 117

6.3.2.2 Non-Linear EH . . . 118
6.3.3 Throughput . . . 120
6.4 Numerical Results . . . 120
6.5 Conclusion . . . 137

7 UAV-Mounted RIS for Cooperative NOMA Systems with Practical Constraints 139
7.1 Introduction . . . 139
7.1.1 Related Works . . . 140
7.1.2 Motivation and Contributions . . . 140
7.2 System and Channel Models . . . 141
7.3 Performance Analysis . . . 144
7.3.1 Bit Error Rate . . . 144
7.3.2 Energy Efficiency . . . 146
7.4 Numerical Results . . . 146
7.5 Conclusion . . . 152

Bibliography 158

A Appendix A: Proof of (2.20) and (2.21) A

B Appendix B: Proof of (2.22) and (2.23) C

C Appendix C: Proof of (3.30) E

D Appendix D: Proof of (5.38) F

E Appendix E: Proof of (5.39) H

List of Figures

1 Evolution of mobile network: From 1G to 6G. . . . 1

2 Key Performance Requirements for 5G and 6G. . . . 3

1.1 (a) Downlink NOMA network, (b) The working principle of superposition coding and successive interference cancellation. . . . 11

1.2 Uplink NOMA network. . . . 13

1.3 Downlink CNOMA network. . . . 13

1.4 Uplink CNOMA network. . . . 14

1.5 The transmission with EH technology. . . . 15

1.6 Power splitting protocol. . . . 16

1.7 Time switching protocol. . . . 17

1.8 A comparison between the linear EH model and the non-linear EH model. . . . 18

1.9 UAV with NOMA network. . . . 19

1.10 Types of RIS. . . . 20

1.11 RIS with NOMA network. . . . 21

2.1 CNOMA WDL scheme. . . . 25

2.2 Constellation diagram of the received signal. . . . 28

2.3 EC of CNOMA WDL. . . . 30

2.4 EC of CNOMA WDL w.r.t. d2. . . . 30

2.5 EC of CNOMA WDL w.r.t. α_2. . . . 31

2.6 EC comparison between CNOMA WDL and COMA WDL. . . . 32

2.7 OP of CNOMA WDL. . . . 32

2.8 OP of CNOMA WDL w.r.t. d_2. . . . 33

2.9 OP of CNOMA WDL w.r.t. α_2. . . . 33

2.10 OP comparison between CNOMA WDL and COMA WDL. . . . 34

2.11 BER of CNOMA WDL. . . . 34

2.12 BER of CNOMA WDL w.r.t. d_2. . . . 35

2.13 BER of CNOMA WDL w.r.t. α_2. . . . 36

2.14 BER comparison between CNOMA WDL and OMA WDL. 36

3.1 CNOMA with DL scheme. 40
3.2 OP of CNOMA with DL. 45
3.3 OP of CNOMA with DL w.r.t. ICSI factor (σ_e^2). 46
3.4 OP of CNOMA with DL w.r.t. α_2. 46
3.5 OP of CNOMA with DL w.r.t. d_2. 47
3.6 BER of CNOMA with DL. 48
3.7 BER of CNOMA with DL w.r.t. ICSI factor (σ_e^2). 49
3.8 BER of CNOMA with DL w.r.t. α_2. 49
3.9 BER of CNOMA with DL w.r.t. d_2. 50

4.1 MH-DF-CNOMA WDL scheme. 56
4.2 MH-DF-CNOMA with DL scheme. 61
4.3 OP of MH-DF-CNOMA WDL w.r.t. SNR: (a) With perfect CSI, (b) With ICSI. . . 65
4.4 OP of MH-DF-CNOMA WDL w.r.t. L relay. 66
4.5 OP of MH-DF-CNOMA WDL vs MH-DF-COMA WDL with different relays 67
4.6 OP of MH-DF-CNOMA WDL vs MH-DF-COMA WDL for one relay 68
4.7 BER of MH-DF-CNOMA WDL w.r.t. SNR: (a) With perfect CSI, (b) With ICSI. . 69
4.8 BER of MH-DF-CNOMA WDL w.r.t. L relay. 70
4.9 BER of MH-DF-CNOMA WDL w.r.t. α_2 with different relays. 70
4.10 BER of MH-DF-CNOMA WDL w.r.t. α_2 with different different distances between R_L and U_2. 71
4.11 OP of MH-DF-CNOMA WDL compared to single relay scheme. 71
4.12 BER of MH-DF-CNOMA WDL compared to single relay scheme. 73
4.13 OP of MH-DF-CNOMA with DL w.r.t. SNR: (a) With perfect CSI, (b) With ICSI. 74
4.14 OP of MH-DF-CNOMA with DL w.r.t. α_2 with different relay. 75
4.15 BER of MH-DF-CNOMA with DL w.r.t. SNR: (a) With perfect CSI, (b) With ICSI. 76
4.16 OP of MH-DF-CNOMA with DL w.r.t. α_2 with different relay. 77

5.1 CNOMA with EH schemes. 83
5.2 CNOMA with HEH schemes. 86
5.3 BER w.r.t. SNR with the TS and PS protocols under ICSI. 92
5.4 BER w.r.t. ICSI for the TS and PS protocols under ICSI. 93
5.5 BER w.r.t. ρ and ν for the TS and PS protocols. 93
5.6 BER w.r.t. η for the TS and PS protocols under ICSI. 94
5.7 BER w.r.t. η for the TS and PS protocols under ICSI. 95
5.8 BER w.r.t. α_2 for the TS and PS protocols under ICSI. 95

5.9 BER w.r.t. SNR for the TS and PS protocols under ICI. 96
5.10 BER performance comparisons between hybrid protocol and benchmarks w.r.t. SNR. 97
5.11 BER performance comparisons between hybrid protocol and benchmarks w.r.t. power allocation. 98
5.12 BER performance comparisons between hybrid protocol and benchmarks w.r.t. EH parameters. 99
5.13 OP performance comparisons between hybrid protocol and benchmarks w.r.t. SNR. 100
5.14 OP performance comparisons between hybrid protocol and benchmarks w.r.t. power allocation. 101
5.15 OP performance comparisons between hybrid protocol and benchmarks w.r.t. EH parameters. 102

6.1 HTC-NOMA-WPCCN scheme. 108
6.2 Block diagram of harvest and information transmission for the proposed system. . . 108
6.3 Outage probability comparison for HTC-NOMA-WPCCN and uplink NOMA with linear and non-linear EH. 122
6.4 Outage probability w.r.t. τ for HTC-NOMA-WPCCN with linear and non-linear EH. 123
6.5 Outage probability w.r.t. α_2 for HTC-NOMA-WPCCN with linear and non-linear EH.124
6.6 Outage probability w.r.t. IRR for HTC-NOMA-WPCCN with linear and non-linear EH. 125
6.7 EC comparison for HTC-NOMA-WPCCN and uplink NOMA with linear and non-linear EH. 126
6.8 EC w.r.t. τ for HTC-NOMA-WPCCN with linear and non-linear EH. 127
6.9 EC w.r.t. α_2 for HTC-NOMA-WPCCN with linear and non-linear EH. 129
6.10 EC w.r.t. IRR for HTC-NOMA-WPCCN with linear and non-linear EH. 130
6.11 Throughput w.r.t. SNR comparison for HTC-NOMA-WPCCN and uplink NOMA with linear and non-linear EH. 132
6.12 Throughput w.r.t. τ for HTC-NOMA-WPCCN with linear and non-linear EH. . . . 133
6.13 Throughput w.r.t. α_2 for HTC-NOMA-WPCCN with linear and non-linear EH. . . . 134
6.14 Throughput w.r.t. IRR for HTC-NOMA-WPCCN with linear and non-linear EH. . . 135
6.15 HTC-NOMA-WPCCN w.r.t. SNR_{th}: OP, EC and Throughput. 136

7.1 UAV-RIS NOMA system model. 142
7.2 BER w.r.t. SNR of UAV-RIS NOMA with the fixed value of the effect of HWI and ICI: (a) U_1; (b) U_2. 147
7.3 BER w.r.t. SNR of UAV-RIS NOMA with the effect of HWI and ICI: (a) U_1; (b) U_2. 148
7.4 BER of system w.r.t. altitude $T_h(m)$ of UAV-RIS NOMA with the effect of HWI and ICI. 150

7.5 EE w.r.t. N with different Plos for NOMA and OMA with ideal and non-ideal (i.e., with and without HWI and ICI). 151
7.6 EE w.r.t. N with different SNR. 151

List of Abbreviations

1G	First generation.
2G	Second generation.
3G	Third generation.
4G	Fourth generation.
5G	Fifth generation.
6G	Sixth generation.
ABER	Average bit error rate.
AF	Amplify and forward.
AI	Artificial intelligence.
AP	Access point.
BER	Bit error rate.
BPSK	Binary phase-shift keying.
B5G	Beyond 5G.
BS	Base station.
CDF	Cumulative distribution function.
CDMA	Code division multiple access.
CNOMA	Cooperative non-orthogonal multiple access.
COMA	Cooperative orthogonal multiple access.
DF	Decode and forward.

DLs	With direct links.
E2E	End-2-End.
EC	Ergodic capacity.
EH	Energy harvesting.
FD	Full-duplex.
FDMA	Frequency division multiplexing access.
HAP	High-altitude platform.
HD	Half-duplex.
HEH	Hybrid energy harvesting.
HI	Hardware impairments.
HTC	Harvest-then-cooperate.
ICSI	Channel state information.
ICSI	Imperfect channel state information.
IoT	Internet-of-Things.
IQI	In-phase and quadrature-phase imbalance.
IUI	Inter-user interference.
IRR	Image rejection ratio.
ISIC	Imperfect successive interference cancelation.
ISIC	Successive interference cancelation.
JML	Joint maximum-likelihood.
KPI	Key performance indicator.
LoS	Line of sight.
MA	Multiple access.
MIMO	Multiple-input multiple-output.
MGF	Moment generating function.

MH-DF-NOMA Multi-hop decode-and-forward-aided cooperative CNOMA.

mMTC Massive machine-type communication.

MLD Maximum likelihood detection.

MRC Maximum ratio combining.

NOMA Non-orthogonal multiple access.

OFDMA Orthogonal frequency division multiplexing access.

OMA Orthogonal Multiple Access.

OP Outage Probability.

PDF Probability density function.

PS Power splitting.

RF Radio frequency.

RIS Reconfigurable intelligence surfaces.

Rx Receiver.

SC Superposition coding.

SC-FDMA Single-carrier frequency division multiplexing access.

SINR Signal-to-interference-plus-noise ratio.

SNR Signal-to-noise ratio.

TDMA Time division multiple access.

Thz Terahertz.

TS Time switching.

Tx Transmitter.

uHDD Ultra-high data density.

uHSLLC Ultra-high-speed with low-latency communications.

uMUB Ubiquitous mobile ultra-broadband.

UAV Unmanned aerial vehicle.

WDLs	Without direct links.
WIT	Wireless information transmission.
WPCN	Wireless-powered cooperative network.
WPCCN	Wireless-powered cooperative communication network.
WPT	Wireless power transfer.

General introduction

1. Towards 6G: Exploring Future Frontiers in Wireless Communication:

Wireless communication technologies have always been among the most important technologies developed in the past few decades. A new generation has emerged almost every decade since 1980. As shown in Figure .1, five wireless communication networks have appeared that support various multiple access (MA) technologies, including frequency division multiplexing access (FDMA), time division multiple access (TDMA), code division multiple access (CDMA), and orthogonal FDMA (OFDMA). The start was marked by the realization of the world's first cellular system, known as the first generation (1G), which allowed the emergence of voice communication via cell phones using FDMA. The second generation (2G) uses digital multiple-access technology such as TDMA and CDMA. It provides services such as short message services (SMS), picture messages, and multimedia message services (MMS). The third generation (3G) uses wideband code division multiple access (WCDMA) technology to deliver internet access as well as substantially enhanced video and audio transmission. The fourth generation (4G) Long Term Evolution (LTE) used OFDMA and single-carrier FDMA (SC-FDMA) to provide high-speed, high-quality, high-capacity, security, and low-cost services for voice data services and the internet. The fifth generation (5G) used OFDMA and massive multiple-input multiple-output (MIMO) to offer a greater user data rate, reduced latency, high system capacity, and a massive number of connections.

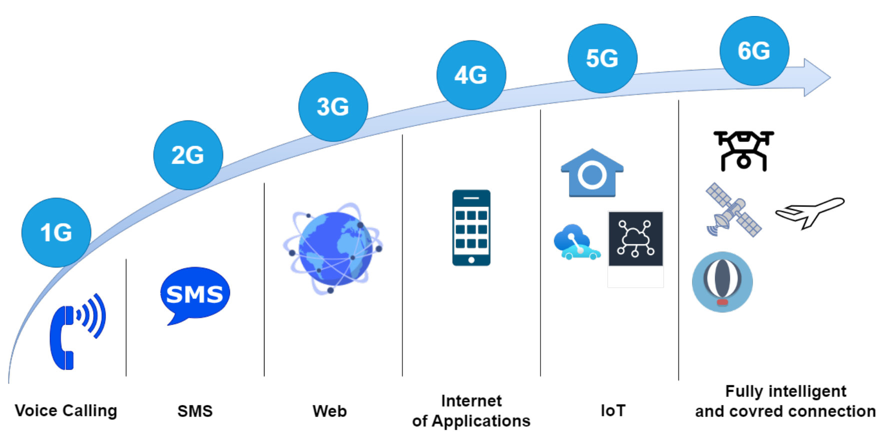

Figure 1: *Evolution of mobile network: From 1G to 6G.*

The implementation of 5G technologies involves balancing multiple considerations, including throughput, latency, energy efficiency (EE), deployment costs, reliability, and hardware complexity. Beyond 2030, 5G will likely face difficulties in meeting the evolving demands of the market. The sixth generation (6G) will bridge the gap between the needs of the market and 5G. The main objectives of 6G systems are based on past trends and future needs projections, which are as follows:

- Extremely high data rates per device.
- Very large number of connected devices.
- Global connectivity and full coverage.
- Very low latency.
- Lowering the energy consumption with battery-free Internet of Things (IoT) devices.
- Ultra-high reliable connectivity.
- Connected intelligence with machine learning capability.

It is anticipated that future research will definitively define several key performance indicators (KPI) classes for 6G. Several academic and industry researchers focus on the following KPIs for 6G communication, including achieving a peak data rate of 1000 Gbps, 10^{-9} reliability, 1000 Mb/s/m^2 area traffic capacity, 10^7 connection density, 10^{-3} ms latency, 100 GHz maximum bandwidth, 30 b/s/Hz peak spectral efficiency, and Km/h mobility, as presented in Figure .2 [1, 2]. These efforts are intended to pave the way for various KPI-related services on 6G communication systems. These services include ubiquitous mobile ultra-broadband (uMUB), ultra-high-speed with low-latency communications (uHSLLC), massive machine-type communication (mMTC), and ultra-high data density (uHDD). Therefore, the upcoming 6G communication system is set to introduce a variety of groundbreaking technologies, including artificial intelligence (AI), terahertz (THz) communications, reconfigurable intelligent surfaces (RIS), non-orthogonal multiple access (NOMA), energy harvesting (EH), and non-terrestrial networks (satellite, high-altitude platform stations or high-altitude pseudo satellites (HAPS), and uncrewed aerial vehicles (UAV)) to provide global coverage [3, 4].

2. Motivation and Objectives:

Each generation of preceding cellular standards (from 1G to 5G) featured different MA techniques, including FDMA, TDMA, CDMA, and OFDMA, which is known as orthogonal MA (OMA). In OMA techniques, the radio resources (in terms of time, code, or frequency) are divided among numerous users. Hence, the amount of accessible orthogonal resources determines the maximum number of users that may be handled. To this end, a new shifting paradigm is proposed in the design philosophy for beyond 5G (B5G) and 6G cellular networks: shifting from orthogonal to

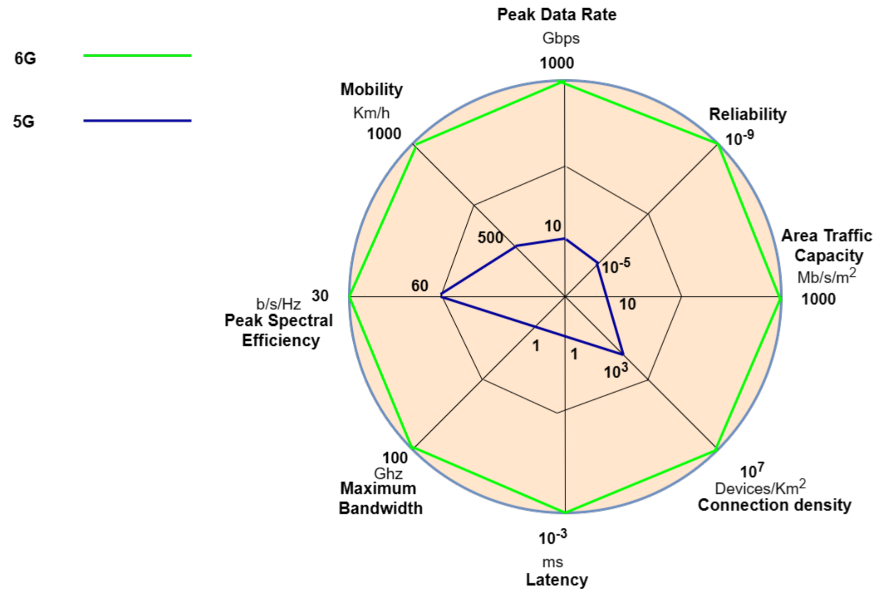

Figure 2: *Key Performance Requirements for 5G and 6G.*

non-orthogonal design in the waveform, MA, and random-access techniques. The key component techniques of NOMA are the superposition coding (SC) signal and successive interference cancellation (SIC) [5, 6, 7]. NOMA was suggested for future radio networks in [8], and its superiority to OMA schemes has been proved in terms of different KPIs such as outage probability (OP) and ergodic capacity (EC), etc [9, 10]. However, NOMA suffers from inter-user interference (IUI), impacting bit error rate (BER) performance, especially with the increasing number of users [11].

Despite its potential to enhance wireless communication systems, NOMA is hindered by several problems, including limited coverage, channel turbulence, IUI, etc. This thesis proposes NOMA-assisted cooperative communication as a solution to resolve these problems and improve system efficiency. In cooperative communications, two main protocols are used in the literature, known as follows: decode and forward (DF) and amplify and forward (AF). In the DF protocol, the relay node needs to decode the received information of the first phase to forward it to the destination. In the AF protocol, without decoding the received information of the first phase, the relay node amplifies the received information of the first phase and forwards it to the destination. Since the AF protocol has more errors based on the investigations in the literature, this thesis focuses on the use of the DF protocol. In CNOMA, multiple nodes collaborate to transmit and receive signals to achieve significant performance gains. To this end, several technologies are used in the CNOMA system, such as cooperative with and without direct links, multiple relays (multi-hop relay), EH, and UAV-RIS. Therefore, we are going to outline each system's objectives as follows:

- CNOMA is one of the important technologies to improve the performance of NOMA and combat channel disorders [12, 13, 14]. Two main schemes in CNOMA are used and known as cooperative with direct links (DL) and cooperative without direct links (WDL). The objectives of each of them are as follows. The first one is used to enhance the system performance when the direct and relay links at the destination are available. The second one is used to increase the coverage area when only the relay link is available at the destination.

- Several schemes are used in multiple relays, such as selection relay and multi-hop relay. In this thesis, we focus on the multi-hop relay. In this scheme, the signal can travel farther without noticeably losing quality by placing relay nodes strategically between the source and the destination. This method efficiently reduces problems that commonly occur in long-distance communications, like path-loss, fading, and interference. Furthermore, multi-hop relay allows for more flexible network deployment and better resource utilization, which makes it especially useful in situations with limited infrastructure or harsh environmental conditions. The main objective of multi-hop relay systems is to maximize coverage, throughput, and communication reliability while making effective use of the available resources.

- The escalated energy consumption in wireless communication presents a significant challenge. In the event of battery depletion or disconnection of power supplies, the task of battery replacement becomes daunting and costly. To overcome this problem, it has been suggested that wireless EH be used to gather and convert ambient radiofrequency signals into electrical power that wireless devices can use. This approach improves the sustainability of wireless applications by eliminating the need for traditional power sources. The two primary protocols used in EH are time switching (TS) and power splitting (PS). The description of each protocol is defined in the first chapter.

- RIS operates as a "smart" surface that can dynamically control electromagnetic waves to increase coverage areas, reduce interference, and maximize signal strength. Moreover, to improve coverage, capacity, and reliability, UAV equipped with advanced communication technologies will act as mobile base stations, relays, or data carriers, enabling the rapid deployment of network infrastructure, supporting emergency communications, and facilitating data offloading in crowded areas. Recently, the RIS has been integrated with UAV by mounting RIS on the UAV, which is called UAV-mounted RIS. Wireless communication performance is improved by installing RIS on UAV by dynamically controlling electromagnetic waves, expanding coverage areas, and mitigating interference.

On the other hand, in reality, the devices suffer from many problems that affect the overall performance of the system, including the RF component of hardware impairment (HWI), such as in-phase and quadrature-phase imbalance (IQI), imperfect channel state information (ICSI), imperfect SIC. These imperfections are taken into account and evaluated in this thesis.

3. Contributions:

As described above, NOMA is one of the promising radio access technologies to improve performance in cellular communications of the next generation. Moreover, the interplay between NOMA and cooperative communication is one of the topics that drew the most attention to achieving higher spectral efficiency and compensation for path-loss. Additionally, the multi-hop relay is crucial for expanding cell coverage to locations outside the cell range or to heavily shadowed areas within the cell. On the other hand, EH has attracted much attention due to its potential to increase EE. UAV-mounted RIS dynamically controls electromagnetic waves, expands coverage areas, and mitigates interference. Based on the author's acknowledgment, these systems have not been studied under practical imperfections. The objective of this thesis is to analyze CNOMA with the mentioned systems for BER, OP, EC, and throughput. We evaluate the ICSI, ISIC, HWI, and IQI in this thesis. During this research, the major contributions of this thesis are provided as follows:

- We investigate the OP, EC, and BER performance of cooperative NOMA (CNOMA) WDL. Moreover, we discuss the impact of power allocation and the position of the helper user. We compare CNOMA WDL with their counterpart cooperative OMA (COMA) and conventional NOMA. The results show that CNOMA WDL outperformed COMA WDL in terms of OP and EC, while COMA WDL have better performance gains in terms of BER.

- We investigate the OP and BER performance of CNOMA with DL under the ISIC and ICSI. The asymptotic OP at a high signal-to-noise ratio (SNR) region is obtained. Moreover, we discuss the impact of power allocation, helper user distance, imperfect SIC, and CSI. The results show that ICSI has a negative impact on the high SNR regions, which affects the SIC to detect the symbols of users.

- We propose the multi-hop CNOMA system with the effect of ISIC and ICSI. The system overcomes the issue of poor channel quality and extends the coverage area to places outside the cell range. Two systems are proposed: CNOMA mult-hop WDL and CNOMA multi-hop with DL. The first one is used to extend the coverage when direct communication between the BS and users is not available. The second system is used to improve the system performance when the direct and indirect links are available. We analyze the OP, EC, and BER performance of both considered systems under the ISIC and ICSI. Moreover, we discuss the effects of power allocation, ISIC, ICSI, and the number of relays.

- Without using the relay's power, the EH is considered to increase EE. We analyze the BER of CNOMA with the EH system over the Rayleigh fading channel for TS and PS protocols. Moreover, to reach the maximum performance of EH, we propose the hybrid EH (HEH) protocols for CNOMA. It is a combination of TS and PS protocols. We derive the BER and OP of three EH protocols (i.e., PT, TS, and HEH) over the Nakagami-m fading channel. we compare the HEH protocol with traditional EH protocols (i.e., TS and PS) and CNOMA without EH. The optimum values for EH CNOMA with EH parameters and power allocation coefficient are discussed.

- We propose an uplink NOMA-assisted wireless-powered cooperative communication network (WPCCN). To improve the system performance, multiple near users are performed to improve the received signal quality. The practical implementations such as IQI and ISIC are ignored in the literature. Thus, we consider these imperfections in our proposed system. In the realistic scenarios, the EH circuits have non-linear properties. Thus, the linear and non-linear EH are considered in our investigation. We derive OP and throughput with linear and non-linear EH under IQI and ISIC. We obtained accurate expressions of EC for our proposed system with linear and non-linear EH under the effects of IQI and ISIC. We compare the proposed scheme with the uplink NOMA without EH as a benchmark.

- To improve the performance and coverage of the UAV, we examine the integration of RIS with UAVs in next-generation wireless communication. In our system, the RIS is intended to be mounted on a UAV. We also consider the practical constraints of HWI at the transceivers, inter-cell interference (ICI), and ISIC. We derive the BER of UAV-RIS under HWI, ICI, and ISIC. As well, we obtain the upper bound of our proposed system. Besides, we obtain the EE for our considered system. We compare our results with UAV without RIS and traditional UAV-RIS OMA. We validate our analysis with Monte-Carlo simulation.

4. Organization of Thesis:

The main structure of this thesis is organized into seven chapters, which are summarized as follows:

- Chapter 1 provides a review of the fundamental concept of wireless communication, such as wireless communications channel models and wireless communications performance metrics. Then, we review the basic concept of the NOMA system. As well, cooperative communication is presented as one of the solutions for future communications to improve the performance and extend the coverage of wireless networks. Then, the EH or wireless energy transfer is presented as a solution to extend the battery lifetime and supply self-sustainable operation without replacing or recharging the devices' batteries of wireless communications systems and networks. Finally, we revise the UAV and RIS in wireless communications systems.

- Chapter 2 focuses on analyzing the performance of CNOMA-WDL. The EC, OP, and BER of the CNOMA-WDL over Rayleigh fading channel. This chapter also presents a comparison of CNOMA-WDL with traditional C-OMA-WDL.

- Chapter 3 investigates CNOMA with DL in the presence of ISIC and ICSI. The OP and BER of the CNOMA and DL over Rayleigh fading channel with the presence of ISIC and ICSI. This chapter presents a comparison of CNOMA and DL with traditional NOMA.
- Chapter 4 investigates the performance of multi-hop CNOMA with WDL and DL. This is performed by deriving the analytical expressions for the OP and BER over ISIC and ICSI. The system is compared with single relay schemes.
- Chapter 5 investigates two CNOMA with EH schemes. Firstly, we examine the BER of CNOMA with TS and PS protocols over the Rayleigh fading channel. Secondly, we propose the CNOMA with HEH protocol in terms of the OP and BER and compared with two EH protocols (TS and PS) over the Nakagami-m fading channel.
- Chapter 6 proposes uplink harvest-then-cooperate assisted NOMA for a wireless-powered cooperative communication network (HTC-NOMA-WPCCN) with linear/non-linear EH. In this chapter, we take into account the presence of IQI and SIC imperfections. This chapter also extends by considering the multi-helper-user scheme to improve the system's performance. We analyze the OP, EC, and throughput expressions with the practical imperfections.
- Chapter 7 investigates UAV-RIS NOMA with practical constraints such as HWI, ICI, and imperfect SIC. In this chapter, we analyze the BER of UAV-RIS NOMA. the chapter also provides a comparison with traditional OMA.
- Finally, we conclude our thesis by conclusion and summarizing the key findings and contributions of our research on CNOMA. Furthermore, we explore the significance of our research for the field of telecommunication networks and propose prospective directions for further investigation based on the outcomes of our study.

Chapter 1

Fundamental Concepts of Wireless Communications

1.1 Introduction

This chapter describes some fundamental concepts related to wireless communication networks and NOMA. Firstly, we revise the wireless communications channel models in section 1.2. Then, section 1.3, describes the ICSI. In section 1.4, we recall some key performance indicators for wireless communication networks. The fundamental concepts of NOMA power domain and CNOMA are presented respectively in section 1.5 and section 1.6. section 1.7 describes the EH for NOMA wireless communication networks. In sections 1.8 and 1.9, we will present UAV and RIS for NOMA networks. Finally, we conclude the chapter with a conclusion.

1.2 Wireless Communications Channel Models

In wireless communication radio, waves travel through space from the transmitter to the receiver. The waves during this period suffer from absorption, reflection, refraction, diffraction, and scattering. Thus, fading is a crucial component of the path between the transmitter and the receiver. Therefore, we present some different channel fading models below [15].

1.2.1 Rayleigh Fading Channel Model

When multipath propagation exists, a model called Rayleigh fading is used to describe the kind of fading that occurs. It is used to estimate the channel's performance when there are lots of scatterers in the path that affect the received signal and there is no line of sight (LoS) between the transmitter and the receiver [15, 16]. The cumulative distribution function (CDF) and probability density function (PDF) of the Rayleigh are defined respectively as in [17] by

$$F_X(x) = 1 - exp(-\frac{x}{\Omega}), \tag{1.1}$$

$$f_X(x) = \frac{1}{\Omega} exp(-\frac{x}{\Omega}), \tag{1.2}$$

where X is the random variable, $\Omega = E[|X|^2]$, $E[|.|^2]$ is the expectation operator and $|.|^2$ absolute value.

1.2.2 Nakagami-m Fading Channel Model

The Rayleigh distribution could not expect channel behavior over long distances and high frequencies. Therefore, the Nakagami-m fading model fits matches empirical data more than the Rayleigh fading model and can describe a variety of fading channel conditions, including Rayleigh fading when m=1 [15, 16]. The CDF and PDF of the Nakagami-m are defined respectively as in [17] by

$$F_X(x) = \frac{\nabla\left(m, \frac{m}{\Omega}x\right)}{\Gamma(m)} = 1 - e^{-\frac{m}{\Omega}x} \sum_{t=0}^{m-1} \frac{1}{t!}\left(\frac{m}{\Omega}x\right)^t, \tag{1.3}$$

$$f_X(x) = \left(\frac{m}{\Omega}\right)^m \frac{m^{m-1}}{\Gamma(m)} e^{-\frac{m}{\Omega}x}, \tag{1.4}$$

where $\nabla(.)$ is the lower incomplete Gamma function, $\Gamma(.)$ is the Gamma function, and m is the parameter of the Nakagami-m distribution.

1.3 Imperfect channel State Information

In practical communication scenarios, it is hard or impossible to consider perfect CSI due to the combined effect of path-loss, channel fading, and power attenuation. Therefore, it is important to consider the CSI condition is imperfect [18]. We define h as the channel coefficient between the base station (BS) and the receiver. We can write h as $h = \hat{h} + e$, where $\hat{h}$ is the factor of the channel estimation, which can be modeled as $\hat{h} \sim \mathcal{CN}(0, \sigma_h^2 - \sigma_e^2)$ and e is the factor of the channel estimation error.

1.4 Wireless Communications Performance Metrics

1.4.1 Ergodic Capacity

The capacity of Shannon is defined as the maximum rate that can be achieved between the transmitter and the receiver. The capacity of Shannon can be expressed as in [19, 20] by

$$C = B\ log_2(1 + \frac{P_t|h|^2}{\sigma^2}) = B\ log_2(1 + \gamma|h|^2), \tag{1.5}$$

where B is the bandwidth, h is the channel coefficient between the transmitter and the receiver, $\gamma = \frac{P_t}{\sigma^2}$ is the received signal-to-noise ratio (SNR), and σ^2 is the Additive white Gaussian noise (AWGN) variance.

The ergodic capacity (EC) is obtained by averaging C of (1.5) as

$$C = E_{|h|^2}[B\ log_2(1 + \gamma|h|^2)] = B \int_0^{\infty} f_{|h|^2}(u)\ log_2(1 + \gamma u), \tag{1.6}$$

where $f_{|h|^2}(u)$ is the PDF of $|h|^2$.

1.4.2 Outage Probability

The outage occurs when the signal cannot be reliably decoded at the receiver or when communication between the transmitter and receiver is missing. Theoretically, the outage occurs when the capacity of Shannon C is less than the transmission rate R ($C < R$) [19]. Thus, OP can be expressed as

$$P(out) = Pr(B\ log_2(1 + \gamma|h|^2) < R) = Pr(\gamma|h|^2 < \gamma_{th}), \tag{1.7}$$

where $\gamma_{th} = 2^{\frac{R}{B}} - 1$ is the threshold of receiver.

1.4.3 Bit Error Rate

The BER is defined as the probability of decoding a signal that has been received in favor of a different symbol from the one that was transmitted [16]. The BER can be defined as

$$P(e) = \int_0^{\infty} P_r(e/x) f_X(x) dx, \tag{1.8}$$

where $P_r(e/x)$ is the conditional error probability.

1.5 NOMA Power Domain

In NOMA, multiple users' signals can be combined and shared over the same time-frequency code resources. Different power levels are allocated for each user signal based on the channel conditions to enable knowing them at the receiver. The principle transmission of NOMA is based on the superposition coding (SC) and SIC at the transmitter and receiver [14, 21, 22, 23]. In this section, we describe the downlink and the uplink of the NOMA network.

1.5.1 Downlink NOMA

In the downlink NOMA, the users' signals are combined with different power allocation coefficients at the transmitter in an SC signal according to the channel gain for each user, as presented in Figure 1.1 (a) and (b).

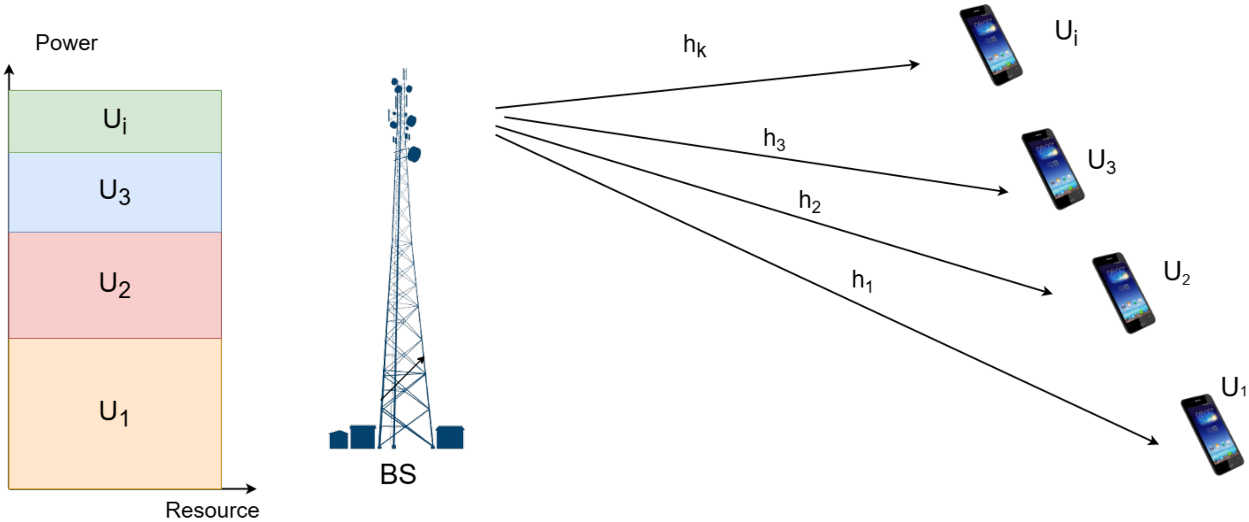

(a)

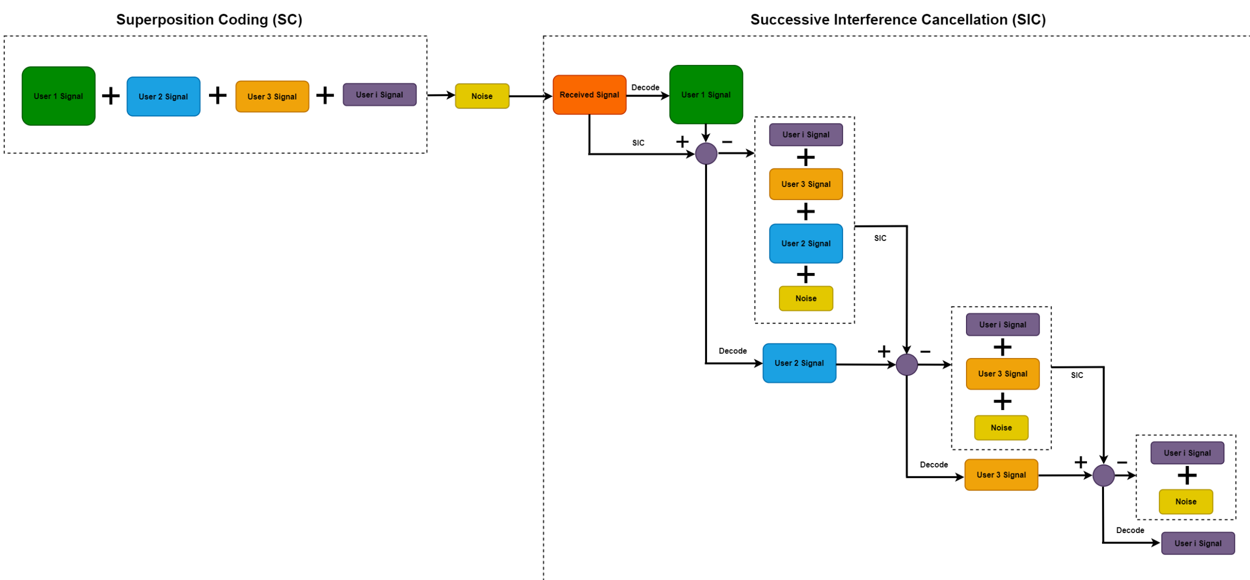

(b)

Figure 1.1: *(a) Downlink NOMA network, (b) The working principle of superposition coding and successive interference cancellation.*

A lower power allocation coefficient is given to the user of a higher channel gain, whereas a larger power allocation coefficient is given to the user of a worse channel gain ($|h_1|^2 < |h_2|^2 < |h_3|^2 < ... < |h_i|^2$). The SC transmitted signal at the BS can be given as

$$X_{SC} = \sum_{k=1}^{i} (\sqrt{\alpha_k} s_k), \tag{1.9}$$

where α_k is the power allocation coefficient for U_i, where $\alpha_1 > \alpha_2 > \alpha_3 > ... > \alpha_i$, in which $\sum_{k=1}^{i} \alpha_k = 1$ and s_k is signals of U_i.

To decode the signals of the users, the SIC process is used by the receivers, as presented in Figure 1.1 (b). The decoding begins with the user of the highest power, then the user of the lowest power, and so forth. The far user decodes its signal without SIC directly by treating the other signals as noise, while at the near user, the far user signal is decoded firstly by treating the near user signal as noise. Then, using the SIC process, the near user decodes its signal. By following the same method, other users can decode their signals. The received signal at users is given by

$$y_k = \sqrt{P_t} X_{SC}\ h_k + n, \qquad k = 1, 2, 3, ..., i, \tag{1.10}$$

where P_t is the total transmitted power, h_k is the channel coefficient of U_i, and n is the AWGN as follows $n \sim \mathcal{CN}(0, \sigma^2)$.

1.5.2 Uplink NOMA

In contrast to downlink NOMA, the uplink NOMA operates very differently. Several transmitters transmit their signals to BS at the same time and frequency blocks, where the near transmitter signal has higher power than the far transmitter signal and so on ($\alpha_1 < \alpha_2 < \alpha_3 < ... < \alpha_i$), as presented in Figure 1.2 [21]. The received signal at the BS can be given as

$$r = \sqrt{P_t}\ \sum_{k=1}^{i} (h_k\ \sqrt{\alpha_k} s_k) + n, \qquad k = 1, 2, 3, ..., i. \tag{1.11}$$

The received signal at the BS is a combination of all transmitted signals with different power levels. We can decode them using the SIC process, where the closest transmitter's signal is first decoded, followed by the next-closest transmitter's signal, and so on. In other words, the signal with the highest energy is decoded first, then the signal with the lowest energy, and so on.

1.6 Cooperative NOMA

A CNOMA system is one of the techniques employed to increase system performance, combat channel disorders, and expand cell coverage. Two famous schemes for CNOMA are as follows. The first one is CNOMA with DL, which is used to improve the system's performance. The second one

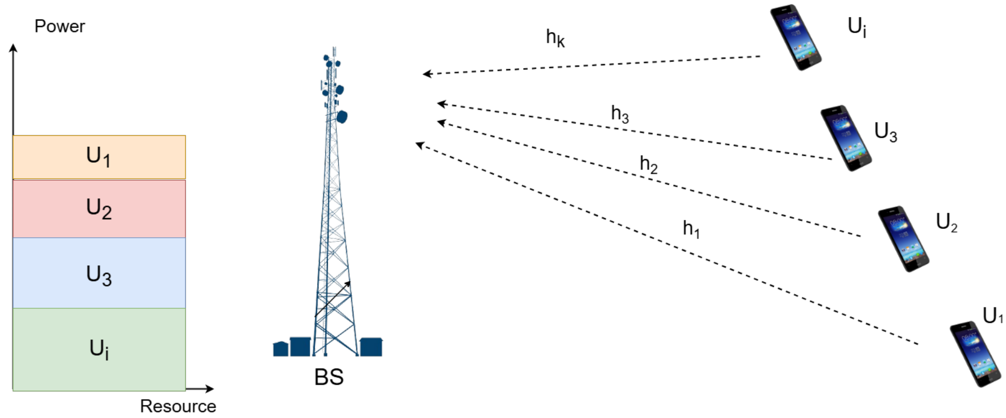

Figure 1.2: *Uplink NOMA network.*

is CNOMA WDL, which is used to help faraway users or users who cannot receive the BS signal due to poor channels [24]. Multiple relay techniques are employed for CNOMA, such as DF and AF. In the DF, the received signal at the relay is decoded, re-encoded, and forwarded to the receivers. In AF, the received signal at the relay is amplified without decoding and forwarded to the receivers [19]. In this section, we concentrate on the CNOMA WDL. Thus, we introduce the downlink and uplink for CNOMA networks.

1.6.1 Downlink Cooperative NOMA

In CNOMA, transmission consists of two phases, as presented in Figure 1.3. In phase 1: Based on the NOMA system, the SC signal is transmitted from the BS to the relay node. The received signal at the relay node is given by

$$y_r = \sqrt{P_t} X_{SC}\ h_r + n, \qquad k = 1, 2, 3, ..., i, \tag{1.12}$$

where h_r is the channel coefficient of the relay node.

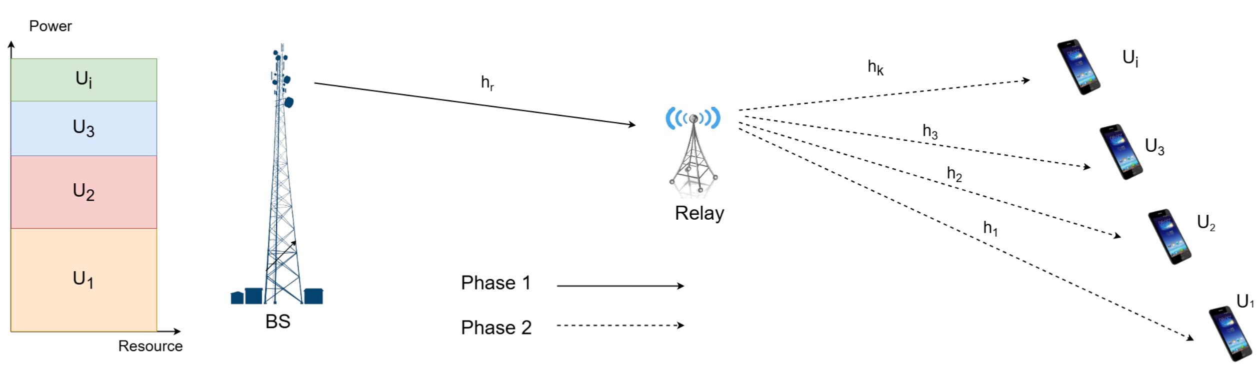

Figure 1.3: *Downlink CNOMA network.*

The relay node decodes all users' signals from the SC received signal using the SIC process, as we described in section 1.4. In phase 2: The relay node re-encodes and combines all the users' signals in the new SC signal as in the BS, then forwards it by its power to the users. Thus, the received signal by the users is given by

$$y_k = \sqrt{P_r} X_{SC}\ h_k + n, \qquad k = 1, 2, 3, ..., i, \tag{1.13}$$

where P_r is the relay power.

1.6.2 Uplink Cooperative NOMA

In uplink CNOMA, the transmission consists of two phases, as shown in Figure 1.4. In phase: Multiple users transmit their signals simultaneously to the relay node, in which each user transmits its signal with the following power levels ($\alpha_1 < \alpha_2 < \alpha_3 < ... < \alpha_i$). The received signal at the relay node will be as (1.11) and is given as

$$y_r = \sqrt{P_t}\ \sum_{k=1}^{i} (h_k\ \sqrt{\alpha_k} s_k) + n, \qquad k = 1, 2, 3, ..., i. \tag{1.14}$$

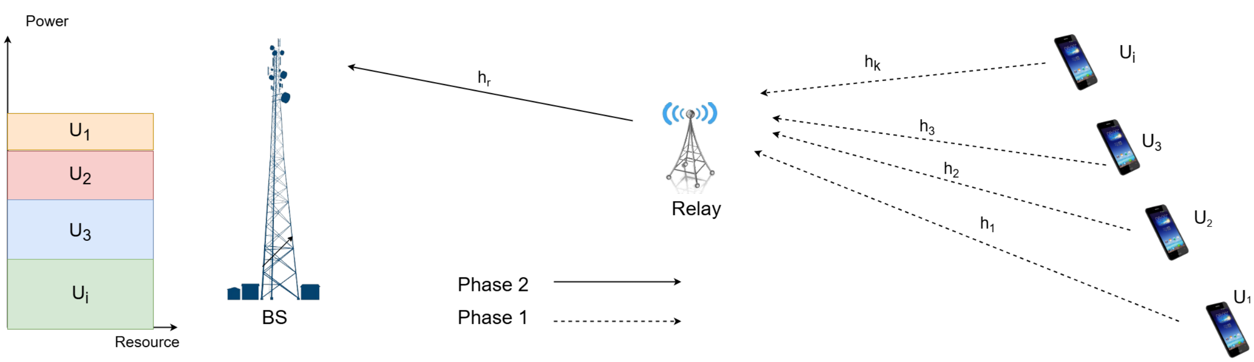

Figure 1.4: *Uplink CNOMA network.*

The relay decodes the SC received signal using the SIC process. The signal with the highest power level is decoded first, then the signal with the lowest power level, and so on. In phase 2: The relay re-encodes the decoded signals and combines them into a new SC signal, then forwards it to the BS by its power. Hence, the received signal at the BS is given by

$$y_{BS} = \sqrt{P_r}\ h_r\ \sum_{k=1}^{i} (\sqrt{\alpha_k} s_k) + n, \qquad k = 1, 2, 3, ..., i. \tag{1.15}$$

In the same way at the relay node, the SIC process is used at the BS to decode the signals. The signal with greater power is decoded first, then the signal with lower power, and so on.

1.7 Energy Harvesting

As it's known, energy is the primary source for operating all devices and systems. Therefore, with the significant increase in the number of devices and the world's orientation towards the IoT and others, devices may suffer from the problem of charging or damaging the batteries. For this purpose, many researchers have proposed EH or wireless energy transfer as a promising solution for wireless communication networks [25, 26].

In future wireless communications, EH from radio frequency (RF) sources is a significant part of green communication that supplies self-sustainable operation without replacing or recharging the devices' batteries of wireless communications systems and networks [26, 27]. In EH, one part is devoted to energy transmission; and the other part is devoted to transferring signals or decoding information, as presented in Figure 1.5. There are two main EH protocols, named as follows: PS and TS. We describe the details of the two EH protocols below.

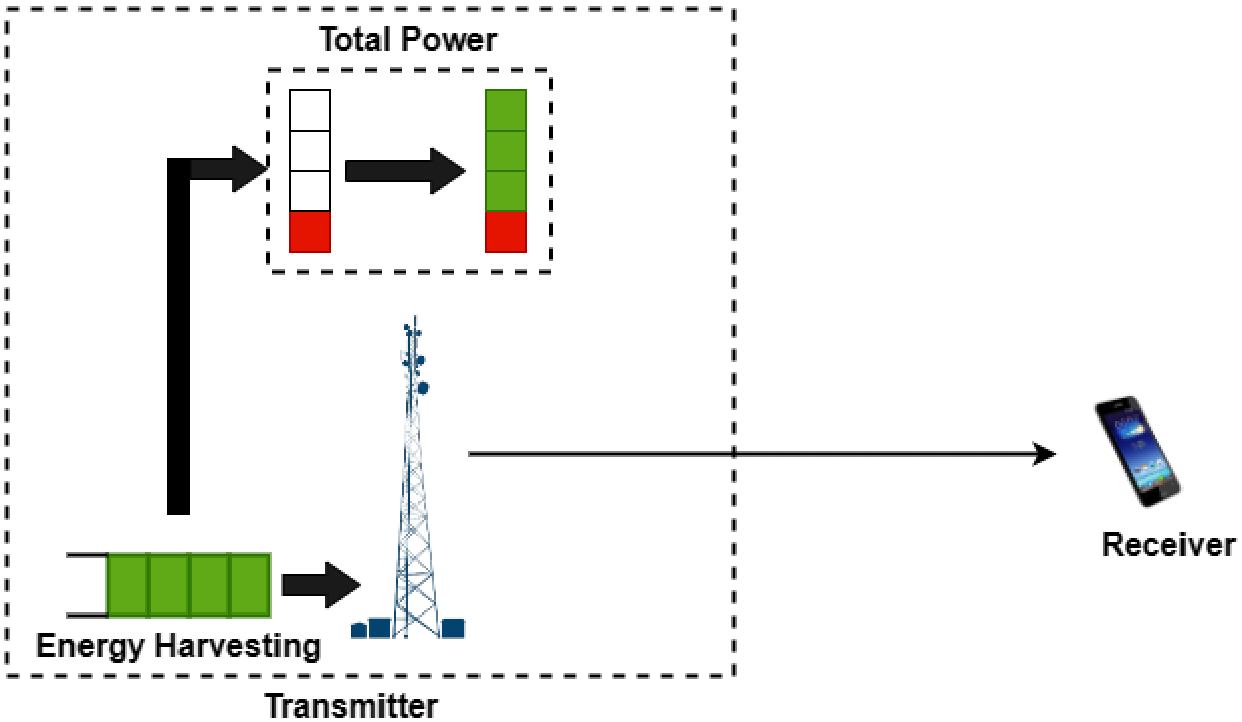

Figure 1.5: *The transmission with EH technology.*

1.7.1 Power Splitting

In the PS protocol, the received signal is split into two parts: one part for EH and the other part for data decoding, as presented in Figure 1.6. Thus, EH and information decoding are simultaneous in the PS protocol [27, 28, 29]. The received signal for EH and data decoding can be written, respectively by

$$y = \sqrt{P_t \rho}\, h \sum_{k=1}^{i} (\sqrt{\alpha_k} s_k) + \sqrt{\rho}\, n, \qquad k = 1, 2, 3, ..., i, \tag{1.16}$$

$$y = \sqrt{P_t(1-\rho)}\; h \sum_{k=1}^{i}(\sqrt{\alpha_k} s_k) + \sqrt{(1-\rho)}\; n, \qquad k = 1, 2, 3, ..., i, \tag{1.17}$$

where ρ is the PS factor, in which $0 < \rho < 1$.

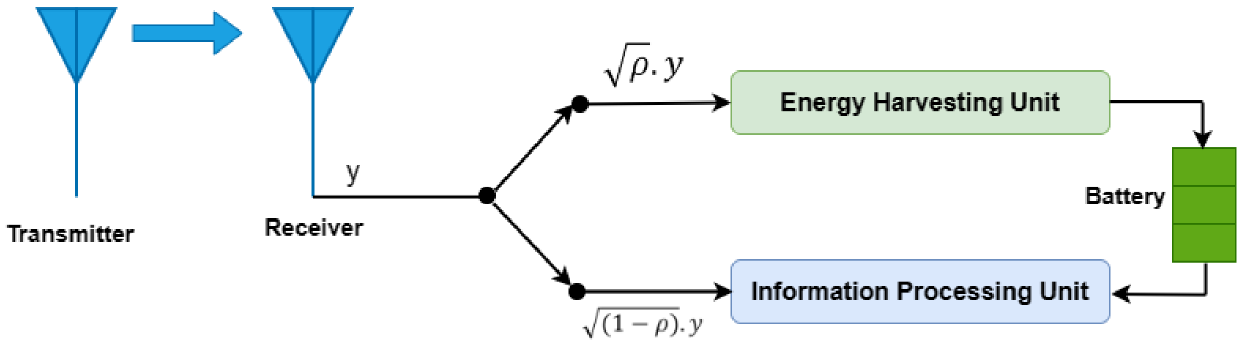

Figure 1.6: *Power splitting protocol.*

The energy harvested from the received signal power is given by

$$E_{PS} = \eta\rho P_t |h|^2 \frac{T}{2}. \tag{1.18}$$

The transmission power of the transmitter through the harvested energy is given by

$$P_{PS} = \frac{2E_{PS}}{T} = \eta\rho P_t |h|^2, \tag{1.19}$$

where T is the total communication period, η is the factor of the energy conversion efficiency, in which $0 < \eta < 1$.

1.7.2 Time Switching

In TS protocol, one part of the transmitting time is devoted to connecting the received signal to an energy harvester for power transfer. The other part of the transmitting time is devoted to switching the received signal to a data decoder for signal delivery, as presented in Figure 1.7. Unlike PS, EH and information decoding are not simultaneous in the TS protocol [27, 28, 29]. The received signal for the data decoding can be written by

$$y = \sqrt{P_t}\; h \sum_{k=1}^{i}(\sqrt{\alpha_k} s_k) + \; n, \qquad k = 1, 2, 3, ..., i, \tag{1.20}$$

The energy harvested from the received signal power is given by

$$E_{TS} = \eta\nu P_t |h|^2 T. \tag{1.21}$$

The transmission power of the transmitter through the harvested energy is given by

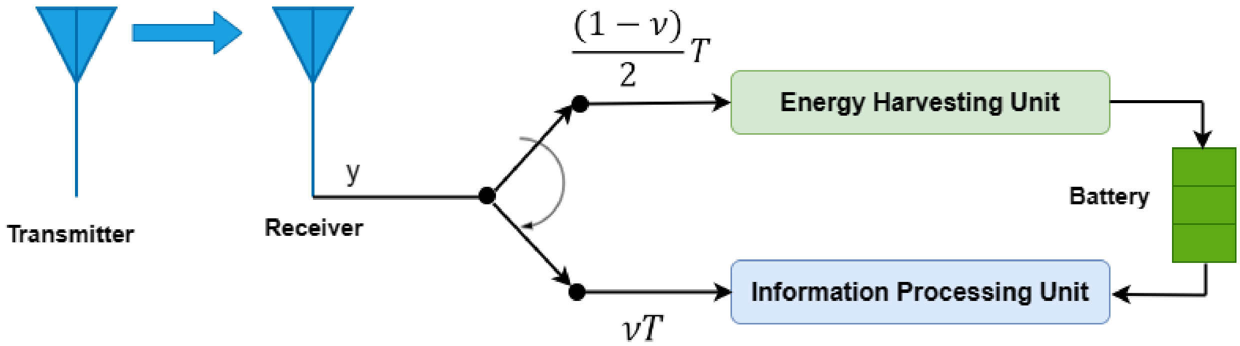

Figure 1.7: *Time switching protocol.*

$$P_{TS} = \frac{E_{TS}}{\frac{(1-\nu)T}{2}} = \frac{2\eta\nu P_t|h|^2}{(1-\nu)}, \tag{1.22}$$

where ν is the TS factor, in which $0 < \nu < 1$.

1.7.3 Non-Linear Energy Harvesting

In this subsection, we explore the intricacies of the non-linear EH model, which takes into account the subtleties of saturation and sensitivity in the EH circuit. In this subsection, we consider the TS as an example. If TS is used, the EH from the received signal power is provided by

$$E_{NL} = \begin{cases} \eta\nu P_t|h_h|^2 T, & P_t|h|^2 \leq P_{th}, \\ \eta\nu P_{th} T, & P_t|h|^2 > P_{th}, \end{cases} \tag{1.23}$$

where P_{th} is the saturation threshold.

However, in the non-linear EH model, the transmit power is given as

$$P_{EH,NL} = \frac{E_{NL}}{(1-\tau)^{T}/2} = \begin{cases} \frac{2\eta\tau P_t|h|^2}{(1-\tau)}, & P_t|h|^2 \leq P_{th}, \\ \frac{2\eta\tau P_{th}}{(1-\tau)}, & P_t|h|^2 > P_{th}. \end{cases} \tag{1.24}$$

The harvested energy is shown in Figure 1.8 for a range of input power values, comparing the results of two EH models: the non-linear EH and linear EH models. In particular, the harvesting energy exhibits an upward trend as the input energy increases in the non-linear EH model until it reaches a saturation point at the value P_{th}. When the harvester's output energy crosses this threshold, it stabilizes and stays at that level.

1.8 Uncrewed Aerial Vehicle

The vehicle and drone-based communications systems field of research is known as UAV communications systems. UAV can fly at a few hundred meters and can be remotely operated through

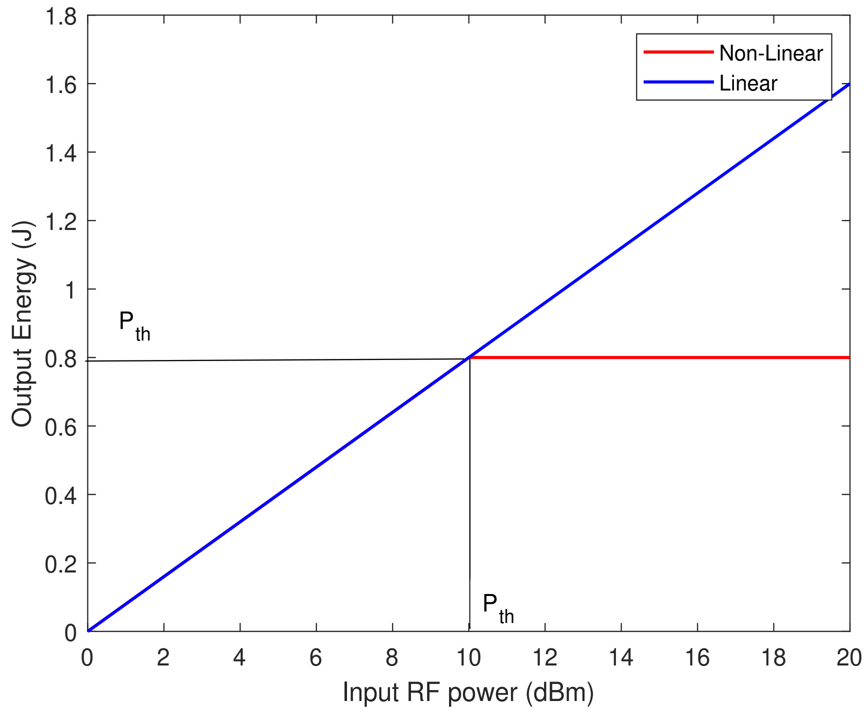

Figure 1.8: *A comparison between the linear EH model and the non-linear EH model.*

different electronic gadgets. Recently, UAV have been considered one of the most significant technologies for future wireless communications networks. Therefore, there is currently a lot of interest in integrating UAV into wireless networks such as satellites to enable more accurate data processing and support continuous information broadcasting [30, 31].

Integrating NOMA with UAV communication networks presents an exciting opportunity to enhance the QoS in congested areas and expand the coverage of existing networks in challenging environments (as shown in Figure 1.9). UAV communication networks are increasingly recognized for their cost-effectiveness, leveraging line-of-sight (LoS) air-to-ground channels and adaptable deployment strategies. By employing NOMA within these networks, we can further optimize spectrum utilization, increase throughput, and improve fairness among users, thereby maximizing the overall efficiency and performance of UAV communication systems [32].

In the downlink scenario, we take into account three-dimensional Cartesian coordinates (x, y, z) for positioning UAV relay and NOMA users as presented in Figure 1.9. We begin by identifying the location of the BS and U_i as follows. The position coordinates of the BS is $\mathsf{S}(-x_{BS}, 0, 0)$, whereas the position coordinates of ground users U_i is indicated as $\mathsf{U_i}(x_k, y_k, z_k)$. The central position of the UAV's circular trajectory, characterized by a radius r and altitude T_h, can be pin-

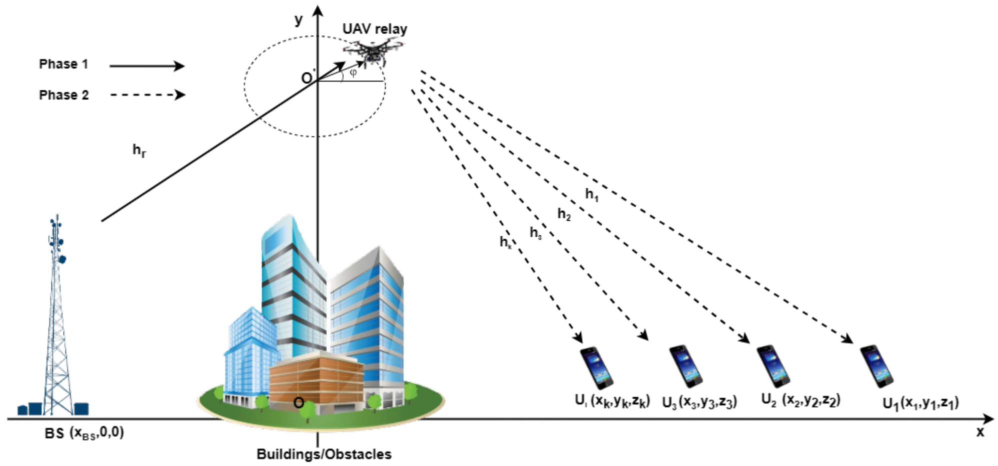

Figure 1.9: *UAV with NOMA network.*

pointed to the coordinates $O'(0, T_h, 0)$. Supposing that φ is the angle between the position of the UAV on the circle and the x-axis, we can easily indicate the position coordinates of the relay UAV as $\mathsf{UAV}(r.\cos(\varphi), r.\sin(\varphi), T_h)$. Based on this analysis, we calculate the Euclidean distance between BS-UAV and UAV-U$_i$, respectively, as $d_i = \sqrt{(r\cos(\varphi) - x_i)^2 + (r\sin(\varphi) - z_i)^2 + T^2}$ and $d_r = \sqrt{(r\cos(\varphi) - x_r)^2 + (r\sin(\varphi) - z_r)^2 + T^2}$.

In CNOMA, transmission consists of two phases, as presented in Figure 1.9. In phase 1: Based on the NOMA system, the SC signal is transmitted from the BS to the UAV relay node. The received signal at the UAV relay node is given by

$$y_r = \sqrt{P_t} X_{SC} \sqrt{d_r^{\varsigma}}\, h_r + n. \tag{1.25}$$

The UAV relay node decodes all users' signals from the SC received signal using the SIC process, as we described in section 1.4. In phase 2: The UAV relay node re-encodes and combines all the users' signals in the new SC signal as in the BS, then forwards it by its power to the users. Thus, the received signal by the users is given by

$$y_k = \sqrt{P_r} X_{SC} \sqrt{d_k^{\varsigma}}\, h_k + n, \qquad k = 1, 2, 3, ..., i. \tag{1.26}$$

1.9 Reconfigurable Intelligent Surfaces

RIS has received growing attention as a potential next-generation technology due to its promising capabilities to control the wireless propagation environment. The structure of RIS is made of a thin and flexible metasurface material that contains passive circuitry. It can intelligently control the propagation of the incident electromagnetic waves and reflect or refract these waves in a desired way, thereby turning the wireless channel into a controllable environment, and enhancing the overall system performance.

As shown in Figure 1.10, RIS can be categorized into three types: reflective, transmissive, and hybrid [33, 34]. We describe each type respectively as follows:

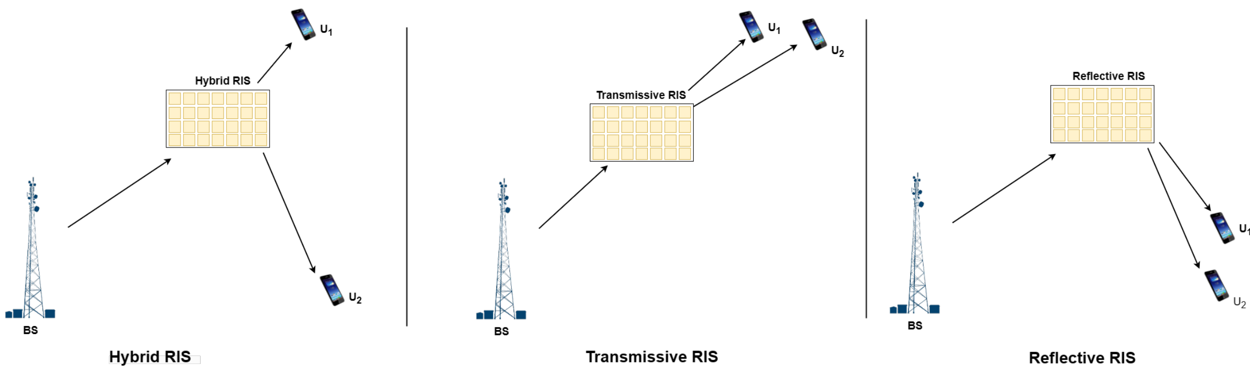

Figure 1.10: *Types of RIS.*

- **Reflective:** This type only reflects incident signals toward the users on the same side of the source. Generally, we can define the response of a reflective RIS element by having the information of ($\flat$, ϕ_z). Hence, the response of a reflective RIS element can be written by

$$\eta = \flat \exp(-j\phi_z), \tag{1.27}$$

where j is the imaginary unit, i.e., $|j|^2 = 1$ and $\flat \in [0, 1]$ is the amplitude of the RIS response. When $\flat = 1$ indicates that the incident signals are fully reflected, while $\flat = 0$ implies that the incident signals are fully absorbed. ϕ_r is the phase shift of the RIS response.

- **Transmissive:** In this type, the incident signals will pass through the RIS and be sent to the users on the opposite side of the source. The response of a transmissive RIS element is similar to (1.27). In this type, the incident signals fully penetrate the RIS element in case of $\flat = 1$.

- **Hybrid:** This kind of RIS offers dual operations of reflection and transmission. This means that the incident signals will be divided into two pieces, one of which will be sent and the other reflected. Generally, we can define the response of a hybrid RIS element by having the information of (β_z, ϕ_r, ϕ_t). Hence, the response of the RIS element to reflected and transmitted signals can be expressed by

$$\eta_r = \sqrt{\frac{\beta_z}{1+\beta_z}} \exp(-j\phi_r), \tag{1.28}$$

$$\eta_t = \sqrt{\frac{\beta_z}{1+\beta_z}} \exp(-j\phi_t), \tag{1.29}$$

where $\beta_z \in [0, \infty)$ is the power ratio of reflected signals to transmitted signals, ϕ_r is the phase shift between the incident and reflected signals, and ϕ_t is the phase shift between the incident and transmitted signals.

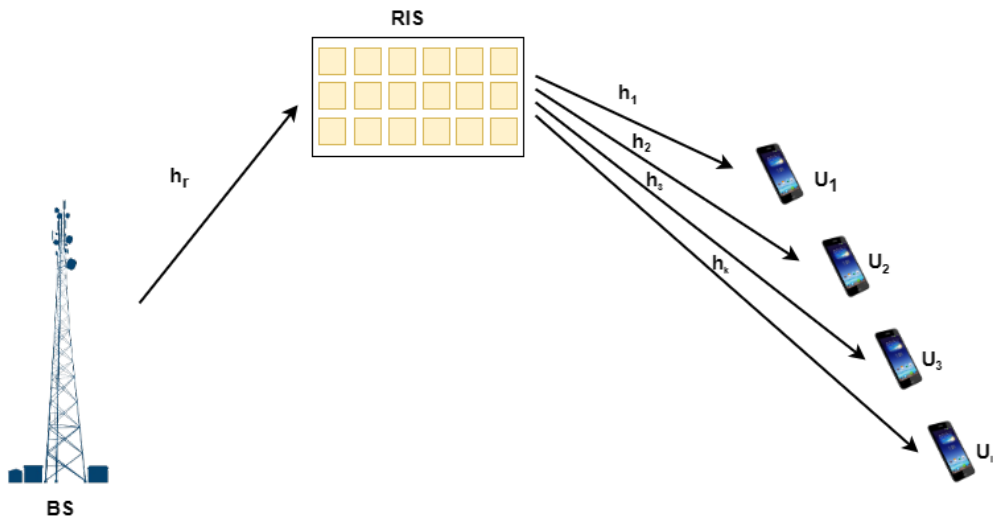

Figure 1.11: *RIS with NOMA network.*

As shown in Figure 1.11, the BS transmits an SC signal to NOMA users through RIS (reflective RIS). The received signal at NOMA users with N number RIS elements is given by

$$y_k = \sqrt{P_t} X_{SC} \sum_{n=1}^{N} h_{r,n} \exp{(j\phi_{k,n})} h_{k,n} + n, \qquad k = 1, 2, 3, ..., i, \tag{1.30}$$

where $\phi_{i,n}$ represents the adjustable phase induced by the n^{th} reflector of the RIS, $h_{r,n}$ and $h_{k,n}$ are channels between BS-RIS, and RIS-U$_i$.

1.10 Conclusion

In this chapter, the fundamental concepts of wireless communication networks and NOMA are defined. Moreover, to increase the system performance and extend the coverage of NOMA, we described the basic concept of cooperative communication with NOMA. Furthermore, we have seen that EH technology is a great solution when the device's batteries are damaged or there is a problem with charging. EH from the ambient wireless sources is a promising solution for future NOMA networks. Finally, the benefits of using UAV and RIS in NOMA presented including improved coverage, spectral efficiency, and overall system performance.

Based on previous literature and our study, the following chapters will investigate the CNOMA system to extend the coverage and improve the system's performance. Furthermore, we will evaluate the EH for CNOMA networks.

Chapter 2

Cooperative NOMA Without Direct Link

2.1 Introduction

In the foreseen future beyond 6G networks, ambitious high data rate applications need new solutions [35]. NOMA is an essential enabling technology to meet the heterogeneous demands of low latency, massive connectivity, high reliability, high throughput, and improved fairness [36]. Moreover, cooperative communications can improve the system performance in cellular networks through higher data rates, more reliable transmission links, and satisfactory quality of service [37].

2.1.1 Related Works

NOMA is superior to OMA in terms of OP and ergodic sum rate [9]. In terms of ergodic sum rate and OP, CNOMA is superior to OMA [10]. On the other hand, under the SIC, the authors of [11] derived the closed-form BER in downlink and uplink NOMA for binary phase shift keying and quadrature phase shift keying (BPSK-QPSK) modulation schemes. Similarly, in [38], the BER of NOMA in the downlink with different modulation schemes BPSK-BPSK, QPSK-BPSK, and QPSK-QPSK have been derived. The closed-form BER of NOMA with VLC system for different modulations has been obtained [39]. The authors of [40] evaluated the BER for QPSK-BPSK modulation for DF relay-assisted NOMA. In [41], the error probability has been determined for cooperative DF relay NOMA via Nakagami-m fading channels. The ergodic rate and symbol error rate (SER) of CNOMA by using QPSK-BPSK have been derived [42]. The BER and diversity for cooperative relay-assisted NOMA have been evaluated by performing joint maximum likelihood (JML) decoding at the destination [43]. The authors of [38] have derived the BER and EC of mobile ad-hoc networking in NOMA. In the downlink and uplink, the BER of CNOMA with FD user relaying has been obtained [44] when there is no direct connection with users. The EC, OP, and error probability have been derived for the reversed DF relaying NOMA with ISIC and CSI to improve user fairness compared to conventional DF with NOMA [45].

2.1.2 Motivation and Contributions

Based on the above research, most of the works focused on deriving the BER by assuming different modulations for encoding the users' messages (i.e., BPSK-QPSK) in DF with CNOMA (DF-CNOMA). The BPSK modulation to encode two users' messages in DF-CNOMA has not been analyzed to the best of the author's knowledge. In this chapter, using the BPSK modulation to encode the users' messages, we analyze the BER of the CNOMA without direct links (CNOMA WDL). We assume the near user helps the far user to receive its signal using DF mode when there is no connection between the BS and the far user. The main contributions of this chapter are as follows:

- We derive the closed-form BER of the near user. Then, we express the end-to-end (e2e) BER of the far user.
- We compare our results with traditional cooperative OMA with WDL (COMA WDL).
- We also evaluate the EC and OP of CNOMA WDL.
- We discuss the optimum power allocation value and the optimal situation for the helper user.

2.2 System Model

Consider a CNOMA WDL system that has one BS and two users, named U_1 and U_2. The last one (U_2) is near the BS, whereas the first one (U_1) is far away and cannot receive the BS signal, as shown in Figure 2.1. It is supposed that U_2 is an assistant user to U_1 to receive its signal, and it works in half-duplex (HD) mode and DF protocol. It is assumed that all nodes are over the Rayleigh fading channel. The users' signals are combined in an SC signal with different power levels according to channel gain of the users, which is transmitted from the BS to U_2 in the first phase. The received signal at the U_2 is given by

$$y_{BS2} = \sqrt{P_t}\; h_2\; (\sqrt{\alpha_1} s_1 + \sqrt{\alpha_2} s_2) + \; n, \tag{2.1}$$

where $h_2 \sim \mathcal{CN}(0, \sigma_{h_2}^2 = d_2^{\varsigma})$ is the channel coefficient of U_2, d_2 is the distance between BS-U_2, and ς is the path-loss factor, and α_1 and α_2 are the power allocation for users and it is distributed according to the downlink NOMA as presented in chapter 1, Subsection 1.5.1, in which $\alpha_1 > \alpha_2$, $\alpha_1 + \alpha_2 = 1$

Using the SIC, U_2 decodes the U_1 signal first and then subtracts it from the total received signal to decode its signal. Thereafter, U_2 re-encodes s_1 and forwards it to U_1 in the second phase. The received signal at U_1 is given by

$$y_{21} = \sqrt{P_r}\ h_1\ s_1 +\ n, \tag{2.2}$$

where $h_1 \sim \mathcal{CN}(0, \sigma_{h_1}^2 = d_1^{\varsigma})$ is the channel coefficient of U_1 and d_1 is the distance between U_2-U_1.

The U_1 uses maximum likelihood detection (MLD) to detect its signal s_1. The signal-to-interference-plus-noise ratio (SINR) of the s_1 at U_2 can be expressed as

$$\gamma_{BS2,s_1} = \frac{P_t\alpha_1|h_2|^2}{P_t\alpha_2|h_2|^2 + \sigma^2}, \tag{2.3}$$

while the SINR of s_2 at U_2 can be expressed as

$$\gamma_{BS2,s_2} = \frac{P_t\alpha_2|h_2|^2}{\sigma^2}, \tag{2.4}$$

and the SINR of s_1 at U_1 in the second phase can be expressed as

$$\gamma_{12,s_1} = \frac{P_r|h_1|^2}{\sigma^2}. \tag{2.5}$$

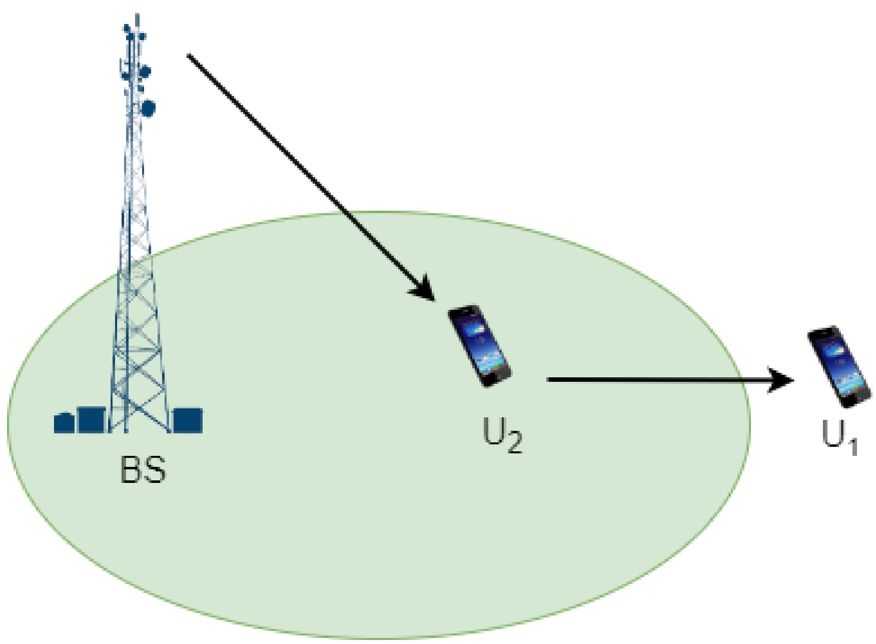

Figure 2.1: *CNOMA WDL scheme.*

2.3 Performance Analysis

In this section, we analyze the EC, OP, and BER for CNOMA WDL over the Rayleigh fading channel.

2.3.1 Ergodic Capacity

In this subsection, we derive the EC expressions for U_1 and U_2. The capacity of Shannon of the s_1 signal should be considered based on both BS-U_2 and U_2-U_1 links. Hence, the capacity of Shannon of the U_1 is given by

$$C_{BS21,s_1} = \frac{1}{2}\log_2(1 + min(\gamma_{BS2,s_1}, \gamma_{21,s_1})). \tag{2.6}$$

By averaging (2.6), we calculate the EC of U_1 as

$$C_{BS21,s_1} = \frac{1}{2}\iint^{\infty} \log_2(1 + min(\gamma_{BS2,s_1}, \gamma_{21,s_1}))f_{|h_2|^2}(|h_2|^2)f_{|h_1|^2}(|h_1|^2)\ d|h_2|^2\ d|h_1|^2, \tag{2.7}$$

where $f_{|h_2|^2}(|h_2|^2)$ and $f_{|h_1|^2}(|h_1|^2)$ are the PDFs of $|h_2|^2$ and $|h_1|^2$, respectively. Let represent W=min(A+B), the CDF of W is expressed by $F_W(x) = 1 - (1 - F_A(x))(1 - F_B(x))$, where $F_A(x)$ and $F_B(x)$ are the CDF of A and B, respectively [45, 46]. Recalling, $\int^{\infty} \log_2(1 + x)f_X(x) = \frac{1}{\ln 2}\int^{\infty} \frac{1-F_X(x)}{1+x}dx$ [47]. Hence, after some algebraic manipulations, we derive the EC of the U_1 as given by

$$C_{BS21,s_1} = \frac{1}{2\ln 2}\int^{\infty} \frac{exp\left(-\frac{\sigma^2 x}{(\alpha_1-\alpha_2 x)P_t E[|h_2|^2]}\right) exp\left(-\frac{\sigma^2 x}{P_r E[|h_1|^2]}\right)}{1 - x}\ dx. \tag{2.8}$$

There is no derivation analytical solution to (2.8) according to the author's knowledge. However, it can be simple to calculate using software like MATLAB.

The capacity of Shannon of the U_2 is given by

$$C_{BS2,s_2} = \frac{1}{2}\log_2(1 + \gamma_{BS2,s_2}). \tag{2.9}$$

Thus, the average of (2.9) is given by

$$C_{BS2,s_2} = \frac{1}{2}\int^{\infty} \log_2(1 + \gamma_{BS2,s_2})f_{|h_2|^2}(|h_2|^2)\ d|h_2|^2. \tag{2.10}$$

By using [47, Eq(3.352.2)], we obtain the EC of U_2 as

$$\begin{aligned} C_{BS2,s_2} &= \frac{1}{2\ln 2}\int^{\infty} \frac{exp\left(-\frac{\sigma^2 x}{\alpha_2 P_t E[|h_2|^2]}\right)}{1 + x}\ dx \\ &= -\frac{1}{2\ln 2}exp\left(-\frac{\sigma^2}{\alpha_2 P_t E[|h_2|^2]}\right) Ei\left(\frac{\sigma^2}{\alpha_2 P_t E[|h_2|^2]}(1 + x)\right). \end{aligned} \tag{2.11}$$

2.3.2 Outage Probability

The OP of U_1 occurs if the received SINR of s_1 in phase one and phase two are less than the threshold θ_1. The OP of U_1 is given by

$$P_{BS21,s_1}(out) = P(min(\gamma_{BS2,s_1}, \gamma_{21,s_1}) < \theta_1). \tag{2.12}$$

By using the PDF and CDF as in (1.1) and (1.2), we find the OP of (2.12) as

$$P_{BS21,s_1}(out) = 1 - exp\left(-\frac{\sigma^2\theta_1}{(\alpha_1 - \alpha_2\theta_1)P_tE[|h_2|^2]}\right) exp\left(-\frac{\sigma^2\theta_1}{P_rE[|h_1|^2]}\right), \tag{2.13}$$

where E[.] is the expectation operator, $\theta_1 = 2^{Tr_1} - 1$ is the threshold rate of s_1, and Tr_1 is the target rate of s_1.

The OP of s_2 at U_2 occurs for the following reasons: If the received SINR of s_1 is less than the threshold θ_1. If the received SINR of s_1 is higher or equal to the threshold θ_1 and the received SINR of s_2 is less than the threshold θ_2. The OP of s_2 at U_2 is given by

$$P_{BS2,s_2}(out) = P\left(\gamma_{BS2,s_1} < \theta_1\right) + [1 - P\left(\gamma_{BS2,s_1} < \theta_1\right)]P\left(\gamma_{BS2,s_2} < \theta_2\right). \tag{2.14}$$

After simplification, we can write (2.14) as

$$P_{BS2,s_2}(out) = 1 - P\left(\gamma_{BS2,s_1} < \theta_1\right) P\left(\gamma_{BS2,s_2} < \theta_2\right). \tag{2.15}$$

By using the PDF and CDF as in (1.1) and (1.2), the OP of (2.15) is given by

$$P_{BS2,s_2}(out) = 1 - exp\left(-\frac{\sigma^2\theta_1}{(\alpha_1 - \alpha_2\theta_1)P_tE[|h_2|^2]}\right) exp\left(-\frac{\sigma^2\theta_2}{\alpha_2P_tE[|h_2|^2]}\right), \tag{2.16}$$

where $\theta_2 = 2^{Tr_2} - 1$ is the threshold rate of s_2 and Tr_2 is the target rate of s_2.

To acquire insight into our system, the asymptotic OP of users is given in high SNR regimes as in [48] by

$$P^{\infty}_{BS21,s_1}(out) \approx 1 - \left(1 - \frac{\sigma^2\theta_1}{(\alpha_1 - \alpha_2\theta_1)P_tE[|h_2|^2]}\right)\left(1 - \frac{\sigma^2\theta_1}{P_rE[|h_1|^2]}\right), \tag{2.17}$$

$$P^{\infty}_{BS2,s_2}(out) \approx 1 - \left(1 - \frac{\sigma^2\theta_1}{(\alpha_1 - \alpha_2\theta_1)P_tE[|h_2|^2]}\right)\left(1 - \frac{\sigma^2\theta_2}{\alpha_2P_tE[|h_2|^2]}\right). \tag{2.18}$$

2.3.3 Bit Error Rate

In this subsection, we derive the closed-form BER for s_1 and s_2 at U_2. Then, we derive the closed-form BER of s_1 at phase two. Finally, we express the e2e BER for U_1. The e2e BER expression for U_1 is given by [13]

$$P_{e2e,WDL}(e) = 1 - (1 - P_{BS2,s_1}(e))(1 - P_{21,s_1}(e)), \tag{2.19}$$

where $P_{BS2,s_1}(e)$ is the BER of s_1 in the first phase and $P_{21,s_1}(e)$ is the BER of s_1 in the second phase.

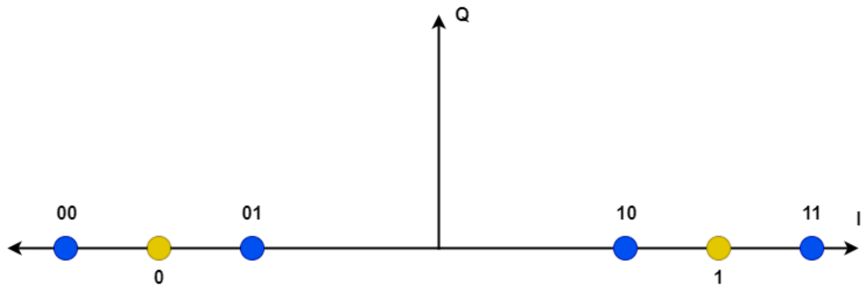

Figure 2.2: *Constellation diagram of the received signal.*

We consider that the BPSK modulation is utilized to encode the users' symbols. As shown in Figure 2.2, we represent the constellation points of the SC signal by (a_1, a_2), in which the (a_1) symbol illustrates s_1, and the (a_2) symbol illustrates s_2. The decision boundary is established by the in-phase component of the received signal, either higher or less than zero.

The U_2 detects s_1 using MLD. Hence, the BER of the s_1 symbols at U_2 is expressed by [13]

$$P_{BS2,s_1}(e) = \frac{1}{2}\sum_{j=1}^{2} Q\left(\sqrt{P_t \gamma \chi_j |h_2|^2}\right), \tag{2.20}$$

where $\chi_j = [(\sqrt{\alpha_1} + \sqrt{\alpha_2})^2, (\sqrt{\alpha_1} - \sqrt{\alpha_2})^2]$.

With helping an alternative form of the Q(.) function and the moment generating function (MGF), and after some algebraic manipulation, (2.20) can be written by

$$P_{BS2,s_1}(e) = \frac{1}{4}\sum_{j=1}^{2} \left(\sqrt{\frac{P_t \gamma \chi_j E[|h_2|^2]}{2 + P_t \gamma \chi_j E[|h_2|^2]}}\right). \tag{2.21}$$

Proof: Please, see Appendix A.

Also, the U_2 implements the SIC to detect its symbols. The detection of s_2 at U_2 is based on the detection of s_1 symbols correct or not. Thus, the BER of s_2 at U2 is expressed by

$$P_{BS2,s_2}(e) = \frac{1}{2}\sum_{v=1}^{6} \kappa_v Q\left(\sqrt{P_t \gamma \aleph_v |h_2|^2}\right), \tag{2.22}$$

where $\kappa_v = [1, 1, -1, 1, 1, -1]$ and $\aleph_v = [\alpha_2, \alpha_2, (\sqrt{\alpha_1}+\sqrt{\alpha_2})^2, (\sqrt{2\alpha_1}+\sqrt{\alpha_2})^2, (\sqrt{\alpha_1}-\sqrt{\alpha_2})^2, (2\sqrt{\alpha_1}-\sqrt{\alpha_2})^2]$.

By assisting an alternative form of the Q(.) function and the MGF, and after some algebraic manipulation, (2.22) can be written by

$$P_{BS2,s_2}(e) = \frac{1}{4}\sum_{v=1}^{6}\kappa_v\left(\sqrt{\frac{P_t\gamma\aleph_v E[|h_2|^2]}{2+P_t\gamma\aleph_v E[|h_2|^2]}}\right). \tag{2.23}$$

Proof: Please, see Appendix B.

In the second phase, U_2 re-encodes the s_1 symbols and forwards them to U_1. The BPSK modulation is assumed to encode the s_1 symbols at U_2. The BER of s_1 in the second phase can be written as

$$P_{21,s_1}(e) = Q\left(\sqrt{P_t\gamma|h_1|^2}\right). \tag{2.24}$$

As we do in the derivations above, by using an alternative form of the Q(.) function and MGF, we can write the average BER (ABER) of (2.24) as

$$P_{21,s_1}(e) = \frac{1}{2}\left(\sqrt{\frac{P_r\gamma E[|h_1|^2]}{2+P_r\gamma E[|h_1|^2]}}\right). \tag{2.25}$$

To find the BER of U_1, we substitute the (2.21) and (2.25) into (2.19) as given by

$$P_{e2e,WDL}(e) = 1-\left(1-\frac{1}{4}\sum_{j=1}^{2}\left(\sqrt{\frac{P_t\gamma\daleth_j E[|h_2|^2]}{2+P_t\gamma\daleth_j E[|h_2|^2]}}\right)\right)\left(1-\frac{1}{2}\left(\sqrt{\frac{P_r\gamma E[|h_1|^2]}{2+P_r\gamma E[|h_1|^2]}}\right)\right). \tag{2.26}$$

2.4 Numerical Results

In this section, We validate our analytical derivations by simulation results. We assume that the parameters used in the simulation are as follows, d_1=3 m, d_2=1 m, ς=3, α_1=0.8, α_2=0.2 and $P_t = P_r$.In our results, the curves represent simulations, while the markers indicate the analytical derivation. It is evident that our analytical derivation precisely matches the simulations, thereby validating our mathematical framework.

Moreover, we evaluate the performance of the EC of CNOMA WDL. In Figure 2.3, we present the EC performance w.r.t. SNR. We observe that the EC of U_2 increases with increasing SNR, while the EC of U_1 increases and then stabilizes at SNR= 30 dB. The EC of U_2 is better than U_1 due to the different distribution of power allocation and channel gain for each user.

To evaluate the impact of U_2 distance on EC performance, Figure 3.4 presents the EC performance of EC w.r.t. d_2, where SNR = 10, 20, 40 dB. It can be seen that the EC of U_2 deteriorates with increasing d_2 while the EC of U_1 improves. The better distance of U_2 to achieve better performance for both users is in the middle between BS and U_1. As well, the EC performance of both users increases with the growth of SNR.

To assess the impact of α_2 on the EC performance for both users, Figure 2.5 presents the EC performance w.r.t. α_2, where SNR = 10, 20, 40 dB. We observe that changing α_2 affects one user

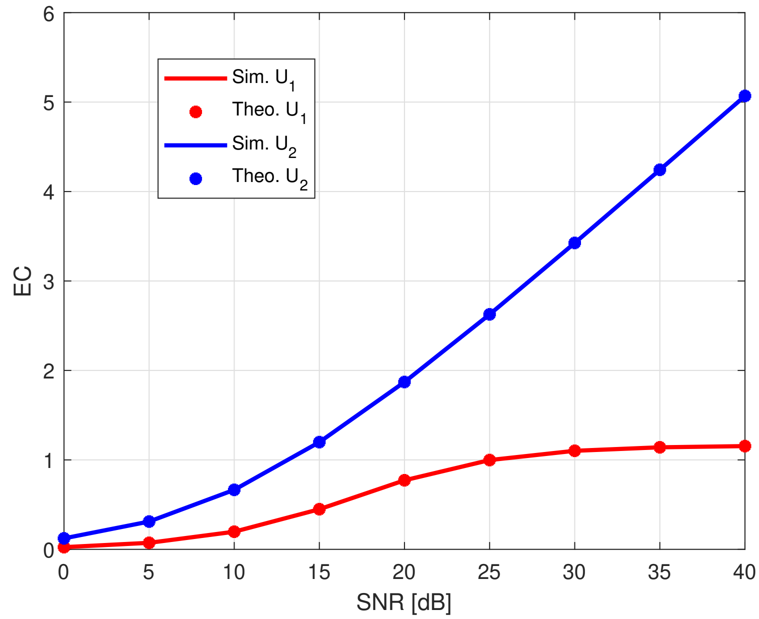

Figure 2.3: *EC of CNOMA WDL.*

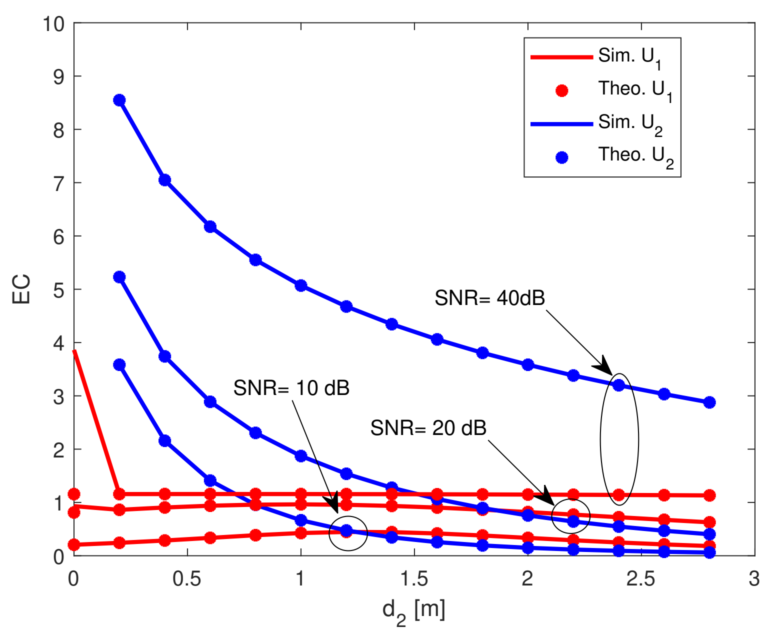

Figure 2.4: *EC of CNOMA WDL w.r.t. d2.*

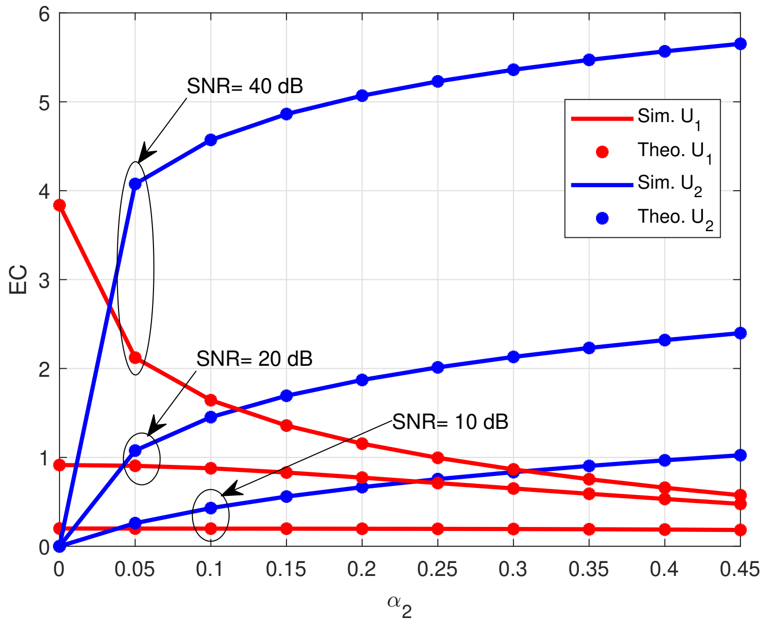

Figure 2.5: *EC of CNOMA WDL w.r.t. α_2.*

at the expense of the other, where increasing α_2 improves the EC of U_2 and decreases the EC of U_1. Additionally, the EC performance of both users increases when SNR increases.

To compare the performance of CNOMA WDL with COMA WDL, we consider that the TDMA is implemented for the COMA WDL scheme. In COMA WDL, we need three time slots for transmission. In the first and the second time slots, the BS transmits the signal of U_1 (s_1) and U_2 (s_2) to U_2, respectively. In the third time slot, the U_2 forwards the s_1 signal to U_1. In contrast, CNOMA WDL needs only two time slots. One time slot is to transmit the SC signal from BS to U_2 and the other time slot is to forward s_1 to U_1. In Figure 2.6, we compare the EC performance of CNOMA WDL and COMA WDL. We observe that the EC of CNOMA WDL achieves better performance gain than OMA WDL. This is due to the difference in transmission time between the two systems, which makes CNOMA WDL superior to its OMA counterpart. In Figure 2.7, we present the OP performance of the two users for CNOMA WDL w.r.t. SNR. By using (2.13) and (2.16), we executed the mathematical simulations. We observe that the OP performance the U_2 is better than U_1. This is due to the different power allocation and channel gain for both users.

To assess the impact of distance on the performance of both users, in Figure 2.8, we present the OP performance with different distances for U_2, where SNR=10, 20, 40 dB. We observe that the OP performance of U_1 decreased compared to U_2, while in the large distance of U_2, the OP of both users increases jointly. Increasing distance means poor channel, so the outage performance of both users degrades. As we can see the best position of U_2 to achieve better outage performance for both users is in the middle between the BS and U_1. Furthermore, the high SNR enhances the

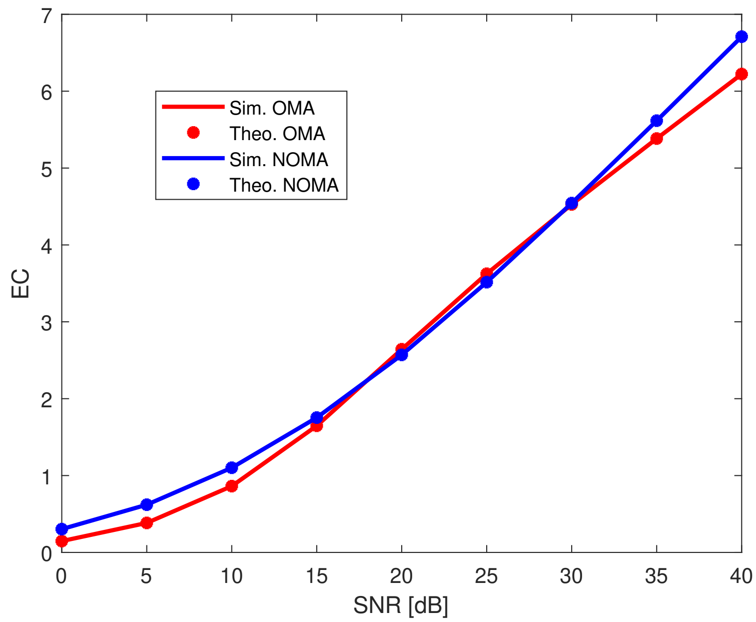

Figure 2.6: *EC comparison between CNOMA WDL and COMA WDL.*

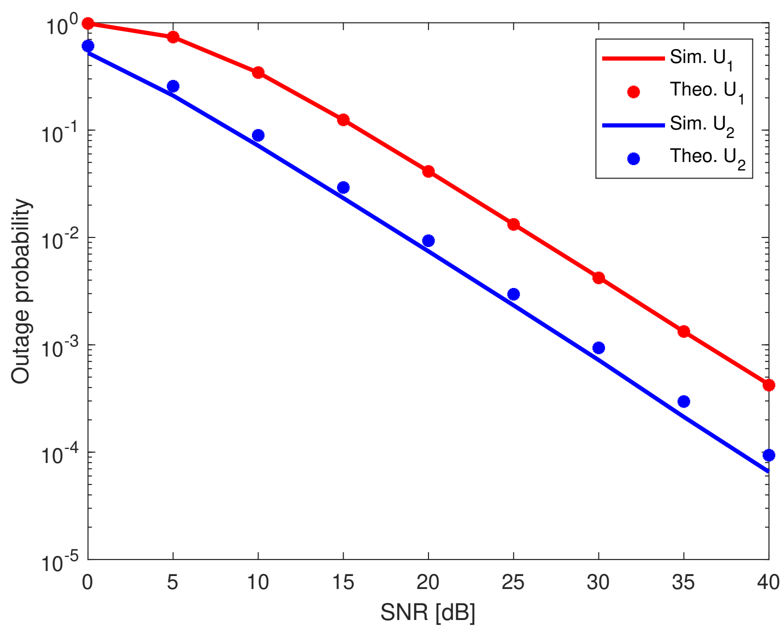

Figure 2.7: *OP of CNOMA WDL.*

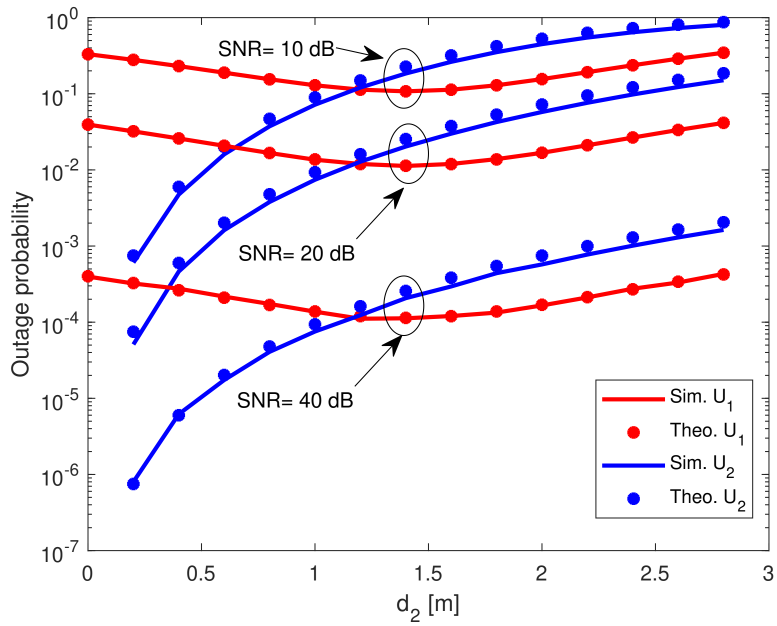

Figure 2.8: *OP of CNOMA WDL w.r.t.* d_2.

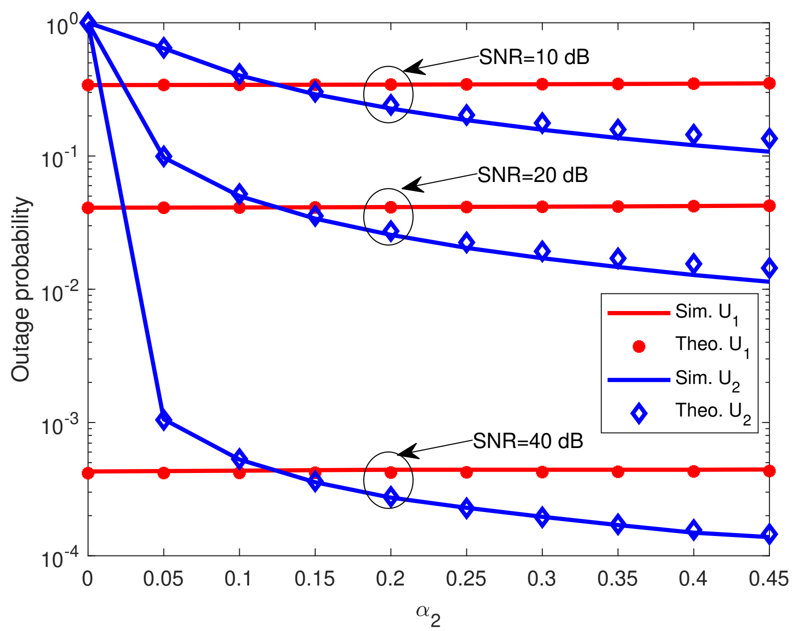

Figure 2.9: *OP of CNOMA WDL w.r.t.* α_2.

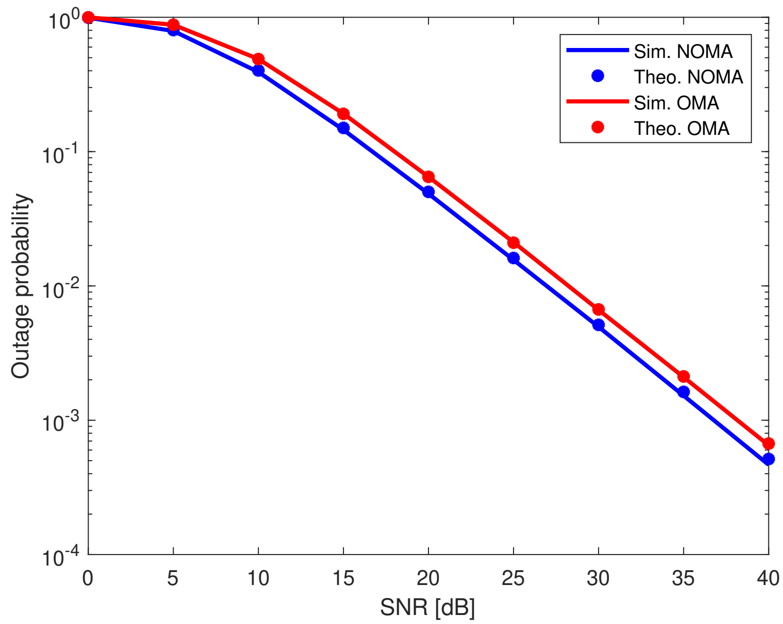

Figure 2.10: *OP comparison between CNOMA WDL and COMA WDL.*

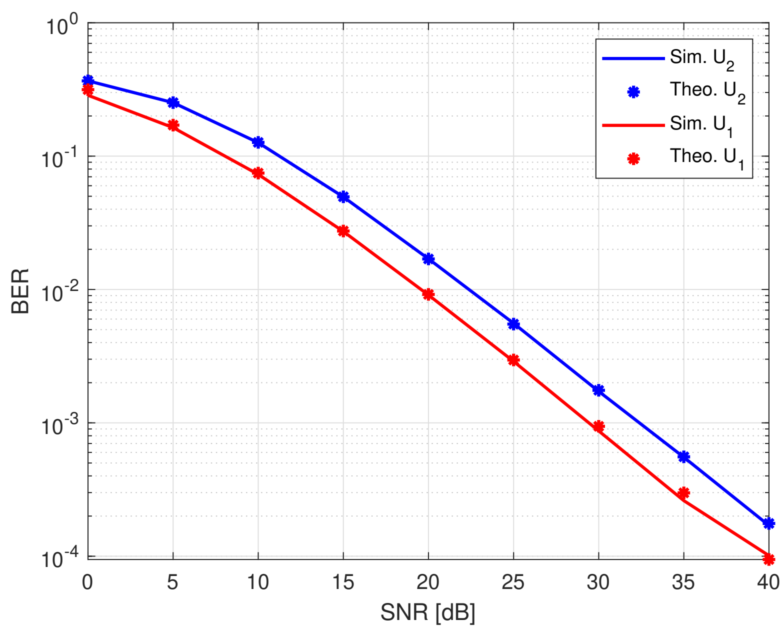

Figure 2.11: *BER of CNOMA WDL.*

OP performance of users.

To evaluate the effect of the α_2 on the performance of both users, Figure 2.9. presents the OP performance with different α_2, where SNR=10, 20, 40 dB. We observe that when α_2 increases, the OP performance changes in opposite way for both users, as the performance of U_2 decreases, while the performance of U_1 increases. The change of α_2 affects the SIC process and signal detection. Also, the increase in the SNR improves the OP performance of users.

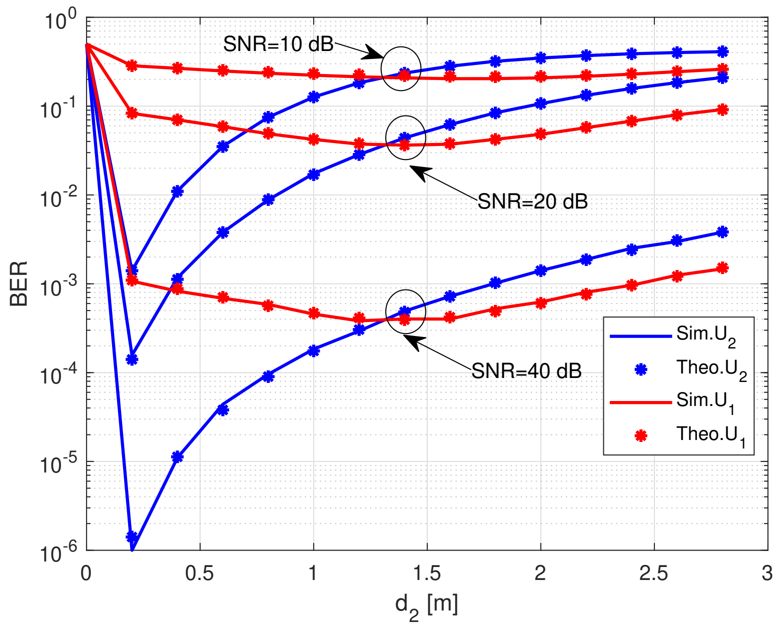

Figure 2.12: *BER of CNOMA WDL w.r.t. d_2.*

In Figure 2.10, we compare the OP performance of the CNOMA WDL and COMA WDL. We observe that the OP performance of CNOMA WDL outperforms COMA WDL due to the different time slots between the two systems. Moreover, we evaluate the BER performance using (2.23) and (2.26). In Figure 2.11, we show the BER performance of users for CNOMA WDL w.r.t. SNR. We observe that the BER of U_1 achieves better performance than U_2. The different distribution of power allocation affects the BER performance of users. In Figure 2.12, we evaluate the BER performance of users for CNOMA WDL w.r.t. d_2. We observe that increasing d_2 deteriorates the BER performance of U_2 and decreases the BER performance of U_1 at lower d_2 values. In the large values of d_2, the BER performance of U_1 and U_2 deteriorates. To achieve better BER performance for both users, the best position of the U_2 is in the middle between BS and U_1. As well, increasing SNR decreases the BER performance of both users.

In Figure 2.13, we evaluate the BER performance of users for CNOMA WDL w.r.t. α_2. It is observed that increasing α_2 affects the BER performance of one user at the expense of the other, as

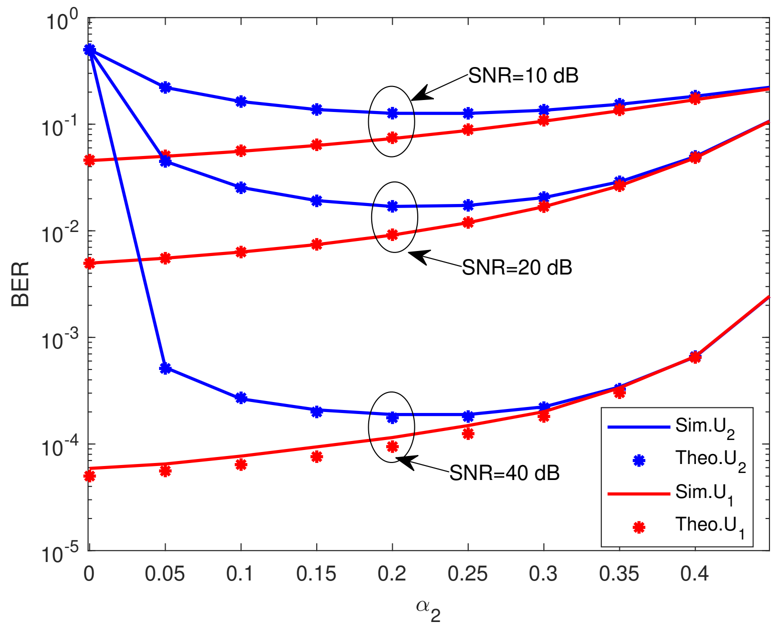

Figure 2.13: *BER of CNOMA WDL w.r.t.* α_2.

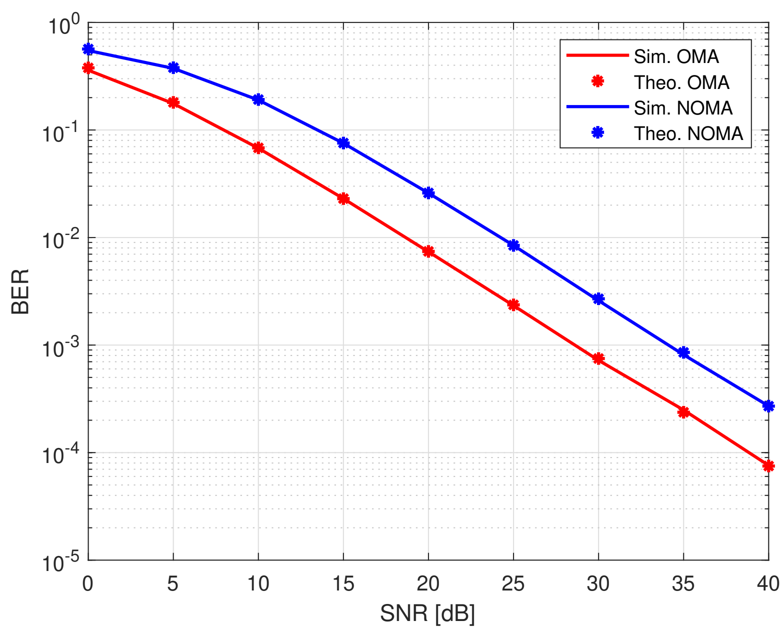

Figure 2.14: *BER comparison between CNOMA WDL and OMA WDL.*

increasing α_2 reduces the BER performance of the U_2 and increases the BER performance of the U_1. Increasing α_2 affects the SIC process at U_2 and the forwarding message in the second phase. Again, increasing SNR improves the BER performance of both users. In Figure 2.14, we compare the BER performance of the CNOMA WDL and COMA WDL. We observe that the BER performance of COMA WDL outperforms CNOMA WDL. Unlike OMA, the users' signals suffer from inter user interference (IUI) in NOMA, which affects the detection of users' signals and the SIC process.

2.5 Conclusion

In this chapter, we investigated the downlink CNOMA WDL. We derive the closed-form EC, OP, and BER over the Rayleigh fading channel. The power allocation factor and helper user distance are evaluated. We have compared our scheme with traditional COMA WDL. Our derivations are matched perfectly with simulation results. We have shown that the power allocation affects the SIC process and does not enhance the users' performance. As well, the distance of the helper user affects the performance of the far user. The best position of the helper user is in the middle between the BS and far user to achieve better performance for both users jointly. Furthermore, the high SNR enhances the performance of the system.

In the following chapter, we will study the performance of the second CNOMA scheme (i.e., CNOMA with DL) to enhance the system performance.

Chapter 3

Cooperative NOMA with Direct Link

3.1 Introduction

Recently, cooperative communication integrated with NOMA networks to increase spectral efficiency, extend coverage, etc [24, 49]. Two cooperative communication schemes are known as cooperative WDL when the users receive their signals only with the help of the relay. The other one is known as cooperative with DL, i.e., when the users receive their signals from different sources. In this chapter, we study and analyze the CNOMA with DL, in which this scheme is used to improve the system performance.

3.1.1 Related Works

In [50], three types of CNOMA schemes have been analyzed to enhance OP performance. The authors of [51, 52] derive the OP performance of the CNOMA with DL by adopting an AF relay. A buffer-aided CNOMA system in the IoT has been investigated in terms of OP in [53]. In [54], CNOMA is evaluated in terms of OP over the Nakagami-m fading channel. In [55], a new scheme of AF CNOMA with DL has been investigated in terms of OP. The delay-tolerant capacity, OP, and delay-limited capacity of a deivce-to-device-aided CNOMA using the overheard signal are analyzed [56]. In [57], the system throughput of CNOMA with DL has been evaluated over the Nakagami-m fading channel. The authors of [58] examine the coverage probability and average data rate of user pairing with FD CNOMA networks. The authors of [59] analyze the OP of DF CNOMA over the Nakagami-m fading channel. In [60], the incremental CNOMA has been investigated in terms of OP to improve the performance of conventional CNOMA. In [61], the OP of FD/HD uplink CNOMA has been considered. The authors of [62] analyzed the EC and OP for threshold-based DF selective CNOMA. All previous works considered the perfect case of SIC and CSI, which is not realistic. The investigation needs to consider and evaluate the systems with more practical assumptions such as imperfect SIC (ISIC), imperfect CSI (ICSI), IQI imbalance, etc. In [63], the

OP and system throughput of DF CNOMA has been examined under ICSI and IQI, while in [64], the authors evaluated the OP of DF CNOMA under ISIC, ICSI, and HWI. On the other hand, the BER of FD/HD CNOMA has been analyzed in [65, 66]. In [67], the authors investigated the BER of the threshold-based DF selective CNOMA to increase the data reliability of conventional CNOMA. For more practical assumptions, under ISIC, ICSI, and HWI the BER of HD CNOMA has been performed and evaluated in [64].

3.1.2 Motivation and Contributions

Based on the discussion above, in this chapter, we analyze the OP and BER of the CNOMA with DL. The main contributions of this chapter are as follows:

- We analyze the OP and BER of CNOMA with DL under ISIC and ICSI. The asymptotic analysis of OP at high SNR regions is performed to reveal the insights of the parameters for ICSI, and ISIC on system performance. We compare our results with traditional NOMA.
- We discuss the optimum power allocation value and the optimal situation for the helper user.

3.2 System Model

As shown in Figure 3.1, we consider a CNOMA with DL network, which includes BS and two users, U_1 is far and U_2 is near the BS. The users can receive the BS signal. We assume that the U_2 works as a helper user to help the U_1 to improve its received signal. It is assumed that the U_1 applies the MRC technique to improve its signal. We assume that each node works in HD mode. It is supposed that each node has a single antenna. All channel links are modeled as an independent Rayleigh fading channel.

The BS sends an SC signal, which includes U_1 and U_2 signals with different power allocation distributed according to the gain of the channel for each user. The received signal at each user can be written by

$$y_k = \sqrt{P_t}\ (\hat{h}_k + e)\ (\sqrt{\alpha_1} s_1 + \sqrt{\alpha_2} s_2) +\ n, \quad k = 1, 2, \tag{3.1}$$

where $\hat{h}_k \sim \mathcal{CN}(0, \sigma^2_{\hat{h}_k} = d_k^{\varsigma})$ is channel estimated coefficient of U_1 and U_2, respectively, d_k is the distance between BS-U_1 and BS-U_2, respectively, ς is the path-loss factor, s_1 and s_2 are the signals of U_1 and U_2, α_1 and α_2 are the power allocation coefficients of U_1 and U_2 signals, in which $\alpha_1 > \alpha_2$, $\alpha_1 + \alpha_2 = 1$, and n is the AWGN as follows $n \sim \mathcal{CN}(0, \sigma^2)$.

Through the SIC process, the U_2 decodes the U_1 signal and then removes it from the total signal to decode its signal. While U_1 decodes its signal without SIC by treating the U_2 signal as noise.

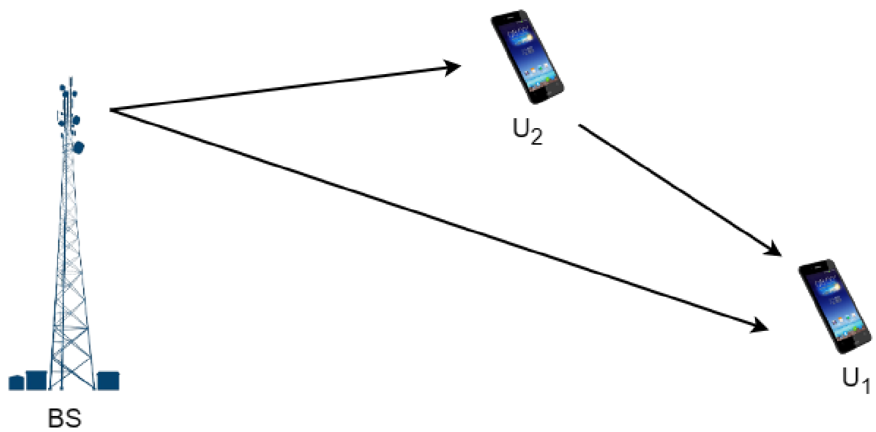

Figure 3.1: *CNOMA with DL scheme.*

As shown in Figure 3.1, in the cooperative scheme, the U_2 re-encodes the U_1 signal and forwards it using its power to U_1 in the second time slot. The received signal in the second time slot at U_1 is given by

$$y_{21} = \sqrt{P_r}\ (\hat{h}_{21} + e)\ s_1 + \ n, \tag{3.2}$$

where $\hat{h}_{21} \sim \mathcal{CN}(0, \sigma^2_{\hat{h}_{21}} = d^{\varsigma}_{21})$ is channel estimated coefficient between U_2-U_1 and d_{21} is the distance between U_2-U_1.

U1 decode its signal s_1 using MLD. The SINR of the phase one and two can be expressed respectively as

$$\gamma_{BS2,s_1} = \frac{P_t \alpha_1 |\hat{h}_2|^2}{P_t \alpha_2 |\hat{h}_2|^2 + P_t \sigma_e^2 + \sigma^2}, \tag{3.3}$$

$$\gamma_{BS2,s_2} = \frac{P_t \alpha_2 |\hat{h}_2|^2}{\varkappa P_t \alpha_1 |\hat{h}_2|^2 + P_t \sigma_e^2 + \sigma^2}, \tag{3.4}$$

$$\gamma_{BS1,s_1} = \frac{P_t \alpha_1 |\hat{h}_1|^2}{P_t \alpha_2 |\hat{h}_1|^2 + P_t \sigma_e^2 + \sigma^2}, \tag{3.5}$$

$$\gamma_{12,s_1} = \frac{P_r |\hat{h}_{21}|^2}{P_t \sigma_e^2 + \sigma^2}, \tag{3.6}$$

where $\varkappa$ is the impact of the SIC factor.

U_1 receives its signals from two different sources (BS and U_2). Thus, U_1 uses one of the diversity combining techniques (in this chapter, we assume that the MRC is used) to improve the received signal quality. The SINR at output MRC at U_1 can be given by

$$\gamma_{MRC,s_1} = \gamma_{BS1,s_1} + \gamma_{12,s_1}. \tag{3.7}$$

3.3 Performance Analysis

In this section, we analyze the OP and BER of CNOMA with DL over the Rayleigh fading channel.

3.3.1 Outage Probability

U_2 detects the U_1 signal and then detects its signal, while U_1 receives its signal from BS and U_2, so U_1 uses the maximum ration combining (MRC) to improve its received signal quality.

3.3.1.1 Outage Probability of Downlink NOMA

The OP of NOMA for U_1 and U_2 are as follows: The OP of U_1 occurs if the γ_{BS1,s_1} is less than the threshold θ_1. Thus, the OP of U_1 is given by

$$P_{BS1,U1}(out) = P(\gamma_{BS1,s_1} < \theta_1). \tag{3.8}$$

By using the PDF and CDF as in (1.1) and (1.2), we find the OP of (3.8) as

$$P_{BS1,U1}(out) = 1 - exp\left(-\frac{(P_t\sigma_e^2 + \sigma^2)\theta_1}{(\alpha_1 - \alpha_2\theta_1)P_tE[|\hat{h}_1|^2]}\right). \tag{3.9}$$

The OP of U_2 occurs if the received γ_{BS2,s_1} or γ_{BS2,s_2} is less than the threshold θ_1 and θ_2, respectively.

$$P_{BS2,U2}(out) = 1 - P(\gamma_{BS2,s_1} > \theta_1)P(\gamma_{BS2,s_2} > \theta_2). \tag{3.10}$$

By using the PDF and CDF as in (1.1) and (1.2), we find the OP of (3.10) by

$$P_{BS2,U2}(out) = 1 - exp\left(-\frac{(P_t\sigma_e^2 + \sigma^2)\theta_1}{(\alpha_1 - \alpha_2\theta_1)P_tE[|\hat{h}_2|^2]}\right) exp\left(-\frac{(P_t\sigma_e^2 + \sigma^2)\theta_2}{(\alpha_2 - \varkappa\alpha_1\theta_2)P_tE[|\hat{h}_2|^2]}\right) \tag{3.11}$$

3.3.1.2 Outage Probability of CNOMA with DL

U_1 uses MRC to combine the two received signals to improve the received signal quality. The OP expression of U_1 using the MRC is given as [68] by

$$\begin{aligned} P_{MRC,U1} =&(1 - P(\gamma_{BS2,s_1} < \theta_1))P(\gamma_{BS1,s_1} + \gamma_{21,s_1} < \theta_1) \\ &+ P(\gamma_{BS2,s_1} < \theta_1)P(\gamma_{BS1,s_1} < \theta_1), \end{aligned} \tag{3.12}$$

where $P(\gamma_{BS2,s_1} < \theta_1)$ is the OP of s_1 at U_2, $P(\gamma_{BS1,s_1} < \theta_1)$ is the OP of s_1 at U_1, and $P(\gamma_{BS1,s_1} + \gamma_{21,s_1} < \theta_1)$ is the OP of s_1 at U_1 when MRC is implemented. We calculate each term of (3.12) as

$$P(\gamma_{BS2,s_1} < \theta_1) = 1 - exp\left(-\frac{(P_t\sigma_e^2 + \sigma^2)\theta_1}{(\alpha_1 - \alpha_2\theta_1)P_tE[|\hat{h}_2|^2]}\right), \tag{3.13}$$

$$P(\gamma_{BS1,s_1} < \theta_1) = 1 - exp\left(-\frac{(P_t\sigma_e^2 + \sigma^2)\theta_1}{(\alpha_1 - \alpha_2\theta_1)P_tE[|\hat{h}_1|^2]}\right). \tag{3.14}$$

Since $P(\gamma_{BS1,s_1} + \gamma_{21,s_1} < \theta_1)$ consists of two independent random variables $W = X + Y$, so, the CDF of W at output MRC is given in [68, eq. (6)] by

$$P(X + Y < M) = 1 - \left[\frac{X}{X - Y}\exp\left(-\frac{M}{X}\right) + \frac{Y}{Y - X}\exp\left(-\frac{M}{Y}\right)\right], \quad X \neq Y. \tag{3.15}$$

Since γ_{BS1,s_1} and γ_{21,s_1} are two independent random variables, where $\gamma_{BS1,s_1} \neq \gamma_{21,s_1}$, so $P(\gamma_{BS1,s_1} + \gamma_{21,s_1} < \theta_1)$ can be computed as (3. 15) by

$$P(\gamma_{BS1,s_1} + \gamma_{21,s_1} < \theta_1) = 1 - \left[\frac{\tau_1}{\tau_1 - \tau_2} \exp\left(-\tau_1\theta_1\right) + \frac{\tau_2}{\tau_2 - \tau_1} \exp\left(-\tau_2\theta_1\right)\right], \quad \tau_1 \neq \tau_2, \tag{3.16}$$

where $\tau_1 = \frac{P_t\sigma_e^2 + \sigma^2}{(\alpha_1 - \alpha_2\theta_1)P_t E[|\hat{h}_1|^2]}$ and $\tau_2 = \frac{P_r\sigma_e^2 + \sigma^2}{P_r E[|\hat{h}_{21}|^2]}$.

The e2e OP using MRC is obtained by substituting (3.13), (3.14) and (3.16) into (3.12) as

$$\begin{aligned} P_{MRC,U1} = & exp\left(-\frac{(P_t\sigma_e^2 + \sigma^2)\theta_1}{(\alpha_1 - \alpha_2\theta_1)P_t E[|\hat{h}_1|^2]}\right)\left(1 - \left[\frac{\tau_1}{\tau_1 - \tau_2} \exp\left(-\tau_1\theta_1\right) + \frac{\tau_2}{\tau_2 - \tau_1} \exp\left(-\tau_2\theta_1\right)\right]\right) \\ & + \left(1 - exp\left(-\frac{(P_t\sigma_e^2 + \sigma^2)\theta_1}{(\alpha_1 - \alpha_2\theta_1)P_t E[|\hat{h}_1|^2]}\right)\right)\left(1 - exp\left(-\frac{(P_t\sigma_e^2 + \sigma^2)\theta_1}{(\alpha_1 - \alpha_2\theta_1)P_t E[|\hat{h}_1|^2]}\right)\right). \end{aligned} \tag{3.17}$$

3.3.1.3 Asymptotic Outage Probability

The asymptotic OP of NOMA and CNOMA for U_1 and U_2 are given, respectively, as follows

$$P^{\infty}_{BS1,U1}(out) \approx \left(1 - \frac{(P_t\sigma_e^2 + \sigma^2)\theta_1}{(\alpha_1 - \alpha_2\theta_1)P_t E[|\hat{h}_1|^2]}\right), \tag{3.18}$$

$$P^{\infty}_{BS2,U2}(out) \approx 1 - \left(1 - \frac{(P_t\sigma_e^2 + \sigma^2)\theta_1}{(\alpha_1 - \alpha_2\theta_1)P_t E[|\hat{h}_2|^2]}\right)\left(1 - \frac{(P_t\sigma_e^2 + \sigma^2)\theta_2}{(\alpha_2 - \varkappa\alpha_1\theta_2)P_t E[|\hat{h}_2|^2]}\right), \tag{3.19}$$

$$\begin{aligned} P^{\infty}_{MRC,U1} \approx & \left(1 - \frac{(P_t\sigma_e^2 + \sigma^2)\theta_1}{(\alpha_1 - \alpha_2\theta_1)P_t E[|\hat{h}_1|^2]}\right)\left(1 - \left[\frac{\tau_1}{\tau_1 - \tau_2}\left(1 - \tau_1\theta_1\right) + \frac{\tau_2}{\tau_2 - \tau_1}\left(1 - \tau_2\theta_1\right)\right]\right) \\ & + \left(1 - \left(1 - \frac{(P_t\sigma_e^2 + \sigma^2)\theta_1}{(\alpha_1 - \alpha_2\theta_1)P_t E[|\hat{h}_1|^2]}\right)\right)\left(1 - \left(1 - \frac{(P_t\sigma_e^2 + \sigma^2)\theta_1}{(\alpha_1 - \alpha_2\theta_1)P_t E[|\hat{h}_1|^2]}\right)\right). \end{aligned} \tag{3.20}$$

3.3.2 Bit Error Rate

In this subsection, we analyze the BER of U_1 and U_2 of NOMA. As well, we analyze the BER of CNOMA with DL. We consider the BPSK modulation is implemented to encode the symbols as described in the previous chapter.

3.3.2.1 BER of Downlink NOMA

The BS transmits an SC symbol consisting of the users' symbols with different power allocation coefficients for each symbol according to the channel gain of each user. U_1 detects its symbols s_1 using MLD. Thus, the BER of U_1 is expressed by

$$P_{BS1,s_1}(e) = \frac{1}{2}\sum_{j=1}^{2} Q\left(\sqrt{P_t\gamma\chi_j|\hat{h}_1|^2/(P_t\gamma\chi_j\sigma_e^2+1)}\right), \tag{3.21}$$

where $\chi_j = [(\sqrt{\alpha_1}+\sqrt{\alpha_2})^2, (\sqrt{\alpha_1}-\sqrt{\alpha_2})^2]$.

By using an alternative form of Q(.) function and the MGF, and after some algebraic manipulation, we can write (3.21) by

$$P_{BS1,s_1}(e) = \frac{1}{4}\sum_{j=1}^{2}\left(\sqrt{\frac{\left(P_t\gamma\chi_j E[|\hat{h}_1|^2]/(P_t\gamma\chi_j\sigma_e^2+1)\right)}{2+\left(P_t\gamma\chi_j E[|\hat{h}_1|^2]/(P_t\gamma\chi_j\sigma_e^2+1)\right)}}\right). \tag{3.22}$$

Likewise, the U_2 implements the SIC to detect its symbols s_2. Thus, the BER of s_2 at U_2 is given by

$$P_{BS2,s_2}(e) = \frac{1}{2}\sum_{v=1}^{6}\kappa_v Q\left(\sqrt{P_t\gamma\aleph_v|\hat{h}_2|^2/(P_t\gamma\delta_v\sigma_e^2+1)}\right), \tag{3.23}$$

where $\kappa_v = [1,1,-1,1,1,-1]$, $\aleph_v = [\alpha_2, \alpha_2, (\sqrt{\alpha_1}+\sqrt{\alpha_2})^2, (\sqrt{2\alpha_1}+\sqrt{\alpha_2})^2, (\sqrt{\alpha_1}-\sqrt{\alpha_2})^2, (2\sqrt{\alpha_1}-\sqrt{\alpha_2})^2]$, $\delta_v = [(\sqrt{\alpha_1}-\sqrt{\alpha_2})^2, (\sqrt{\alpha_1}+\sqrt{\alpha_2})^2, (\sqrt{\alpha_1}+\sqrt{\alpha_2})^2, (\sqrt{\alpha_1}+\sqrt{\alpha_2})^2, (\sqrt{\alpha_1}-\sqrt{\alpha_2})^2, (\sqrt{\alpha_1}-\sqrt{\alpha_2})^2]$.

By using an alternative form of the Q(.) function and the MGF, and after some algebraic manipulation, we write (3.23) by

$$P_{BS2,s_2}(e) = \frac{1}{4}\sum_{v=1}^{6}\kappa_v\left(\sqrt{\frac{\left(P_t\gamma\aleph_v E[|\hat{h}_2|^2]/(P_t\gamma\delta_v\sigma_e^2+1)\right)}{2+\left(P_t\gamma\aleph_v E[|\hat{h}_2|^2]/(P_t\gamma\delta_v\sigma_e^2+1)\right)}}\right). \tag{3.24}$$

3.3.2.2 BER of CNOMA with DL

In the CNOMA with DL, after the U_2 detects all transmitted symbols, it re-encodes the s_1 symbol and forwards it to U_1 in the second phase. In this case, the U_1 receives its signal s_1 from two different sources (i.e., BS and U_2). Hence, we consider that U_1 implements the diversity combining technique MRC to improve its received signal quality. We obtain the e2e BER expression of CNOMA with DL for U_1 as [66]

$$P_{e2e,CNOMA-DL}(e) = \frac{1}{2}\sum_{j=1}^{2}[P_{prop}(e|j)\times P_{BS2,s_1}(e|j) + (1-P_{BS2,s_1}(e|j))P_{coop}(e|j)], \tag{3.25}$$

where $P_{prop}(e|j)$ is the BER in the presence of error propagation from U_2 to U_1, $P_{BS2,s_1}(e|j)$ is the BER of the s_1 at U_2, and $P_{coop}(e|j)$ is the BER when the symbols of U_1 are detected correctly at the U_2 and forwarded to the U_1 and then combined with MRC.

Thus, the BER of the s_1 at U_2 under ICSI is given by

$$P_{BS2,s_1}(e|j) = \frac{1}{2}Q\left(\sqrt{P_t\gamma\chi_j|\hat{h}_2|^2/(P_t\gamma\chi_j\sigma_e^2+1)}\right). \tag{3.26}$$

By using an alternative form of Q(.) function and the MGF, and after some algebraic manipulation, we can write (3.26) by

$$P_{BS2,s_1}(e|j) = \frac{1}{4}\left(\sqrt{\frac{\left(P_t\gamma\chi_j E[|\hat{h}_2|^2]/(P_t\gamma\chi_j\sigma_e^2+1)\right)}{2+\left(P_t\gamma\chi_j E[|\hat{h}_2|^2]/(P_t\gamma\chi_j\sigma_e^2+1)\right)}}\right). \tag{3.27}$$

Since the U_1 receives its signal from BS and U_2, the U_1 employs MRC, the total SNR is the sum of the SNRs after combining the two received signals. Hence, the BER of the cooperative when the MRC is implemented at U_1 under ICSI is calculated by

$$P_{\text{Coop}}(e|j) = Q\left(\sqrt{2\left(\gamma_{21,s1}+\gamma_{BS2,s1,j}\right)}\right), \tag{3.28}$$

where $\gamma_{21,s1} = P_r\gamma|\hat{h}_{21}|^2/(P_r\gamma\sigma_e^2+1)$ and $\gamma_{BS2,s1,j} = P_t\gamma\chi_j|\hat{h}_1|^2/(P_t\gamma\chi_j\sigma_e^2+1)$

The average BER of the cooperative system with two branches using MRC over Rayleigh fading, as given in (3.28), considers the scenario where the mean SNRs of the branches are different, $\overline{\gamma}_{21,s1} \neq \overline{\gamma}_{BS2,s1}$, as presented in [66] by

$$P_{Coop}(e|j) = \frac{1}{2}\left(1-\frac{1}{\overline{\gamma}_{BS2,s1,j}-\overline{\gamma}_{21,s1}}\left(\overline{\gamma}_{BS2,s1,j}\sqrt{\frac{\overline{\gamma}_{BS2,s1,j}}{1+\overline{\gamma}_{BS2,s1,j}}}-\overline{\gamma}_{12,s1}\sqrt{\frac{\overline{\gamma}_{12,s1}}{1+\overline{\gamma}_{12,s1}}}\right)\right), \tag{3.29}$$

where $\overline{\gamma}_{21,s1} = P_r\gamma E[|\hat{h}_{12}|^2]/(P_r\gamma\sigma_e^2+\sigma^2)$ and $\overline{\gamma}_{BS2,s1,j} = P_t\gamma\chi_j E[|\hat{h}_1|^2]/(P_t\gamma\chi_j\sigma_e^2+\sigma^2)$

After utilizing MRC at U_1, the incoming signals from BS and U_2 are summed. If U_2 detects the symbol of U_1 erroneously, it will be forwarded to U_1 as an error propagation. Hence, the received signals will be combined at U_1 using MRC in the case of error propagation. Thus, the BER using MRC with error propagation at the U_1 is given by

$$P_{Prop,s1}(e|j) = \frac{\overline{\gamma}_{21,s1}}{\overline{\gamma}_{21,s1}+\overline{\gamma}_{BS1,s1,j}}. \tag{3.30}$$

Proof: Please, see Appendix C.

The e2e BER using MRC is obtained by substituting (3.27), (3.29) and (3.30) into (3.25) as

$$\begin{aligned} &P_{e2e,CNOMA-DL}(e) = \\ &\frac{1}{2}\sum_j\left[\frac{\overline{\gamma}_{21,s1}}{\overline{\gamma}_{21,s1}+\overline{\gamma}_{BS1,s1,j}}\times\frac{1}{4}\left(\sqrt{\frac{\left(P_t\gamma\chi_j E[|\hat{h}_2|^2]/(P_t\gamma\chi_j\sigma_e^2+1)\right)}{2+\left(P_t\gamma\chi_j E[|\hat{h}_2|^2]/(P_t\gamma\chi_j\sigma_e^2+1)\right)}}\right)\right. \\ &+\left(1-\frac{1}{4}\left(\sqrt{\frac{\left(P_t\gamma\chi_j E[|\hat{h}_2|^2]/(P_t\gamma\chi_j\sigma_e^2+1)\right)}{2+\left(P_t\gamma\chi_j E[|\hat{h}_2|^2]/(P_t\gamma\chi_j\sigma_e^2+1)\right)}}\right)\right) \\ &\left.\frac{1}{2}\left(1-\frac{1}{\overline{\gamma}_{BS2,s1,j}-\overline{\gamma}_{21,s1}}\left(\overline{\gamma}_{BS2,s1,j}\sqrt{\frac{\overline{\gamma}_{BS2,s1,j}}{1+\overline{\gamma}_{BS2,s1,j}}}-\overline{\gamma}_{12,s1}\sqrt{\frac{\overline{\gamma}_{12,s1}}{1+\overline{\gamma}_{12,s1}}}\right)\right)\right]. \end{aligned} \tag{3.31}$$

3.4 Numerical Results

In this section, we validate our analytical derivations by simulation results. We assume that the parameters used in the simulation are as follows, d_1=2 m, $d_2 = d_{21}$=1 m, ς=3, α_1=0.8, α_2=0.2, and $P_t = P_r$. In our results, the curves denote simulations, and markers represent the analytical derivation. It can be easily seen that our analytical derivation matches exactly with the simulations, validating our analytical approach.

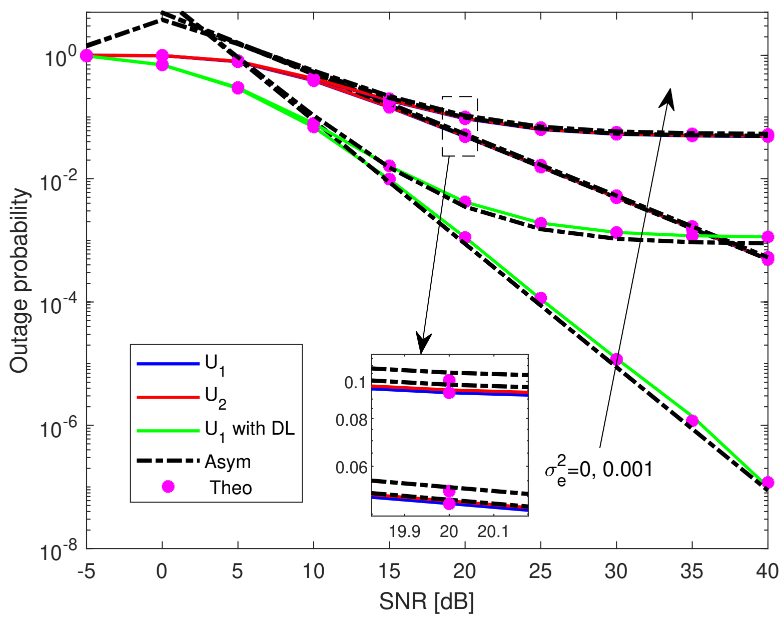

Figure 3.2: *OP of CNOMA with DL.*

Figure 3.2 presents the OP of users versus transmit SNR with the effects of ICSI and ISIC factors. It can be seen that our derived equations are identical to the simulation results, proving the validity of our approach. We observe that the OP of CNOMA for U_1 achieves better performance compared to U_1 without CNOMA. Additionally, ICSI and ISIC degrade the OP performance of all users, resulting in an error floor at high SNR. The effect of ICSI at high SNR impacts the detection of signals and the SIC process.

In order to assess the effect of ICSI, Figure 3.3 presents the OP of users versus ICSI. We observe that the OP of all users in both NOMA and CNOMA degrades with an increase in ICSI. The OP of CNOMA for U_1 achieves better performance compared to U_1 without CNOMA across all ICSI values. The increase in ICSI affects the detection of the U_1 signal and the SIC process for detecting the U_2 signal.

We evaluate the OP w.r.t. α_2 with the effect of ICSI and ISIC as presented in Figure 3.4. We observe that the increasing α_2 affects one user at the expense of the other, which means that in-

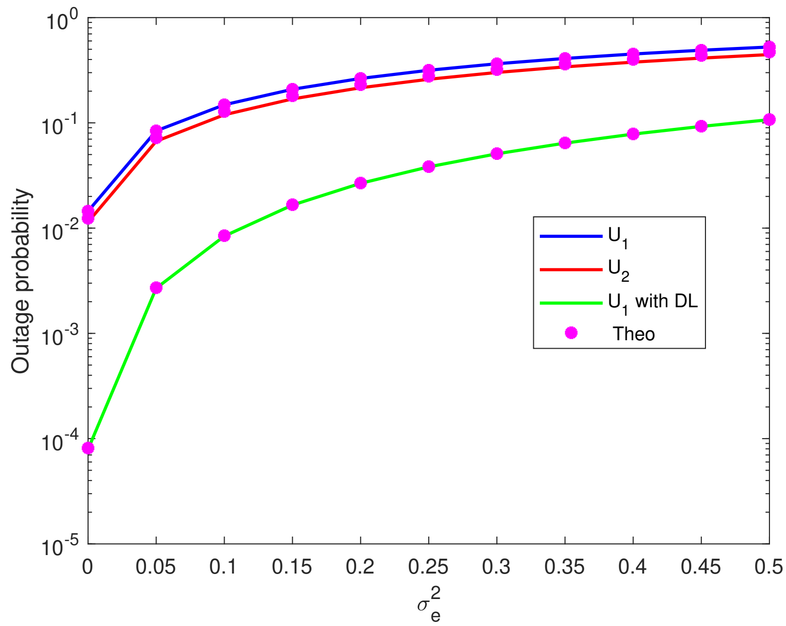

Figure 3.3: *OP of CNOMA with DL w.r.t. ICSI factor (σ_e^2).*

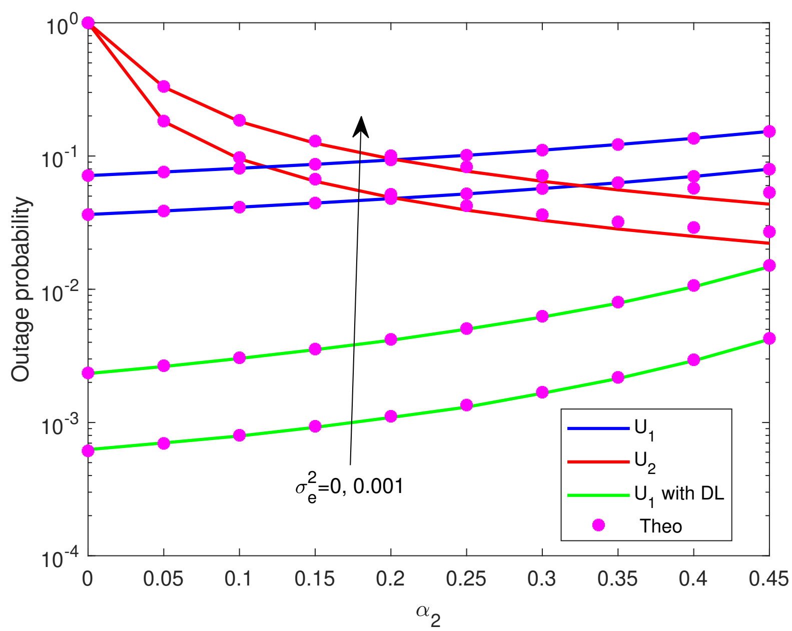

Figure 3.4: *OP of CNOMA with DL w.r.t. α_2.*

creasing α_2 improves the OP performance of U_2 and degrades the OP performance of U_1. Moreover, the U_1 in CNOMA with DL achieves better performance gain compared to NOMA. In addition, the ICSI degrades the OP performance of the users and the SIC process to detect the signals, where the higher values of α_2 with the effect of ICSI degrade the OP performance more than lower α_2 values. The high values of α_2 affect the detection of the U_1 signal and SIC to detect the U_2 signal.

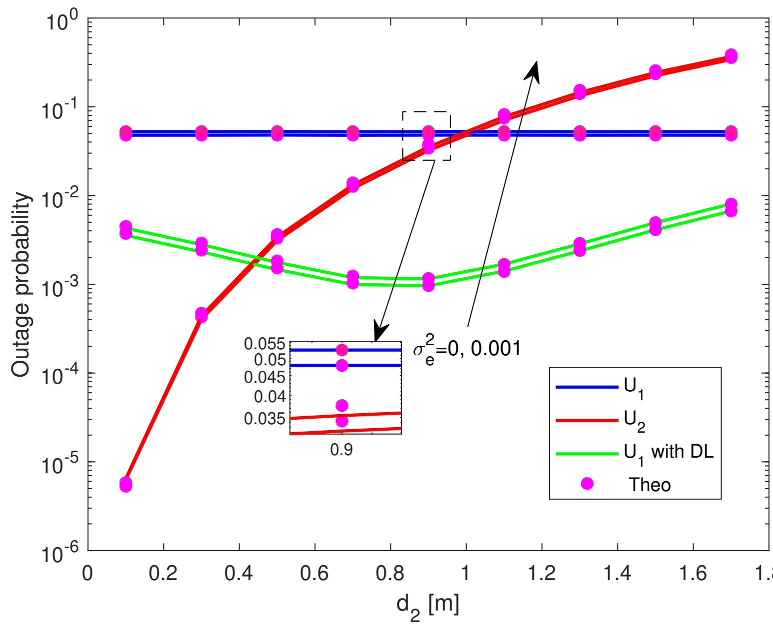

Figure 3.5: *OP of CNOMA with DL w.r.t. d_2.*

The OP w.r.t. d_2 with the effect of ICSI and ISIC is presented in Figure 3.5. We observe that increasing d_2 degrades the OP of U_2, while the OP of U_1 with CNOMA improves and achieves better performance when the U_2 was in the middle. When U_2 falls in the middle, the channel of U_2 will be better, so the detection of signals and SIC will be better than the higher distance between the BS and U_2. Thus, the forwarding signal in the second phase will have fewer errors compared to a high distance of U_2, in which the detection of signals at the U_2 is more error. Therefore, the forwarding signal in the second phase has more errors, which degrades OP performance. Moreover, ICSI influences the SIC process, as well as the second phase's signal forwarding and detection of user signals, which decreases the OP performance of the users.

The OP w.r.t. d_2 considering the effects of ICSI and ISIC is presented in Figure 3.5. We observe that increasing d_2 degrades the OP of U_2, while the OP of U_1 with CNOMA improves and achieves better performance when U_2 is positioned in the middle. When U_2 is in the middle, its channel quality improves, enhancing the detection of signals and the SIC process compared to a higher distance between the BS and U_2. Consequently, the forwarding signal in the second phase will have fewer errors compared to when U_2 is farther away, where signal detection at U_2 is more error-prone. Therefore, the forwarding signal in the second phase has more errors, degrading the OP performance. Moreover, ICSI influences the SIC process, as well as the second phase's signal forwarding and detection of user signals, which decreases the OP performance of the users.

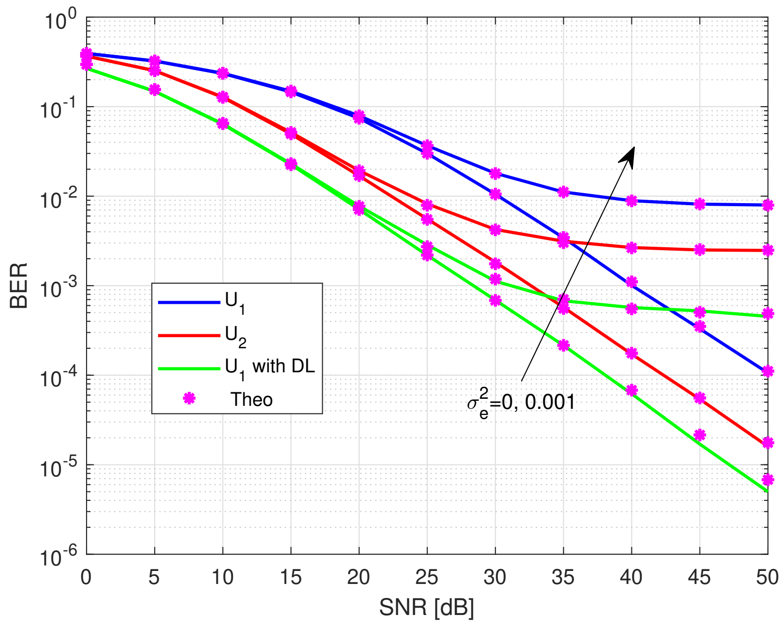

Figure 3.6: *BER of CNOMA with DL.*

Figure 3.6 presents the BER of CNOMA compared to NOMA with the effect of ICSI. We observe that the BER performance of CNOMA for U_1 is superior to that of NOMA. Moreover, ICSI degrades the system's BER performance and introduces an error floor at high SNR. To further evaluate the impact of the ICSI factor on our system, Figure 3.7 presents the BER of CNOMA compared to NOMA. It is observed that the BER performance decreases as the effect of ICSI increases. ICSI affects the SIC process, the detection of signals at users, and the forwarding signals in the second phase. Additionally, it can be seen that the BER performance of CNOMA for U_1 is improved compared to NOMA.

As shown in the previous figures, power allocation impacts the detection of user signals. It is important to evaluate the BER performance for different power allocation factors. Figure 3.8 presents the BER of CNOMA compared to NOMA w.r.t. α_2 under the effect of ICSI. We observe that the BER performance of one user is negatively impacted by the other as α_2 increases. Additionally, ICSI decreases the BER performance of the users. Increasing α_2 with ICSI affects the SIC process, and the detection of users' signals and forwarding signals in the second phase will have more errors, degrading the BER performance.

To assess the impact of d_2 on the BER performance, Figure 3.9 presents the BER of CNOMA compared to NOMA w.r.t. d_2 under the effect of ICSI. We observe that increasing d_2 degrades the

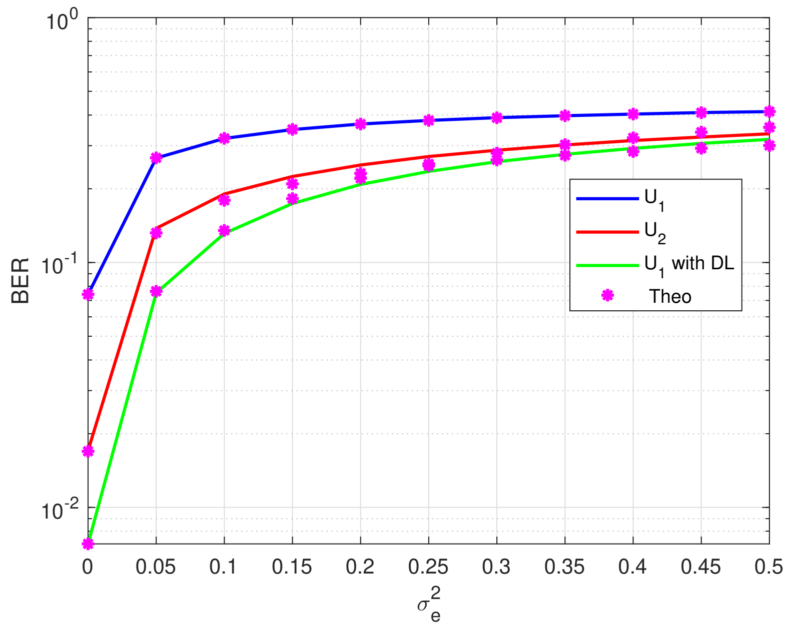

Figure 3.7: *BER of CNOMA with DL w.r.t. ICSI factor (σ_e^2).*

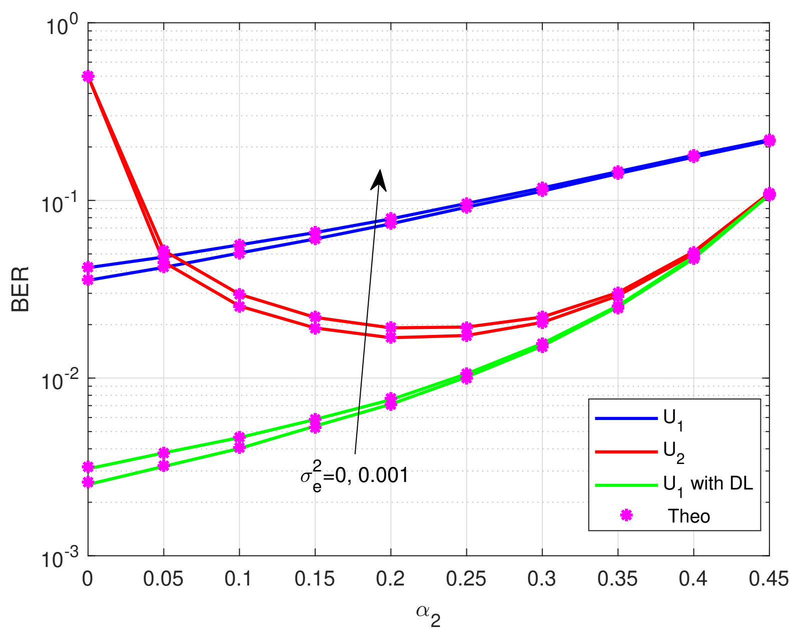

Figure 3.8: *BER of CNOMA with DL w.r.t. α_2.*

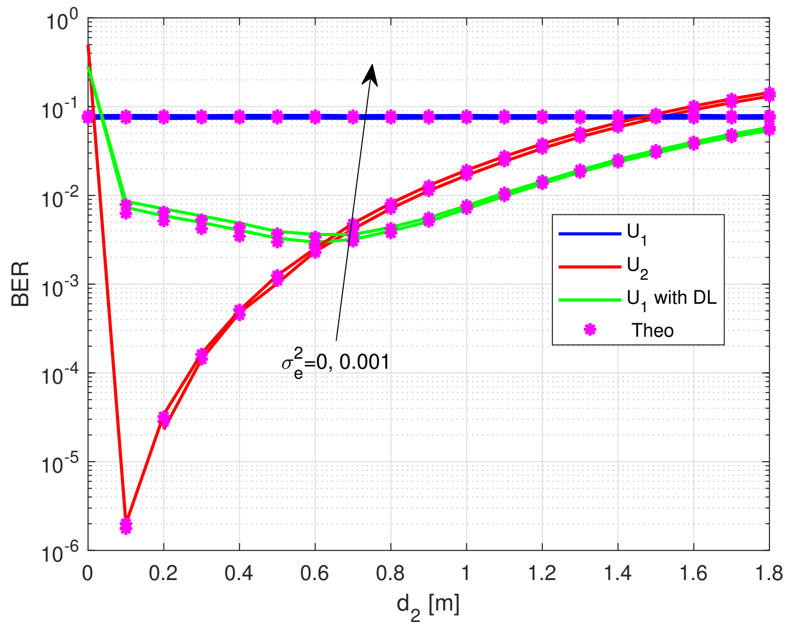

Figure 3.9: *BER of CNOMA with DL w.r.t. d_2.*

BER performance of U_2 and improves the BER performance of U_1. It can be easily seen that when U_2 is near the middle, the BER of U_1 is better. A shorter distance for U_2 means better channel gain, so the detection of signals and the SIC process are more effective. Thus, detection will have fewer errors, and forwarding signals to the second phase will also have fewer errors. Additionally, we observe that ICSI degrades the BER performance of the system. ICSI affects the SIC process and the detected signals at users, increasing the errors in the forwarded signals in the second phase.

3.5 Conclusion

In this chapter, we investigated the downlink CNOMA with DL. We derived closed-form expressions for the OP and BER with both ISIC and ICSI over the Rayleigh fading channel. We evaluated the impact of power allocation factors and helper user distances. Our results were compared with traditional NOMA, and we found that our analytical derivations matched perfectly with simulation results. We demonstrated that both power allocation and helper user distance are affected by ISIC and ICSI, with the optimal location for the helper user being in the middle between the BS and the far user, leading to improved performance for both users jointly.

As observed in the results of previous chapters, the system's performance is significantly influenced by the distance of the relay or helper user. Poor channel conditions can notably reduce system performance. Therefore, it is imperative to address this issue. One suggested solution is the multiple relay scheme. In the following chapter, we will study and evaluate the performance of the multiple relay scheme for CNOMA.

Chapter 4

Cooperative NOMA with Multiple Relays

4.1 Introduction

The ambitious high data rate applications in the beyond 5G wireless networks will require new solutions and technologies [35]. NOMA is one of the promising radio access technologies for improved performance in cellular communications of the next generation [69]. Compared to OMA, NOMA can serve multiple users in the same resource block. Thus, it reduces latency and promotes massive connectivity. NOMA also enhances spectral efficiency, user fairness, and increases reliability [23]. The concept of NOMA is based on using SC at the transmitter and SIC at the receiver [70]. On the other hand, cooperative communications provide a useful method of combating channel disorders, such as fading, path-loss, and shadowing [24]. Thus, it extends the communication coverage area, improves the quality of service, and increases spectral efficiency [71].

4.1.1 Related Works

The advantages of NOMA over OMA are validated in [9]. The CNOMA system outperforms OMA in terms of ergodic sum rate and OP [10]. The OP and ergodic sum capacity performance of the FD CNOMA under the realistic assumption of imperfect self-interference cancellation has been performed [72]. The uplink FD-CNOMA has been investigated in terms of ergodic sum rate and OP [73]. In [74], the performance of the device-to-device aided FD-NOMA has been evaluated in terms of EC and OP. The OP and ergodic rates of NOMA-FD in coordinated direct and relay transmission have been investigated in [75] under the realistic assumptions of ICSI and ISIC over Nakagami-m fading. In [76], the authors proved the advantages of a novel detection scheme for CNOMA, in terms of OP and ergodic sum rate. The OP of cooperative vehicular communications transmission with NOMA at intersections using MRC has been analyzed in [77]. In [78], the OP of the joint user and relay selection (RS) algorithm for CNOMA has been investigated. The OPs over Nakagami-m fading of the two RS schemes (the max-min RS and the two-stage RS) are evaluated in [79]. The authors of [80] compared an opportunistic RS strategy with a balanced and random RS in terms of OP, throughput, and ergodic sum rate. The opportunistic RS showed significant performance gain over the existing works and OMA. Unlike previous discussions, the BER analysis for NOMA has been conducted in [11, 38, 39, 40, 45, 42, 81, 82, 83, 44]. In [11], the exact closed-form BER under SIC error for downlink and uplink NOMA has been derived. The BER with different modulation was investigated in the downlink NOMA [38]. The authors of [39] obtained the closed-form BER for visible light communication NOMA using different modulations. In [81, 82, 83], the BER of the NOMA systems for an arbitrary number of users and modulation orders has been derived. The results indicate that when the number of users and the modulation order increase, the feasible power coefficients range becomes significantly small, and the users' performances decrease due to increased IUI. The bit error probability of CNOMA has been determined in [40]. The performance of the reversed DF CNOMA in the presence of ISIC and CSI were evaluated [45] to improve user fairness compared to conventional DF CNOMA. In [42], the closed-form symbol error rate for DF CNOMA has been derived. The BER and EC of mobile ad-hoc networking NOMA have been analyzed in [38]. The analytical BER of the user relay FD NOMA has been investigated [44].

On the other hand, the multi-hop relay has gotten great attention in academia and industry because it can efficiently extend coverage to severely shadowed areas in the cell or places outside of the cell range. Meanwhile, it improves throughput, especially at the cell edge [84, 85, 86, 87]. The multi-hop relay schemes' have been also investigated with the NOMA implementation. In the presence of an active eavesdropper for the multi-hop relay, the OP and throughput have been derived [88]. The OP and throughput have been examined for multi-point cooperative relay NOMA with EH [89].

4.1.2 Motivation and Contributions

The interaction between NOMA and cooperative communication is one of the topics that drew the most attention to achieve higher spectral efficiency and compensation for path-loss [40]. As mentioned above, CNOMA with assisted one relay has been investigated in terms of BER, EC, and OP [10, 72, 73, 74, 75, 76, 77, 38, 40, 45, 42, 44]. The idea is to help the very far user or when the direct link between the BS and users is not available due to the large distance or obstacles, etc. The EC and OP of the cooperative RS in NOMA have been analyzed [78, 79, 80]. Although there is a relay to help users, the channel quality may still be poor between each node (i.e., BS-relay and relay-users), and the performance will not be good. Therefore, channel degradation and long distances between nodes may cause a significant deterioration in performance for users. Hence, it is very important to resolve this problem. As mentioned, studies in the open literature consider single relay (or RS) in CNOMA. In the end, they are all two-hop scenarios. However, we consider a multi-hop scenario which is quite important to extend cell coverage to heavily shadowed areas in the cell or places outside the cell range [84, 85, 86, 87]. Therefore, a NOMA with multi-hop relaying can be employed through intermediate relays that form a multi-hop path from the BS to users to compensate the path-loss, expand network coverage, and deliver messages to users everywhere. In this regard, based on the investigations that we have mentioned above, and to the best of the authors' knowledge, the e2e BER expressions of multi-hop DF-aided CNOMA (MH-DF-CNOMA) have not been reported. Therefore, through the path of intermediate relays from BS to two users to deliver messages to the users, this chapter investigates two downlink MH-DF-CNOMA schemes (i.e., MH-DF-CNOMA WDL and MH-DF-CNOMA with DL) to achieve ubiquitous coverage and connectivity in the future NOMA network. The e2e BER expressions of MH-DF-CNOMA are analyzed at each hop under ICSI and ISIC, which are practical assumptions. In addition, we investigate the effect of the OP of MH-DF-CNOMA differently from [88] in the presence of ICSI and ISIC. We compare our model with traditional OMA. Moreover, we discuss the superiority of the MH-DF-CNOMA over a single relay scheme. The original contributions of this chapter are as follows:

- We present two downlink MH-DF-CNOMA (i.e., MH-DF-CNOMA WDL and MH-DF-CNOMA with DL) system models. The model consists of a BS and a group of intermediate relays that form a multi-hop path. The first scheme: The users can't receive the BS signal directly, and the multi-hop path delivers the messages of the two users. The second scheme: The users can receive the BS signal directly, and the multi-hop path.

- The BER analysis for even single relay schemes is limited. In this chapter, we perform a comprehensive analysis of the considered schemes. The considerations of the ISIC and ICSI are more accurate/realistic for the practical scenarios. We investigate ISIC and ICSI in the MH-DF-CNOMA. We derive the closed-form BER expression at each intermediate relay node for each user symbol with the ICSI. Then, we derive the closed-form BER expression for every user in the last phase with ICSI. After that, we express the e2e BER for each user. We discuss the effect of the ICSI and ISIC on the BER performance of the users.

- We discuss the optimum power allocation coefficient for different hops to minimize BER/OP.

- Moreover, we derive the closed-form expression of the OP of each user message at each intermediate relay node with ICSI and ISIC for both schemes. We derive the closed-form expression of the OP at each user in the last phase with ICSI and ISIC. Besides, we express the e2e OP for each user. The OP performance of users on each hop with the effect of ICSI and ISIC is evaluated.

- In BER and OP performance, we examine the impact of the increasing number of relays with different SNR values.

- Finally, the performance of downlink MH-DF-R-NOMA and downlink multi-hop DF COMA (MH-DF-COMA) are compared. We discuss the superiority of the MH-DF-CNOMA over existing single relay schemes.

4.2 Cooperative NOMA assisted Multiple Relays Without Direct Links

4.2.1 System Model

We consider a downlink CNOMA consisting of one BS, L relays (R_L) and two users named as follows, U_1 is far, while U_2 is near the last relay (see Figure 4.1). We assume that all relays work in DF and HD modes. Due to the very long distance between the BS and users, the users receive their signals with the help of the relay nodes only. Thus, it is assumed that the relay nodes create a way or path from BS to the users. We suppose that the CSI between all nodes is imperfect. The Rayleigh fading channel coefficient between all relay links denoted by $g_{RL} \sim \mathcal{CN}(0, \sigma_{RL}^2 = d_{RL}^{\varsigma})$, where $L = 1, 2, 3, ..., N$ and the Rayleigh fading channel coefficient between the last relay and users links are denoted by $h_k \sim \mathcal{CN}(0, \sigma_k^2 = d_k^{\varsigma})$, where $k = 1, 2$. The channel estimation coefficients are presented as $\hat{g}_{RL} = g_{RL} - e \sim \mathcal{CN}(0, \hat{\sigma}_{RL}^2 = \sigma_{RL}^2 - \sigma_e^2)$ and $\hat{h}_k = h_k - e \sim \mathcal{CN}(0, \hat{\sigma}_k^2 = \sigma_k^2 - \sigma_e^2)$, where e is the error factor of the channel estimation.

In the MH-DF-CNOMA, the SC signal is implemented at the BS and transmitted over the path of multiple relays until reaches the users. At relay nodes, the SIC and SC are implemented at each hop to detect the received signal and re-combine them, then forward it to the next relay node until it reaches the users (see Figure 4.1). We assume that the power of the BS and relay nodes are equal and named P_t. The received signals at each relay can be written as

$$y_L = \sqrt{P_t}\ (\hat{g}_{RL} + e)\ (\sqrt{\alpha_1} s_1 + \sqrt{\alpha_2} s_2) +\ n, \qquad L = 1, 2, 3, ..., N, \tag{4.1}$$

where $\hat{g}_{RL}$ is channel estimation coefficient of between BS-R_1, R_1-R_2 and R_{L-1}-R_L. d_L is the distance between BS-R_1, R_1-R_2 and R_{L-1}-R_L, ς is the path loss factor, s_1 and s_2 are users signals of U_i, $i = 1, 2$, and α_1 and α_2 are the power allocation coefficient for U_i, where $\alpha_1 > \alpha_2$, in which $\alpha_1 + \alpha_2 = 1$, and n is the AWGN as follows $n \sim \mathcal{CN}(0, \sigma^2)$.

The relay nodes decode the s_1 signal first then using the SIC decode the s_2 signal. The SINRs of the decoded signals under ICSI and ISIC can be expressed by

$$\gamma_{L,s_1} = \frac{P_t \alpha_1 |\hat{g}_{RL}|^2}{P_t \alpha_2 |\hat{g}_{RL}|^2 + P_t \sigma_e^2 + \sigma^2}, \tag{4.2}$$

$$\gamma_{L,s_2} = \frac{P_t \alpha_2 |\hat{g}_{RL}|^2}{\varrho P_t \alpha_1 |\hat{g}_{RL}|^2 + P_t \sigma_e^2 + \sigma^2}, \tag{4.3}$$

where ϱ is the factor of ISIC.

In the last relay node, the SC signal is forwarded to the users. The received signal by the users can be expressed by

$$y_k = \sqrt{P_t}\,(\hat{h}_k + e)\,(\sqrt{\alpha_1}s_1 + \sqrt{\alpha_2}s_2) + \ n. \tag{4.4}$$

The U_1 decodes its signal directly using the MLD, while the U_2 implements the SIC to detect its signal. In practical scenarios, the SIC and CSI are not imperfect. Thus, the decoding error is expected in the detection and SIC process. Thus, the SINRs of the decoded signals at users under ICSI and ISIC can be expressed by

$$\gamma_{2,s_1} = \frac{P_t\alpha_1|\hat{h}_2|^2}{P_t\alpha_2|\hat{h}_2|^2 + P_t\sigma_e^2 + \sigma^2}, \tag{4.5}$$

$$\gamma_{2,s_2} = \frac{P_t\alpha_2|\hat{h}_2|^2}{\varrho P_t\alpha_1|\hat{h}_2|^2 + P_t\sigma_e^2 + \sigma^2}, \tag{4.6}$$

$$\gamma_{1,s_1} = \frac{P_t\alpha_1|\hat{h}_1|^2}{P_t\alpha_2|\hat{h}_1|^2 + P_t\sigma_e^2 + \sigma^2}. \tag{4.7}$$

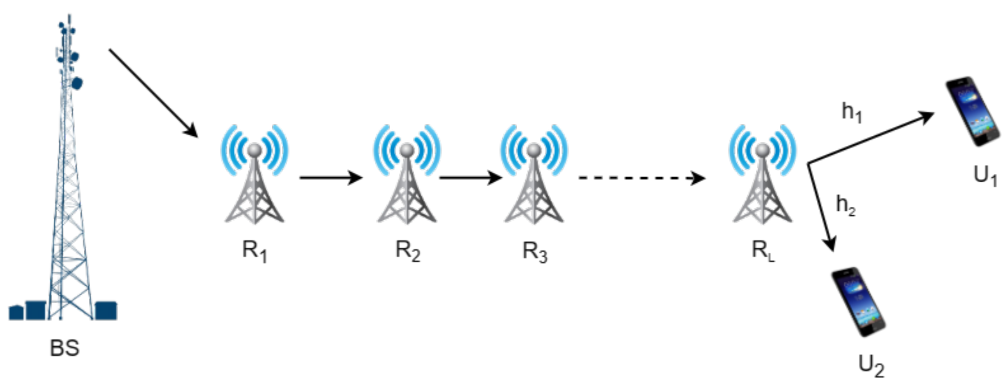

Figure 4.1: *MH-DF-CNOMA WDL scheme.*

4.2.2 Performance Analysis

In this subsection, we derive the e2e OP and BER at each hop for MH-DF-CNOMA with the effect of ICSI and ISIC.

4.2.2.1 Outage Probablity

The SC signal is transferred from BS to users over the path of L relay nodes. The signal should be decoded successfully at all intermediate relay nodes to forward to the next relay. Hence, the e2e OP of users with L relay can be expressed by

$$P_{e2e,U_k,L+1}(out) = 1 - \prod_{l}^{L} \left(1 - P_{U_k}(out)\right)\left(1 - P_{U_k,L}(out)\right), \quad k = 1, 2., \tag{4.8}$$

where $P_{U_k}(out)$ is the OP of users' signals at L relay nodes and $P_{U_k,L}(out)$ is the OP at users in the last phase $(R_L - U_k)$.

The OP of s_1 at each L relay node with ICSI and ISIC occurs when γ_{L,s_1} is less than the threshold $\theta_1^{(L+1)}$ as

$$P_{U_1,L}(out) = P\left(\gamma_{L,s_1} < \theta_1^{(L+1)}\right). \tag{4.9}$$

With the help of the CDF and PDF, (4.9) can be expressed as

$$P_{U_1,L}(out) = 1 - exp\left(-\frac{(P_t\sigma_e^2 + \sigma^2)\theta_1^{(L+1)}}{(\alpha_1 - \alpha_2\theta_1^{(L+1)})P_tE[|\hat{g}_{RL}|^2]}\right), \tag{4.10}$$

where $\theta_1^{(L+1)} = 2^{Tr_1(L+1)} - 1$ is the threshold rate of s_1 at $L+1$ hop and Tr_1 is the target rate of s_1.

Likewise, the OP of s_2 at L relays with ICSI and ISIC occurs when the two following cases event: when γ_{L,s_1} is less than $\theta_1^{(L+1)}$. when γ_{L,s_1} is greater or equal than the threshold $\theta_1^{(L+1)}$ and $\theta_1^{(L+1)}$ is less than the threshold $\theta_2^{(L+1)}$. Hence, the OP of s_2 at L relays with ICSI and ISIC can be summarized as

$$P_{U_2,L}(out) = 1 - P\left(\gamma_{L,s_1} > \theta_1^{(L+1)}\right)P\left(\gamma_{L,s_2} > \theta_2^{(L+1)}\right). \tag{4.11}$$

By using the CDF and PDF, (4.11) can be expressed as

$$P_{U_2,L}(out) = 1 - exp\left(-\frac{(P_t\sigma_e^2 + \sigma^2)\theta_1^{(L+1)}}{(\alpha_1 - \alpha_2\theta_1^{(L+1)})P_tE[|\hat{g}_{RL}|^2]}\right)exp\left(-\frac{(P_t\sigma_e^2 + \sigma^2)\theta_2^{(L+1)}}{(\alpha_2 - \varrho\alpha_1\theta_2^{(L+1)})P_tE[|\hat{g}_{RL}|^2]}\right), \tag{4.12}$$

where $\theta_2^{(L+1)} = 2^{Tr_2(L+1)} - 1$ is the threshold rate of s_2 at $L+1$ hop and Tr_2 is the target rate of s_2.

In the last phase, the last relay forwards the SC signal to the users. The U_1 detects its signal directly by treating the other signal as noise, while the U_2 uses the SIC to detect its signal. The OP at U1 under ICSI and ISIC can be written as

$$P_{U_1}(out) = P\left(\gamma_{1,s_1} < \theta_1^{(L+1)}\right). \tag{4.13}$$

With the help of the CDF and PDF, (4.13) can be expressed as

$$P_{U_1}(out) = 1 - exp\left(-\frac{(P_t\sigma_e^2 + \sigma^2)\theta_1^{(L+1)}}{(\alpha_1 - \alpha_2\theta_1^{(L+1)})P_tE[|\hat{h}_1|^2]}\right). \tag{4.14}$$

Also, we detect the s_2 at U_2 by using the same way to detect s_2 at relays. Hence, the OP of U_2 with ICSI and ISIC can be expressed as

$$P_{U_2}(out) = 1 - P\left(\gamma_{2,s_1} > \theta_1^{(L+1)}\right) P\left(\gamma_{2,s_2} > \theta_2^{(L+1)}\right). \tag{4.15}$$

By using the CDF and PDF, (4.15) can be expressed as

$$P_{U_2}(out) = 1 - exp\left(-\frac{(P_t\sigma_e^2 + \sigma^2)\theta_1^{(L+1)}}{(\alpha_1 - \alpha_2\theta_1^{(L+1)})P_t E[|\hat{g}_L|^2]}\right) exp\left(-\frac{(P_t\sigma_e^2 + \sigma^2)\theta_2^{(L+1)}}{(\alpha_2 - \varrho\alpha_1\theta_2^{(L+1)})P_t E[|\hat{g}_L|^2]}\right). \tag{4.16}$$

4.2.2.2 Bit Error Rate

The SC signal is transferred from the BS to users over a path of relay nodes. In the previous literature, the e2e BER for two hops i.e., BS-R_1 users is given as in [66, 45, 90] by

$$P_{e2e,2hop}^{U_k}(e) = P_{R_1}^{U_k}(e)\ (1 - P_{U_k}(e)) + P_{U_k}(e)\ (1 - P_{R_1}^{U_k}(e)). \tag{4.17}$$

Furthermore, for more than two hops (i.e., $(L+1)$ hops) (BS-RL-users), we express e2e BER of $(L+1)$ hops as in [90, 91] by

$$P_{e2e,(L+1)hop}^{U_k}(e) = \underbrace{P_{e2e,BS-R_L}^{U_k}(e)}_{\iota}\ (1 - P_{U_k}(e)) + P_{U_k}(e)\ (1 - \underbrace{P_{e2e,BS-R_L}^{U_k}(e)}_{\iota}), \tag{4.18}$$

where ι is the e2e BER from BS to R_L. To simplify, if $L = 2$ i.e., two relays or two hops, ι it will be expressed as

$$P_{e2e,BS-R_L}^{U_k}(e) = P_{R_1}^{U_k}(e)\ (1 - P_{R_2}^{U_k}(e)) + P_{R_2}^{U_k}(e)\ (1 - P_{R_1}^{U_k}(e)), \tag{4.19}$$

and, in the case of more than two relays, we generalized ι as

$$P_{e2e,BS-R_L}^{U_k}(e) = P_{e2e,BS-R_{L-1}}^{U_k}(e)\ (1 - P_{R_L}^{U_k}(e)) + P_{R_L}^{U_k}(e)\ (1 - P_{e2e,BS-R_{L-1}}^{U_k}(e)), \tag{4.20}$$

where $P_{R_1}^{U_k}(e)$ is the BER of users in the first phase from BS to R_1 (case of one relay), $P_{U_k}(e)$ is the BER of users in the last phase from R_L to users, $P_{e2e,BS-R_L}^{U_k}(e)$ is the e2e BER of users' signals from BS to L relay (R_L), $P_{R_2}^{U_k}(e)$ is the BER of users' signals in the second phase from R_1 to R_2 (case of two relays), $P_{e2e,BS-R_{L-1}}^{U_k}(e)$ is the e2e BER of users' signals from BS to R_{L-1}, and $P_{R_L}^{U_k}(e)$ is the ABER of the users' signals from R_{L-1} to R_L.

We consider that the BPSK modulation is used to encode the users' signals at each node. Also, the ICSI is available at all nodes. At all relay nodes, the s_1 signal is detected through MLD, while by using the SIC process, the s_1 is removed from the total received signal, and then by using MLD s_2 is detected. Hence, the BER of s_1 at al relay nodes with ICSI can be expressed as

$$P_{R_L}^{U_1}(e) = \frac{1}{2}\sum_{j=1}^{2} Q\left(\sqrt{P_t\gamma\chi_j|\hat{g}_{RL}|^2/(P_t\gamma\chi_j\sigma_e^2+1)}\right). \tag{4.21}$$

By using an alternative form of Q(.) function and the MGF, and after some algebraic manipulation, we can write (4.21) by

$$P_{R_L}^{U_1}(e) = \frac{1}{4}\sum_{j=1}^{2}\left(\sqrt{\frac{(P_t\gamma\chi_j E[|\hat{g}_{RL}|^2]/(P_t\gamma\chi_j\sigma_e^2+1))}{2+(P_t\gamma\chi_j E[|\hat{g}_{RL}|^2]/(P_t\gamma\chi_j\sigma_e^2+1))}}\right). \tag{4.22}$$

Likewise, we obtain the BER of s_2 at all relay nodes with ICSI as

$$P_{R_L}^{U_2}(e) = \frac{1}{2}\sum_{v=1}^{6}\kappa_v Q\left(\sqrt{P_t\gamma\aleph_v|\hat{g}_{RL}|^2/(P_t\gamma\daleth_v\sigma_e^2+1)}\right), \tag{4.23}$$

where $\daleth_v = [(\sqrt{\alpha_1}-\sqrt{\alpha_2})^2, (\sqrt{\alpha_1}+\sqrt{\alpha_2})^2, (\sqrt{\alpha_1}+\sqrt{\alpha_2})^2, (\sqrt{\alpha_1}+\sqrt{\alpha_2})^2, (\sqrt{\alpha_1}-\sqrt{\alpha_2})^2, (\sqrt{\alpha_1}-\sqrt{\alpha_2})^2]$.

By using an alternative form of the Q(.) function and the MGF), and after some algebraic manipulation, we write (4.23) by

$$P_{R_L}^{U_2}(e) = \frac{1}{4}\sum_{v=1}^{6}\kappa_v\left(\sqrt{\frac{(P_t\gamma\aleph_v E[|\hat{g}_{RL}|^2]/(P_t\gamma\daleth_v\sigma_e^2+1))}{2+(P_t\gamma\aleph_v E[|\hat{g}_{RL}|^2]/(P_t\gamma\daleth_v\sigma_e^2+1))}}\right). \tag{4.24}$$

During the last phase, the last relay detects signals, re-combines them into a new SC signal, and forwards it to the users. Hence, the BER of U_1 with ICSI can be expressed by

$$P^{U_1}(e) = \frac{1}{2}\sum_{j=1}^{2} Q\left(\sqrt{P_t\gamma\chi_j|\hat{h}_1|^2/(P_t\gamma\chi_j\sigma_e^2+1)}\right). \tag{4.25}$$

By using an alternative form of Q(.) function and the MGF, and after some algebraic manipulation, we can write (4.25) by

$$P^{U_1}(e) = \frac{1}{4}\sum_{j=1}^{2}\left(\sqrt{\frac{\left(P_t\gamma\chi_j E[|\hat{h}_1|^2]/(P_t\gamma\chi_j\sigma_e^2+1)\right)}{2+\left(P_t\gamma\chi_j E[|\hat{h}_1|^2]/(P_t\gamma\chi_j\sigma_e^2+1)\right)}}\right). \tag{4.26}$$

Also, the BER of U_2 with ICSI is given as

$$P^{U_2}(e) = \frac{1}{2}\sum_{v=1}^{6}\kappa_v Q\left(\sqrt{P_t\gamma\aleph_v|\hat{h}_2|^2/(P_t\gamma\daleth_v\sigma_e^2+1)}\right). \tag{4.27}$$

By using an alternative form of the Q(.) function and the MGF, and after some algebraic manipulation, we write (4.27) by

$$P^{U_2}(e) = \frac{1}{4}\sum_{v=1}^{6}\kappa_v\left(\sqrt{\frac{\left(P_t\gamma\aleph_v E[|\hat{h}_2|^2]/(P_t\gamma\daleth_v\sigma_e^2+1)\right)}{2+\left(P_t\gamma\aleph_v E[|\hat{h}_2|^2]/(P_t\gamma\daleth_v\sigma_e^2+1)\right)}}\right). \quad (4.28)$$

4.3 Cooperative NOMA assisted Multiple Relays with Direct Links

4.3.1 System Model

We consider a downlink MH-DF-CNOMA with DL consisting of one BS, U_1, and a group of relay named R_L, where $L = 1, 2, 3, ..., N$ which creates a way to U_1 as shown in Figure 4.2. We assume that U_1 is far from the BS. Our assumption is that only R_1 from the group of relays is capable of directly receiving the signal from the BS signal, while R_{L+1} facilitates forwarding the signal to U_1. We assume all node works in DF and HD modes. We suppose also the CSI between all nodes is imperfect. The Rayleigh fading channel coefficient of R_L links is denoted by $g_{RL} \sim \mathcal{CN}(0, \sigma_{RL}^2 = d_{RL}^{\varsigma})$ and the Rayleigh fading channel coefficient of the U_1 link is denoted by $h_1 \sim \mathcal{CN}(0, \sigma_1^2 = d_1^{\varsigma})$. The channel estimation coefficients are presented as $\hat{g}_{RL} = g_{RL} - e \sim \mathcal{CN}(0, \hat{\sigma}_{RL}^2 = \sigma_{RL}^2 - \sigma_e^2)$ and $\hat{h}_1 = h_1 - e \sim \mathcal{CN}(0, \hat{\sigma}_1^2 = \sigma_1^2 - \sigma_e^2)$, where e is the error factor of the channel estimation, d_1 is the distance between BS-U_1, d_{R1} is the distance between BS-R_1, and ς is the path loss factor.

In this system, We consider that the BS transmits as an SC signal consisting of s_1 and s_2 to U_1 and R_1 directly. U_1 detect its signal directly while R_1 uses the SIC to detect s_1 and s_2 signals. We suppose that the R_1 re-encode the U_1 signal (s_1) and forward it to R_{L+1} until it reaches U_1 (see Figure 4.2). The power of the BS and relay nodes R_L are assumed to be equal and named P_t. The received signals at U_1 and R_1 can be written, respectively, as

$$y_1 = \sqrt{P_t}\ (\hat{h}_1 + e)\ (\sqrt{\alpha_1}s_1 + \sqrt{\alpha_2}s_2) +\ n, \quad (4.29)$$

$$y_{R1} = \sqrt{P_t}\ (\hat{g}_{R1} + e)\ (\sqrt{\alpha_1}s_1 + \sqrt{\alpha_2}s_2) +\ n, \quad (4.30)$$

where α_1 and α_2 are the power allocation coefficient for U_i, i=1, 2, $\alpha_1 > \alpha_2$ in which $\alpha_1 + \alpha_2 = 1$.

The U_1 decodes its signal using MLD while the R_1 nodes decode the s_1 signal first then using the SIC decodes the s_2 signal. The SINRs of the decoded signals at U_1 and R_1 under ICSI and ISIC can be expressed, respectively, by

$$\gamma_{1,s_1} = \frac{P_t\alpha_1|\hat{h}_1|^2}{P_t\alpha_2|\hat{h}_1|^2 + P_t\sigma_e^2 + \sigma^2}, \quad (4.31)$$

$$\gamma_{2,s_1} = \frac{P_t\alpha_1|\hat{g}_1|^2}{P_t\alpha_2|\hat{g}_1|^2 + P_t\sigma_e^2 + \sigma^2}, \quad (4.32)$$

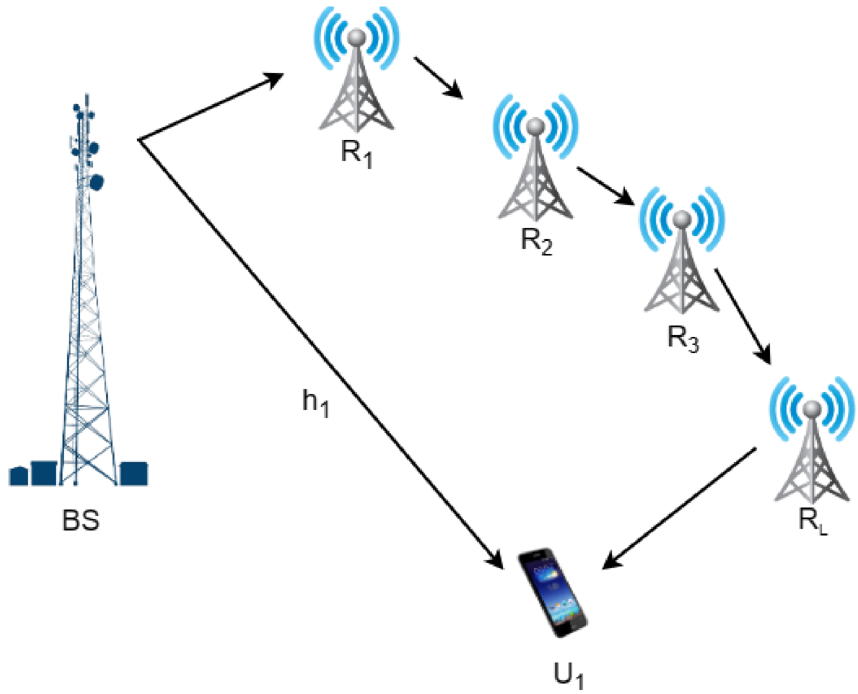

Figure 4.2: *MH-DF-CNOMA with DL scheme.*

$$\gamma_{2,s_2} = \frac{P_t \alpha_2 |\hat{g}_1|^2}{\varrho P_t \alpha_1 |\hat{g}_1|^2 + P_t \sigma_e^2 + \sigma^2}, \tag{4.33}$$

where ϱ is the factor of ISIC.

The R_1 re-encode s_1 and forward it over the path of R_{L+1} to U_1. Thus, s_1 is decoded and forwarded over R_{L+1} until reaches U_1. The received signal at R_{L+1} and U_1 over L hop under ICSI can be expressed by

$$y_{L+1} = \sqrt{P_t}\ (\hat{g}_{R(L+1)} + e)\ s_1 + \ n, \tag{4.34}$$

where $\hat{g}_{R(L+1)} = g_{R(L+1)} - e \sim \mathcal{CN}(0, \hat{\sigma}^2_{R(L+1)} = \sigma^2_{R(L+1)} - \sigma_e^2)$ is channel estimation coefficient of between R_1-R_2 and R_{L-1}-R_L. $d_{R(L+1)}$ is the distance between R_1-R_2 and R_{L-1}-R_L.

The R_{L+1} and U_1 decodes s_1 signal using the MLD. In practical scenarios, the CSI is not imperfect. Therefore, the decoding error is expected in the detection and SIC process. Thus, the SINR of the decoded signals at R_{L+1} and U_1 under ICSI and ISIC can be expressed by

$$\gamma_{L+1,s_1} = \frac{P_t |\hat{g}_{R(L+1)}|^2}{P_t \sigma_e^2 + \sigma^2}. \tag{4.35}$$

4.3.2 Performance Analysis

4.3.2.1 Outage Probability

The user U_1 uses MRC to combine the two received signals (directly from BS and indirectly from $R(L+1)$) to improve the received signal quality. The OP expression of U_1 using the MRC is given as [68] by

$$\begin{aligned} P_{MRC,U1}(out) =&(1 - P_{BS-L}(out))P(\gamma_{1,s_1} + \gamma_{L+1,s_1} < \theta_1^{(L)}) \\ &+ P_{BS-L}(out)P(\gamma_{1,s_1} < \theta_1^{(L)}), \end{aligned} \tag{4.36}$$

where $P_{BS-L}(out)$ is the OP of s_1 at U_1 over the path of R_L, $P(\gamma_{BS1,s_1} < \theta_1)$ is the OP of s_1 at U_1 in the direct like, and $P(\gamma_{1,s_1} + \gamma_{L+1,s_1} < \theta_1^{(L)})$ is the OP of s_1 at U_1 when MRC is implemented $\theta_1^{(L)} = 2^{Tr_1(L)} - 1$. We calculate each term of (4.36) as

$$P(\gamma_{1,s_1} < \theta_1^{(L)}) = 1 - exp\left(-\frac{(P_t\sigma_e^2 + \sigma^2)\theta_1^{(L)}}{(\alpha_1 - \alpha_2\theta_1^{(L)})P_tE[|\hat{h}_1|^2]}\right). \tag{4.37}$$

$P_{BS-L}(out)$ is the e2e OP of s_1 at R_L over L hop, so the e2e OP of 2 hops can be calculated as

$$P_{BS-2}(out) = \left(1 - P_{BS-R_1}(out)\right) P_{R_1-R_2}(out) + P_{BS-R_1}(out) \left(1 - P_{R_1-R_2}(out)\right). \tag{4.38}$$

For more than two hops i.e., $L > 2$, the e2e OP of s_1 at R_L can be expressed as

$$P_{BS-L}(out) = \left(1 - P_{BS,R_{L-1}}(out)\right) P_{R_{L-1}-R_L}(out) + P_{BS,R_{L-1}}(out) \left(1 - P_{R_{L-1}-R_L}(out)\right). \tag{4.39}$$

Note: If $L = 1$ which means that R_1, the OP of BS-R_1 can be calculated as in (4.37).

Each term in (4.38) and (4.39) can be calculated in general as

$$P_{R_{L-1}-R_L}(out) = P_{BS-R_1,L}(out) = 1 - exp\left(-\frac{(P_t\sigma_e^2 + \sigma^2)\theta_1^{(L)}}{(\alpha_1 - \alpha_2\theta_1^{(L)})P_tE[|\hat{g}_{RL}|^2]}\right). \tag{4.40}$$

By substituting (4.40) into (4.38) and (4.39), we find the e2e OP of s_1 at R_L over L hop.

The last R_L forward s_1 to U_1. Thus, the U_1 implements the MRC to combine the received signal. Since γ_{BS1,s_1} and γ_{L+1,s_1} are two independent random variables, where $\gamma_{BS1,s_1} \neq \gamma_{L+1,s_1}$, so $P(\gamma_{BS1,s_1} + \gamma_{L+1,s_1} < \theta_1^{(L)})$ can be computed as [68]

$$P(\gamma_{1,s_1} + \gamma_{L+1,s_1} < \theta_1^{(L)}) =1 - \left[\frac{\tau_a}{\tau_a - \tau_b} \exp\left(-\tau_a\theta_1^{(L)}\right) + \frac{\tau_b}{\tau_b - \tau_a} \exp\left(-\tau_b\theta_1^{(L)}\right)\right], \quad \tau_a \neq \tau_b, \tag{4.41}$$

where $\tau_a = \frac{P_t\sigma_e^2+\sigma^2}{(\alpha_1-\alpha_2\theta_1^{(L)})P_tE[|\hat{h}_1|^2]}$, and $\tau_b = \frac{P_t\sigma_e^2+\sigma^2}{P_tE[|\hat{g}_{R(L+1)}|^2]}$.

The e2e OP of s_1 using MRC is obtained by substituting (4.37), (4.38), (4.39), and (4.41) into (4.36).

4.3.2.2 Bit Error Rate

In the MH-DF-CNOMA with DL, after the R_1 detects the transmitted symbols, it re-encodes the s_1 symbol and forwards it to R_{L+1}. In this case, the U_1 receives its signal s_1 from two different sources (i.e., BS and R_L). Hence, we consider that U_1 implements the diversity combining technique MRC to improve its received signal quality. We obtain the e2e BER expression of MH-DF-CNOMA with DL for U_1 as in [45, 66, 90] by

$$P_{e2e,CNOMA-DL}(e) = \frac{1}{2}\sum_{j=1}^{2}[P_{prop,MH}(e|j) \times P_{e2e,s_1,(L)hop}(e|j) + (1 - P_{e2e,s_1,(L)hop}(e|j))P_{coop,MH}(e|j)], \tag{4.42}$$

where $P_{prop,MH}(e|j)$ is the BER in the presence of error propagation from R_L to U_1 achieved by the MRC to users achieved by the MRC, $P_{e2e,s_1,(L)hop}(e|j)$ is the BER of the s_1 at R_L, and $P_{coop,MH}(e|j)$ is the BER when the symbols of U_1 are detected correctly at the R_L and forwarded to the U_1 and then combined with MRC. Each term of (4.42) is calculated below.

The e2e BER of $P_{e2e,s_1,(L)hop}(e|j)$ for two hops i.e., BS-R_1-U_1 is given as in [90, 91] by

$$P_{e2e,s_1,(2)hop}(e|j) = P_{R_1,s_1}(e|j)\ (1 - P_{R_2,s_1}(e|j)) + P_{R_2,s_1}(e|j)\ (1 - P_{R_1,s_1}(e|j)). \tag{4.43}$$

Further, for more than two hops i.e., $L > 2$ (BS-R_{L-1}-R_L), we express e2e BER of L hops as in [90, 91] by

$$P_{e2e,s_1,(L)hop}(e|j) = \underbrace{P_{e2e,s_1,(L-1)hop}(e|j)}_{\iota_1}\ (1 - P_{R_L,s_1}(e|j)) + P_{R_L,s_1}(e|j)\ (1 - \underbrace{P_{e2e,s_1,(L-1)hop}(e|j)}_{\iota_1}), \tag{4.44}$$

where ι_1 is the e2e BER from BS to R_{L-1} which can be expressed as

$$P_{e2e,s_1,(L-1)hop}(e|j) = P_{R_L,s_1}(e|j)\ (1 - P_{e2e,s_1,(L-1)hop}(e|j)) + P_{e2e,s_1,(L-1)hop}(e|j)\ (1 - P_{R_L,s_1,s_1}(e|j)). \tag{4.45}$$

Each term of (4.43), (4.44), and 4.45) can be calculated by

$$P_{R_L,s_1}(e|j) = \frac{1}{2}Q\left(\sqrt{P_t\gamma\chi_j|\hat{g}_{R_L}|^2/(P_t\gamma\chi_j\sigma_e^2 + 1)}\right). \tag{4.46}$$

where $\chi_j = [(\sqrt{\alpha_1} + \sqrt{\alpha_2})^2, (\sqrt{\alpha_1} - \sqrt{\alpha_2})^2]$,

By using an alternative form of the Q(.) function and the MGF, and after some algebraic manipulation, we can write (4.46) by

$$P_{R_L,s_1}(e|j) = \frac{1}{4}\left(\sqrt{\frac{(P_t\gamma\chi_j E[|\hat{g}_{R_L}|^2]/(P_t\gamma\chi_j\sigma_e^2+1))}{2+(P_t\gamma\chi_j E[|\hat{g}_{R_L}|^2]/(P_t\gamma\chi_j\sigma_e^2+1))}}\right). \tag{4.47}$$

The e2e BER of s_1 over the path of R_L is obtained by substituting (4.47) and (4.45) into (4.44).

Since the U_1 receives its signal from BS and, the U_1 employs MRC, the total SNR is the sum of the SNRs after combining the two received signals. Hence, the BER of the cooperative when the MRC is implemented at U_1 is calculated by

$$P_{coop,MH}(e|j) = Q\left(\sqrt{2\left(\gamma_{Lhop,s1}+\gamma_{1,s1,j}\right)}\right), \tag{4.48}$$

where $\gamma_{Lhop,s1} = P_t\gamma|\hat{g_{R_L}}|^2/(P_t\gamma\sigma_e^2+1)$ and $\gamma_{1,s1,j} = P_t\gamma\chi_j|\hat{h}_1|^2/(P_t\gamma\chi_j\sigma_e^2+1)$.

The ABER of the cooperative of two branches using MRC over Rayleigh fading in (4.48) when the mean of the SNRs of branches are different $\overline{\gamma}_{Lhop,s1} \neq \overline{\gamma}_{1,s1,j}$ as given in [92] by

$$P_{coop,MH}(e|j) = \frac{1}{2}\left(1-\frac{1}{\overline{\gamma}_{1,s1,j}-\overline{\gamma}_{Lhop,s1}}\left(\overline{\gamma}_{1,s1,j}\sqrt{\frac{\overline{\gamma}_{1,s1,j}}{1+\overline{\gamma}_{1,s1,j}}}-\overline{\gamma}_{Lhop,s1}\sqrt{\frac{\overline{\gamma}_{Lhop,s1}}{1+\overline{\gamma}_{Lhop,s1}}}\right)\right), \tag{4.49}$$

where $\overline{\gamma}_{Lhop,s1} = P_t\gamma E[|\hat{g}_{R_L}|^2]/(P_t\gamma\sigma_e^2+\sigma^2)$ and $\overline{\gamma}_{1,s1,j} = P_t\gamma\chi_j E[|\hat{h}_1|^2]/(P_t\gamma\chi_j\sigma_e^2+\sigma^2)$.

After utilizing MRC at U_1, the incoming signals from BS and over the path of R_L are summed. If R_L (i.e., the last one) detects the symbol of U_1 erroneously, it will be forwarded to U_1 as an error propagation. Hence, the received signals will be combined at U_1 using MRC in the case of error propagation. Thus, the BER using MRC with error propagation at the U_1 is given as in [92] by

$$P_{Prop,MH}(e|j) = \frac{\overline{\gamma}_{Lhop,s1}}{\overline{\gamma}_{Lhop,s1}+\overline{\gamma}_{1,s1,j}}. \tag{4.50}$$

The e2e BER of MH-DF-CNOMA with DL using MRC is obtained by substituting (4.50), (4.49), and (4.44) into (4.42).

4.4 Numerical Results

In this section, we validate the analytical expressions of the previous section using the Mont-Carlo simulation.

4.4.1 Cooperative NOMA assisted Multiple Relays Without Direct Links

The parameters used in the simulation are as follows, d_L=1 m ,d_1=2 m, d_2=1 m, ς=4, α_1=0.85, α_2=0.15, ϱ=0.001 and σ_e^2=0.01. The curves denote simulations, and markers represent the analytical derivation in our results. It can be easily observed that our derivations are matched perfectly

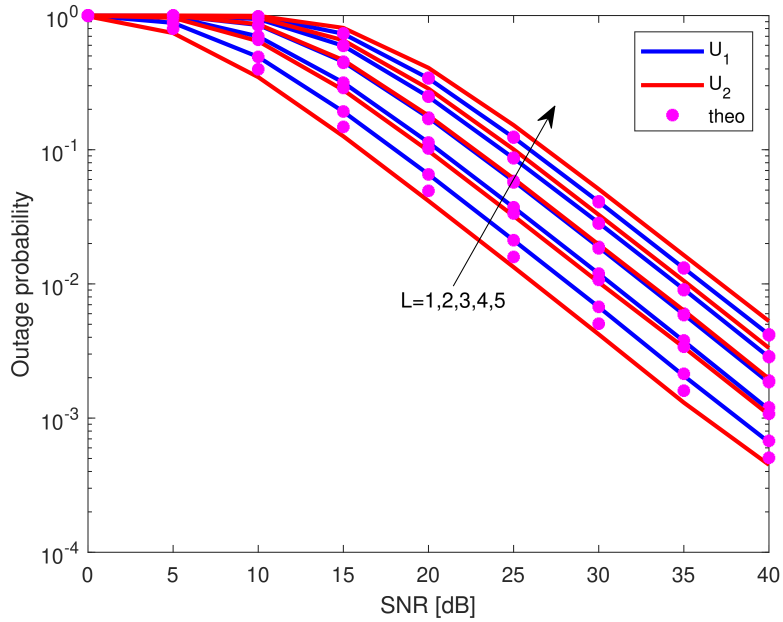

(a)

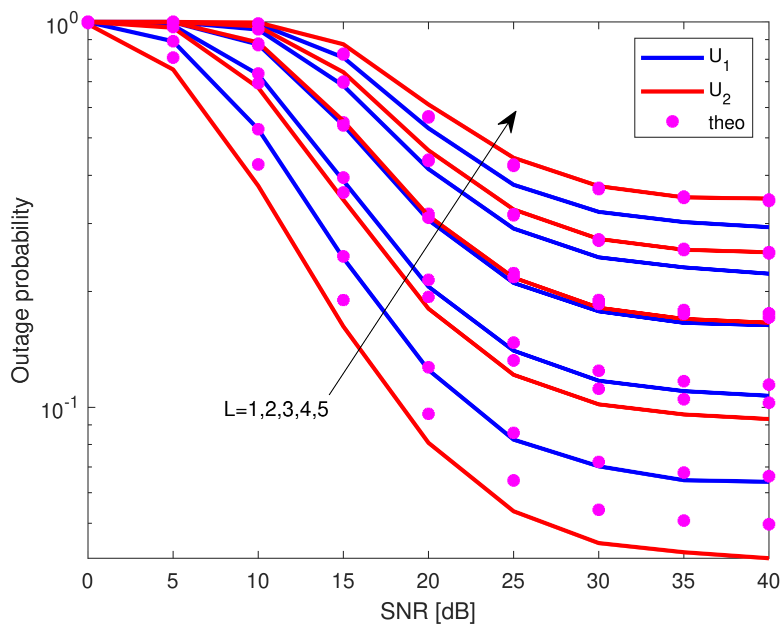

(b)

Figure 4.3: *OP of MH-DF-CNOMA WDL w.r.t. SNR: (a) With perfect CSI, (b) With ICSI.*

with the simulations that validate our derivations.

In Figure 4.3, we present the OP of MH-DF-CNOMA WDL with perfect CSI and ICSI when Tr_1=Tr_2=0.1. We observe that the OP of the two users worsens as the number of relays increases in the two scenarios of CSI, where an error floor occurs in the case of ICSI. It is observed also the performance of U_1 was better than U_2 when $L > 2$, and as the number of relays increased, the degradation of U_2 was more than U_1. It can be explained as follows. The detection of U_2 signal depends on the SIC process. In other words, the outage of the U_2 signal depends on whether the detection of the U_1 signal is better or not i.e., the outage of the U_1 signal is less or bigger. Also, the forwarding signals in the following phases are according to the signals detection of the earlier phases i.e., the outage performance of the users will increase when the reliability of the detection decreases at each phase. Hence, decreasing the reliability of the detection means the error is growing with each phase, which affects the SIC process.

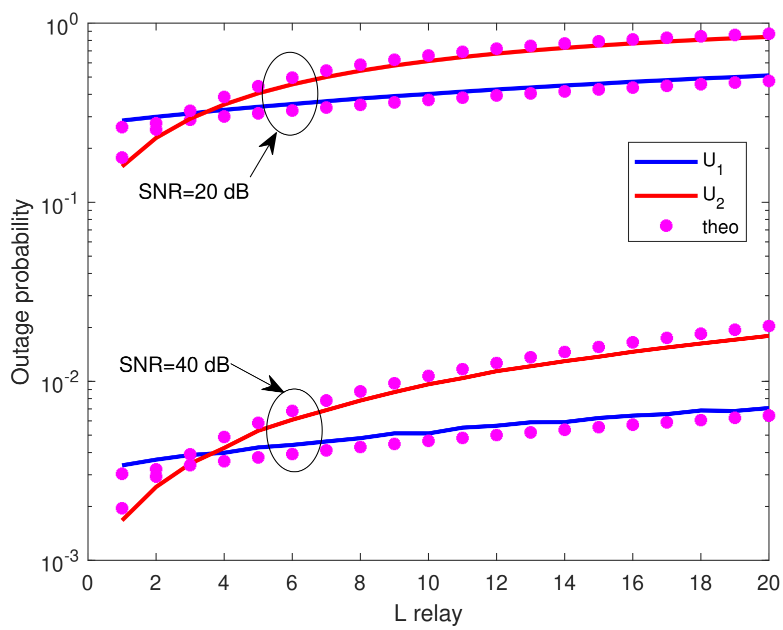

Figure 4.4: *OP of MH-DF-CNOMA WDL w.r.t. L relay.*

To evaluate the effect of the number of relays on the OP performance, in Figure 4.4, we present the OP performance of the MH-DF-CNOMA WDL w.r.t. L relay when $\theta_1^{(L+1)} = \theta_2^{(L+1)} = 1.2$. We observe that the OP performance gets worse as the number of relays increases. Again, it can be seen that the OP performance of U_2 deteriorates more than U_1 when $L > 4$. This is due to the SIC process at each node and the power allocation coefficient of each user. The SIC process is affected at each hop because it always depends on whether the U_1 signal is detected correctly or not. Furthermore, the SIC process is affected at each hop because the signal detected is forwarded with its errors at each phase, so the error detection of all phases will move and increase with the signals until reach the users. Moreover, increasing SNR improves the OP performance of two users.

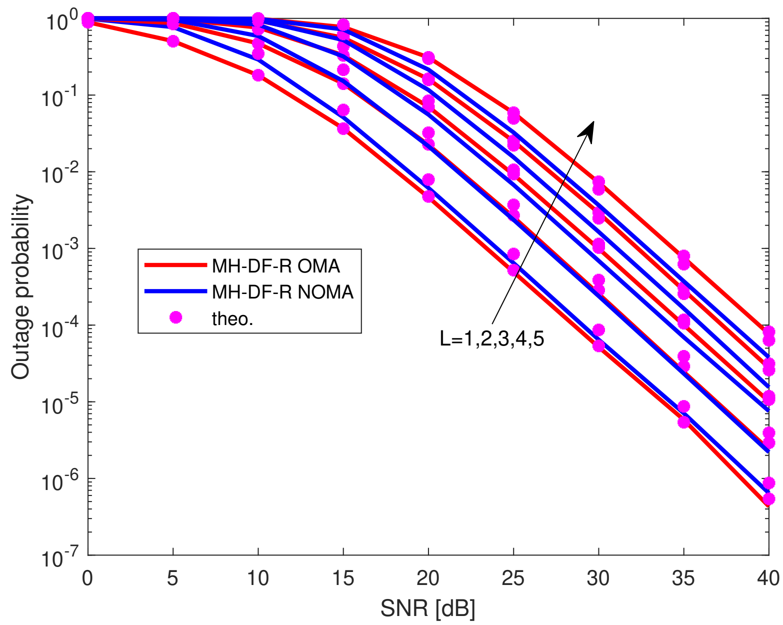

Figure 4.5: *OP of MH-DF-CNOMA WDL vs MH-DF-COMA WDL with different relays*

To compare our model with COMA, we suppose that the threshold of our model is $\theta_1^{(L+1)} = 2^{Tr_1(L+1)} - 1$ and $\theta_2^{(L+1)} = 2^{Tr_2(L+1)} - 1$, and for OMA is $\theta_{OMA}^{(2L+2)}{}_1 = 2^{Tr_1(2L+2)} - 1$ and $\theta_{OMA}^{(2L+2)}{}_2 = 2^{Tr_2(2L+2)} - 1$. We use these parameters in Figure 4.5 and Figure 4.6, it's assumed that the transmit power is to be half of the total power, α_1=0.8, α_2=0.2, and Tr_1=Tr_2= 0.2. In Figure 4.5, we compare the OP of MH-DF-CNOMA WDL with conventional MH-DF-OMA WDL. We observe that the OP of MH-DF-COMA is superior to MH-DF-CNOMA in the first hop. when $L > 1$, the OP of MH-DF-CNOMA is suprior to MH-DF-COMA. It can be explained as follows. The difference in the time slot to transmit the signals from BS to the users is lower in MH-DF-CNOMA compared to MH-DF-COMA. MH-DF-COMA needs a (2L+2) time slot to transmit the signals to the users while MH-DF-CNOMA needs an (L+1) time slot. To confirm the superiority of our proposed scheme, in Figure 4.6, we present a comparison between the OP of MH-DF-CNOMA and the conventional MH-DF-COMA for one relay. It can be seen that our proposed scheme achieves high-performance gain compared to MH-DF-COMA.

On the other hand, Figure 4.7, presents the BER of MH-DF-CNOMA WDL with perfect CSI and ICSI. We observe that BER performance degrades as the number of hops increases with perfect

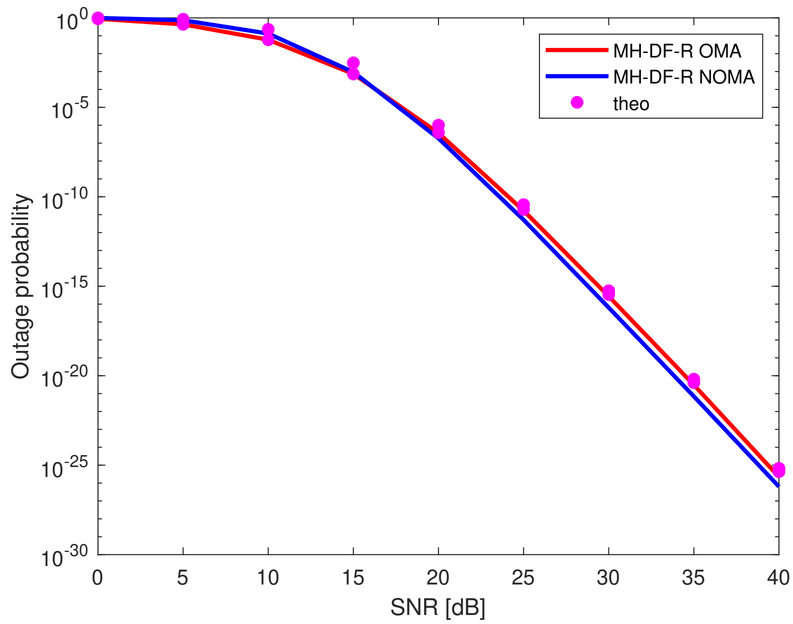

Figure 4.6: *OP of MH-DF-CNOMA WDL vs MH-DF-COMA WDL for one relay*

CSI and ICSI. The ICSI degrades the BER performance of the users and causes an error floor at the high SNR. In Figure 4.7 (a), in the perfect CSI case: The U_2 achieves better performance gain in the first two hops, while the performance of the U_1 was better than U_2 when $L > 2$. In Figure 4.7 (b), in the case of ICSI: The U_2 was better than U_1 only in the first hop, while the U_1 was better when $L > 1$. It is observed that the ICSI affected the performance of the U_2 more than U_1 when $L > 1$. The ICSI causes more errors in the detection of users' signals and the SIC process. Thus, the error will be transmitted with the next hops, and the error will grow. Hence, it affects the SIC process and the signals detected at each node.

To evaluate the effect of relay number, Figure 4.8 presents the BER performance of MH-DF-CNOMA WDL w.r.t. L relay when SNR= 20 dB, 40 dB. It is observed that the BER performance gets worse as the number of relays increases. Also, the BER performance of U_2 degrades more than U_1 where when $L > 3$ and SNR=20 dB and $L > 4$ and SNR=40 dB, the BER of U_1 is better than U_2. To detect the U_2 signals, all nodes need to perform the SIC process. The U_2 is detected based on the detection of the U_1 signal at each hop. The signal transmission over each hop until reaching the users will increase the error of SIC operation. Hence, the U_2 signal is affected more than the U_1 signal because U_1 signal detection does not depend on the SIC. It is observed also increasing SNR improves the performance of the users.

Figure 4.9, presents the BER of MH-DF-CNOMA WDL w.r.t. α_2 when SNR=20 dB, 40 dB.

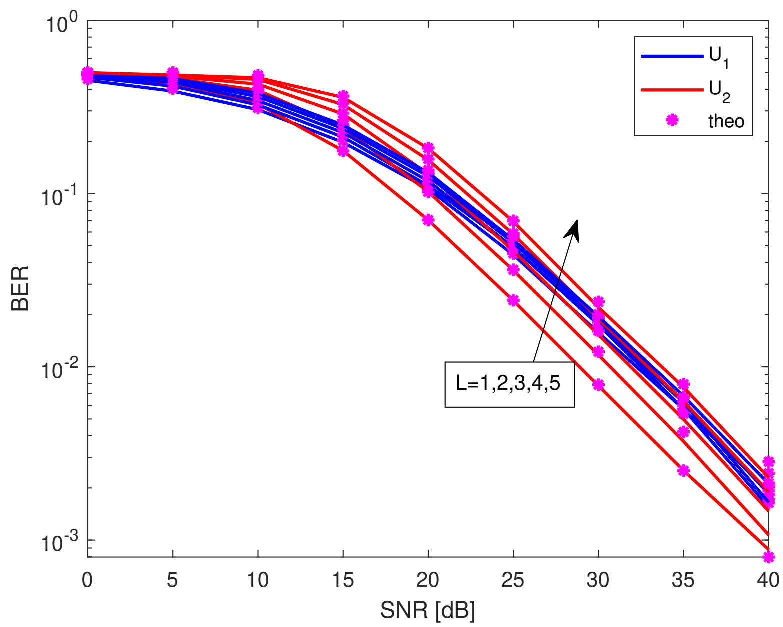

(a)

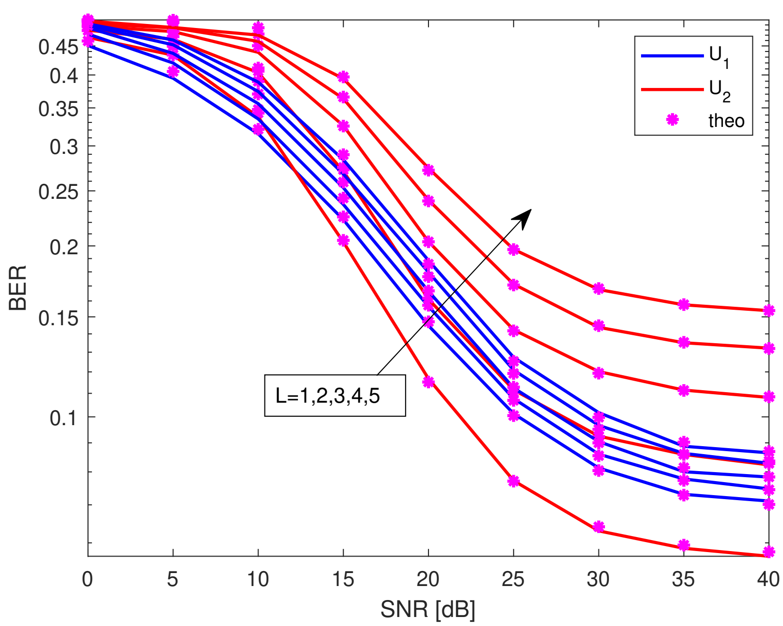

(b)

Figure 4.7: *BER of MH-DF-CNOMA WDL w.r.t. SNR: (a) With perfect CSI, (b) With ICSI.*

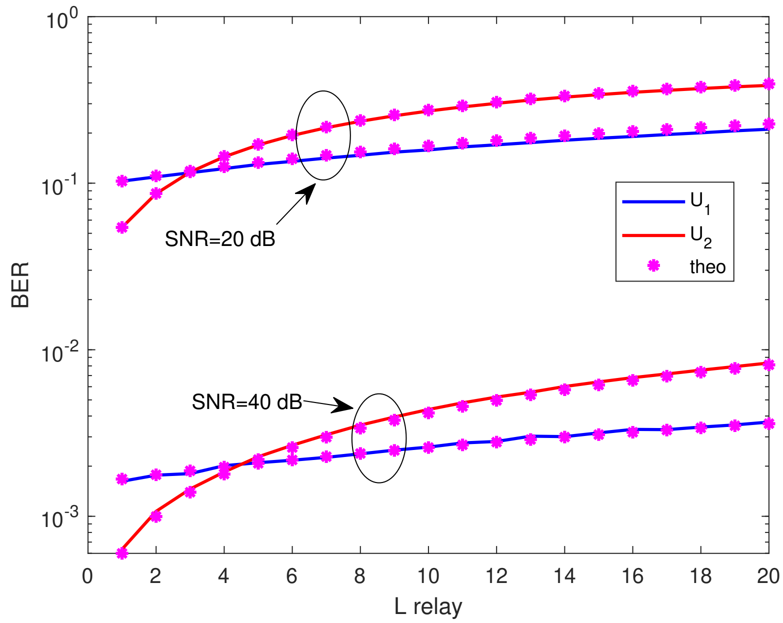

Figure 4.8: *BER of MH-DF-CNOMA WDL w.r.t. L relay.*

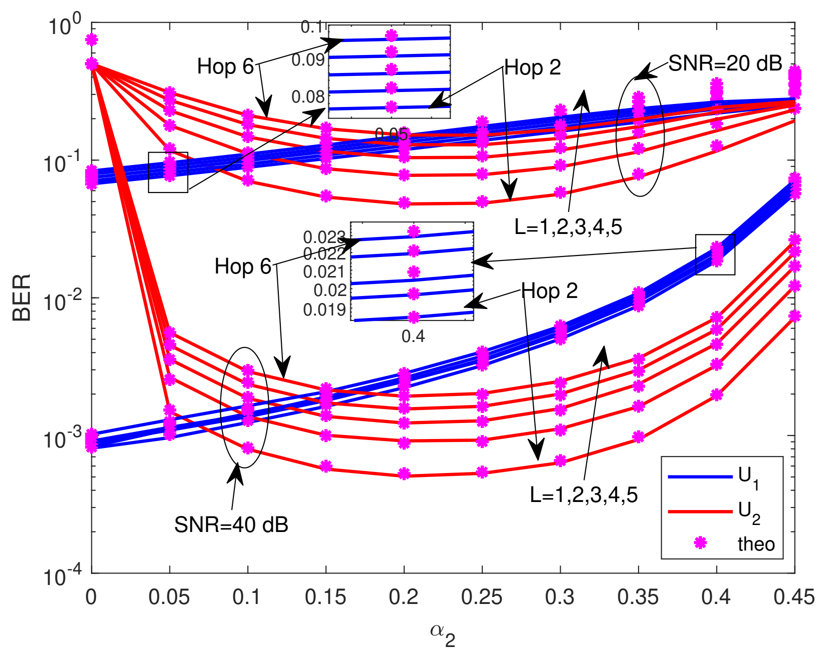

Figure 4.9: *BER of MH-DF-CNOMA WDL w.r.t. α_2 with different relays.*

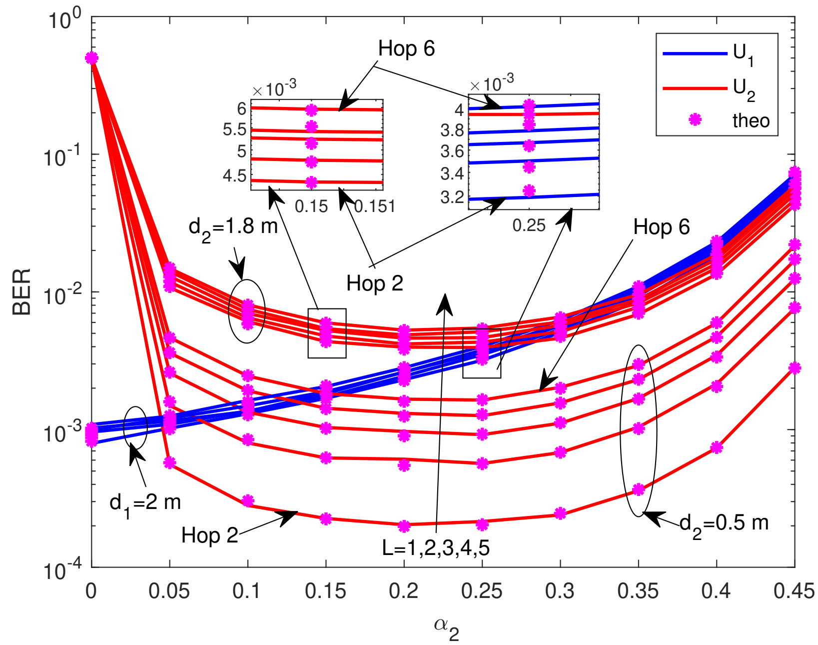

Figure 4.10: *BER of MH-DF-CNOMA WDL w.r.t. α_2 with different different distances between R_L and U_2.*

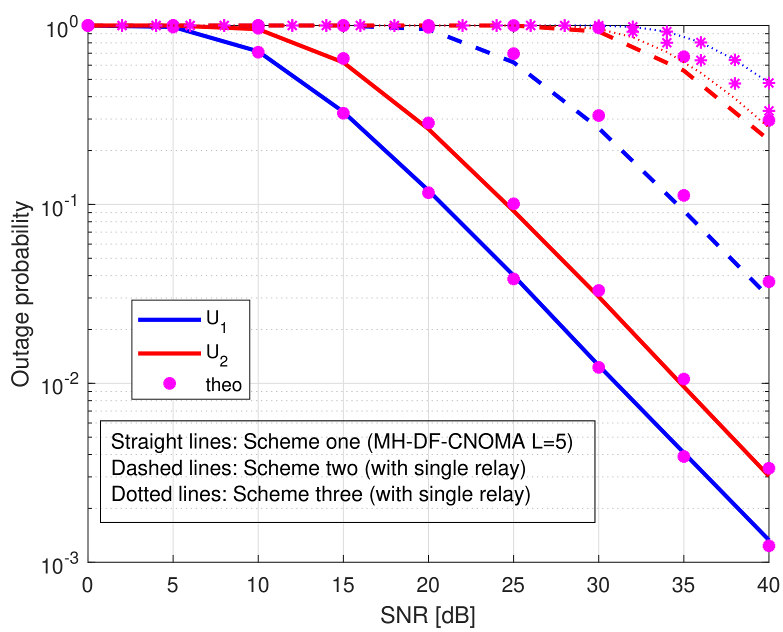

Figure 4.11: *OP of MH-DF-CNOMA WDL compared to single relay scheme.*

We observe that the change of α_2 affects one user at the expense of another. The change of α_2 affects the SIC process and the detection of the U_2 signal. It is observed again that increasing relays reduces the performance of the users. Also, increasing SNR improves the BER performance of the users. In MH-DF-CNOMA WDL, it is important to choose the value of α_2 carefully to ensure reaching the signals to the destination with good quality.

Table 4.1: Distances used for schemes.

	Distances
scheme one (MH-DF-CNOMA)	$d_{RL}= 1m, d_1 = 2$m, $d_2 = 1$m
scheme two (with single relay)	$d_{R1} = 5$m, $d_1 = 2$m, $d_2 = 1$m
scheme three (with single relay)	$d_{R1} = 1$m, $d_1 = 6$m, $d_2 = 5$m

To demonstrate the impact of α_2 in detail, Figure 4.10 presents the BER w.r.t. α_2 with different distances $d_2 = 0.5$ m, 1.8 m, $d_1 = 2$ m when SNR= 40 dB. We observe that increasing relays degrades the BER performance in all α_2 values. It can be seen that reducing the distance of U_2 improves its BER performance. Hence, to acquire an optimum value of α_2 in the MH-DF-CNOMA WDL should be adapted according to the transmit SNR and channel conditions.

To show the superiority of the MH-DF-CNOMA WDL over a single relay scheme, we compare our proposed system with two possible schemes for a single relay (i.e., scheme two and scheme three). Scheme one: MH-DF-CNOMA WDL (we use 5 relays $L = 5$). Scheme two: The relay is far from the BS and near to the users. In Scheme three, the relay is near the BS and far from the users. Thus, the parameters used for each scheme are presented in Table. 4.1.

In Figure 4.11 and Figure 4.12, we present a comparison of our proposed scheme with a single relay NOMA scheme in terms of the OP and BER. In these figures, it is observed that our proposed scheme achieves higher performance gain compared to the two cases of a single relay NOMA scheme. Also, scheme two is superior to scheme three. The near distance of the relay increases the error of the second phase at the users because the distance of this phase is bigger (i.e., the channel is poor). On the contrary, the poor channel of the first phase means the relay receives the signals with more errors and will forward the signals to the users with these errors.

4.4.2 Cooperative NOMA Assisted Multiple Relay with Direct Links

The simulation parameters of [66] are used to evaluate the performance gain of our proposed system. Thus, the distance parameters of the simulation of [66] and our system are presented in Table. 4.2

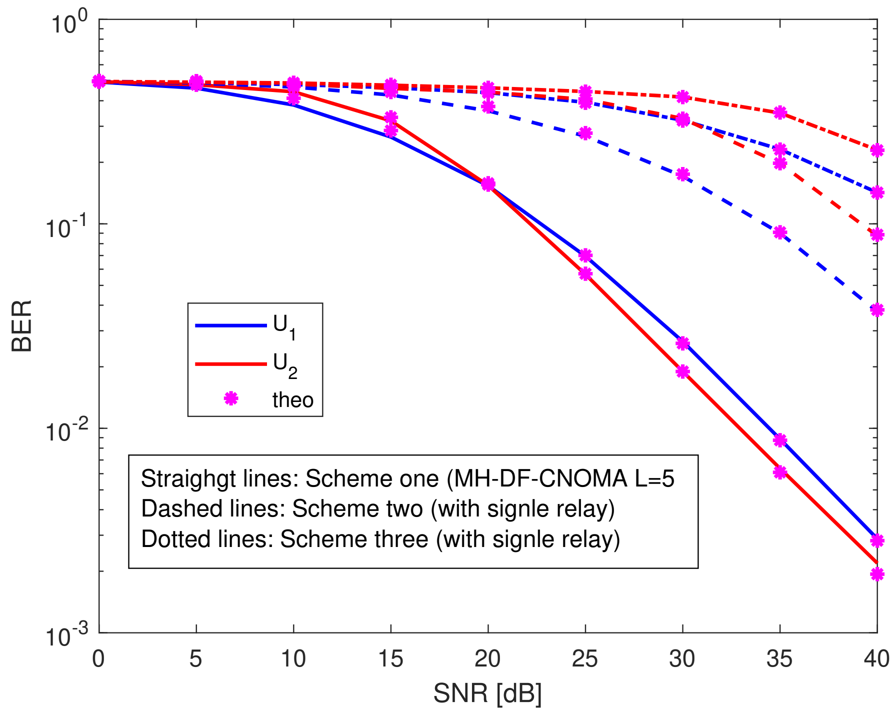

Figure 4.12: *BER of MH-DF-CNOMA WDL compared to single relay scheme.*

Table 4.2: Distances used for scenarios.

	Distances
Scenario I	d_1=5, d_{R1}=1, d_{R2}=4
Scenario II	d_1=5, d_{R1}=1, d_{R2}=2, D_{R3}=2
Scenario III	d_1=5, d_{R1}=1, d_{R2}=1.5, d_{R3}=1.5, d_{R4}=1
Scenario IV	d_1=5, d_{R1}=1, d_{R2}=1, D_{R3}=1, d_{R4}=1, d_{R5}=1
Scenario V ([66])	d_1=5, d_{R1}=2.5, d_{R2}=2.5

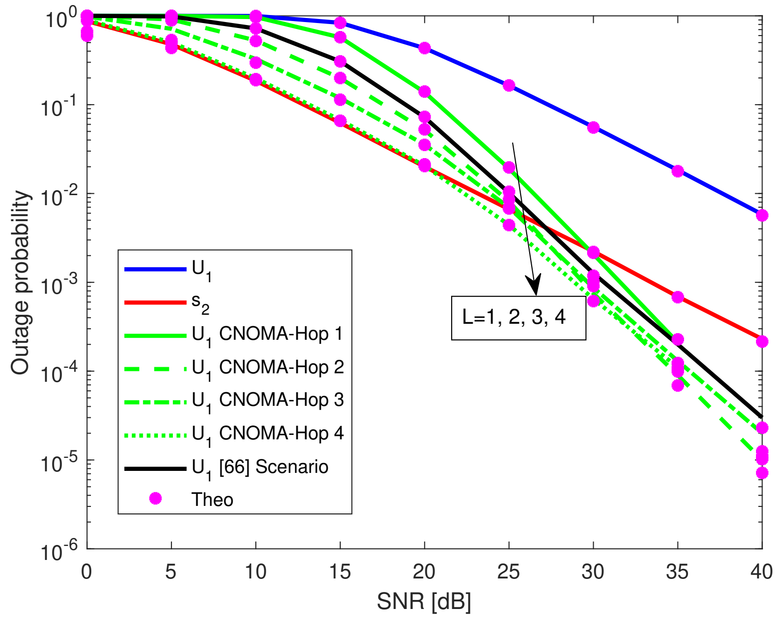

(a)

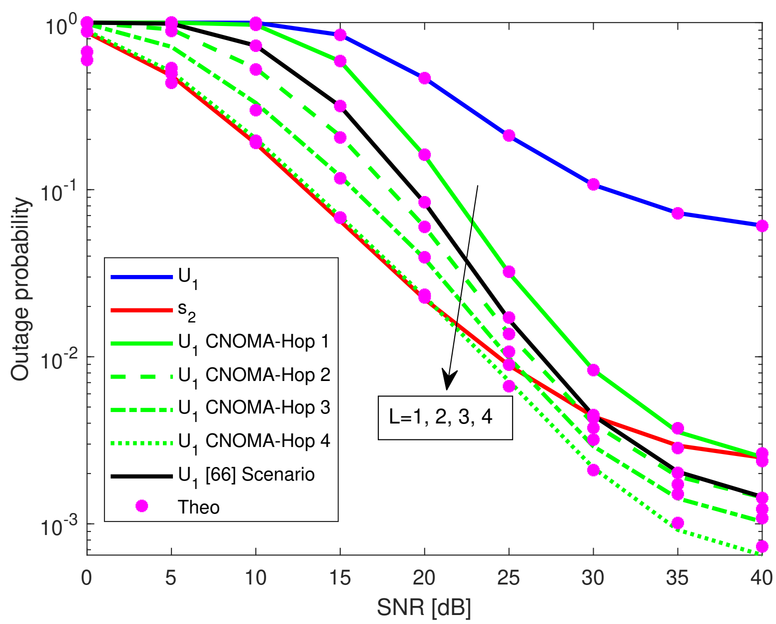

(b)

Figure 4.13: OP of MH-DF-CNOMA with DL w.r.t. SNR: (a) With perfect CSI, (b) With ICSI.

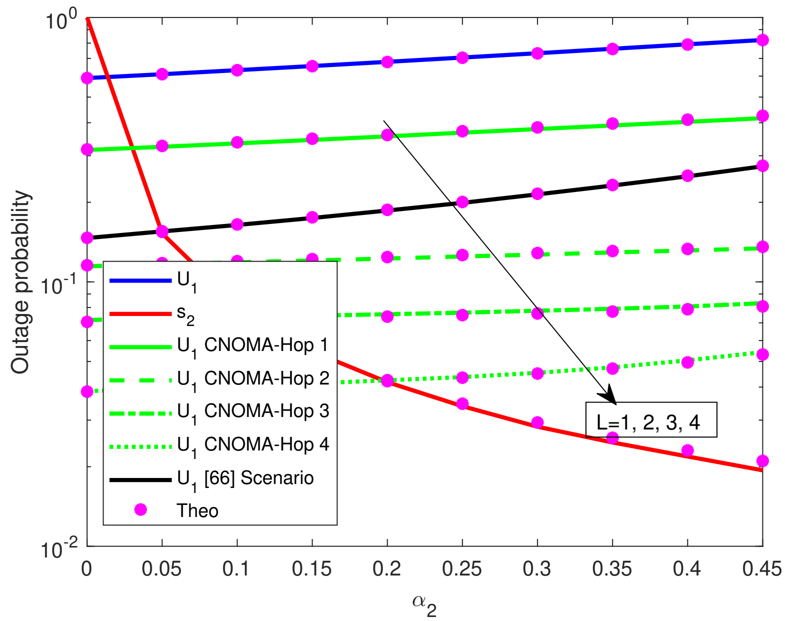

Figure 4.14: *OP of MH-DF-CNOMA with DL w.r.t. α_2 with different relay.*

As we can see through Table. 4.2, the relays are placed differently, where users are distributed almost with equal distances between them until reaching U_1. The fixed simulation parameters are presented as follows, ς=3, α_1=0.8, α_2=0.2, ϱ=0.001, and σ_e^2=0.001. The curves denote simulations, and markers represent the analytical derivation in our results. It can be easily observed that our derivations are matched perfectly with the simulations that validate our derivations.

In Figure 4.13, we present the OP performance of MH-DF-CNOMA with DL under perfect CSI, ICSI, SIC, and ISIC. We observe that the proposed scheme improved the performance of U_1. It is observed also the OP of our proposed scheme improved as the number of relays increased. It can be easily seen that the proposed scheme achieves higher performance gain compared to [66]. Figure 4.13 (b) presents the OP performance of our system under ICSI and ISIC. It is observed that in the presence of ICSI and ISIC, the OP performance of our proposed system deteriorates compared to the perfect case in Figure 4.13 (a) and causes an error floor at the high SNR.

To evaluate the effect of power allocation on the performance of our proposed system, Figure 4.14, presents the OP of MH-DF-CNOMA with DL when SNR= 20 dB. It is observed that increasing α_2 decreases the OP of s_2 and increases the performance of U_1. Also, increasing the number of relays improves the performance of our system. It can be seen that the OP performance of our proposed system achieves higher performance gains compared to [66] in all power allocation values.

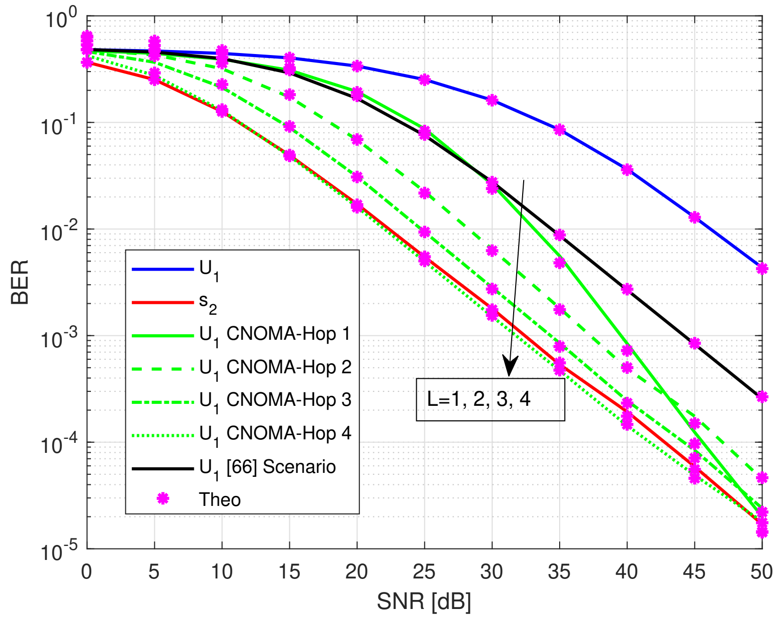

(a)

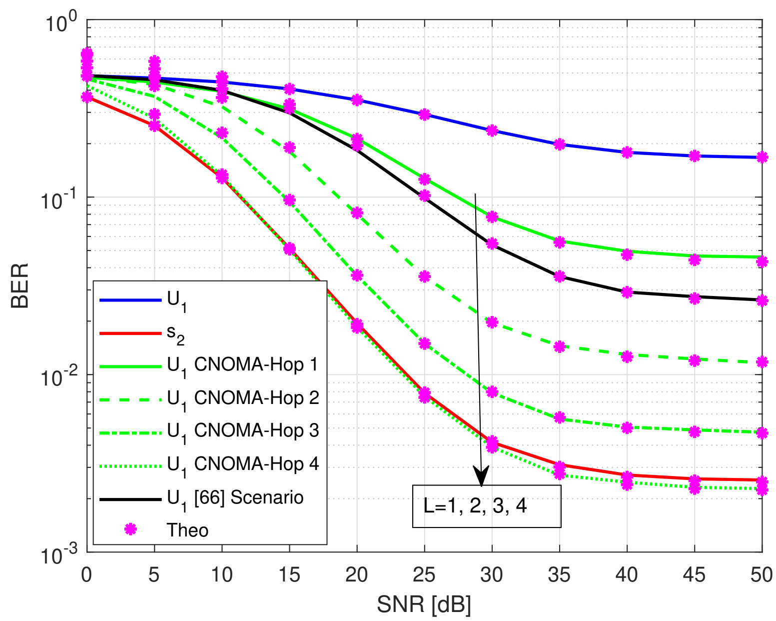

(b)

Figure 4.15: BER of MH-DF-CNOMA with DL w.r.t. SNR: (a) With perfect CSI, (b) With ICSI.

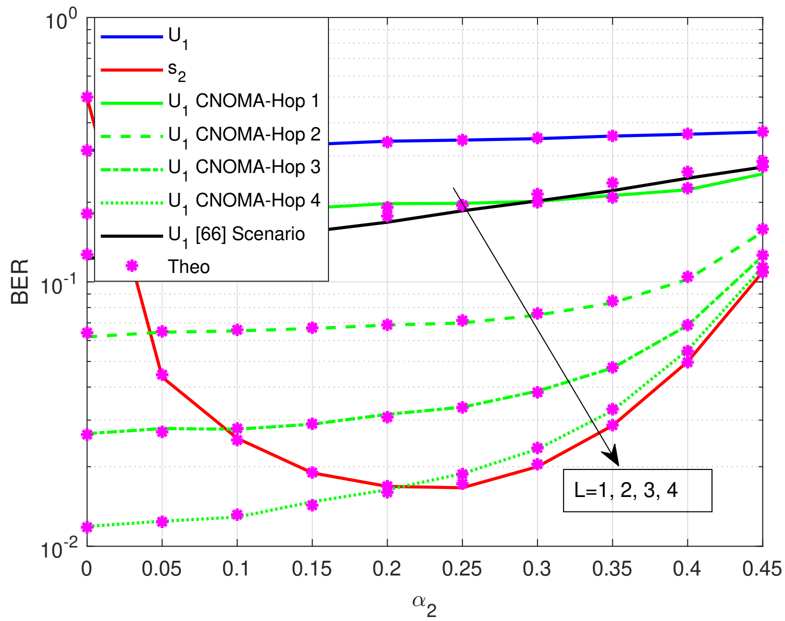

Figure 4.16: *OP of MH-DF-CNOMA with DL w.r.t. α_2 with different relay.*

On the other hand, Figure 4.15 and Figure 4.16 present the BER performance of MH-DF-CNOMA with DL compared to a single relay scheme. In Figure 4.15, we present the BER performance of our proposed system compared to a single relay scheme of [66]. We observe that the BER performance of MH-DF-CNOMA with DL improves as the number of relays increases. Moreover, the BER performance of our proposed system achieves higher performance gain compared to [66] of a single relay scheme. In Figure 4.15 (a) and Figure 4.15 (b), we present the BER of our system with perfect CSI and ICSI respectively. It can be seen that the BER performance of the system degrades in the presence of ICSI and achieves an error floor at the high SNR.

To examine the impacts of the power allocation of our system, in Figure 4.16, we present the BER of our system w.r.t α_2 when SNR= 20dB. We observe that the change of α_2 leads to a change performance of the users which affects the SIC process of each node. Again, increasing the number of relays improves the performance of our scheme. Furthermore, it can be easily seen that our proposed scheme outperforms the single relay scheme of [66].

4.5 Conclusion

This chapter has investigated the MH-DF-CNOMA with two schemes with and without DL. For practical scenarios, the ICSI and ISIC are taken into account. We have derived the e2e OP and

BER expressions for the considered systems under ICSI and ISIC. We have discussed the effect of power allocation, the number of relays, ICSI, and SIC on the performance of systems. We have validated our mathematical derivations by using Monte Carlo simulations. The results demonstrate that increasing the number of relays reduces the OP and BER in the two MH-DF-CNOMA schemes. The MH-DF-CNOMA of our proposed system achieves high-performance gain compared to a single relay scheme and [66], and the performance improves as the number of relays increases. Moreover, the changes in the power allocation affect the performance of the systems, which affects the SIC process. The ICSI decreases the performance of the systems and leads to an error floor at the high SNR. The presence of the ICSI affects signal detection and the SIC process at nodes.

In this chapter, we have presented the investigation of the multi-relay schemes, where the multi-hop schemes are used when the nodes use their power in the transmission. New wireless information and power transmission techniques are crucial for the long-term viability of wireless communications, particularly given the significant increase in energy consumption brought on by the increase in the number of connected devices. In the next chapter, we will investigate RF EH to improve EE and recharge battery-limited devices.

Chapter 5

Cooperative NOMA with Wireless Energy Harvesting

5.1 Introduction

NOMA is widely renowned for increasing the number of users and improving spectral efficiency in next-generation wireless networks [93, 94, 95]. Besides, NOMA can be easily integrated with other physical layer schemes. Hence, the CNOMA has recently received a great deal of attention due to its ability to increase spectral efficiency, and user fairness and expand network coverage [96]. On the other hand, to increase EE and recharge the battery-limited devices, EH in CNOMA has been adopted [97, 98]. In the literature, there are two major EH protocols, namely, PS and TS. In the PS protocol, the EH and information detection are performed simultaneously, whereas in the TS protocol, the EH and information detection are implemented at different time slots [99].

5.1.1 Related Works

In the past years, the performances of NOMA schemes have been evaluated in terms of OP and EC to prove the superiority of NOMA over OMA [100, 101, 102, 103, 104, 105]. Furthermore, to increase the system capacity, a nearly comprehensive analysis of CNOMA issues in terms of EC and OP with FD/HD in the presence of ICSI, ISIC, and imperfection of the HWI has been performed [45, 106, 107, 108, 67, 109, 63, 110, 111]. Multiple relays scheme (e.g., SR and multi-hop relays) is one of the promising directions for increasing the system performance and expanding coverage area. In [73, 112, 12], the EC and OP for multiple relays have been evaluated. Moreover, the BER is another KPI that has been examined for CNOMA FD/HD with single/multiple relays under the imperfection of the ICSI and ISIC [45, 67, 12, 44, 113, 114, 115, 65, 64]. Through the earlier literature, NOMA can serve multiple users at the same time and achieve superiority over OMA schemes in terms of OP and EC, while the error performance of OMA is better because NOMA schemes suffer from IUI [11]. Therefore, increasing the number of users will increase errors and reduce the performance of all NOMA schemes.

On the other hand, alternative wireless information and power transfer strategies are significant for the sustainable growth of wireless communications, especially with enormous energy consumption growth with ever-increasing connected devices [97, 99]. To show the performance gain of EH with CNOMA (EH-CNOMA) over CNOMA without EH, the EC and OP of simultaneous wireless information and power transfer (SWIPT) aided CNOMA (SWIPT-CNOMA) have been evaluated [111, 116, 117, 118]. The EH (TS and PS) for FD/HD CNOMA has been evaluated in terms of the OP and compared with conventional OMA [119]. In [120, 121], the OP of CNOMA with PS has been performed. The OP, EC, and throughput for TS selection relay CNOMA with the effect of ICSI and ISIC have been analyzed in [122]. In [123], TS FD CNOMA has been analyzed in terms of OP and throughput. A CNOMA for PS and TS has been investigated in terms of OP and EC over Nakagami-m fading channel [124]. A DF CNOMA-assisted EH in three different EH protocols, namely: PS, TS, and ideal protocols with ISIC and ICSI have been implemented and compared in terms of the OP over Rayleigh fading channel [125]. The sum rate and EE have been examined for FD CNOMA with EH [126]. In [127], a PS CNOMA IoT network has been analyzed in terms of the OP under practical variations (ISIC and different incentive transmission power levels for the IoT). To handle the co-channel interference, the problem of joint power allocation and sub-channel assignment for device-to-device-enabled IoT NOMA, the sum rate, fairness, access rate, and computational complexity have been investigated [128]. In [129], the CNOMA-IoT user scheduling strategy is used to enhance the secrecy OP. The authors in [130] evaluate overlay networks NOMA in terms of secrecy throughput and secrecy OP.

Regardless of the superiority of EH over schemes without EH, it is possible to improve EH to reach the best performance. Previously, an optimized protocol called hybrid EH that combines PS and TS jointly to improve the EE of EH OMA has been proposed and evaluated in terms of throughput [131]. According to the findings in [131], the hybrid protocol outperforms both TS and PS protocols. The hybrid protocol has been adopted to the EH CNOMA scheme in [132, 133, 134] to improve the performance of EH CNOMA. It has been analyzed in terms of EC and OP for CNOMA over the Rayleigh fading channel. These works do not provide a complete study of the hybrid protocol with their evaluation due to the following reasons: 1) The optimal value of the hybrid protocol has not been indicated compared to other EH protocols (i.e., PS and TS). 2) Does the hybrid protocol always outperform the existing EH protocols in all EH values? 3) Also, all these works assumed one of the users works as an assistant user to help the far user, so with only this assumption, the investigation is not enough. The case without the direct links between the source and users is very important to evaluate the performance. 4) All of these works analyze performance with the assumption of the Rayleigh fading channel, so the evaluation needs more realistic assumptions for the channel, e.g., the Nakagami-m fading channel, which is considered a practical fading channel.

Through examining the previous works, although most of the existing EH-CNOMA papers discuss investigating OP and EC, the error performance (one of the most important KPIs) investigation is very limited. In [115, 135, 136], the error performance of CNOMA with EH (with PS protocol) AF relay has been performed. The authors of [136] evaluated the error performance of the mth best relay selection in EH (with PS protocol) AF multiple relay-assisted CNOMA. Then in [137], the authors investigate the error performance of CNOMA with an EH relay (with TS protocol). As seen in the above discussion, the related EH-CNOMA papers deal with only one EH protocol. However, a comparison of the existing EH protocols is important to select the proper protocol to guarantee the best performance in CNOMA.

5.1.2 Motivation and Contributions

As mentioned above, EH CNOMA for PS or TS has been implemented in [111, 115, 116, 118, 119, 120, 121, 122, 126, 127, 135, 136, 137, 138], and OP, EC and BER have been analyzed. The comparison of the EH CNOMA schemes (TS and PS) is important to select which EH protocol is superior and which is performed in terms of OP and EC in [124, 125]. Based on these discussions, the BER of CNOMA with EH under ICSI, ISIC, and ICI has not been considered over the Rayleigh fading channel to the best of the author's knowledge. Furthermore, to improve the EH CNOMA scheme, the hybrid protocol has been analyzed over the Rayleigh fading channel in terms of OP and EC in [132, 133, 134]. The channel behavior over large distances is not accurately predicted by the Rayleigh distribution. For more flexibility, the Nakagami-m distribution represents a bigger range of channel models, which is considered a practical fading channel. According to the authors' best knowledge, the hybrid protocol has not been evaluated over the Nakagami-m fading channel. Therefore, we analyze and compare the OP of the hybrid protocol with the exiting EH protocols (i.e., PS and TS) and without EH over the Nakagami-m fading channel. Also, to the best of the authors' knowledge, most of the existing papers investigate the EH-CNOMA schemes by using either TS or PS protocol and no work provides hybrid EH for CNOMA in terms of BER. In addition, the BER performance of the EH-CNOMA schemes has not been studied well by considering different EH protocols. Motivated by the aforementioned discussions, in this chapter, first, we investigate the BER of CNOMA with EH under ICSI, ISIC, and ICI over the Rayleigh fading channel. Secondly, the HEH-CNOMA in terms of BER and OP over the Nakagami-m fading channel. The main contributions of the chapter are given as follows.

- First, we analyze the BER of CNOMA with EH (using TS and PS protocols) under ICSI, ISIC, and ICI over the Rayleigh fading channel.
- We examine the effect of ISIC and CSI on BER performance under the parameters of EH (i.e., EH factors and energy conversion efficiency). We also discuss the effect of CSI errors on SIC

performance.

- Secondly, we present the HEH-CNOMA scheme where the relay applies the HEH protocol to improve the performance of the existing EH schemes in CNOMA networks.
- We also present three benchmark schemes (i.e., PS, TS and no-EH) to evaluate the performance of the HEH-CNOMA. We derive the exact e2e BER expressions for HEH-CNOMA and three benchmarks over Nakagami-m fading channels. The simulations validate the perfect match of the analysis. Based on the extensive simulations, we reveal that the BER of HEH-CNOMA outperforms all three benchmarks remarkably.
- Moreover, we derive the exact e2e OP expressions for HEH-CNOMA and three benchmarks over Nakagami-m fading channels. The results are identical to simulations, and it shows the superiority of the hybrid protocol on all three benchmarks significantly.
- We also discuss the optimum values for EH parameters and power allocation coefficient, and we present that optimum values can be obtained to improve the performance of both users.

5.2 Cooperative NOMA with EH over Rayleigh Fading Channel

5.2.1 System Model

As illustrated in Figure 5.1, we consider a CNOMA system with a BS, relay node, and two users named as follows U_1 and U_2. It is assumed that each node is equipped with a single antenna and the relay node works in HD mode. It is further supposed that the communication between the BS and users is not available, so users receive the BS signal only with the help of the relay node. Rayleigh fading affects all communication links. Since the relay has no power to forward the information in the second phase, it is assumed that the relay node harvests energy from the RF signal transmitted by the BS and uses it to forward the information to the users. Two EH protocols are assumed to be used named TS and PS protocols, which are described in Section 1.7, so the received signal at the relay node is given by

$$y_r = \sqrt{\digamma P_t}\ (\hat{h}_r + e)\ (\sqrt{\alpha_1} s_1 + \alpha_2 s_2) +\ n_{r,a} +\ n_{r,c}, \tag{5.1}$$

where s_1 and s_2 are the signals of U_i, in which $i = 1, 2$, $\hat{h}_r = h_r - e \sim \mathcal{CN}(0, \hat{\sigma}_r^2 = \sigma_r^2 - \sigma_e^2)$ is channel estimation coefficient of between BS-relay, $h_r \sim \mathcal{CN}(0, \sigma_r^2 = d_r^{\varsigma})$ is channel coefficient of between BS and relay, $e \sim \mathcal{CN}(0, \sigma_e^2)$ is the error factor of the channel estimation, d_r is the distance between BS-R_r and ς is the path loss factor, $n_{r,a} \sim \mathcal{CN}(0, \sigma_{r,a}^2)$ and $n_{r,a} \sim \mathcal{CN}(0, \sigma_{r,c}^2)$ are the AWGN of the noise from the antenna and the RF to-baseband conversion [139, 140, 141], and α_1 and α_2 are the power allocation coefficient for U_i, where $\alpha_1 > \alpha_2$ in which $\alpha_1 + \alpha_2 = 1$, and $\digamma$ denotes how much source power is dedicated to transmitting information, it will be (1 - ρ) for PS and 1 for TS.

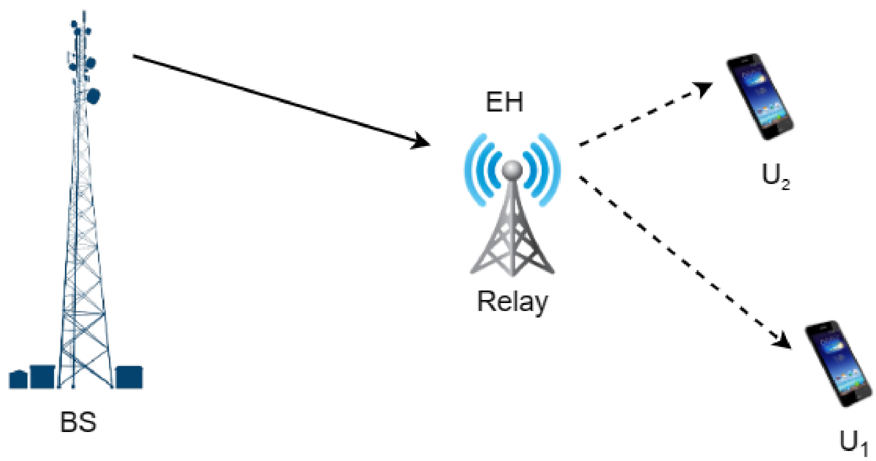

Figure 5.1: *CNOMA with EH schemes.*

The harvested energy at the relay during the power transfer is given by

$$E_h = \begin{cases} \eta P_t \rho \frac{T}{2} |h_r|^2, & \text{PS}, \\ \eta P_t \nu T |h_r|^2, & \text{TS}. \end{cases} \tag{5.2}$$

The transmission power of the relay can be given as

$$P_r = \begin{cases} \eta P_t \rho |h_r|^2, & \text{PS}, \\ \frac{2\eta P_t \nu T |h_r|^2}{1-\nu}, & \text{TS}. \end{cases} \tag{5.3}$$

The relay node decodes the s_1 first by treating the other signal as noise. Then, the relay node decodes s_2 using the SIC process. Thereafter, the relay re-encodes the decoded signal in a new SC signal as in BS and forwards it to the users using the harvested power. The users are considered to be vulnerable to broadcasts from the BS of nearby cells[1]. The received signal at users is given by

$$y_k = \sqrt{P_r}\ (\hat{h}_k + e)\ (\sqrt{\alpha_1} s_1 + \alpha_2 s_2) + \ I_k + \ n_{r,a} + \ n_{r,c},, \qquad k = 1, 2, \tag{5.4}$$

where s_1 and s_2 are the signals of U_i, in which $i = 1, 2$, $\hat{h}_k = h_k - e \sim \mathcal{CN}(0, \hat{\sigma}_k^2 = \sigma_k^2 - \sigma_e^2)$ is channel estimation coefficient between relay and users, $h_k \sim \mathcal{CN}(0, \sigma_k^2 = d_k^{\varsigma})$ is channel coefficient between BS and users, d_k is the distance between BS and users. $I_k = \sum_{o \neq k}^{N} \sqrt{P_{t,o}} s_o\ (\hat{h}_o + e)$ is the ICI. where N is the total number of neighbor cells and o is the index of neighbor cells. $\hat{h}_o \sim \mathcal{CN}(0, \hat{\sigma}_o^2)$ is the estimated channel coefficient between the neighbor cells and users, $P_{t,o}$ is the cell BS's transmit

[1]Since a direct link is unavailable to the users because they are close to cell edges, the relay helps to connect them with BS. Thus, the relay is located between BS and users, far enough away from the cell edge, so it does not suffer from ICI.

power, and s_o is the SC signal of the neighbor cells. The ICI can be assumed as complex Gaussian distributed as in [142, 143] by $I_k \sim \mathcal{CN}(0, \sigma^2_{ICI})$, in which $\sigma^2_{ICI} = \varpi_{ICI} \sum_o^N P_{t,o}$, and ϖ_{ICI} is the ICI factor.

5.2.2 Performance Analysis

In this subsection, we derive the e2e BER for U$_1$ and U$_2$ respectively. We consider the BPSK modulation to be used to encode the users' signals in the BS and relay nodes. The e2e BER expression for users is given as in [144] by

$$P_{e2e,k}(e) = 1 - (1 - P_{I,s_k}(e))(1 - P_{II,s_k}(e)), \qquad k = 1, 2, \tag{5.5}$$

where $P_{I,s_k}(e)$ is the BER of users in the first phase and $P_{I,s_k}(e)$ is the BER of users in the second phase.

The relay detects s_1 using MLD. Hence, the BER of the s_1 symbols at relay can be expressed by

$$P_{I,s_k}(e) = \frac{1}{2} \sum_{j=1}^{2} Q\left(\sqrt{P_t \gamma \chi_j |\hat{h}_r|^2 / (P_t \gamma \chi_j \sigma_e^2 + \sigma_{r,a}^2 + \sigma_{r,c}^2)}\right), \tag{5.6}$$

where $\chi_j = [(\sqrt{\alpha_1} + \sqrt{\alpha_2})^2, (\sqrt{\alpha_1} - \sqrt{\alpha_2})^2]$.

With the help of an alternative form of the Q(.) function and the MGF, and after some algebraic manipulation, (5.6) can be obtained as in [137, 144] by

$$P_{I,s_k}(e) = \frac{1}{4} \sum_{j=1}^{2} \left(\sqrt{\frac{\left(P_t \gamma \chi_j E[|\hat{h}_r|^2] / (P_t \gamma \chi_j \sigma_e^2 + \sigma_{r,a}^2 + \sigma_{r,c}^2)\right)}{2 + \left(P_t \gamma \chi_j E[|\hat{h}_r|^2] / (P_t \gamma \chi_j \sigma_e^2 + \sigma_{r,a}^2 + \sigma_{r,c}^2)\right)}}\right). \tag{5.7}$$

Furthermore, the relay implements the SIC to detect the s_2 symbols. The detection of s_2 at the relay is based on the detection of s_1 symbols correct or not. Hence, the BER of s_2 at relay can be expressed by

$$P_{I,s_2}(e) = \frac{1}{2} \sum_{v=1}^{6} \kappa_v Q\left(\sqrt{P_t \gamma \aleph_v |\hat{h}_r|^2 / (P_t \gamma \delta_v \sigma_e^2 + \sigma_{r,a}^2 + \sigma_{r,c}^2)}\right), \tag{5.8}$$

where $\delta_v = [(\sqrt{\alpha_1} - \sqrt{\alpha_2})^2, (\sqrt{\alpha_1} + \sqrt{\alpha_2})^2, (\sqrt{\alpha_1} + \sqrt{\alpha_2})^2, (\sqrt{\alpha_1} + \sqrt{\alpha_2})^2, (\sqrt{\alpha_1} - \sqrt{\alpha_2})^2, (\sqrt{\alpha_1} - \sqrt{\alpha_2})^2]$, $\kappa_v = [1, 1, -1, 1, 1, -1]$, and $\aleph_v = [\alpha_2, \alpha_2, (\sqrt{\alpha_1} + \sqrt{\alpha_2})^2, (\sqrt{2\alpha_1} + \sqrt{\alpha_2})^2, (\sqrt{\alpha_1} - \sqrt{\alpha_2})^2, (2\sqrt{\alpha_1} - \sqrt{\alpha_2})^2]$.

By assisting an alternative form of the Q(.) function and the MGF, and after some algebraic manipulation, (5.8) can be written by [137, 144]

$$P_{I,s_2}(e) = \frac{1}{4} \sum_{v=1}^{6} \kappa_v \left(\sqrt{\frac{\left(P_t \gamma \aleph_v E[|\hat{h}_r|^2] / (P_t \gamma \delta_v \sigma_e^2 + \sigma_{r,a}^2 + \sigma_{r,c}^2)\right)}{2 + \left(P_t \gamma \aleph_v E[|\hat{h}_r|^2] / (P_t \gamma \delta_v \sigma_e^2 + \sigma_{r,a}^2 + \sigma_{r,c}^2)\right)}}\right). \tag{5.9}$$

In the second phase, the relay re-encodes s_1 and s_2 symbols in a new SC signal as in BS and forwards it to users using the harvested power[2]. The BPSK modulation is assumed to be used to encode the s_1 and s_2 symbols at the relay. The BER of U_1 in the second phase can be written as

$$P_{II,s_1}(e) = \frac{1}{2}\sum_{j=1}^{2} Q\left(\sqrt{P_r\gamma\chi_j|\hat{h}_1|^2/(P_r\gamma\chi_j\sigma_e^2+\sigma_{r,a}^2+\sigma_{r,c}^2)}\right). \tag{5.10}$$

With the help of an alternative form of Q(.) function and the MGF, and after some algebraic manipulation, (5.10) can be obtained as

$$P_{II,s_1}(e) = \frac{1}{4}\sum_{j=1}^{2}\left(\sqrt{\frac{\left(P_r\gamma\chi_j E[|\hat{h}_1|^2]/(P_r\gamma\chi_j\sigma_e^2+\sigma_{r,a}^2+\sigma_{r,c}^2+\sigma_{ICI}^2)\right)}{2+\left(P_r\gamma\chi_j E[|\hat{h}_1|^2]/(P_r\gamma\chi_j\sigma_e^2+\sigma_{r,a}^2+\sigma_{r,c}^2+\sigma_{ICI}^2+)\right)}}\right). \tag{5.11}$$

The U_2 implements the SIC to detect its symbols. s_2 is detected based on whether or not the s_1 symbols are correctly detected. Hence, the BER of U_2 can be expressed by

$$P_{II,s_2}(e) = \frac{1}{2}\sum_{v=1}^{6}\kappa_v Q\left(\sqrt{P_r\gamma\aleph_v|\hat{h}_2|^2/(P_r\gamma\delta_v\sigma_e^2+\sigma_{r,a}^2+\sigma_{r,c}^2+\sigma_{ICI}^2)}\right). \tag{5.12}$$

By assisting an alternative form of the Q(.) function and the MGF, and after some algebraic manipulation, (5.12) can be written by

$$P_{II,s_2}(e) = \frac{1}{4}\sum_{v=1}^{6}\kappa_v\left(\sqrt{\frac{\left(P_r\gamma\aleph_v E[|\hat{h}_2|^2]/(P_r\gamma\delta_v\sigma_e^2+\sigma_{r,a}^2+\sigma_{r,c}^2+\sigma_{ICI}^2)\right)}{2+\left(P_r\gamma\aleph_v E[|\hat{h}_2|^2]/(P_r\gamma\delta_v\sigma_e^2+\sigma_{r,a}^2+\sigma_{r,c}^2+\sigma_{ICI}^2)\right)}}\right). \tag{5.13}$$

To find the BER of U_1 and U_2, we substitute the (5.7) and (5.11) into (5.5) and (5.9) and (5.13) into (5.5) as given by

$$\begin{aligned}P_{e2e,1}(e) = 1 - &\left(1-\frac{1}{4}\sum_{j=1}^{2}\left(\sqrt{\frac{\left(P_t\gamma\chi_j E[|\hat{h}_r|^2]/(P_t\gamma\chi_j\sigma_e^2+\sigma_{r,a}^2+\sigma_{r,c}^2)\right)}{2+\left(P_t\gamma\chi_j E[|\hat{h}_r|^2]/(P_t\gamma\chi_j\sigma_e^2+\sigma_{r,a}^2+\sigma_{r,c}^2)\right)}}\right)\right)\\ &\left(1-\frac{1}{4}\sum_{j=1}^{2}\left(\sqrt{\frac{\left(P_r\gamma\chi_j E[|\hat{h}_1|^2]/(P_r\gamma\chi_j\sigma_e^2+\sigma_{r,a}^2+\sigma_{r,c}^2+\sigma_{ICI}^2)\right)}{2+\left(P_r\gamma\chi_j E[|\hat{h}_1|^2]/(P_r\gamma\chi_j\sigma_e^2+\sigma_{r,a}^2+\sigma_{r,c}^2+\sigma_{ICI}^2+)\right)}}\right)\right),\end{aligned} \tag{5.14}$$

[2]As is well known, P_r calculates its value under EH. We consider P_r to be a constant value (i.e., P_r as the average value of the harvested power) and assume that it will remain constant during the derivation.

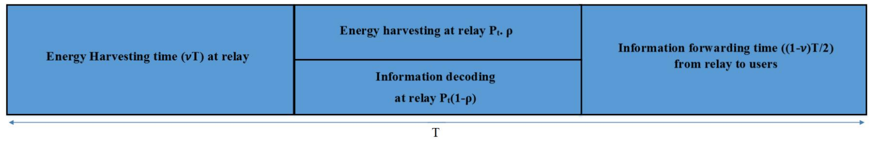

Figure 5.2: *CNOMA with HEH schemes.*

$$
\begin{aligned}
P_{e2e,2}(e) = 1 - &\left(1 - \frac{1}{4}\sum_{v=1}^{6}\kappa_v\left(\sqrt{\frac{\left(P_t\gamma\aleph_v E[|\hat{h}_r|^2]/(P_t\gamma\delta_v\sigma_e^2+\sigma_{r,a}^2+\sigma_{r,c}^2)\right)}{2+\left(P_t\gamma\aleph_v E[|\hat{h}_r|^2]/(P_t\gamma\delta_v\sigma_e^2+\sigma_{r,a}^2+\sigma_{r,c}^2)\right)}}\right)\right) \\
&\left(1 - \frac{1}{4}\sum_{v=1}^{6}\kappa_v\left(\sqrt{\frac{\left(P_r\gamma\aleph_v E[|\hat{h}_2|^2]/(P_r\gamma\delta_v\sigma_e^2+\sigma_{r,a}^2+\sigma_{r,c}^2+\sigma_{ICI}^2)\right)}{2+\left(P_r\gamma\aleph_v E[|\hat{h}_2|^2]/(P_r\gamma\delta_v\sigma_e^2+\sigma_{r,a}^2+\sigma_{r,c}^2+\sigma_{ICI}^2)\right)}}\right)\right).
\end{aligned}
\tag{5.15}
$$

5.3 Cooperative NOMA with EH over Nagakamai-m Fading Channel

5.3.1 System Model

We consider a CNOMA system with BS, one relay, and two users named U_1 and U_2, as shown in Figure 5.2. It is assumed that the users cannot receive the BS signal directly due to large path-loss or obstacles. The relay works in HD mode and helps the users to receive the BS signal. The Nakagami-m fading affects all communication links. It is assumed that the relay node has no power to forward the signal in the second phase, and can harvest energy from the RF signals using three EH protocols, PT, TS, and hybrid. We describe the TS and PS protocols in Section 1.7 and the hybrid protocol below.

In the hybrid protocol, the νT time slot is devoted to harvesting energy as in the TS protocol. In the first (1-ν) T/2 time slot, the BS transmits an SC signal to the relay node. Also, during this time, the relay harvests energy (ρ) from the received signal as in the PS protocol. During the second (1-ν) T/2 time slot, the relay uses the sum of the harvested energy from previous times to forward the information to the users.

In the no EH, the relay uses its energy source because it is unable to collect energy. In the no EH, both BS and relay cover half of the communication time (T/2 time) and use the same amount of power during these data transfers.

The BS transmits an SC signal consisting of the users' signals with different power levels according to the channel gain $|h_1|^2 < |h_2|^2$. The received information signal during the first phase at the relay is given by

$$
y_r = \sqrt{\digamma P_t}\; h_r\; (\sqrt{\alpha_1}s_1 + \sqrt{\alpha_2}s_2) + \; n, \tag{5.16}
$$

where s_1 and s_2 are the signals of U_i, in which $i = 1, 2$, h_r is the Nakagami-m fading channel coefficient between BS-relay with Ω_r spread and m_r shape parameters, $n \sim \mathcal{CN}(0, \sigma^2)$ is the AWGN, α_1 and α_2 are the power allocation coefficient for U_i, where $\alpha_1 > \alpha_2$ in which $\alpha_1 + \alpha_2 = 1$. $\digamma$ denotes how much source power is dedicated to transmitting information, it will be (1 - ρ) for PS and hybrid whereas will be 1 for TS and no-EH.

The relay implements the SIC to detect the signals of users where the s_1 is detected first then s_2. The SINR of the received signals at the relay is expressed by

$$\gamma_{BSR,s_1} = \frac{P_t \digamma \alpha_1 |h_r|^2}{P_t \digamma \alpha_2 |h_r|^2 + \sigma^2}, \tag{5.17}$$

$$\gamma_{BSR,s_2} = \frac{P_t \digamma \varpi \alpha_2 |h_r|^2}{\sigma^2}. \tag{5.18}$$

For the sake of equality, we assume that the consumed energy by all protocols is equal to ϵ_T. In the no-EH, ϵ_T is consumed equally by the BS and relay, whereas in EH protocols, it is consumed only by the BS. Thus, the source power can be expressed as

$$P_t = \Psi P_T, \text{ where } P_T = \epsilon_T / T, \tag{5.19}$$

where Ψ is equal to 1 for no-EH, 2 for PS and $\frac{2}{\nu+1}$ for TS and hybrid. Hence, the harvested energy during the power transfer in the EH protocols is given by

$$E_h = \begin{cases} \eta P_t \rho \frac{T}{2} |h_r|^2, & \text{PS}, \\ \eta P_t \nu T |h_r|^2, & \text{TS}, \\ \eta P_t (\frac{2\nu + \rho(1-\nu))}{2}) T |h_r|^2, & \text{Hybrid}. \end{cases} \tag{5.20}$$

Additionally, the transmit power of the relay in the EH protocols is expressed by

$$P_r = \begin{cases} P_t |h_r|^2 \Psi, & \text{PS, TS and Hybrid}, \\ P_t, & \text{no-EH}, \end{cases} \tag{5.21}$$

where

$$\Psi = \begin{cases} \eta \rho, & \text{PS}, \\ {}^{2\eta\nu}/(1-\nu), & \text{TS}, \\ \eta(\rho + {}^{2\nu}/(1-\nu)), & \text{Hybrid}. \end{cases} \tag{5.22}$$

where η $(0 \leq \eta \leq 1)$ is the factor of the energy conversion efficiency, $(0 \leq \rho \leq 1)$, and $(0 \leq \nu \leq 1)$ are the factors of the PS and TS respectively.

As in BS, the relay re-encodes the decoded signals in a new SC signal and forwards it using the harvested power to the users. The received signal at users is given by

$$y_k = \sqrt{\digamma P_r}\ h_k\ (\sqrt{\alpha_1} s_1 + \sqrt{\alpha_2} s_2) + \ n, \tag{5.23}$$

where h_k is the Nakagami-m fading channel coefficient between relay-users with Ω_k spread and m_k shape parameters. The U_1 decodes its signal directly while the U_2 uses the SIC to decode its signal. Hence, the SINRs at U_1 and U_2 are given as

$$\gamma_{U1,s_1} = \frac{P_r \digamma \alpha_1 |h_1|^2}{P_r \digamma \alpha_2 |h_1|^2 + \sigma^2}, \tag{5.24}$$

$$\gamma_{U_2,s_1} = \frac{P_r \digamma \alpha_1 |h_2|^2}{P_r \digamma \alpha_2 |h_2|^2 + \sigma^2}, \tag{5.25}$$

$$\gamma_{U_2,s_2} = \frac{P_r \digamma \alpha_2 |h_2|^2}{\sigma^2}. \tag{5.26}$$

5.3.2 Performance Analysis

In this subsection, we derive the e2e OP and BER for our system with all EH protocols over the Nakagami-m fading channel.

5.3.2.1 Outage Probablity

As we described above, the relay detects the signals of users through SIC and forwards the information to users using the harvested power (i.e., using one of the following EH protocols, PS, TS and hybrid). In the no-EH, the relay forwards the information to the users by its power. Thus, we derive the e2e OP of users for three EH protocols and no-EH over the Nakagami-m fading channel below. The e2e BER at each user is given as in [145] by

$$P_{e2e,U_1}(out) = 1 - \left(1 - P_{BSR,s_1}(out)\right)\left(1 - P_{U_1,s_1}(out)\right), \tag{5.27}$$

The e2e OP of U_1 is obtained by using the PDF and CDF of the Nakagami-m fading channel [146, Eq. (19) and Eq. (20)] as

$$P_{e2e,U_1}(out) = 1 - \left(1 - e^{-\frac{m_r}{\Omega_r}\ell_1} \sum_{t=0}^{m_r-1} \frac{1}{t!}\left(\frac{m_r}{\Omega_r}\ell_1\right)^t\right) \times \left(1 - \frac{G_{1\,3}^{2\,1}\left({}_{m_r,m_1,0}^{\quad 1} \middle| \frac{\flat_1}{\Omega_r \Omega_1}\right)}{\Gamma(m_r)\Gamma(m_1)}\right). \tag{5.28}$$

where $\ell_1 = \frac{\theta_1 \sigma^2}{(\alpha_1 - \alpha_2\theta_1)P_t \digamma}$, $\flat_1 = \frac{\theta_1 \sigma^2}{(\alpha_1 - \alpha_2\theta_1)P_t \Psi \digamma}$ and $\theta_i = 2^{R_i/\hbar} - 1$. R_i is target rate of s_1 and s_2, $\hbar$ is equal to $\frac{1-\nu}{2}$ for TS and hybrid, and $\frac{1}{2}$ for PS and no-EH

Proof: Please, see Appendix D.

The OP of U_2 occurs when two events occur when s_1 fails to detect and when s_1 successfully detects at the relay and U_2. Hence, the BER at U_2 is given by

$$P_{e2e,U_2}(out) = 1 - \left(1 - P_{BSR,s_2}(out)\right)\left(1 - P_{U_2,s_2}(out)\right), \tag{5.29}$$

where $P_{BSR,s_2}(x)$ and $P_{U_2,s_2}(x)$ are OP at relay and U_2 in the first and second phases, respectively which are expressed below

$$P_{BSR,s_2}(out) = 1 - e^{-\frac{m_r}{\Omega_r}(\ell_1+\ell_2)} \sum_{t=0}^{m_r-1} \sum_{k=0}^{m_r-1} \frac{1}{t!} \frac{1}{k!} \left(\frac{m_r}{\Omega_r}\ell_1\right)^t \left(\frac{m_r}{\Omega_r}\ell_2\right)^k, \tag{5.30}$$

$$\begin{aligned} P_{U_2,s_2}(out) = & \frac{G^{2\,1}_{1\,3}\left(\frac{\flat_1}{\Omega_r\Omega_2}\middle|\begin{smallmatrix}1\\ m_r,m_2,0\end{smallmatrix}\right)}{\Gamma(m_r)\Gamma(m_2)} + \frac{G^{2\,1}_{1\,3}\left(\frac{\flat_2}{\Omega_r\Omega_2}\middle|\begin{smallmatrix}1\\ m_r,m_2,0\end{smallmatrix}\right)}{\Gamma(m_r)\Gamma(m_2)} \\ & - \frac{G^{2\,1}_{1\,3}\left(\frac{\flat_1}{\Omega_r\Omega_2}\middle|\begin{smallmatrix}1\\ m_r,m_2,0\end{smallmatrix}\right)}{\Gamma(m_r)\Gamma(m_2)} \frac{G^{2\,1}_{1\,3}\left(\frac{\flat_2}{\Omega_r\Omega_2}\middle|\begin{smallmatrix}1\\ m_r,m_2,0\end{smallmatrix}\right)}{\Gamma(m_r)\Gamma(m_2)}, \end{aligned} \tag{5.31}$$

where $\ell_2 = \frac{\theta_2\sigma^2}{\alpha_2 P_t F}$ and $\flat_2 = \frac{\theta_2\sigma^2}{\alpha_2 \Psi P_t F}$.

To find the e2e OP of U_2, we substitute (5.30) and (5.31) into (5.29) as

$$\begin{aligned} P_{e2e,U_2}(out) = 1 - & \left(e^{-\frac{m_r}{\Omega_r}(\ell_1+\ell_2)} \sum_{t=0}^{m_r-1} \sum_{k=0}^{m_r-1} \frac{1}{t!} \frac{1}{k!} \left(\frac{m_r}{\Omega_r}\ell_1\right)^t \left(\frac{m_r}{\Omega_r}\ell_2\right)^k\right) \\ & \left(1 - \frac{G^{2\,1}_{1\,3}\left(\frac{\flat_1}{\Omega_r\Omega_2}\middle|\begin{smallmatrix}1\\ m_r,m_2,0\end{smallmatrix}\right)}{\Gamma(m_r)\Gamma(m_2)} - \frac{G^{2\,1}_{1\,3}\left(\frac{\flat_2}{\Omega_r\Omega_2}\middle|\begin{smallmatrix}1\\ m_r,m_2,0\end{smallmatrix}\right)}{\Gamma(m_r)\Gamma(m_2)} + \frac{G^{2\,1}_{1\,3}\left(\frac{\flat_1}{\Omega_r\Omega_2}\middle|\begin{smallmatrix}1\\ m_r,m_2,0\end{smallmatrix}\right)}{\Gamma(m_r)\Gamma(m_2)} \frac{G^{2\,1}_{1\,3}\left(\frac{\flat_2}{\Omega_r\Omega_2}\middle|\begin{smallmatrix}1\\ m_r,m_2,0\end{smallmatrix}\right)}{\Gamma(m_r)\Gamma(m_2)}\right). \end{aligned} \tag{5.32}$$

To calculate the e2e OP of users in the no-EH case, we need only to determine the OP of the second phase. Thus, we can obtain the OP of s_2 of the second phase using the same way as the first phase, where the change is only in the channel.

5.3.2.2 Bit Error Rate

The BS and relay encode the signals of users using BPSK modulation. Thus, it is possible to present two different energy levels with equal probabilities. In all EH protocols and no-EH, by treating s_2 as noise, the relay detects s_1 first, then using the SIC, it detects s_2. Thereafter, the relay re-encodes the detected signals in a novel SC signal and forwards it to the users using the harvested power (in the no-EH, it is assumed that the relay uses it is own power to forward the information to the users). The e2e BER of users can be written as in [145] by

$$P_{e2e,k}(e) = 1 - (1 - P_{I,s_k}(e))(1 - P_{II,s_k}(e)), \qquad k = 1, 2, \tag{5.33}$$

where $P_{I,s_k}(e)$ is the BER of users in the first phase and $P_{I,s_k}(e)$ is the BER of users in the second phase.

In all EH protocols and no-EH, the relay detects s_1 first. Hence, the BER of s_1 at the relay is given by

$$P_{I,s_1}(e) = \frac{1}{2}\sum_{j=1}^{2} \mathrm{Q}(\sqrt{\digamma\gamma\chi_j|h_r|^2}), \tag{5.34}$$

where $\chi_j = [(\sqrt{\alpha_1}+\sqrt{\alpha_2})^2, (\sqrt{\alpha_1}-\sqrt{\alpha_2})^2]$.

To average the BER of (5.34), we use the alternate representation of the Q-function and the PDF of the Nakagami-m fading channel [81, 17, 147]. After some algebraic manipulation, the ABER of (5.34) over a Nakagami-m fading channel is given as

$$P_{I,s_1}(e) = \frac{1}{2}\sum_{j=1}^{2} \frac{1}{\sqrt{2\pi}}\frac{\Gamma(m_r+0.5)}{\Gamma(m_r+1)} \times (\frac{\sqrt{\digamma\gamma\chi_j\delta/2m_r}}{(1+\sqrt{\digamma\gamma\chi_j\delta/2m_r})^{(m_r+0.5)}})\nabla_1(m_r, \digamma\gamma\chi_j\delta), \tag{5.35}$$

where $\nabla_1(m_r, \varpi\gamma\zeta_i\delta) =_2 F_1(1, m_r+0.5, m_r+1, \frac{2m_r}{2m_r+\digamma\gamma\chi_j\delta})$ and $\delta = \Omega_r$. ${}_2F_1(.,.;.,.)$ is the Gauss hypergeometric function.

Furthermore, to derive the BER of s_2 at the relay node, we derive the BER of the correct and erroneous SIC. Hence, the BER of s_2 at the relay node is given by

$$P_{I,s_2}(e) = \frac{1}{2}\sum_{v=1}^{5} \kappa_v \mathrm{Q}(\sqrt{\digamma\gamma\aleph_v|h_r|^2}), \tag{5.36}$$

where $\kappa_v = [2,-1,1,1,-1]$ and $\aleph_v = [\alpha_2, (\sqrt{\alpha_1}+\sqrt{\alpha_2})^2, (\sqrt{2\alpha_1}+\sqrt{\alpha_2})^2, (\sqrt{\alpha_1}-\sqrt{\alpha_2})^2, (2\sqrt{\alpha_1}-\sqrt{\alpha_2})^2]$.

The ABER over the Nakagami-m fading channel of (5.36) can be expressed as

$$P_{I,s_2}(e) = \frac{1}{2}\sum_{v=1}^{5} \kappa_v \frac{1}{\sqrt{2\pi}}\frac{\Gamma(m_r+0.5)}{\Gamma(m_r+1)} \times (\frac{\sqrt{\digamma\gamma\aleph_v\delta/2m_r}}{(1+\sqrt{\digamma\gamma\aleph_v\delta/2m_r})^{(m_r+0.5)}})\nabla_2(m_r, \digamma\gamma\aleph_v\delta), \tag{5.37}$$

where $\nabla_2(m_r, \varpi\gamma\zeta_j\delta) =_2 F_1(1, m_r+0.5, m_r+1, \frac{2m_r}{2m_r+\digamma\gamma\aleph_v\delta})$.

In the second phase, the relay uses harvested power in the EH protocols or its power in the no-EH to forward the SC information to the users. The U_1 detects its signal without SIC. The BER of U_2 in the second phase is given by

$$P_{II,s_1}(e) = \frac{1}{2}\sum_{j=1}^{2} \mathrm{Q}(\sqrt{\digamma\gamma\chi_j\psi|h_1|^2|h_r|^2}). \tag{5.38}$$

After some algebraic manipulation, the ABER of (5.38) can be expressed as

$$P_{II,s_1}(e) = \frac{1}{4\sqrt{\pi}}\sum_{j=1}^{2} \Delta_1 G_{4\ 5}^{3\ 3}\left({}^{0,1-u_2,0.5-u_2,1-u_2}_{0.5u_1,-0.5u_1,1-u_2,u_2,0} \middle| \frac{\Delta_3}{4} \right), \tag{5.39}$$

where $u_1 = m_r - m_1, u_2 = 0.5(m_r + m_1), \Delta_1 = \Delta_2(\frac{m_1\Omega_r}{m_r\Omega_1})^{\frac{u_1}{2}}(\frac{1}{\digamma\gamma\chi_j\psi})^{u_2}, \Delta_2 = \frac{(\frac{mr}{\Omega_r})^{mr}(\frac{m1}{\Omega_1})^{m1}}{\Gamma(m_r)\Gamma(m_1)}, \Delta_3 = 2\sqrt{\frac{m_1m_r}{\Omega_1\Omega_r\digamma\gamma\chi_j\psi}}$, m_r and m_k are the Nakagami fading parameters.

Proof: Please see Appendix E.

Likewise, the U_2 uses the SIC to detect its signal. Thus, through both the correct and erroneous SIC, we determine the BER at U_2. The BER at U_2 is expressed by

$$P_{II,s_2}(e) = \frac{1}{2}\sum_{v=1}^{5}\kappa_v \mathrm{Q}(\sqrt{\digamma\gamma\aleph_v\psi|h_2|^2|h_r|^2}). \tag{5.40}$$

The ABER of (5.40) is expressed as

$$P_{II,s_2}(e) = \frac{1}{4\sqrt{\pi}}\sum_{v=1}^{5}\kappa_v\Delta_4 G_{4\ 5}^{3\ 3}\left({}^{0,1-u_4,0.5-u_4,1-u_4}_{0.5u_3,-0.5u_3,1-u_4,u_4,0} \middle| \frac{\Delta_6}{4}\right), \tag{5.41}$$

where $u_3 = m_r - m_2, u_4 = 0.5(m_r + m_2), \Delta_4 = \Delta_5(\frac{m_2\Omega_r}{m_r\Omega_2})^{\frac{u_1}{2}}(\frac{1}{\digamma\gamma\aleph_v\psi})^{u_4}, \Delta_5 = \frac{(\frac{mr}{\Omega_r})^{mr}(\frac{m2}{\Omega_2})^{m_2}}{\Gamma(m_r)\Gamma(m_2)}$ and $\Delta_6 = 2\sqrt{\frac{m_2m_r}{\Omega_2\Omega_r\digamma\gamma\aleph_v\psi}}$.

To find the e2e BER for U_1 and U_2, we substitute (5.35) and (5.39) into (5.33) and (5.41), and (5.35) into (5.33) as

$$P_{e2e,1}(e) = 1 - \left(1 - \frac{1}{2}\sum_{j=1}^{2}\frac{1}{\sqrt{2\pi}}\frac{\Gamma(m_r+0.5)}{\Gamma(m_r+1)} \times (\frac{\sqrt{\digamma\gamma\chi_j\delta/2m_r}}{(1+\sqrt{\digamma\gamma\chi_j\delta/2m_r})^{(m_r+0.5)}})\nabla_1(m_r,\digamma\gamma\chi_j\delta)\right) \left(1 - \frac{1}{4\sqrt{\pi}}\sum_{j=1}^{2}\Delta_1 G_{4\ 5}^{3\ 3}\left({}^{0,1-u_2,0.5-u_2,1-u_2}_{0.5u_1,-0.5u_1,1-u_2,u_2,0} \middle| \frac{\Delta_3}{4}\right)\right), \tag{5.42}$$

$$P_{e2e,2}(e) = 1 - \left(1 - \frac{1}{2}\sum_{v=1}^{5}\kappa_v\frac{1}{\sqrt{2\pi}}\frac{\Gamma(m_r+0.5)}{\Gamma(m_r+1)} \times (\frac{\sqrt{\digamma\gamma\aleph_v\delta/2m_r}}{(1+\sqrt{\digamma\gamma\aleph_v\delta/2m_r})^{(m_r+0.5)}})\nabla_2(m_r,\digamma\gamma\aleph_v\delta)\right) \left(1 - \frac{1}{4\sqrt{\pi}}\sum_{v=1}^{5}\kappa_v\Delta_4 G_{4\ 5}^{3\ 3}\left({}^{0,1-u_4,0.5-u_4,1-u_4}_{0.5u_3,-0.5u_3,1-u_4,u_4,0} \middle| \frac{\Delta_6}{4}\right)\right). \tag{5.43}$$

To calculate the e2e BER of users in the no-EH case, we need only to determine the BER of the second phase. The BER of the first phase is the same. Thus, we can obtain the BER of s_2 of the second phase using the same way as the first phase, where the derivation will be according to the change of the channel.

5.4 Numerical Results

5.4.1 Cooperative NOMA with EH over Rayleigh Fading Channel

In this subsection, the theoretical derivations over the Rayleigh fading channel are verified by the Mont-Carlo simulation. The parameters used in this subsection are as follows. d_r=d_2=1 m, $d_1 = 2m$, ς=3, α_1=0.8, α_2=0.2, ρ=ν=0.3 and η=0.95. It can be easily observed that our derivations are matched perfectly with the simulations that validate our derivations.

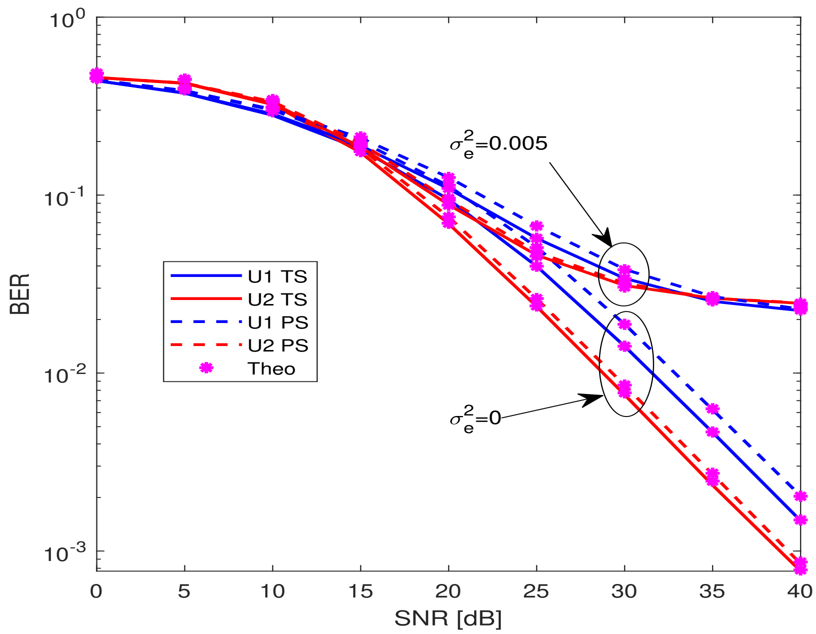

Figure 5.3: *BER w.r.t. SNR with the TS and PS protocols under ICSI.*

In Figure 5.3, we present the BER w.r.t. SNR for TS and PS protocols under ICSI when σ_e^2=0, 0.005. We observe that the BER of the TS protocol is better than the PS protocol. Furthermore, the presence of ICSI reduces the BER performance of the two protocols. Additionally, it is noted that when ICSI existed with the two protocols, U_1 performed better performance than U_2. The ICSI affects the SIC process and the detection of U_2 symbols in the two phases.

To evaluate the effect of ICSI on the BER performance, in Figure 5.4, we present the BER performance w.r.t. ICSI for the TS and PS protocols with α_2=0.1, 0.4. We observe that the BER performance of the users with the two EH protocols is degraded as the ICSI factor increases. It is seen also the BER performance of U_1 is better than U_2 for the two EH protocols when α_2=0.1. When α_2=0.4, the BER performance of U_2 is better than U_1. It is clear that the change of power allocation in the presence of ICSI reduces the system performance, which affects the SIC.

To evaluate the performance of users for the EH protocols, in Figure 5.5, we present the BER performance w.r.t. ρ and ν when SNR=20 dB. We observe that the BER of users with the TS

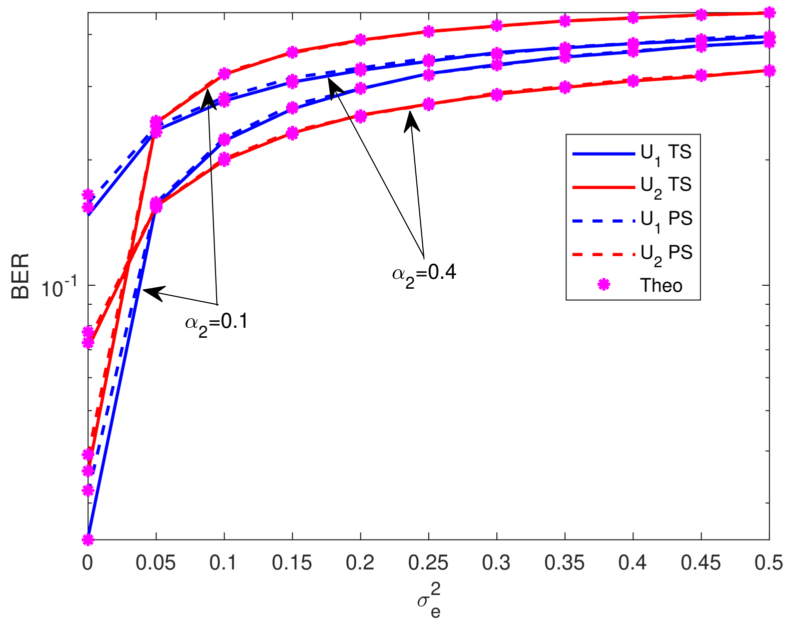

Figure 5.4: *BER w.r.t. ICSI for the TS and PS protocols under ICSI.*

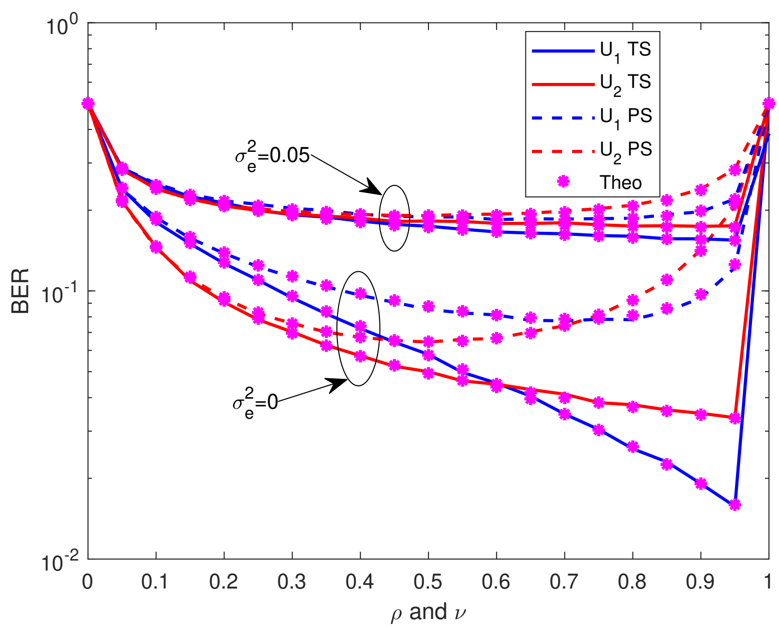

Figure 5.5: *BER w.r.t. ρ and ν for the TS and PS protocols.*

protocol increases when ρ increases. It is seen also the BER of users with the PS protocol increases in the lower ν values. In the high ν values, the BER performance reduces. High values of ν mean that the energy harvested in the first phase of the PS protocol is high, and this affects the quality of the signal decoded and forwarded in the second phase. Furthermore, the TS protocol outperforms the PS protocol. The ICSI affects the SIC and reduces the system performance of users.

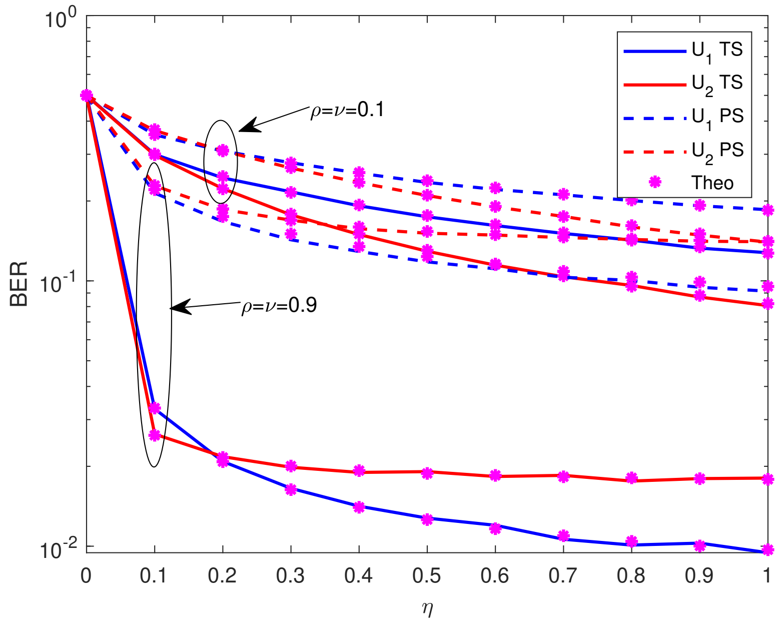

Figure 5.6: *BER w.r.t. η for the TS and PS protocols under ICSI.*

In Figure 5.6, we present the BER performance of the users w.r.t. η for TS and PS protocols when ρ=ν=0.1, 0.9, and SNR=20 dB. We observe that as η increases, the BER performance of users improves in the two protocols. In the TS protocols, when ρ=0.1, the performance of U_2 is better than U_1, while when ρ=0.9, the performance of U_1 was better than U_2. It can be explained as follows. In NOMA schemes, the U_1 (i.e., far user) should have more power to receive its signal with high quality. The increase of ρ increases the harvested power at the relay, which improves the received signal quality at U_1 in the second phase more than U_2 because it suffers from SIC. In the PS protocol, when ν=0.1, the performance of U2 is better than U_1, while when ν=0.9, the performance of U_1 outperforms U_2. The high ν values increase the harvested power at the relay, but it reduces the power of the received signal in the first phase, which leads to forwarding the signal to the users with more error. This affects the SIC and the detection of s_2 at relay and U_2.

In Figure 5.7, we present the BER performance of the users w.r.t. η for TS and PS protocols under ICSI when ρ=ν=0.3, and SNR=20 dB. We observe that increases η improve the BER performance of users in the two protocols. Also, the presence of the ICSI reduces the BER performance. It influences the signal detected and SIC at the relay and U_2.

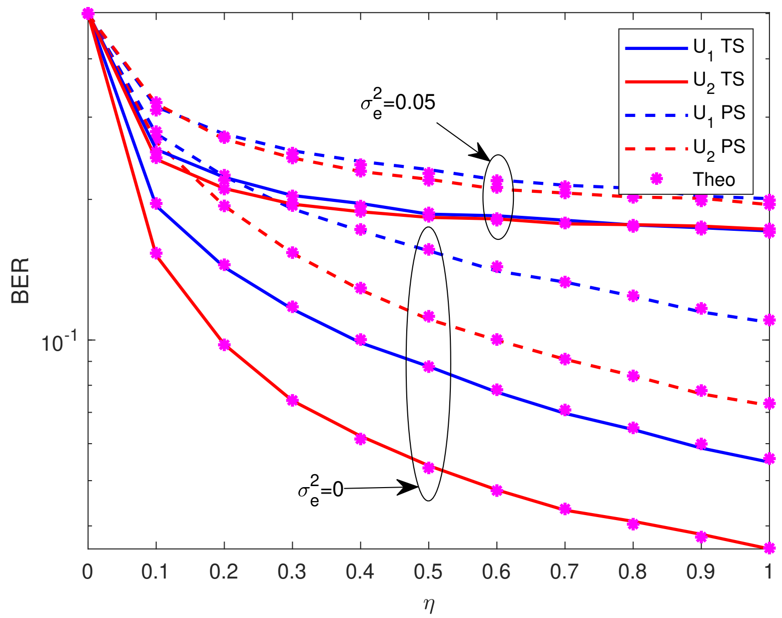

Figure 5.7: *BER w.r.t. η for the TS and PS protocols under ICSI.*

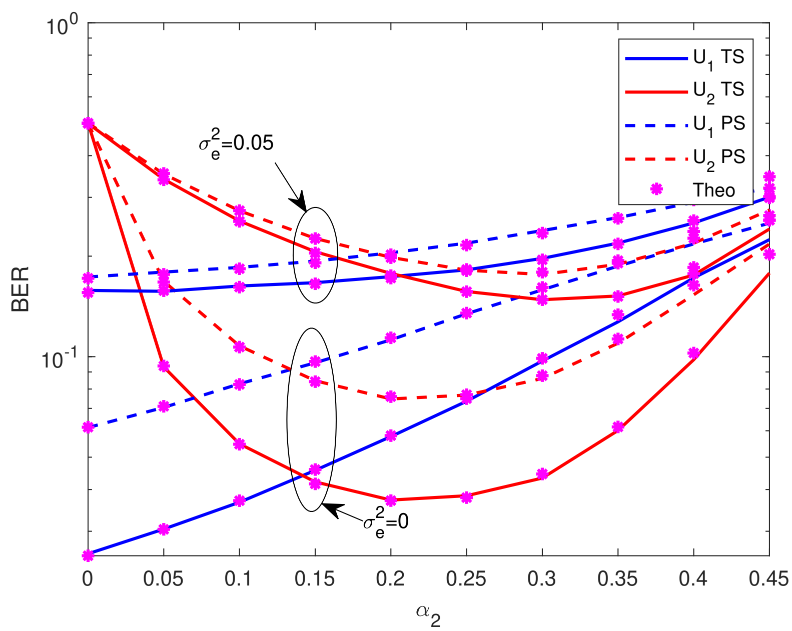

Figure 5.8: *BER w.r.t. α_2 for the TS and PS protocols under ICSI.*

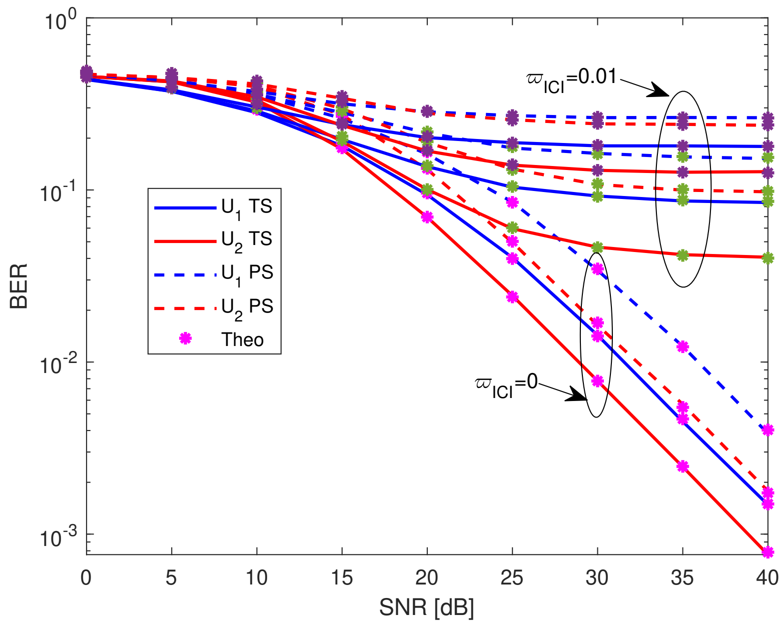

Figure 5.9: *BER w.r.t. SNR for the TS and PS protocols under ICI.*

In Figure 5.8, we present the BER performance of the users w.r.t. α_2 for TS and PS protocols under ICSI when ρ=ν=0.3, and SNR=20 dB. We observe that the change of α_2 affects the BER performance of users in the two protocols. Again, the presence of the ICSI reduces the BER performance in all α_2 values. The change of α_2 affects the signal detected by users and the SIC at the relay and users. The effect of SIC increased in the presence of ICSI with the change of $alpha_2$ and a greater reduction in performance due to increased error. In Figure 5.9, we present the BER performance of the users w.r.t. SNR for TS and PS protocols under ICI when ρ=ν=0.3. We observe that the BER performance of users degrades in the presence of ICI and causes an error floor at the high SNR. The increase of ϖ_{ICI} increases the error floor of the users' performance. The presence of ICI increases the error and impacts the signal detection of the users.

5.4.2 Cooperative NOMA with EH over Nagakamai-m Fading Channel

In this subsection, we validate the theoretical expressions by Monte Carlo simulations over the Nakagami-m fading channel. The channel parameters for all simulations are given in Table 5.1 and in all simulations, $\alpha_2 = 0.2$, $\alpha_1 = 0.8$, $\eta = 0.95$, R_1=0.1, and R_2=0.2.

In Figure 5.10, we present the BER performances of users for three EH protocols with different scenarios as presented in Table 5.1, where $\alpha_1 = 0.9$, and $\nu = \rho = 0.1$. It can be seen that the analytical and simulation results are matched perfectly, which validates our derivation. Additionally, both integer and non-integer values of m are presented, and it can be demonstrated that this shape parameter m determines the diversity order. In this figure, we observe that the hybrid

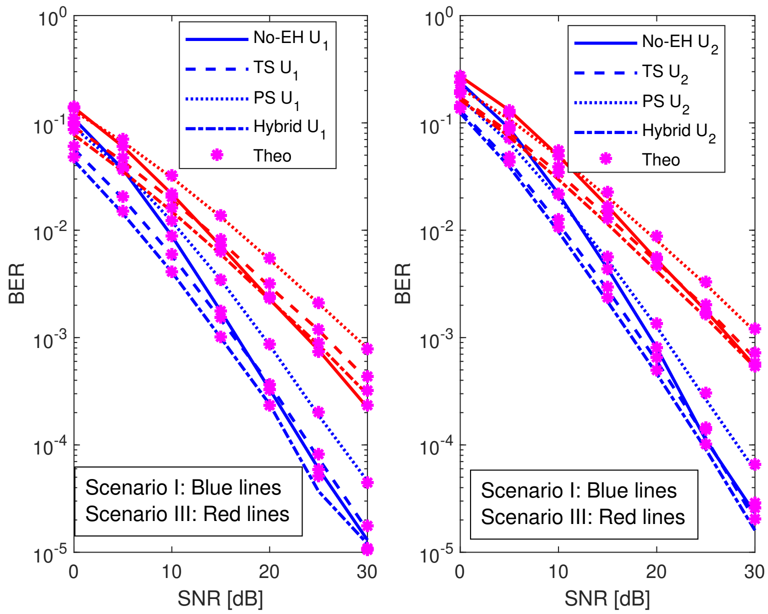

(a) *Comparison between Scenarios I and III*

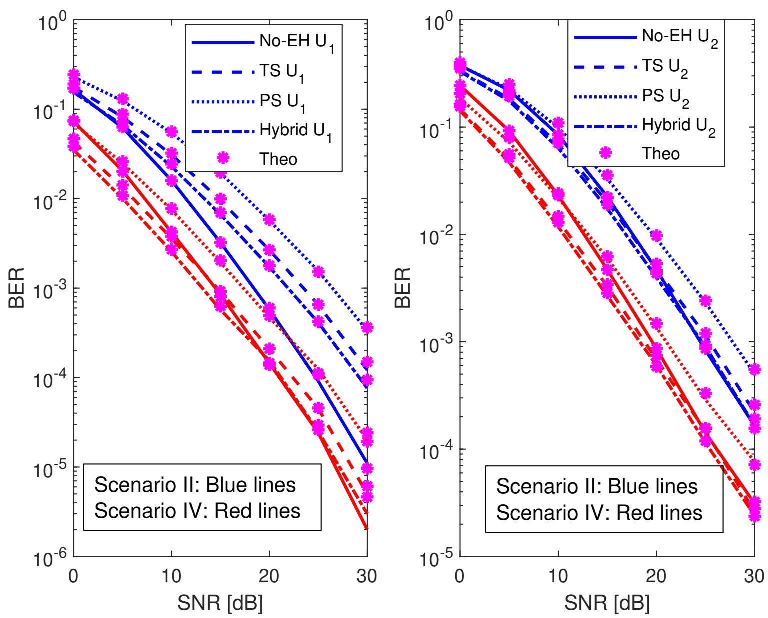

(b) Comparison between Scenarios II and IV

Figure 5.10: BER performance comparisons between hybrid protocol and benchmarks w.r.t. SNR.

Table 5.1: Channel parameters in simulations.

	Ω_r	Ω_1	Ω_2	m_r	m_1	m_2
Scenario I	10	2	10	1.5	1.5	1.5
Scenario II	2	2	10	1.5	1.5	1.5
Scenario III	10	2	10	1	1	1
Scenario IV	8	4	12	1.5	1.5	1.5

achieves better performance gain compared to all three benchmarks. Through the comparisons with different spread (i.e., Ω_r and Ω_k) and shape (i.e., m_r and m_k) parameters, in this figure, we observe that Scenario I outperforms Scenario III due the shape parameter in Scenario I is greater than in Scenario III, which enhanced diversity order because there is less erroneous detection in both phases. Likewise, we observe that Scenario IV outperforms Scenario II. It is due to the spread parameters being higher, which enhanced performance. Also, the linear sum of spread parameters (i.e., $\Omega_r + \Omega_k$) in Scenario I and Scenario IV are fixed, which reflects the relay position. We can see that Scenario IV is superior to Scenario I. Thus, we achieve better performance gain when the relay is close to the middle of the BS and users.

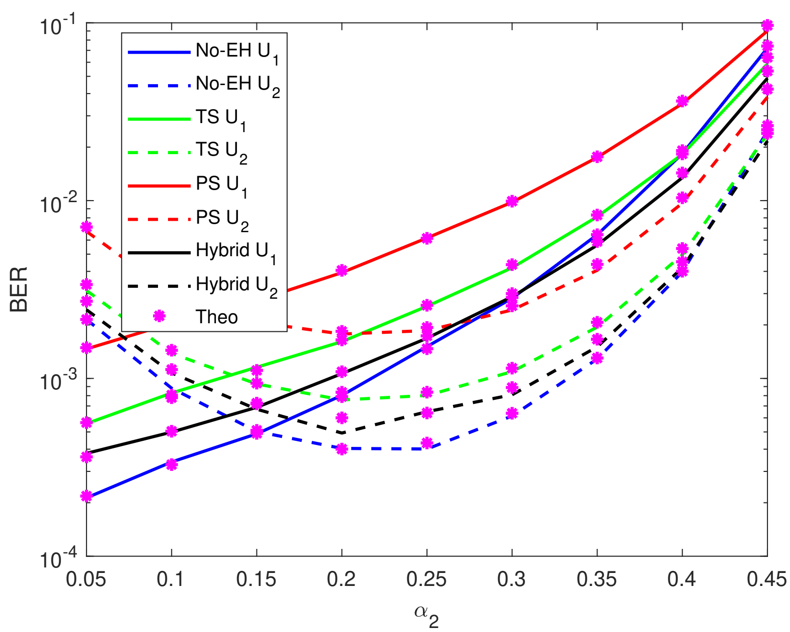

Figure 5.11: *BER performance comparisons between hybrid protocol and benchmarks w.r.t. power allocation.*

Since power allocation impacts the system performance, we evaluate the effect of power allocation on the BER performance in all schemes proposed. In Figure 5.11, we present the BER performance

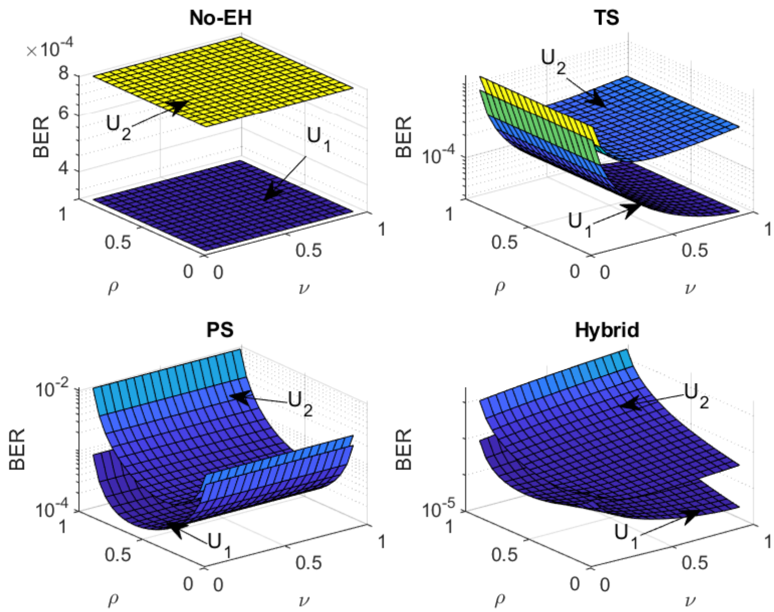

(a) *Scenario I*

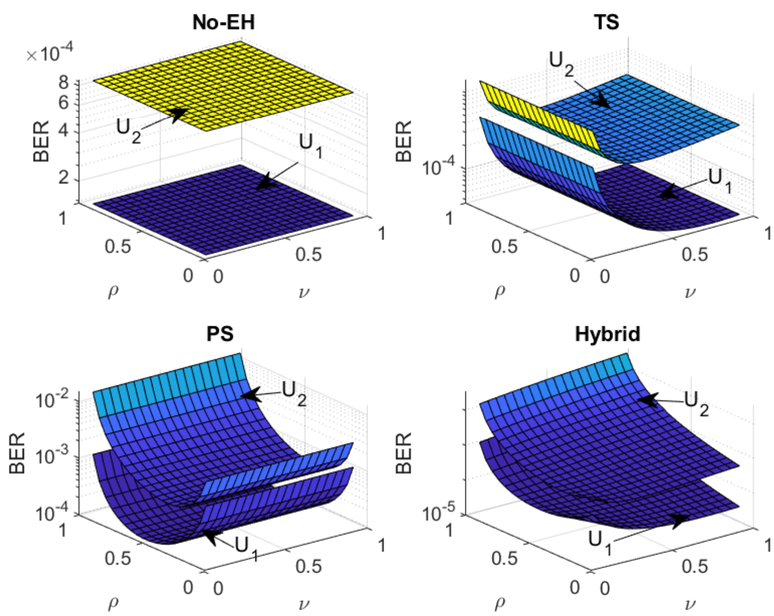

(b) *Scenario IV*

Figure 5.12: *BER performance comparisons between hybrid protocol and benchmarks w.r.t. EH parameters.*

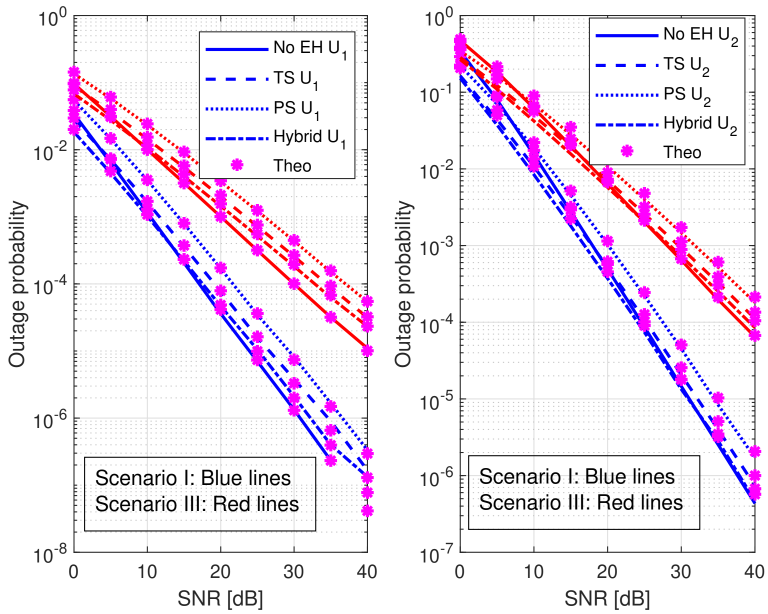

(a) *Comparison between Scenarios I and III*

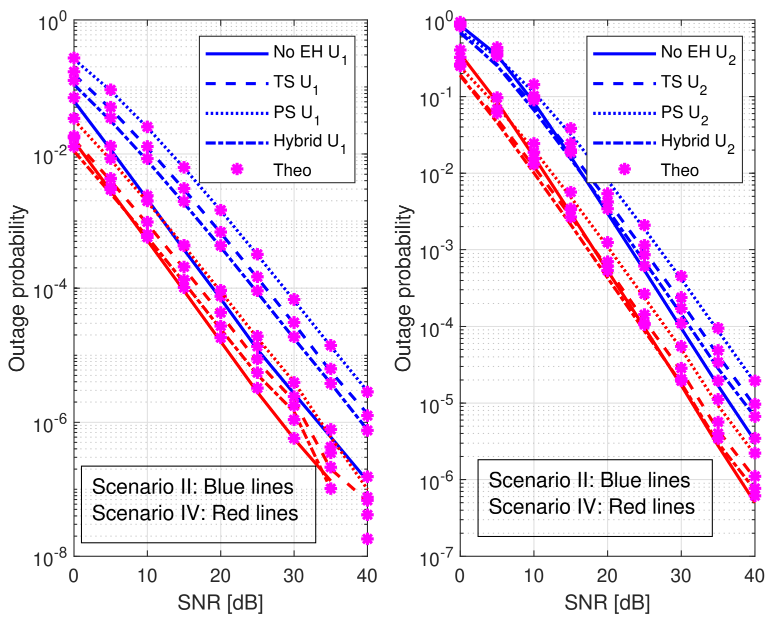

(b) *Comparison between Scenarios II and IV*

Figure 5.13: *OP performance comparisons between hybrid protocol and benchmarks w.r.t. SNR.*

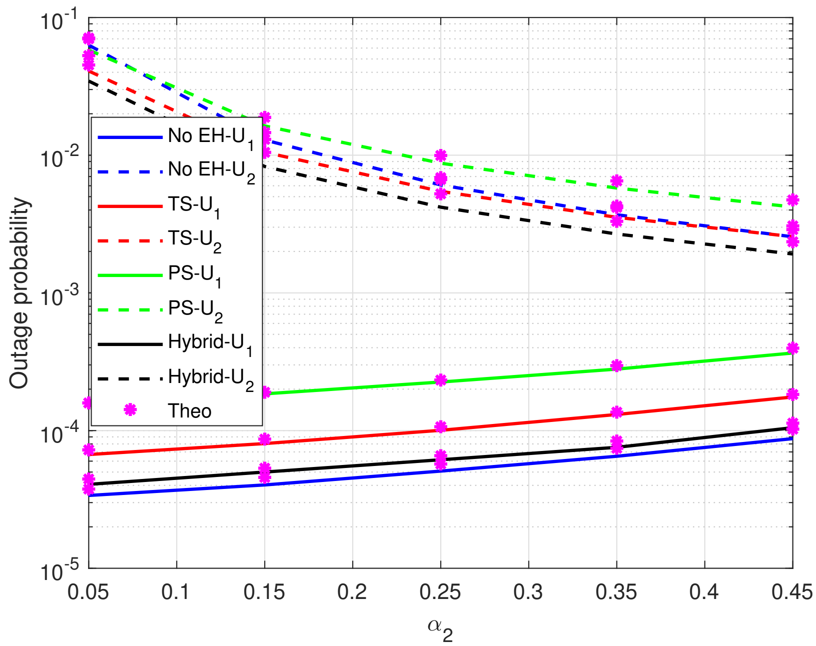

Figure 5.14: *OP performance comparisons between hybrid protocol and benchmarks w.r.t. power allocation.*

of users in Scenario I when SNR=20 dB. We observe that the hybrid still outperforms all three benchmarks despite the changes of α_2. The changes of α_2 affect one user at the expense of the other. The increase of α_2 leads to degrading the performance of U_1 and enhances the performance of U_2; however, the U_2 becomes worse with so much increase in α_2. It can be explained as follows. The increase of α_2 improves the performance of U_2 and with more increase of α_2 will affect the SIC and the detection of the symbols at relay and U_2. Thus, we can say that the optimum value of α_2 for both users should be $0.1 \leq \alpha_2 \leq 0.25$.

To clarify the impacts of the EH parameters (ν, ρ) on the system performance, in Figure 5.12, we present BER w.r.t. ν and ρ in Scenario I and Scenario IV. We can see from both comparisons, that the optimal ν-ρ can be chosen jointly to reduce the BER in a hybrid protocol depending on the channel conditions. For instance, in Scenario I, the link between the BS-relay is already good quality, which means that the relay is near the BS. Thus, the relay has less erroneous detection. Therefore, we can raise ν and ρ to increase the transmit power of the relay and provide reliable communication in the second phase. Furthermore, in Scenario IV, We should choose lower values of ν and ρ if the relay location is near the middle (i.e. the channel quality of the first phase is relatively worse). Thus, the increase of ν and ρ too much will affect the information processing in the first phase because less power is devoted to information transfer. Thus, the erroneous detection at the relay increases, which causes an error propagation in the second phase.

On the other hand, we illustrate the OP performance for all protocols in Figure 5.13 with

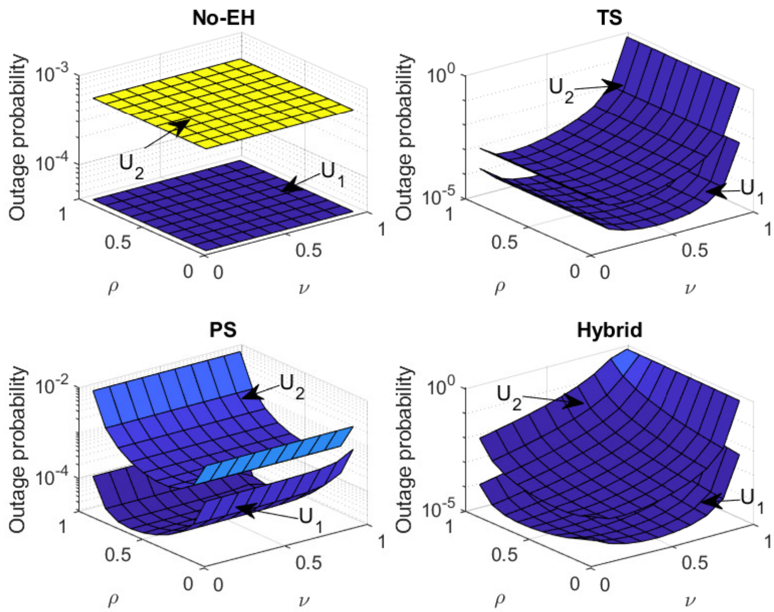

(a) *Scenario I*

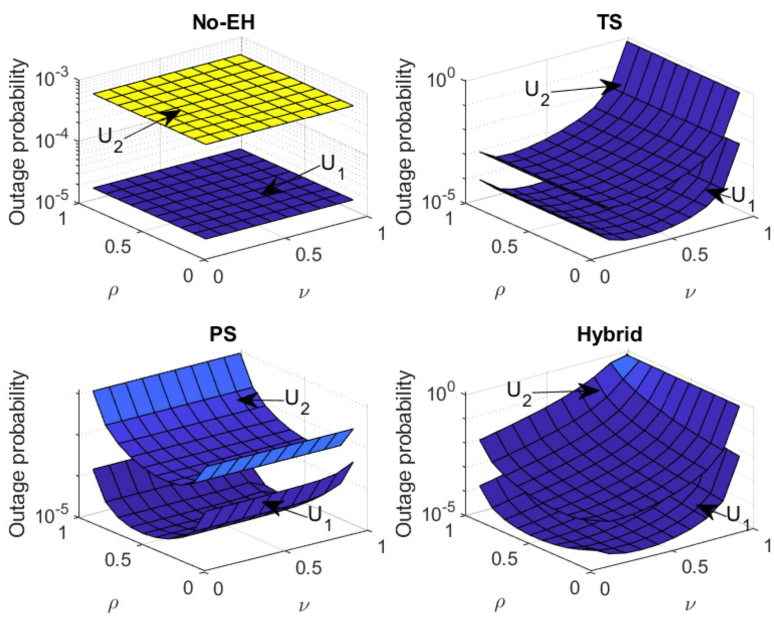

(b) *Scenario IV*

Figure 5.15: *OP performance comparisons between hybrid protocol and benchmarks w.r.t. EH parameters.*

different Scenarios as presented in Table 5.1. We observe that the hybrid protocol is superior to all benchmarks. Through comparisons, we observe that Scenario I is superior to Scenario III and Scenario IV is superior to Scenario II. As a result, it is clear that a greater shape parameter value decreases OP performance and enhances diversity order since a lower OP is acquired in both phases. Moreover, as can be seen, the lower spread parameter values denote a worse channel quality between BS and relay which affects the harvested power and the signal detection at the relay and the signal forwarded in the second phase. Thus, the minimal OP for both users can be attained depending on the relay position (e.g., when the relay is located near the middle). To illustrate the impact of power allocation on the OP performance, in Figure 5.14, we present the OP performance of both users in Scenario I when SNR=20 dB, R_1=0.1, and R_2=1.3. It is observed that the hybrid protocol outperforms TS and PS. It is seen also that increasing α_2 enhances the OP of U_2 and degrades the OP of U_1. It can be explained as follows. The higher α_2 values cause convergence of the power distribution between users, which leads to difficulty in the users' signals detection. Thus, taking into account the performances of both users, the optimal values for α_2 should be $0.1 \leq \alpha_2 \leq 0.25$. To present the impact of EH parameters (ρ, ν) on the OP performance, in Figure 5.15, we present the OP performance w.r.t. ρ and ν in Scenario I and Scenario IV. For both comparisons, an optimal ρ-ν pair to reduce OP can be chosen jointly based on the channel quality as shown in the previous discussion, so to reduce the OP, the state is the same here. The good channel between BS and the relay (i.e., the close location of the relay) reduces the outage in this link. Thus, increasing ρ and ν increases the harvested energy to obtain reliable communication in the second phase by raising the relay transmit power. Also, in Scenario IV, it should select a lower of ρ and ν when the relay position is near the middle. The greater ρ and ν values augment the outage in the first phase. Thus, it affects the information forwarded in the second phase.

5.5 Conclusion

This chapter has investigated two CNOMA with EH schemes. Firstly, the BER of CNOMA with TS and PS protocols has been analyzed over the Rayleigh fading channel when the ICSI, ISIC, and ICI are considered. Secondly, the OP and BER of CNOMA with three EH protocols (TS, PS, and hybrid) have been analyzed over the Nakagami-m fading channel. We have discussed the effect of power allocation, ICSI, ICI, and EH parameters on the performance of the systems. We have validated our analytical derivations by using Monte Carlo simulations. The results demonstrate that the hybrid protocol is superior to all benchmarks. In more detail, the performance improvement of the hybrid protocol over other schemes can be in the range of 1–3 dB and 0.5–1.5 dB for OP and BER performances, respectively, depending on channel characteristics. This proved that the same performance objectives could be met with decreased power consumption, which has significance for energy-limited devices. Also, the optimal values of the EH and power allocation parameters to reach a better performance gain for both users in the hybrid protocol can be selected based on the spread and shape parameter values. Furthermore, the hybrid protocol can improve the system performance by 10 times greater performance (e.g., $10^4 \rightarrow 10^5$).

Chapter 6

Wireless-Powered Cooperative Communication Network for Dual-Hop Uplink NOMA

6.1 Introduction

NOMA has been identified as a promising technology for 6G wireless mobile networks [148]. To improve spectral efficiency, QoS and the coverage area, the interplay between cooperative communication and NOMA has attracted tremendous attention from researchers [35, 12, 64]. With the rapid growth of the IoT and the increasing number of mobile devices, EH has attracted much interest as a sustainable means of extending the lifespan of wireless networks that are energy-limited [149].

6.1.1 Related Works

In [150], the coverage probability, ergodic rate, and EE have been analyzed for downlink cooperative NOMA-assisted simultaneous wireless information and power transfer (CNOMA SWIPT). The optimal power allocation factor and optimal TS with the effect of ISIC for downlink CNOMA with EH are derived to minimize the OP and maximize the system throughput [123]. The authors of [151] maximize the sum rate of PS and TS for downlink CNOMA with EH. The adaptive power allocation with FD CNOMA under TS protocol has been performed to improve OP and throughput performance [152]. With the perfect SIC and ISIC, the authors of [153, 154, 155] evaluate EC, throughput, and OP performance of the downlink CNOMA SWIPT for IoT. Furthermore, the authors of [156, 157] investigated the achievable rate, sum throughput, and EE for downlink and uplink jointly with PS-based SWIPT MIMO-NOMA systems. In [158], uplink NOMA with EH jammers has been analyzed in terms of OP and secrecy OP. On the other hand, a novel wireless network type known as a wireless-powered communication network (WPCN) has received increasing interest as a viable research subject. In this wireless network type, wireless stations are only powered by wireless energy transfer and use the collected energy to transfer information [159]. In [160], the capability of the resource allocation and time scheduling algorithms for a NOMA-based device-to-device and WPCN system has been investigated. A sum-throughput maximization problem for a NOMA-assisted WPCN with cluster-specific beamforming was developed by the authors of [161]. In [162], a multi-cell WPCN based on NOMA has been analyzed, along with a proposed algorithm to increase the sum throughput of the network. In [163, 164], a newly emerged NOMA and WPCNs with the aid of RIS technology has been carried out for sum-rate maximization.

As we discussed above, most of the existing studies consider a linear EH model, in which the energy harvested by the EH circuit rises linearly with the energy received from the RF signal. However, the reality is that the practical EH circuits have non-linear properties. An incremental CNOMA with non-linear EH has been analyzed in terms of OP and throughput [165]. In [166], the OP of FD-CNOMA with non-linear EH has been performed. The authors of [167, 168] investigate the OP, throughput, and sum rate of cognitive radio CNOMA-assisted multi-antenna with non-linear EH. In [169], FD-CNOMA with non-linear EH has been analyzed in terms of OP and throughput. In [170], CNOMA with linear and non-linear EH has been evaluated in terms of OP. The downlink CNOMA has been adopted for linear and non-linear EH with power beacon in terms of OP and throughput [171].

All aforementioned works consider the ideal RF front-end operating conditions. However, in reality, the transceiver RF front-end is prone to IQI since non-ideal mixers and phase shifters are used [172, 173, 174]. In [175, 176], the OP and the error probability are evaluated with the effects of IQI and ISIC. The authors of [63, 172] analyzed the OP and ergodic rate of the downlink FD/HD CNOMA with ISIC. In [177], the OP and intercept probability (IP) are obtained, to explore the reliable and secure performance of a cognitive ambient backscatter for NOMA with an internet-of-vehicle maritime transportation systems network when the IQI is considered for practical proposes. The OP and IP are derived for non-linear EH with downlink NOMA multi-relay with IQI and ICSI [178]. The OP of CNOMA-aided EH has been examined with the effect of residual hardware impairments (RHI) and ICSI [179].

6.1.2 Motivation and Contributions

As we have mentioned above, the OP of the downlink SWIPT CNOMA has been analyzed in [123, 150, 151, 152, 153, 154, 155] with and without ISIC under ideal RF front-end condition when the EH is linear. In [165, 166, 167, 168, 169, 171], the non-linear EH for downlink SWIPT CNOMA has been performed. Likewise, the uplink NOMA with SWIPT in terms of the OP, throughput, and EE are examined in [156, 157, 158], where the RF front-end condition is ideal and the EH is linear. Also, the OP and ergodic rate with the IQI imperfections for downlink SWIPT CNOMA has been evaluated in [63, 172, 175, 176] for linear EH and non-linear in [178]. Moreover, the throughput and sum rate of WPCN based on NOMA has been performed in [160, 161, 162, 163, 164]. The impact of practical proposals such as IQI with WPCN or EH has not received extensive attention in the literature. Therefore, it is important to consider practical proposals in the literature to evaluate the performance of systems. To the best of the authors' knowledge, the uplink CNOMA assisted WPCN with non-linear EH has not been studied in the literature. Moreover, most papers neglected the negative impact of the RF front-end deficiencies on uplink CNOMA with or without SWIPT. Therefore, this topic is critical to the actual implementation of practical systems, which is considered the first investigation in the open literature with non-linear EH. Motivated by this, we propose harvest-then-cooperate assisted NOMA for a wireless-powered cooperative communication network (HTC-NOMA-WPCCN), where the wireless power transfer (WPT) in the downlink and wireless information transmission (WIT) in uplink. The linear and non-linear EH are considered in our investigation. To make the investigation more realistic and practical, we take into account the IQI and SIC imperfections. Thus, the main contributions of this chapter are given as follows

- We propose the HTC-NOMA-WPCCN system with linear/non-linear EH and to improve the performance of the proposed system, we consider a group of multiple near users, which help to increase the quality of the received signal at the access point.
- For a more realistic scenario, the ideal and non-ideal IQI with ISIC have been considered in our system. We derive closed-form analytical expressions for OP and throughput with linear and non-linear EH. We obtained accurate analytical expressions of EC for our proposed system with linear and non-linear EH under the effects of IQI and ISIC.
- We employ the commonly utilized image-rejection ratio (IRR) metric to evaluate the impacts of IQI. Hence, we discuss the effect of the IQI and SIC imperfections with different WPCCN parameters and power allocation on the proposed scheme. We validate our numerical derivations by simulation results.
- As a benchmark, we compare the proposed scheme with the uplink NOMA without EH. The simulation results validate the presented analyses and show the superiority of the proposed scheme over the benchmark. Moreover, the IQI has negative effects on OP, EC and the throughput of systems. In a non-linear model, IQI and ISIC have a significant impact on system performance.

6.2 System Model

The proposed system consists of one access point (AP), one far user (U_F) and L near users U_{NJ}, where $J = 1, 2, 3, ..., L$ as shown in Figure 6.1. We assume that the U_{NJ} works as assistant users in DF protocol to improve the received signal of U_F at AP. It is assumed that each node works in HD mode and the communication links experience Rayleigh fading. It is assumed that the channel coefficients between each other are independent. We consider that all users have no other embedded energy supply, and they collect energy[1] from the AP in the downlink, which can be stored in a rechargeable battery and afterward utilized to transmit the signal to the AP in the uplink. It is assumed that CSI is available at all nodes.

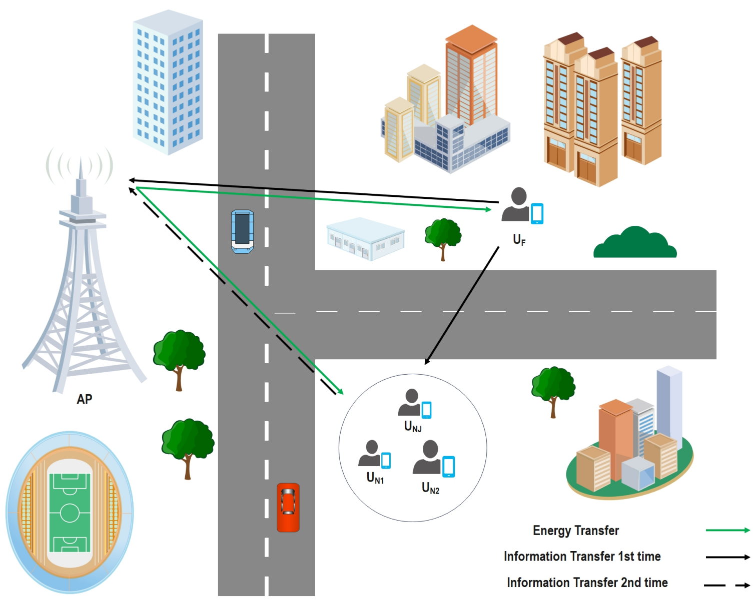

Figure 6.1: *HTC-NOMA-WPCCN scheme.*

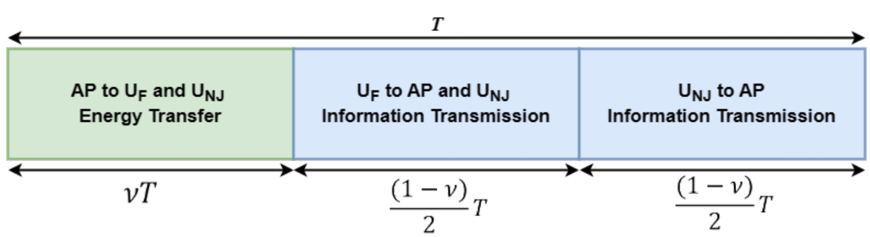

Figure 6.2: *Block diagram of harvest and information transmission for the proposed system.*

We assume that the RF impairment is described as IQI in both TX and RX, which is the phase and/or amplitude imbalance between the in-phase and quadrature-phase branches. Hence, the baseband form of the IQI-impaired signal is written by [63]

$$y_{IQI} = \mu_{t/r} s + \nu_{t/r} s^*, \tag{6.1}$$

[1] The WPCN is assumed to be used in our proposed system. A WPCN is only powered by wireless energy transfer and uses the harvested energy to transfer information i.e., the nodes need to harvest energy during the first time and then use it to forward information during the second time [159].

where $\mu_{t/r}$ and $\nu_{t/r}$ are the IQI coefficients at the TX/RX respectively, s is the baseband transmit signal, and $(.)^*$ denotes conjugation. It is noticed that in the absence of IQI, $\mu_t = \mu_r = 1$ and $\nu_t = \nu_r = 0$. The IQI coefficients $\mu_{t/r}$ and $\nu_{t/r}$ are expressed by [63] as $\mu_t = \frac{1}{2}(1 + \epsilon_t \exp(\mathfrak{i}\, \phi_t))$, $\nu_t = \frac{1}{2}(1 - \epsilon_t \exp(-\mathfrak{i}\, \phi_t))$, $\mu_r = \frac{1}{2}(1 + \epsilon_r \exp(-\mathfrak{i}\, \phi_r))$ and $\nu_r = \frac{1}{2}(1 - \epsilon_r \exp(\mathfrak{i}\, \phi_r))$, where $\epsilon_{t/r}$ and $\phi_{t/r}$ are the amplitude and the phase imbalance levels of TX/RX, $\mathfrak{i} = \sqrt{-1}$ is the unit of the imaginary. The IRR calculates the frequency band used for images' attenuation. The IRR is generally between 20 and 40 dB in the literature for practical analog RF front-end circuits [63]. Thus, the IRR is expressed by

$$IRR_{t/r} = \frac{|\ \mu_{t/r}|^2}{|\ \nu_{t/r}|^2}. \tag{6.2}$$

As shown in Figure 6.2, in the first νT time slot, the users harvest energy from AP. Both linear and non-linear EH models are adopted in this system. In the linear EH model, the harvested energy during the power transfer phase in each user is given as

$$E_F^{Lin} = \eta \nu P_t |h_{AF}|^2 T, \tag{6.3}$$

$$E_{NJ}^{Lin} = \eta \nu P_t |h_{ANJ}|^2 T. \tag{6.4}$$

Nevertheless, taking into account the non-linear feature of a practical EH circuit, the corresponding expressions during the power transfer phase in each user can be given by

$$E_F^{NL} = \begin{cases} \eta \nu P_t |h_{AF}|^2 T, & P_t |h_{AF}|^2 \leq P_{th}, \\ \eta \nu P_{th} T, & P_t |h_{AF}|^2 > P_{th}, \end{cases} \tag{6.5}$$

$$E_{NJ}^{NL} = \begin{cases} \eta \nu P_t |h_{ANJ}|^2 T, & P_t |h_{ANJ}|^2 \leq P_{th}, \\ \eta \nu P_{th} T, & P_t |h_{ANJ}|^2 > P_{th}, \end{cases} \tag{6.6}$$

where P_t and P_{th} are the total transmit power and the saturation threshold respectively, h_{AF} and h_{ANJ} are the channels between AP-U$_F$ and AP-U$_{NJ}$, η is the EH efficiency, in which $0 \leq \eta \leq 1$, ν is the energy transfer factor and T is the transmission block period.

The remaining fraction (1 - ν) of the block is divided into two-time slots with an equal length of $(1 - \nu)T/2$ for cooperative information transmission in the uplink (please see Figure 6.2).

Accordingly, in the linear EH model, the transmit power of users in the second (uplink) phase is given as

$$P_F^{Lin} = \frac{E_F^{Lin}}{(1-\nu)^T/2} = \frac{2\eta\nu |h_{AF}|^2}{(1-\nu)} = P_t \psi_1 |h_{AF}|^2, \tag{6.7}$$

$$P_{NJ}^{Lin} = \frac{E_{NJ}^{Lin}}{(1-\nu)^T/2} = \frac{2\eta\nu P_t |h_{ANJ}|^2}{(1-\nu)} = P_t \psi_1 |h_{ANJ}|^2. \tag{6.8}$$

However, in the non-linear EH model, the transmit power of users in the second (uplink) phase is given as

$$P_F^{NL} = \frac{E_F^{NL}}{(1-\nu)T/2} = \begin{cases} P_t\psi_1|h_{AF}|^2, & P_t|h_{AF}|^2 \leq P_{th}, \\ P_{th}\psi_1, & P_t|h_{AF}|^2 > P_{th}, \end{cases} \tag{6.9}$$

$$P_{NJ}^{NL} = \frac{E_{NJ}^{NL}}{(1-\nu)T/2} = \begin{cases} P_t\psi_1|h_{ANJ}|^2, & P_t|h_{ANJ}|^2 \leq P_{th}, \\ P_{th}\psi_1, & P_t|h_{ANJ}|^2 > P_{th}, \end{cases} \tag{6.10}$$

where $\psi_1 = \frac{2\eta\nu}{(1-\nu)}$, $h_{AF} \sim \mathcal{CN}(0, \sigma_{AF}^2 = d_{AF}^{\varsigma})$ and $h_{ANJ} \sim \mathcal{CN}(0, \sigma_{ANJ}^2 = d_{ANJ}^{\varsigma})$ are the channels between AP-U$_F$ and AP-U$_{NJ}$, respectively, and ς is the path loss factor.

During the first time slot $(1-\nu)T/2$ of the uplink WPCCN NOMA, the U$_F$ transmits its signal s_1 to AP and U$_{NJ}$. The received signals at AP and U$_{NJ}$ are given respectively as

$$\begin{aligned} {y_{FA,o}}^{IQI} &= \mu_{r,1A}(\sqrt{P_F^o}(\mu_{t,FA}s_1h_{FA} + \nu_{t,FA}{s_1}^*h_{FA}^*) + n) \\ &+ \nu_{r,FA}(\sqrt{P_F^o}(\mu_{t,FA}s_1h_{FA} + \nu_{t,FA}{s_1}^*h_{FA}^*) + n)^*, \end{aligned} \tag{6.11}$$

$$\begin{aligned} {y_{FNJ,o}}^{IQI} &= \mu_{r,FNJ}(\sqrt{P_F^o}(\mu_{t,FNJ}s_1h_{FNæ} + \nu_{t,FNJ}{s_1}^*h_{FNJ}^*) + n) \\ &+ \nu_{r,FNJ}(\sqrt{P_F^o}(\mu_{t,FNJ}s_1h_{FNJ} + \nu_{t,FNJ}{s_1}^*h_{FNJ}^*) + n)^*, \end{aligned} \tag{6.12}$$

where $h_{FA} \sim \mathcal{CN}(0, \sigma_{FA}^2 = d_{FA}^{\varsigma})$ and $h_{FNJ} \sim \mathcal{CN}(0, \sigma_{FNJ}^2 = d_{FNJ}^{\varsigma})$ are the channels between U$_F$-AP and U$_F$-U$_{FNJ}$ [2], n is the AWGN, s_1 is the signal of U$_F$, $\mu_{t,FNJ/r,FNJ}$, $\mu_{t,FA/r,FA}$, $\nu_{t,FNJ/r,FNJ}$, and $\nu_{t,FA/r,FA}$ are the IQI coefficients at the TX/RX and equal to $\mu_{t/r}$ and $\nu_{t/r}$ in (6.1). P_F^o denotes the transmit power of U$_F$, which depends on the linear or non-linear EH models as in (6.7) and (6.9), where $o = Lin, NL$.

The AP and U$_{NJ}$ decode s_1 using MLD. In the linear model, the SINRs during the first $(1-\nu)T/2$ time at AP and U$_{NJ}$ are given as

$$\gamma_{1,Lin}^{FA} = \frac{P_t\psi_1|h_{AF}|^2|h_{FA}|^2A_{FA}}{P_t\psi_1|h_{AF}|^2|h_{FA}|^2B_{FA} + \sigma^2C_{FA}}, \tag{6.13}$$

$$\gamma_{1,Lin}^{FNJ} = \frac{P_t\psi_1|h_{AF}|^2|h_{FNJ}|^2A_{FNJ}}{P_t\psi_1|h_{AF}|^2|h_{FNJ}|^2B_{FNJ} + \sigma^2C_{FNJ}}. \tag{6.14}$$

However, in the non-linear model, the SINRs during the first $(1-\nu)T/2$ time at AP and U$_{NJ}$ are given as

$$\gamma_{1,NL}^{FA} = \begin{cases} \emptyset_1^{FA}, & P_t|h_{AF}|^2 \leq P_{th}, \\ \emptyset_2^{FA}, & P_t|h_{AF}|^2 > P_{th}, \end{cases} \tag{6.15}$$

[2]Since the transmission of power and information occurs in two different phases (i.e., in downlink and uplink), it is supposed that $h_{AF} \neq h_{FA}$ and $h_{ANJ} \neq h_{NJA}$.

$$\gamma_{1,NL}^{FNJ} = \begin{cases} \emptyset_1^{FNJ}, & P_t|h_{AF}|^2 \leq P_{th}, \\ \emptyset_2^{FNJ}, & P_t|h_{AF}|^2 > P_{th}, \end{cases} \tag{6.16}$$

where $\mathrm{A}_{FA} = (\mu_{r,FA}^2\mu_{t,FA}^2 + \nu_{r,FA}^2\nu_{t,FA}^2)$, $\mathrm{B}_{FA} = (\mu_{r,FA}^2\nu_{t,FA}^2 + \nu_{r,FA}^2\mu_{t,FA}^2)$, $\mathrm{C}_{FA} = (\mu_{r,FA}^2 + \nu_{r,FA}^2)$, $\mathrm{A}_{FNJ} = (\mu_{r,FNJ}^2\mu_{t,FNJ}^2 + \nu_{r,FNJ}^2\nu_{t,FNJ}^2)$, $\mathrm{B}_{FNJ} = (\mu_{r,FNJ}^2\nu_{t,FNJ}^2 + \nu_{r,FNJ}^2\mu_{t,FNJ}^2)$, $\mathrm{C}_{FNJ} = (\mu_{r,FNJ}^2 + \nu_{r,FNJ}^2)$, $\emptyset_1^{FA} = \frac{P_t\psi_1|h_{AF}|^2|h_{FA}|^2A_{FA}}{P_t\psi_1|h_{AF}|^2|h_{FA}|^2B_{FA}+\sigma^2C_{FA}}$, $\emptyset_1^{FNJ} = \frac{P_t\psi_1|h_{AF}|^2|h_{FNJ}|^2A_{FNJ}}{P_t\psi_1|h_{AF}|^2|h_{FNJ}|^2B_{FNJ}+\sigma^2C_{FNJ}}$, $\emptyset_2^{FA} = \frac{P_{th}\psi_1|h_{FA}|^2A_{FA}}{P_{th}\psi_1|h_{FA}|^2B_{FA}+\sigma^2C_{FA}}$, and $\emptyset_2^{FNJ} = \frac{P_{th}\psi_1|h_{FNJ}|^2A_{FNJ}}{P_{th}\psi_1|h_{FNJ}|^2B_{FNJ}+\sigma^2C_{FNJ}}$.

During the second $(1-\nu)T/2$ time, all U_{NJ} combines their signal s_2 with the coming signal from U_F in a superimposed coding signal[3] and transmits the total signal simultaneously using the harvested power to AP. Thus, the AP received the same signal from L U_{NJ} (i.e., L path). Hence, the received signal by AP in the channel corresponding to U_{NJ} is given by

$$\begin{aligned} &{y_{NJA,o}}^{IQI} = \\ &\mu_{r,NJA}(\sqrt{P_{NJ}^o}(\mu_{t,NJA}X_{SC}h_{NJA} + \nu_{t,NJA}{X_{SC}}^*h_{NJA}^*) + n) \\ &+ \nu_{r,NJA}(\sqrt{P_{NJ}^o}(\mu_{t,NJA}{X_{SC}}^*h_{NJA} + \nu_{t,NJA}X_{SC}^*h_{NJA}^*) + n)^*, \end{aligned} \tag{6.17}$$

where $X_{SC} = \sqrt{\alpha_1}s_1 + \sqrt{\alpha_2}s_2$, α_1 and α_2 are the power allocation coefficients of s_1 and s_2, $h_{NJA} \sim \mathcal{CN}(0, \sigma_{NJA}^2 = d_{NJA}^\varsigma)$ is the channel between L U_{NJ} and AP. $\mu_{t,NJA/r,NJA}$ and $\nu_{t,NJA/r,NæA}$ are the IQI coefficients at the TX/RX and equal to $\mu_{t/r}$ and $\nu_{t/r}$ in (6.1). P_{NJ}^o denotes the transmit power of U_{NJ}, which depends on the linear or non-linear EH models as in (6.8) and (6.10), where $o = Lin, NL$.

At AP, s_1 is detected firstly using MLD and s_2 is detected using the SIC. Thus, during this time, the SINRs of the linear model to detect s_1 and s_2 in the channel corresponding to U_{NJ} at AP can be expressed as

$$\gamma_{1,Lin}^{NJA} = \frac{P_t\alpha_1\psi_1|h_{NJA}|^2|h_{ANJ}|^2A_{NJA}}{P_t\alpha_1\psi_1|h_{NJA}|^2|h_{ANJ}|^2A_{NJA} + P_t\psi_1|h_{NJA}|^2|h_{ANJ}|^2B_{NJA} + \sigma^2C_{NJA}}, \tag{6.18}$$

$$\gamma_{2,Lin}^{NJA} = \frac{P_t\alpha_2\psi_1|h_{NJA}|^2|h_{ANJ}|^2A_{NJA}}{\varrho P_t\alpha_1\psi_1|h_{NJA}|^2|h_{ANJ}|^2A_{NJA} + P_t\psi_1|h_{NJA}|^2|h_{ANJ}|^2B_{NJA} + \sigma^2C_{NJA}}. \tag{6.19}$$

Likewise, the SINRs of the non-linear model to detect s_1 and s_2 in the channel corresponding to U_{NJ} at AP can be expressed as

$$\gamma_{1,NL}^{NJA} = \begin{cases} \emptyset_1^{NJA} = \frac{P_t\alpha_1\psi_1|h_{NJA}|^2|h_{ANJ}|^2A_{NJA}}{P_t\alpha_1\psi_1|h_{NJA}|^2|h_{ANJ}|^2A_{NJA}+P_t\psi_1|h_{NJA}|^2|h_{ANJ}|^2B_{NJA}+\sigma^2C_{NJA}}, & P_t|h_{ANJ}|^2 \leq P_{th}, \\ \emptyset_2^{NJA} = \frac{P_{th}\alpha_1\psi_1|h_{NJA}|^2A_{NJA}}{P_{th}\alpha_1\psi_1|h_{NJA}|^2A_{NJA}+P_{th}\psi_1|h_{NJA}|^2B_{NJA}+\sigma^2C_{NJA}}, & P_t|h_{ANJ}|^2 > P_{th}, \end{cases} \tag{6.20}$$

[3]Based on NOMA schemes, the L U_{NJ} combines s_1 and s_2 and it is assumed that s_1 has high power allocation than s_2 based on the channel gain $E[|h_{FA}|^2] < E[|h_{NJA}|^2]$, $\alpha_1 > \alpha_2$, in which $\alpha_1 + \alpha_2$=1 [61].

$$\gamma_{2,NL}^{NJA} = \begin{cases} \emptyset_3^{NJA} = \frac{P_t\alpha_2\psi_1|h_{NJA}|^2|h_{ANJ}|^2A_{NJA}}{\varrho P_t\alpha_1\psi_1|h_{NJA}|^2|h_{ANJ}|^2A_{NJA}+P_t\psi_1|h_{NJA}|^2|h_{ANJ}|^2B_{NJA}+\sigma^2C_{NJA}}, & P_t|h_{ANJ}|^2 \le P_{th}, \\ \emptyset_4^{NJA} = \frac{P_{th}\alpha_2\psi_1|h_{NJA}|^2A_{NJA}}{\varrho P_{th}\alpha_1\psi_1|h_{NJA}|^2A_{NJA}+P_{th}\psi_1|h_{NJA}|^2B_{NJA}+\sigma^2C_{NJA}}, & P_t|h_{ANJ}|^2 > P_{th}, \end{cases} \tag{6.21}$$

where $\mathrm{A}_{NJA} = (\mu_{r,NJA}^2\mu_{t,NJA}^2+\nu_{r,NJA}^2\nu_{t,NJA}^2)$, $\mathrm{B}_{NJA} = (\mu_{r,NJA}^2\nu_{t,NJA}^2+\nu_{r,NJA}^2\mu_{t,NJA}^2)$, $\mathrm{C}_{NJA} = (\mu_{r,NJA}^2+\nu_{r,NJA}^2)$, and ϱ is the effect of the SIC process.

The AP receives multiple signals from L U_{NJ} and U_F. Thus, the AP received the signals from multi-path. Hence, the selection combining technique is assumed to be used at AP to select the best-received signal[4] based on all received signals from L U_{NJ} and U_F. Hence, the SINRs of s_1 and x_2 when the SC is implemented in the linear or non-linear models are given as

$$\gamma_{1,o}^{SC} = \max_{J=1,2,3,\ldots,L} \left(\gamma_{1,o}^{FA}, \gamma_{1,o}^{NJA}\right), \tag{6.22}$$

$$\gamma_{2,o}^{SC} = \max_{J=1,2,3,\ldots,L} \left(\gamma_{2,o}^{NJA}\right), \tag{6.23}$$

where $o = Lin, NL$.

6.3 Performance analysis

In this section, we derive the OP, throughput, and EC expressions of HTC-NOMA-WPCCN with linear and non-linear EH models under IQI and SIC imperfections.

6.3.1 Outage Probability

6.3.1.1 Linear EH

The AP received the signal s_1 from different sources i.e., U_F and U_{NJ}. The SC is implemented at AP, where only the signal with the highest SINR among those received is utilized for detection. The OP of the SC for s_1 at AP can be written as [180]

$$P_{x_1,Lin}^{SC}(out) = P\left(\gamma_{1,Lin}^{SC} < \theta_1\right) = P\left(\max_{J=1,2,3,\ldots,L} \left(\gamma_{1,Lin}^{FA}, \gamma_{1,Lin}^{NJA}\right) < \theta_1\right). \tag{6.24}$$

Thus, (6.24) can be written as

$$P_{s_1,Lin}^{SC}(out) = \prod_{J}^{L} P\left(|h_{AF}|^2|h_{FA}|^2 < \zeta_F\right) P\left(|h_{ANJ}|^2|h_{NJA}|^2 < \zeta_{NJ}^1\right). \tag{6.25}$$

By employing the PDF and the CDF of the dedicated Rayleigh fading channel as in [125, 180], (6.25) can be calculated as

[4] It is assumed that the selection in the selection combining technique at the receiver is based on the higher channel quality of the received signals similar to the antenna selection strategy [19]. Generally, we can obtain a selection signal according to the higher-received SINR at AP [19].

$$\begin{aligned} P^{SC}_{x_1,Lin}(out) &= \prod_{J}^{L} \left(1 - \int_0^\infty P\left(|h_{AF}|^2 < \frac{\zeta_F}{y}\right) f_{|h_{FA}|^2}(y)\ \mathrm{d}y\right) \\ &\times \left(1 - \int_0^\infty P\left(|h_{ANJ}|^2 < \frac{\zeta^1_{NJ}}{y}\right) f_{|h_{NJA}|^2}(y)\ \mathrm{d}y\right) \\ &= \prod_{J}^{L} \left(1 - \frac{1}{\sigma^2_{FA}} \int_0^\infty \exp\left(-\frac{\zeta_F}{\sigma^2_{AF} y} - \frac{y}{\sigma^2_{FA}}\right)\ \mathrm{d}y\right) \\ &\times \left(1 - \frac{1}{\sigma^2_{NJA}} \int_0^\infty \exp\left(-\frac{\zeta^1_{NJ}}{\sigma^2_{ANJ} y} - \frac{y}{\sigma^2_{NJA}}\right)\ \mathrm{d}y\right). \end{aligned} \tag{6.26}$$

By using [181, Eq. (3.324.1)], the integral of (6.26) can be written as

$$P^{SC}_{x_1,Lin}(out) = \prod_{J}^{L} \left(1 - \Lambda\left(\frac{4\zeta_F}{\sigma^2_{AF}\sigma^2_{FA}}\right)\right)\left(1 - \Lambda\left(\frac{4\zeta^1_{NJ}}{\sigma^2_{ANJ}\sigma^2_{NJA}}\right)\right), \tag{6.27}$$

where $\zeta^1_{NJ} = \frac{\sigma^2 C_{NJA}\theta_1}{P_t\psi_1(A_{NJA}\alpha_1 - \alpha_2 A_{NJA}\theta_1 - B_{NJA}\theta_1)}$, $\zeta_F = \frac{\sigma^2 C_{FA}\theta_1}{(A_{FA} - B_{FA}\theta_1)P_t\psi_1}$, $\theta_1 = 2^{\frac{2Tr_1}{1-\tau}} - 1$, Tr_1 is the target rate of s_1, θ_1 is the transmission threshold of s_1 and $\Lambda(x) = \sqrt{x}K_1(\sqrt{x})$ is defined for notation simplification with $\mathrm{K}_1(\cdot)$ denoting the modified Bessel function of the second kind with first order [181]. It is noted that through (6.27), the effects of IQI and ISIC influence OP performance.

Also, the OP of s_2 occurs when AP can not successfully decode the s_1 signal and s_2 signal. Based on these events, the OP of s_2 can be expressed as in [63, 64, 180] as

$$\begin{aligned} P^{SC}_{x_2,Lin}(out) &= P\left(\max_{J=1,2,3,\ldots,L} (\gamma^{NJA}_{1,Lin}) < \theta_1\right) + \left[1 - P\left(\max_{J=1,2,3,\ldots,L} (\gamma^{NJA}_{1,Lin}) < \theta_1\right)\right] \\ &\times P\left(\max_{J=1,2,3,\ldots,L} (\gamma^{NJA}_{2,Lin}) < \theta_2\right). \end{aligned} \tag{6.28}$$

Each term of (6.28) is calculated as

$$\begin{aligned} P\left(\max_{J=1,2,3,\ldots,L} (\gamma^{NJA}_{1,Lin}) < \theta_1\right) &= \prod_{J}^{L} P\left(|h_{ANJ}|^2 |h_{NJA}|^2 < \zeta^1_{NJ}\right) \\ &= \prod_{J}^{L} \left(1 - \int_0^\infty P\left(|h_{ANJ}|^2 > \frac{\zeta^1_{NJ}}{y}\right) f_{|h_{NJA}|^2}(y)\ \mathrm{d}y\right) \\ &= \prod_{J}^{L} \left(1 - \frac{1}{\sigma^2_{NJA}} \int_0^\infty \exp\left(-\frac{\zeta^1_{NJ}}{\sigma^2_{ANJ} y} - \frac{y}{\sigma^2_{NJA}}\right)\ \mathrm{d}y\right) \\ &= \prod_{J}^{L} \left(1 - \Lambda\left(\frac{4\zeta^1_{NJ}}{\sigma^2_{ANJ}\sigma^2_{NJA}}\right)\right), \end{aligned} \tag{6.29}$$

$$
\begin{aligned}
P\left(\max_{J=1,2,3,\ldots,L}(\gamma_{2,Lin}^{NJA})<\theta_2\right) &= P\left(|h_{ANJ}|^2|h_{NJA}|^2<\zeta_{NJ}^2\right)\\
&=\prod_{J}^{L}\left(1-\int_0^{\infty}P\left(|h_{ANJ}|^2>\frac{\zeta_{NJ}^2}{y}\right)f_{|h_{NJA}|^2}(y)\,\mathrm{d}y\right)\\
&=\prod_{J}^{L}\left(1-\frac{1}{\sigma_{NJA}^2}\int_0^{\infty}\exp\left(-\frac{\zeta_{NJ}^2}{\sigma_{ANJ}^2 y}-\frac{y}{\sigma_{NJA}^2}\right)\mathrm{d}y\right)\\
&=\prod_{J}^{L}\left(1-\Lambda\left(\frac{4\zeta_{NJ}^2}{\sigma_{ANJ}^2\sigma_{NJA}^2}\right)\right),
\end{aligned}
\tag{6.30}
$$

where $\zeta_{NJ}^2=\frac{\sigma^2 C_{NJA}\theta_2}{P_t\psi_1(A_{NJA}\alpha_2-\varrho\alpha_1 A_{NJA}\theta_2-B_{NJA}\theta_2)}$, $\theta_2=2^{\frac{2Tr_2}{1-\tau}}-1$, Tr_2 is the target rate of s_2 and θ_2 is the transmission threshold of s_2.

By substituting (6.29) and (6.30) into (6.28), we find the OP of s_2 at AP as given by

$$
\begin{aligned}
P_{x_2,Lin}^{SC}(out) &= \prod_{J}^{L}\left(1-\Lambda\left(\frac{4\zeta_{NJ}^1}{\sigma_{ANJ}^2\sigma_{NJA}^2}\right)\right)+\left[1-\prod_{J}^{L}\left(1-\Lambda\left(\frac{4\zeta_{NJ}^1}{\sigma_{ANJ}^2\sigma_{NJA}^2}\right)\right)\right]\\
&\times\prod_{J}^{L}\left(1-\Lambda\left(\frac{4\zeta_{NJ}^2}{\sigma_{ANJ}^2\sigma_{NJA}^2}\right)\right),
\end{aligned}
\tag{6.31}
$$

Through (6.29) and (6.30), it appears that the IQI and ISIC affect the OP performance of s_1 and s_2 respectively, and this leads to influences the OP performance of s_2 in (6.31).

6.3.1.2 Non-Linear EH

The outage performance of NOMA can be utilized in the non-linear EH model. In this instance, when implementing wireless power transfer architecture, our focus is on the threshold power of harvested value. Thus, to transmit the signal in the NOMA scheme, we take into account two instances of harvested power or transmit power deployed. As a result, the analytical formulas can be obtained using a method similar to that of the preceding sub-subsection, which dealt with a linear EH model. Thus, in the non-linear case, the outage behavior for s_1 at AP can be expressed as [180]

$$
P_{x_1,NL}^{SC}(out)=P\left(\gamma_{1,NL}^{SC}<\theta_1\right)=P\left(\max_{J=1,2,3,\ldots,L}(\gamma_{1,NL}^{FA},\gamma_{1,NL}^{NJA})<\theta_1\right). \tag{6.32}
$$

Thus, (6.32) can be re-written as [166, 170, 180]

$$
P_{x_1,NL}^{SC}(out)=\prod_{J}^{L}\left(I_1+I_2\right)\times\left(I_3+I_4\right), \tag{6.33}
$$

where $I_1 = P\left(|h_{AF}|^2|h_{FA}|^2 < \zeta_F, P_t|h_{AF}|^2 \leq P_{th}\right)$, $I_2 = P\left(|h_{FA}|^2 < \zeta_{F,1}, P_t|h_{AF}|^2 > P_{th}\right)$, $I_3 = P\left(|h_{ANJ}|^2|h_{NJA}|^2 < \zeta_{NJ}^1, P_t|h_{ANJ}|^2 \leq P_{th}\right)$ and $I_4 = P\left(|h_{NJA}|^2 < \zeta_{NJ,1}^1, P_t|h_{ANJ}|^2 > P_{th}\right)$.

We compute each term of (6.33) respectively below.

I_1 can be written as

$$I_1 = P\left(|h_{AF}|^2|h_{FA}|^2 < \zeta_F, |h_{AF}|^2 \leq \frac{P_{th}}{P_t}\right). \tag{6.34}$$

Thus, (6.34) can be obtained as [166, 170, 180]

$$\begin{aligned} I_1 &= \frac{1}{\sigma_{AF}^2}\int_0^{\frac{P_{th}}{P_t}}\left(\exp\left(-\frac{y}{\sigma_{AF}^2}\right) - \exp\left(-\frac{\zeta_F}{\sigma_{FA}^2 y} - \frac{y}{\sigma_{AF}^2}\right)\right)\,dy \\ &= 1 - \exp\left(-\frac{P_{th}}{\sigma_{AF}^2 P_t}\right) - \frac{1}{\sigma_{AF}^2}\int_0^{\frac{P_{th}}{P_t}}\exp\left(-\frac{\zeta_F}{\sigma_{FA}^2 y} - \frac{y}{\sigma_{AF}^2}\right)\,dy. \end{aligned} \tag{6.35}$$

Also, we obtain I_2 as

$$I_2 = P\left(|h_{FA}|^2 < \zeta_{F,1}, |h_{AF}|^2 > \frac{P_{th}}{P_t}\right) = P\left(|h_{FA}|^2 < \zeta_{F,1}\right), P\left(|h_{AF}|^2 > \frac{P_{th}}{P_t}\right). \tag{6.36}$$

By employing the PDF and CDF of the dedicated Rayleigh fading channel as in [166, 170], (6.36) is obtained as

$$I_2 = \exp\left(-\frac{P_{th}}{\sigma_{AF}^2 P_t}\right) - \exp\left(-\frac{\zeta_{F,1}}{\sigma_{FA}^2} - \frac{P_{th}}{\sigma_{AF}^2 P_t}\right). \tag{6.37}$$

By using the same way, we obtain I_3 and I_4 respectively as given by

$$\begin{aligned} I_3 &= P\left(|h_{ANJ}|^2|h_{NJA}|^2 < \zeta_{NJ}^1, |h_{ANJ}|^2 \leq \frac{P_{th}}{P_t}\right) \\ &= \frac{1}{\sigma_{ANJ}^2}\int_0^{\frac{P_{th}}{P_t}}\left(\exp\left(-\frac{y}{\sigma_{ANJ}^2}\right) - \exp\left(-\frac{\zeta_{NJ}^1}{\sigma_{NJA}^2 y} - \frac{y}{\sigma_{ANJ}^2}\right)\right)\,dy \\ &= 1 - \exp\left(-\frac{P_{th}}{\sigma_{ANJ}^2 P_t}\right) - \frac{1}{\sigma_{ANJ}^2}\int_0^{\frac{P_{th}}{P_t}}\exp\left(-\frac{\zeta_{NJ}^1}{\sigma_{NJA}^2 y} - \frac{y}{\sigma_{ANJ}^2}\right)\,dy. \end{aligned} \tag{6.38}$$

$$\begin{aligned} I_4 &= P\left(|h_{NJA}|^2 < \zeta_{NJ,1}^1, P_t|h_{ANJ}|^2 > P_{th}\right) = P\left(|h_{NJA}|^2 < \zeta_{NJ,1}^1\right), P\left(|h_{ANJ}|^2 > \frac{P_{th}}{P_t}\right) \\ &= \exp\left(-\frac{P_{th}}{\sigma_{ANJ}^2 P_t}\right) - \exp\left(-\frac{\zeta_{NJ,1}^1}{\sigma_{NJA}^2} - \frac{P_{th}}{\sigma_{ANJ}^2 P_t}\right). \end{aligned} \tag{6.39}$$

, where $\zeta_{NJ,1}^1 = \frac{\sigma^2 C_{NJA,1}\theta_1}{P_{th}\psi_1(A_{NJA}\alpha_1 - \alpha_2 A_{NJA}\theta_1 - B_{NJA}\theta_1)}$, $\zeta_{F,1} = \frac{\sigma^2 C_{FA}\theta_1}{(A_{FA} - B_{FA}\theta_1)P_{th}\psi_1}$.

Thus, to find the OP for s_1 at AP of the non-linear model, we substitute the (6.35), (6.37), (6.38), and (6.39) into (6.33) as given by

$$\begin{aligned} P_{x_1,NL}^{SC}(out) = \prod_J^L &\left(1 - \exp\left(-\frac{\zeta_{F,1}}{\sigma_{FA}^2} - \frac{P_{th}}{\sigma_{AF}^2 P_t}\right) - \frac{1}{\sigma_{AF}^2}\int_0^{\frac{P_{th}}{P_t}}\exp\left(-\frac{\zeta_F}{\sigma_{FA}^2 y} - \frac{y}{\sigma_{AF}^2}\right)\,dy\right) \\ &\times\left(1 - \exp\left(-\frac{\zeta_{NJ,1}^1}{\sigma_{NJA}^2} - \frac{P_{th}}{\sigma_{ANJ}^2 P_t}\right) - \frac{1}{\sigma_{ANJ}^2}\int_0^{\frac{P_{th}}{P_t}}\exp\left(-\frac{\zeta_{NJ}^1}{\sigma_{NJA}^2 y} - \frac{y}{\sigma_{ANJ}^2}\right)\,dy\right). \end{aligned} \tag{6.40}$$

Likewise, the OP of s_2 in the non-linear model can be expressed as

$$\begin{aligned} P^{SC}_{x_2,NL}(out) = &\underbrace{P\left(\max_{J=1,2,3,\ldots,L}(\gamma^{NJA}_{1,NL}) < \theta_1\right)}_{M_1} + \left[1 - \underbrace{P\left(\max_{J=1,2,3,\ldots,L}(\gamma^{NJA}_{1,NL}) < \theta_1\right)}_{M_1}\right] \\ &\times \underbrace{P\left(\max_{J=1,2,3,\ldots,L}(\gamma^{NJA}_{2,NL}) < \theta_2\right)}_{M_2}. \end{aligned} \tag{6.41}$$

The term M_1 of (41) is calculated in (42) given by

$$\begin{aligned} M_1 &= P\left(\max_{J=1,2,3,\ldots,L}(\gamma^{NJA}_{1,NL}) < \theta_1\right) = \prod_J^L \ (I_3 + I_4) \\ &= \prod_J^L \ \left(1 - \exp\left(-\frac{\zeta^1_{NJ,1}}{\sigma^2_{NJA}} - \frac{P_{th}}{\sigma^2_{ANJ}P_t}\right) - \frac{1}{\sigma^2_{ANJ}}\int_0^{\frac{P_{th}}{P_t}} \exp\left(-\frac{\zeta^1_{NJ}}{\sigma^2_{ANJ}y} - \frac{y}{\sigma^2_{NJA}}\right)\,\mathrm{d}y\right). \end{aligned} \tag{6.42}$$

The term M_2 of (41) is calculated as

$$M_2 = P\left(\max_{J=1,2,3,\ldots,L}(\gamma^{NJA}_{2,NL}) < \theta_2\right) = \prod_J^L \ (I_5 + I_6)\,, \tag{6.43}$$

where $I_5 = P\ (|h_{ANJ}|^2|h_{NJA}|^2 < \zeta^2_{NJ}, P_t|h_{ANJ}|^2 \le P_{th})$ and $I_6 = P\ (|h_{NJA}|^2 < \zeta^2_{NJ,1}, P_t|h_{ANJ}|^2 > P_{th})$.

We obtain I_5 and I_6 respectively as

$$\begin{aligned} I_5 &= P\left(|h_{ANJ}|^2|h_{NJA}|^2 < \zeta^2_{NJ}, |h_{ANJ}|^2 \le \frac{P_{th}}{P_t}\right) \\ &= \frac{1}{\sigma^2_{ANJ}}\int_0^{\frac{P_{th}}{P_t}} \left(\exp\left(-\frac{y}{\sigma^2_{ANJ}}\right) - \exp\left(-\frac{\zeta^2_{NJ}}{\sigma^2_{NJA}y} - \frac{y}{\sigma^2_{ANJ}}\right)\right)\,\mathrm{d}y \\ &= 1 - \exp\left(-\frac{P_{th}}{\sigma^2_{ANJ}P_t}\right) - \frac{1}{\sigma^2_{ANJ}}\int_0^{\frac{P_{th}}{P_t}} \exp\left(-\frac{\zeta^2_{NJ}}{\sigma^2_{ANJ}y} - \frac{y}{\sigma^2_{NJA}}\right)\,\mathrm{d}y, \end{aligned} \tag{6.44}$$

$$\begin{aligned} I_6 &= P\left(|h_{NJA}|^2 < \zeta^2_{NJ,1}, P_t|h_{ANJ}|^2 > P_{th}\right) = P\left(|h_{NJA}|^2 < \zeta^2_{NJ,1}\right) P\left(|h_{ANJ}|^2 > \frac{P_{th}}{P_t}\right) \\ &= \exp\left(-\frac{P_{th}}{\sigma^2_{ANJ}P_t}\right) - \exp\left(-\frac{\zeta^2_{NJ,1}}{\sigma^2_{NJA}} - \frac{P_{th}}{\sigma^2_{ANJ}P_t}\right). \end{aligned} \tag{6.45}$$

where $\zeta^2_{NJ,1} = \frac{\sigma^2 C_{NJA}\theta_2}{P_{th}\psi_1(A_{NJA}\alpha_2 - \varrho\alpha_1 A_{NJA}\theta_2 - B_{NJA}\theta_2)}$.

By substituting the (6.44) and (6.45) into (6.43), we obtain

$$\begin{aligned} P&\left(\max_{J=1,2,3,\ldots,L}(\gamma^{NJA}_{2,NL}) < \theta_2\right) = \prod_J^L \ (I_4 + I_5) \\ &= \prod_J^L \ \left(1 - \exp\left(-\frac{\zeta^2_{NJ,1}}{\sigma^2_{NJA}} - \frac{P_{th}}{\sigma^2_{ANJ}P_t}\right) - \frac{1}{\sigma^2_{ANJ}}\int_0^{\frac{P_{th}}{P_t}} \exp\left(-\frac{\zeta^2_{NJ}}{\sigma^2_{NJA}y} - \frac{y}{\sigma^2_{ANJ}}\right)\,\mathrm{d}y\right). \end{aligned} \tag{6.46}$$

Thus, to find the OP for x_2 at AP of the non-linear model, we substitute the (42) and (46) into (41) as given by

$$P^{SC}_{x_2,NL}(out) = \prod_{J}^{L} \left(1 - \exp\left(-\frac{\zeta^1_{NJ,1}}{\sigma^2_{NJA}} - \frac{P_{th}}{\sigma^2_{ANJ}P_t}\right) - \frac{1}{\sigma^2_{ANJ}} \int_0^{\frac{P_{th}}{P_t}} \exp\left(-\frac{\zeta^1_{NJ}}{\sigma^2_{NJA}y} - \frac{y}{\sigma^2_{ANJ}}\right) \mathrm{d}y\right)$$
$$+ \left[1 - \prod_{J}^{L} \left(1 - \exp\left(-\frac{\zeta^1_{NJ,1}}{\sigma^2_{NJA}} - \frac{P_{th}}{\sigma^2_{ANJ}P_t}\right) - \frac{1}{\sigma^2_{ANJ}} \int_0^{\frac{P_{th}}{P_t}} \exp\left(-\frac{\zeta^1_{NJ}}{\sigma^2_{NJA}y} - \frac{y}{\sigma^2_{ANJ}}\right) \mathrm{d}y\right)\right]$$
$$\times \prod_{J}^{L} \left(1 - \exp\left(-\frac{\zeta^2_{NJ,1}}{\sigma^2_{NJA}} - \frac{P_{th}}{\sigma^2_{ANJ}P_t}\right) - \frac{1}{\sigma^2_{ANJ}} \int_0^{\frac{P_{th}}{P_t}} \exp\left(-\frac{\zeta^2_{NJ}}{\sigma^2_{NJA}y} - \frac{y}{\sigma^2_{ANJ}}\right) \mathrm{d}y\right). \tag{6.47}$$

The integral of equations (6.40) and (6.47) cannot be obtained in closed forms based on the authors' knowledge. However, they can be easily determined by numerical tools.

6.3.2 Ergodic Capacity

6.3.2.1 Linear EH

Since the AP receives signals from multiple sources (U_F, U_{NJ}), the SC is implemented to select the highest SINR from all received signals as given in (6.22) and (6.23) to employ it for detection. Thus, the achievable (Shannon) rate of s_1 can be written as [180]

$$R_{1,Lin} = \frac{1-\nu}{2} \log_2\left(1 + \gamma^{SC}_{1,Lin}\right). \tag{6.48}$$

By averaging $R_{1,Lin}$ over SINRs in (6.48), we obtain the EC of s_1 as

$$C_{1,Lin} = \frac{1-\nu}{2} \int^{\infty} \log_2\left(1 + \gamma^{SC}_{1,Lin}\right) f_{\gamma^{SC}_{1,Lin}}(z)\, \mathrm{d}\hat{\gamma}^{SC}_{1,Lin}, \tag{6.49}$$

where $f_{\gamma^{SC}_{1,Lin}}(z)$ is the PDF of $\gamma^{SC}_{1,Lin}$. Recalling, $\int_0^\infty \log_2(1+z) f_Z(z)\ \mathrm{d}z = \frac{1}{\ln 2}\int_0^\infty \frac{1-F_Z(z)}{1+z}\ \mathrm{d}z$, where $F_Z(z)$ is the CDF of Z [181]. Thus, the EC of s_1 is given by

$$C_{1,Lin} = \frac{1-\nu}{2\ln 2} \int_0^{\infty} \frac{1-F_Z(z)}{1+z} \mathrm{d}z, \tag{6.50}$$

where

$$F_Z(z) = \prod_{J}^{L} \left(1 - \Lambda\left(\frac{4\zeta^a_F}{\sigma^2_{AF}\sigma^2_{FA}}\right)\right)\left(1 - \Lambda\left(\frac{4\zeta^a_{NJ}}{\sigma^2_{ANJ}\sigma^2_{NJA}}\right)\right), \tag{6.51}$$

where $\zeta^a_{NJ} = \frac{\sigma^2 C_{NJA} z}{P_t\psi_1(A_{NJA}\alpha_1 - \alpha_2 A_{NJA} z - B_{NJA} z)}$ and $\zeta^a_F = \frac{\sigma^2 C_{FA} z}{(A_{FA} - B_{FA} z) P_t \psi_1}$.

Likewise, the achievable rate of s_2 at AP can be written as

$$R_{2,Lin} = \frac{1-\nu}{2} \log_2\left(1 + \gamma^{SC}_{2,Lin}\right). \tag{6.52}$$

By averaging $R_{2,Lin}$, we obtain the EC of s_2 as

$$C_{2,Lin} = \frac{1-\nu}{2} \int^{\infty} \log_2 \left(1 + \gamma_{2,Lin}^{SC}\right) f_{\gamma_{2,Lin}^{SC}}(z) \, \mathrm{d}\gamma_{2,Lin}^{SC}, \tag{6.53}$$

where $f_{\gamma_{2,Lin}^{SC}}(z)$ is the PDF of $\gamma_{2,Lin}^{SC}$.

Hence, the EC of s_2 at AP can be expressed as

$$C_{2,Lin} = \frac{1-\nu}{2\ln 2} \int_0^{\infty} \frac{1 - F_K(z)}{1+z} \, \mathrm{d}z, \tag{6.54}$$

where

$$F_K(z) = \prod_{J}^{L} \left(1 - \Lambda\left(\frac{4\zeta_{NJ}^b}{\sigma_{ANJ}^2 \sigma_{NJA}^2}\right)\right), \tag{6.55}$$

where $\zeta_{NJ}^b = \frac{\sigma^2 C_{NJA} z}{P_t \psi_1 (A_{NJA}\alpha_2 - \varrho\alpha_1 A_{NJA} z - B_{NJA} z)}$.

To the best of the authors' knowledge, (6.50) and (6.54) cannot be determined mathematically in closed forms. However, they can be easily determined by numerical tools.

6.3.2.2 Non-Linear EH

In the non-linear model, the achievable rate of s_1 can be written as [180]

$$R_{1,NL} = \frac{1-\nu}{2} \begin{cases} \log_2 \left(1 + \Im_1\right), & \wp_1 \leq \frac{P_{th}}{P_t}, \\ \log_2 \left(1 + \Im_2\right), & \wp_1 > \frac{P_{th}}{P_t}, \end{cases} \tag{6.56}$$

where $\Im_1 = \max_{J=1,2,3,\ldots,L} \left(\emptyset_1^{FA}, \emptyset_1^{NJA}\right)$, $\Im_2 = \max_{J=1,2,3,\ldots,L} \left(\emptyset_2^{FA}, \emptyset_2^{NJA}\right)$ and $\wp_1 = \max_{J=1,2,3,\ldots,L}$ $\left(|h_{AF}|^2, |h_{ANJ}|^2\right)$.

To derive EC, we should average (6.56) by taking into account whether the condition $\wp_1 > \frac{P_{th}}{P_t}$ is able to succeed or not. Firstly, (6.56) can be re-written as

$$R_{1,NL} = P\left(\wp_1 \leq \frac{P_{th}}{P_t}\right) \frac{1-\nu}{2} \log_2 \left(1 + \Im_1\right) + P\left(\wp_1 > \frac{P_{th}}{P_t}\right) \frac{1-\nu}{2} \log_2 \left(1 + \Im_2\right). \tag{6.57}$$

By averaging (6.57), we obtain

$$\begin{aligned} C_{1,NL} = {} & P\left(\wp_1 \leq \frac{P_{th}}{P_t}\right) \frac{1-\tau}{2} \int^{\infty} \log_2 \left(1 + \Im_1\right) \, f_{\Im_1}(z) \, \mathrm{d}\Im_1 \\ & + P\left(\wp_1 > \frac{P_{th}}{P_t}\right) \frac{1-\tau}{2} \int^{\infty} \log_2 \left(1 + \Im_2\right) \, f_{\Im_2}(z) \, \mathrm{d}\Im_2, \end{aligned} \tag{6.58}$$

where $f_{\Im_1}(z)$ and $f_{\Im_2}(z)$ is the PDF of $\Im_1$ and $\Im_2$ respectively.

Hence, the (6.58) can be expressed as

$$\begin{aligned} C_{1,NL} = {} & \underbrace{P\left(\wp_1 \leq \frac{P_{th}}{P_t}\right)}_{I_7} \frac{1-\nu}{2\ln 2} \int_0^{\infty} \frac{1 - F_{W_1}(z)}{1+z} \mathrm{d}z \\ & + \left(1 - \underbrace{P\left(\wp_1 \leq \frac{P_{th}}{P_t}\right)}_{I_7}\right) \frac{1-\nu}{2\ln 2} \int_0^{\infty} \frac{1 - F_{W_2}(z)}{1+z} \mathrm{d}z, \end{aligned} \tag{6.59}$$

where

$$F_{W_1}(z) = \prod_{J}^{L} \left(1 - \Lambda\left(\frac{4\zeta_F^a}{\sigma_{AF}^2\sigma_{FA}^2}\right)\right)\left(1 - \Lambda\left(\frac{4\zeta_{NJ}^a}{\sigma_{ANJ}^2\sigma_{NJA}^2}\right)\right), \tag{6.60}$$

$$F_{W_2}(z) = \prod_{J}^{L} \left(1 - \exp\left(-\frac{\zeta_{F,1}^a}{\sigma_{FA}^2}\right)\right)\left(1 - \exp\left(-\frac{\zeta_{NJ,1}^a}{\sigma_{NJA}^2}\right)\right). \tag{6.61}$$

where $\zeta_{NJ,1}^a = \frac{\sigma^2 C_{NJA} z}{P_{th}\psi_1(A_{NJA}\alpha_1 - \alpha_2 A_{NJA} z - B_{NJA} z)}$ and $\zeta_{F,1}^a = \frac{\sigma^2 C_{FA} z}{(A_{FA} - B_{FA} z) P_{th}\psi_1}$.

We compute I_7 of (6.59) as

$$I_7 = P\left(\wp_1 \le \frac{P_{th}}{P_t}\right) = \prod_{J}^{L} \left(1 - \exp\left(-\frac{P_{th}}{\sigma_{AF}^2 P_t}\right)\right) \times \left(1 - \exp\left(-\frac{P_{th}}{\sigma_{ANJ}^2 P_t}\right)\right). \tag{6.62}$$

Likewise, the achievable rate of s_2 can be written as

$$R_{2,NL} = \frac{1-\nu}{2} \begin{cases} \log_2\left(1 + \Im_3\right), & \wp_2 \le \frac{P_{th}}{P_t}, \\ \log_2\left(1 + \Im_4\right), & \wp_2 > \frac{P_{th}}{P_t}, \end{cases} \tag{6.63}$$

where $\Im_3 = \max_{J=1,2,3,\ldots,L}\left(\emptyset_3^{NJA}\right)$, $\Im_4 = \max_{J=1,2,3,\ldots,L}\left(\emptyset_4^{NJA}\right)$ and $\wp_2 = \max_{J=1,2,3,\ldots,L}\left(|h_{ANJ}|^2\right)$.

Hence, (6.63) can be re-written as

$$R_{2,NL} = P\left(\wp_2 \le \frac{P_{th}}{P_t}\right)\frac{1-\nu}{2}\log_2\left(1 + \Im_3\right) + P\left(\wp_2 > \frac{P_{th}}{P_t}\right)\frac{1-\nu}{2}\log_2\left(1 + \Im_4\right). \tag{6.64}$$

By averaging (6.64), we obtain

$$\begin{aligned} C_{2,NL} = {} & P\left(\wp_2 \le \frac{P_{th}}{P_t}\right)\frac{1-\nu}{2}\int^{\infty} \log_2\left(1 + \Im_3\right)\, \mathrm{d}\hat{\Im}_3 \\ & + P\left(\wp_2 > \frac{P_{th}}{P_t}\right)\frac{1-\nu}{2}\int^{\infty} \log_2\left(1 + \Im_4\right)\, \mathrm{d}\hat{\Im}_4, \end{aligned} \tag{6.65}$$

where $f_{\Im_3}(z)$ and $f_{\Im_4}(z)$ is the PDF of $\Im_3$ and $\Im_4$ respectively.

Hence, the (6.65) can be expressed as

$$\begin{aligned} C_{2,NL} = {} & \underbrace{P\left(\wp_2 \le \frac{P_{th}}{P_t}\right)}_{I_8}\frac{1-\nu}{2\ln 2}\int_0^{\infty} \frac{1 - F_{W_3}(z)}{1+z}\mathrm{d}z \\ & + \left(1 - \underbrace{P\left(\wp_2 \le \frac{P_{th}}{P_t}\right)}_{I_8}\right)\frac{1-\nu}{2\ln 2}\int_0^{\infty} \frac{1 - F_{W_4}(z)}{1+z}\mathrm{d}z, \end{aligned} \tag{6.66}$$

where

$$F_{W_3}(z) = \prod_{J}^{L} \left(1 - \Lambda\left(\frac{4\zeta_{NJ}^b}{\sigma_{ANJ}^2\sigma_{NJA}^2}\right)\right), \tag{6.67}$$

$$F_{W_4}(z) = \prod_{J}^{L} \left(1 - \exp\left(-\frac{\zeta_{NJ,1}^{b}}{\sigma_{NJA}^{2}}\right)\right), \tag{6.68}$$

where $\zeta_{NJ,1}^{b} = \frac{\sigma^2 C_{NJA} z}{P_{th}\psi_1(A_{NJA}\alpha_2 - \varrho\alpha_1 A_{NJA} z - B_{NJA} z)}$.

We compute I_8 as

$$I_8 = P\left(\wp_2 \le \frac{P_{th}}{P_t}\right) = \prod_{J}^{L} \left(1 - \exp\left(-\frac{P_{th}}{\sigma_{ANJ}^{2} P_t}\right)\right). \tag{6.69}$$

To find the EC for s_1 at AP of the non-linear model, we substitute the (6.60), (6.61), and (6.62) into (6.59). Also, we obtain the EC for s_2 at AP of the non-linear model, we substitute the (6.67), (6.68), and (6.69) into (6.66). To the best of the authors' knowledge, the integral of (6.59) and (6.66) cannot be determined mathematically in closed forms. However, they can be easily determined by numerical tools.

6.3.3 Throughput

In this subsection, we analyze the throughput (with linear and non-linear EH) which is defined as the number of signals transmitted per period successfully. Thus, the throughput is formulated as [182]

$$\Phi_{\beth,o} = \frac{1-\tau}{2}\left(1 - P_{s_{\beth},o}^{SC}(out)\right) Tr_{\beth}, \quad \beth = 1, 2. \ , \tag{6.70}$$

where $P_{x_{\beth},o}^{SC}(out)$ is the OP of s_1 and s_2 at AP for linear or non-linear EH and are obtained in (6.27), (6.31), (6.40), and (6.47).

6.4 Numerical Results

In this section, we compute Monte Carlo simulations to prove the theoretical analysis. The lines in all figures indicate the simulation results, while the markers indicate the theoretical derivations. For a fair comparison, it is supposed that σ^2=1 [140], SNR= P_t/σ^2 and SNR$_{th}$ = P_{th}/σ^2. The parameters used in all simulations are given [183], $\varrho = 0.01$, $\eta = 0.95$, $\tau = 0.1$, $\alpha_1 = 0.8$, $\alpha_2 = 0.2$, $\varsigma = 4$, $d_{FA} = d_{AF} = 3m$, $d_{NJA} = d_{ANJ} = 1m$, $d_{FNJ} = 2m$, SNR_{th}=5 dB and $IRR = IRR_{t/r} = |\mu_{t/r}|^2/|\nu_{t/r}|^2$.

As a benchmark scheme, we consider that the uplink NOMA scheme has two users far U_F and near U_{N1} from the AP. It is assumed that the users transmit their signal with their power to the AP simultaneously, where the U_{N1} has higher energy than U_F. For fairness, as described in [145, 154, 184], transmitted energy by users in the uplink NOMA is equal to the total power P_t while the transmitted energy by the users in HTC-NOMA-WPCCN is equal to P_t/τ. The SIC is implemented at AP, where the U_{N1} signal is detected directly using MLD due to its higher power, and then using the SIC, U_F signal is detected. To improve the performance of the U_F, the HTC-NOMA-WPCCN is proposed as presented in Section II. The comparison between uplink NOMA and our proposed scheme (with linear and non-linear EH model) under ideal and non-ideal IQI with ISIC when Tr_1 =0.2, Tr_2 = 0.3, and IRR=20 dB is presented in Figure 6.3. In this figure, we observe that the OP of U_F of our scheme with linear and non-linear EH outperforms the uplink NOMA while the OP of U_{N1} with ideal/non-ideal IQI was better only with J=1 and when J>1, the U_{NJ} with ideal/non-ideal IQI and linear/non-linear EH outperforms the U_{N1} of uplink NOMA. In the non-linear EH, the U_{N1} with ideal/non-ideal IQI in the high SNR regions was better than U_{NJ}. It can be seen that the OP in the non-linear EH reaches a performance floor when SNR_{th}=5 dB. The presence of IQI and ISIC in the non-linear EH increases the error floor at the high SNR regions and degrades the performance. It is clear that the non-linear EH with IQI affects the SIC performance and the detection signals at AP. We observe also the OP of both signals U_F and U_{NJ} improved as the number of J increased with ideal/non-ideal IQI, linear/non-linear EH and with perfect/imperfect SIC. Moreover, it can be easily seen that the OP of both users with ideal IQI with all J is superior to the non-ideal condition. Also, the ISIC with linear/non-linear EH degrades the OP performance of the U_{NJ} signal with ideal/non-ideal IQI conditions. In the case of an ISIC, the residual detection of the s_1 affects the detection of the s_2 signal, and this leads to a decrease in the OP performance of the s_2 with all U_{NJ}.

In Figure 6.4, we evaluate the effect of τ on the OP performance of both users' signals with U_{NJ} under ideal/non-ideal IQI and linear/non-linear EH with ISIC when Tr_1=0.009, Tr_2=0.01, SNR= 10 dB and IRR= 20 dB. We observe that in the linear and non-linear EH, the OP of both users' signals decreased as τ increased with all J values under ideal/non-ideal IQI conditions. Again, the OP of both users' signals with J values under ideal IQI is superior to the non-ideal condition in all τ values. It can also be seen the non-linear EH degrades the performance of both signals, which more closely approaches a practical transmission.

As known in NOMA schemes, power distribution is important in detecting signals at receivers for evaluating systems performance. To evaluate the impact of α_2 on our system, Figure 6.5, presents the OP of both users' signals with linear and non-linear EH w.r.t α_2 with U_{NJ} under ideal and non-ideal IQI with ISIC when Tr_1=0.05, Tr_2=0.01, SNR= 20 dB and IRR= 20 dB. In the linear/non-linear EH, we observe that incrementing α_2 increases the performance of U_F and decreases the performance of U_{NJ} for the ideal/non-ideal IQI conditions. The non-linear EH degrades the OP performance of both users in all α_2 values. Again, the OP of both users' signals with J values under ideal IQI with the linear/non-linear EH outperforms the non-ideal condition in all α_2 values. It is clearly also with increasing J, the gaps between the ideal and non-ideal curves increase. Increasing α_2 with ideal/non-ideal IQI conditions and linear/non-linear EH affects the SIC process and the detected signals at AP, however, the non-ideal IQI and non-linear EH have more influence on the SIC process because it creates more errors in the system, which emphasizes the significant influence of power allocation on the RF impairment.

In Figure 6.6, we evaluate the impact of IRR on the OP of both users' signals for linear and

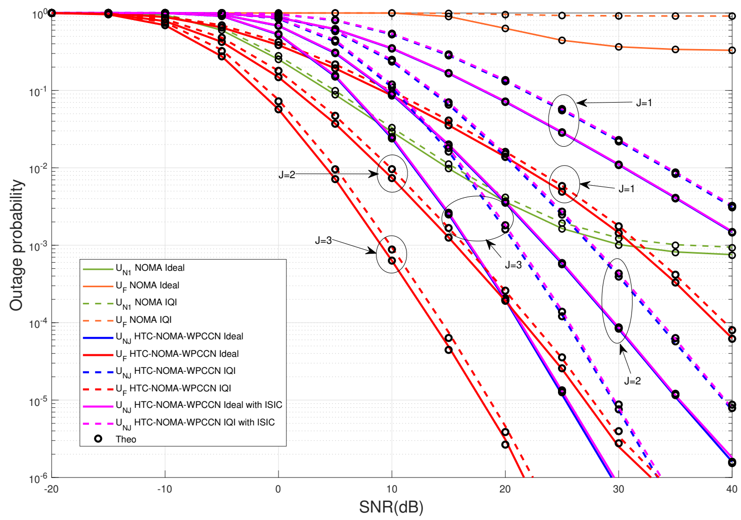

(a) *Linear EH.*

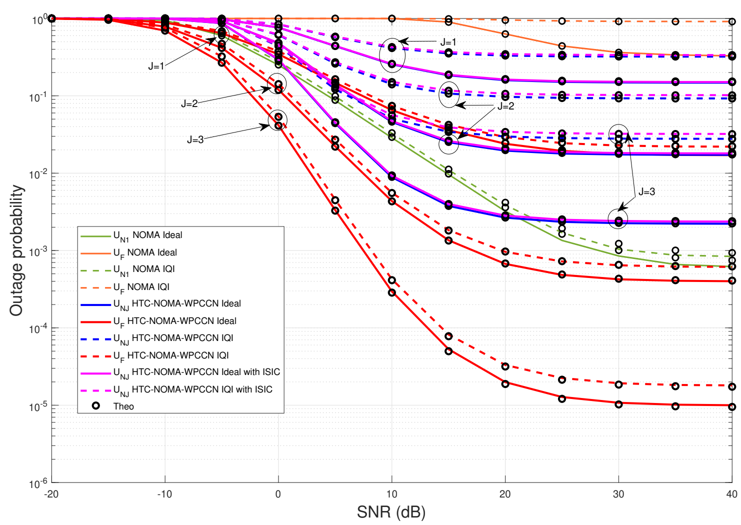

(b) *Non-linear EH.*

Figure 6.3: *Outage probability comparison for HTC-NOMA-WPCCN and uplink NOMA with linear and non-linear EH.*

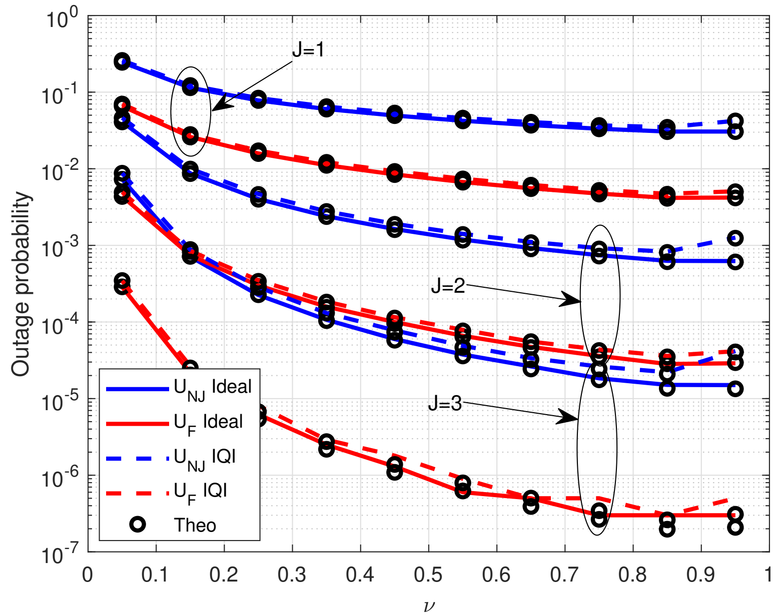

(a) *Linear EH.*

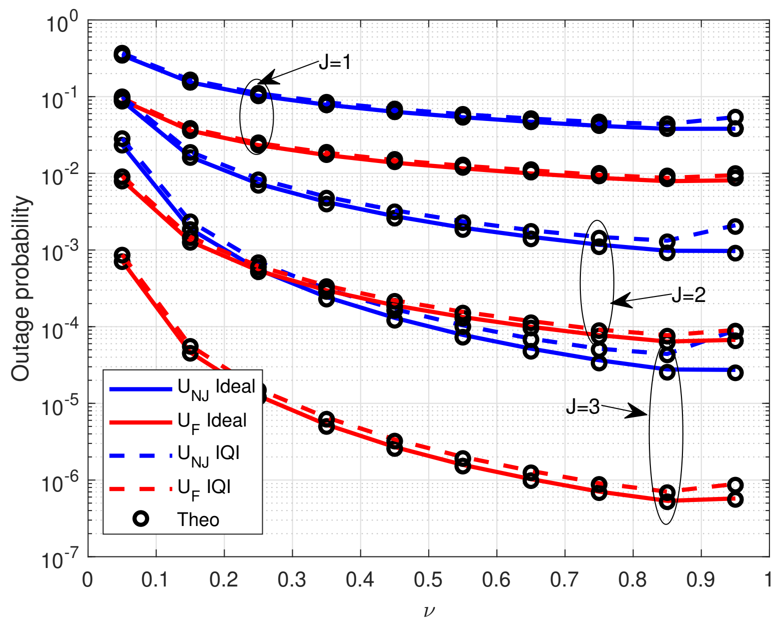

(b) *Non-linear EH.*

Figure 6.4: *Outage probability w.r.t. τ for HTC-NOMA-WPCCN with linear and non-linear EH.*

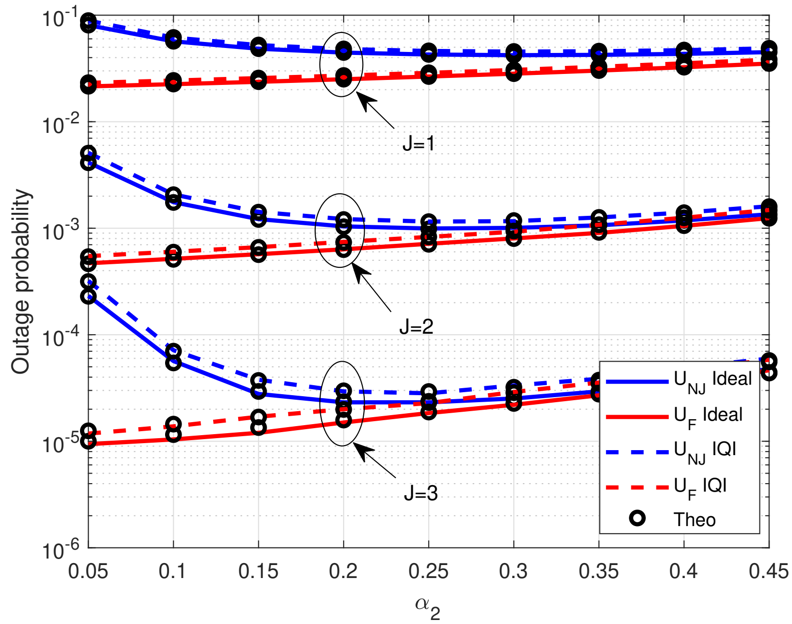

(a) *Linear EH.*

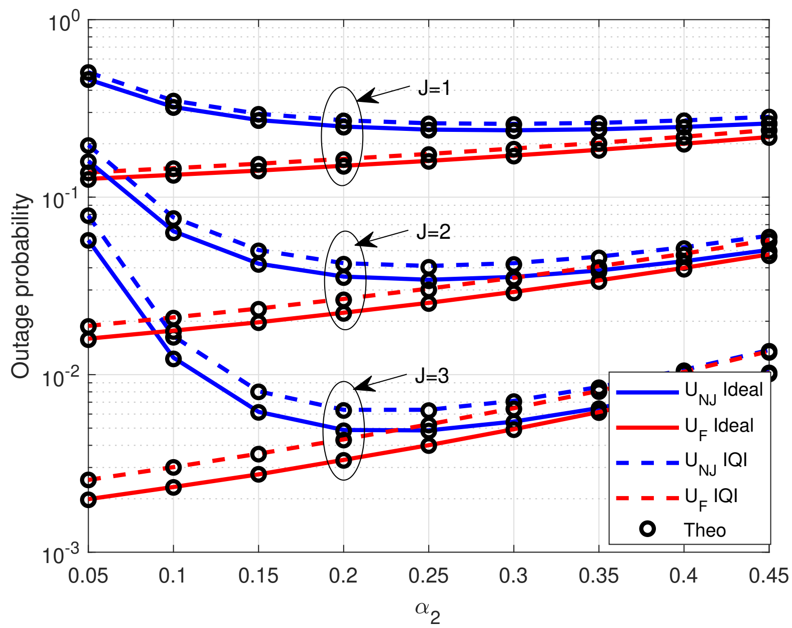

(b) *Non-linear EH.*

Figure 6.5: *Outage probability w.r.t. α_2 for HTC-NOMA-WPCCN with linear and non-linear EH.*

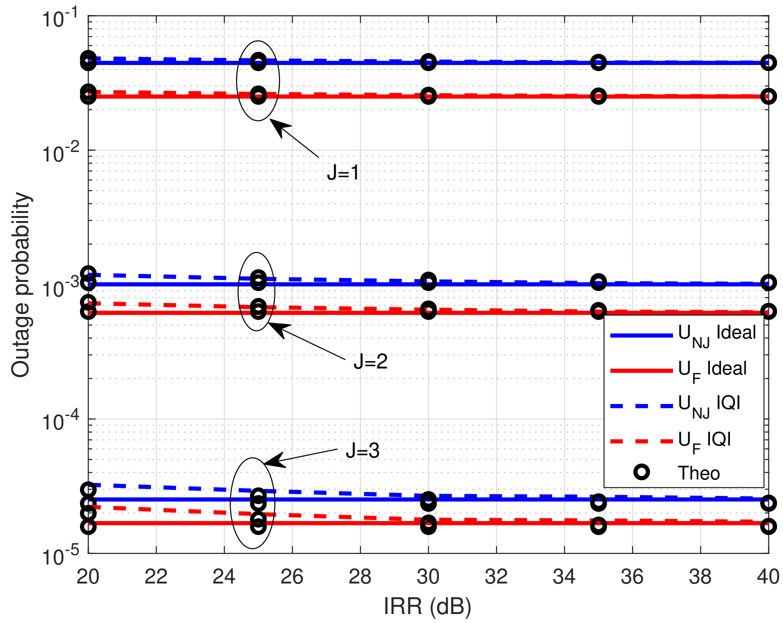

(a) *Linear EH.*

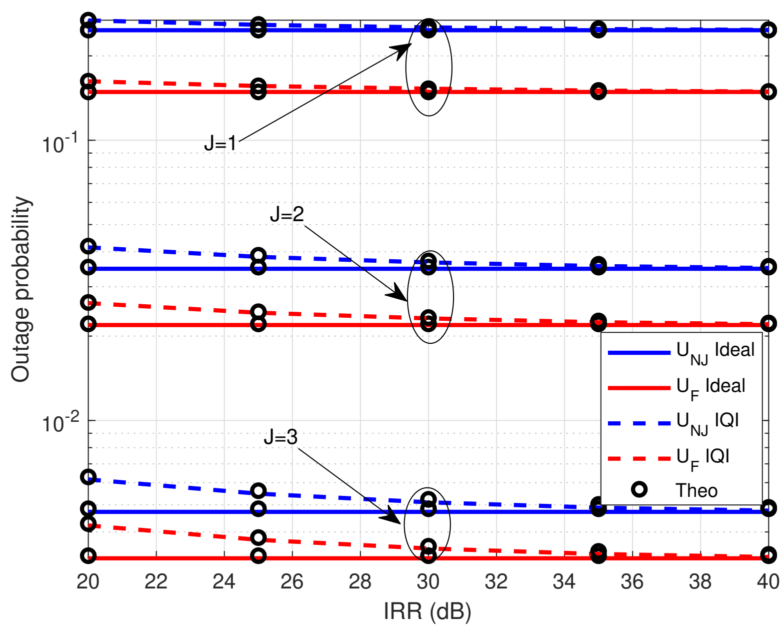

(b) *Non-linear EH.*

Figure 6.6: *Outage probability w.r.t. IRR for HTC-NOMA-WPCCN with linear and non-linear EH.*

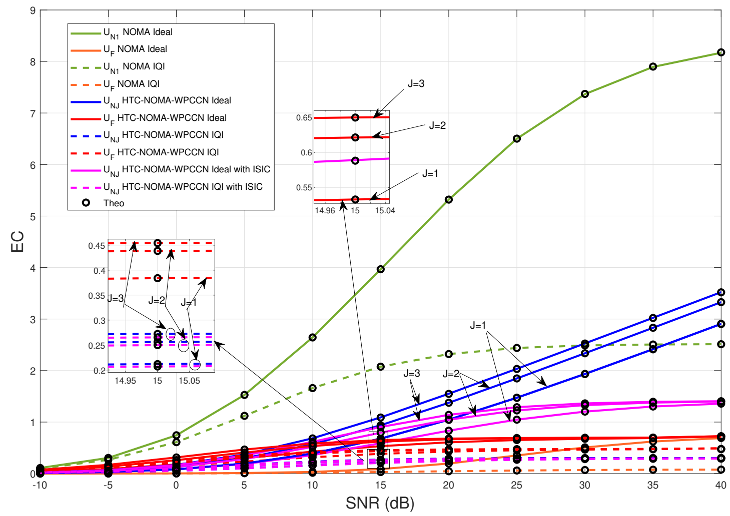

(a) *Linear EH.*

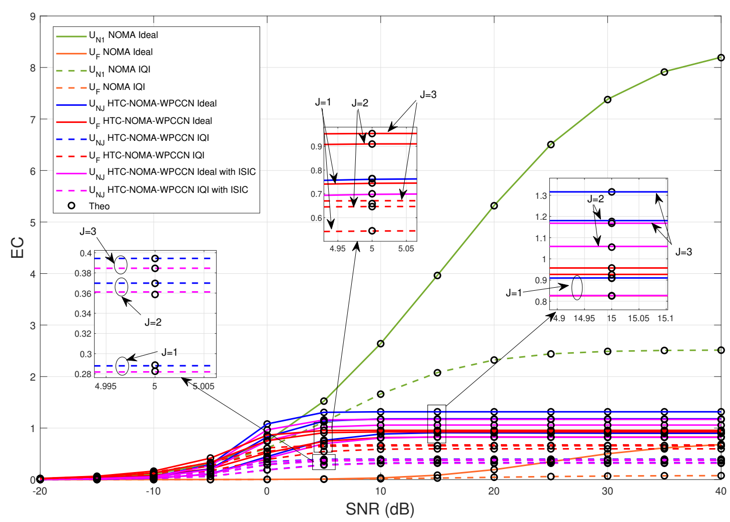

(b) *Non-linear EH.*

Figure 6.7: *EC comparison for HTC-NOMA-WPCCN and uplink NOMA with linear and non-linear EH.*

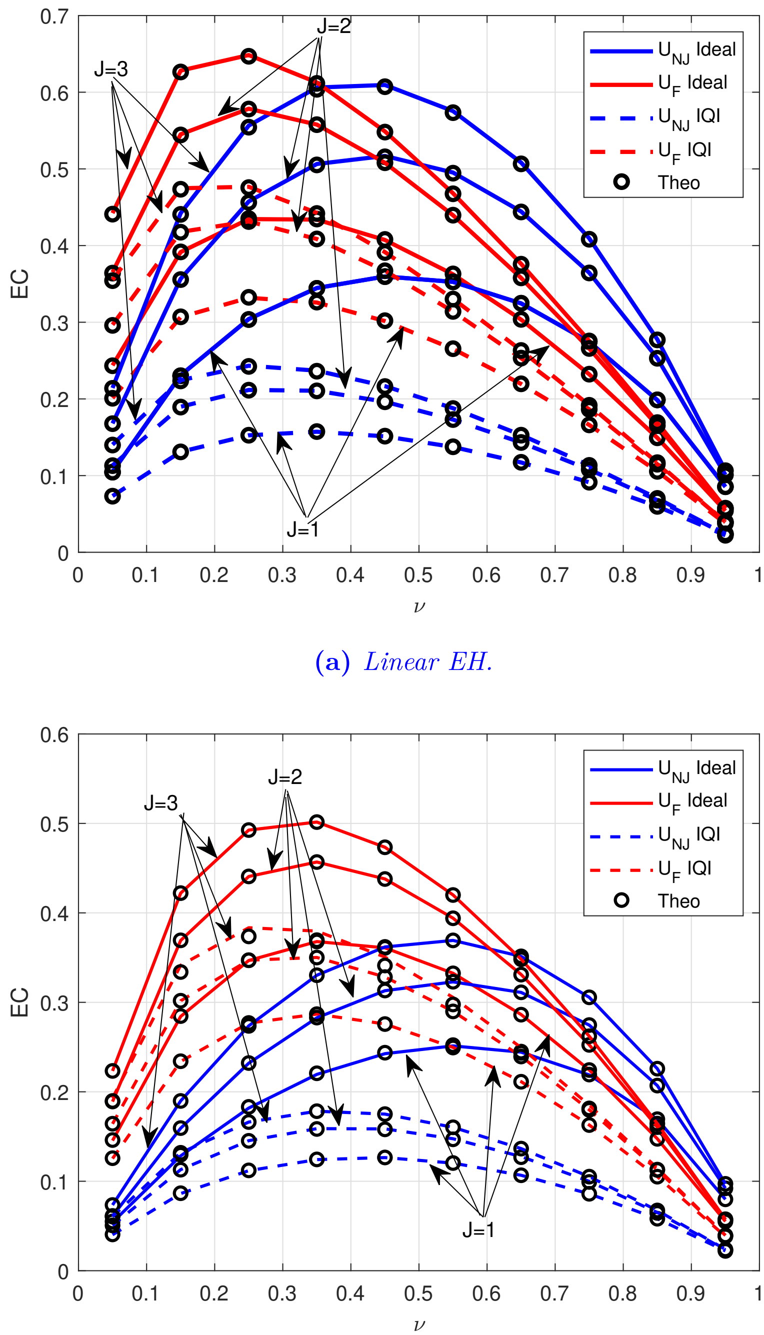

(a) *Linear EH.*

(b) *Non-linear EH.*

Figure 6.8: *EC w.r.t. τ for HTC-NOMA-WPCCN with linear and non-linear EH.*

non-linear EH with J values under ideal and non-ideal IQI with ISIC when Tr_1=0.05, Tr_2=0.01, and SNR= 20 dB. It is clear that as the IRR grows, the OP performance of the users for linear and non-linear EH with all J values increases and becomes almost exact to that of the ideal scenario (ideal IQI) in the high IRR. It means that a low IRR is a more severe condition of IQI. Also, the non-linear EH degrades the performance of both users. It more closely corresponds to practical transmission. Again, increasing J improves the OP of users with ideal/non-ideal conditions at the AP. It is seen that the IQI has a variety of effects on the OP performance of the users in our considered system, according to the gaps between the curves representing perfect IQ matching and the IQI. These results present and emphasize the detrimental impacts of IQI and underscore the importance of bringing RF impairments into consideration.

Figure 6.7 presents the EC performance of HTC-NOMA-WPCCN and uplink NOMA with ideal/non-ideal IQI, linear/ non-linear EH and perfect/imperfect SIC when SNR= 20 dB and IRR= 20 dB. It can be seen that the EC of U_F of our proposed scheme outperforms the U_F uplink NOMA with ideal-non ideal IQI and linear/non-linear EH while the U_{N1} for uplink NOMA has better performance than U_{NJ} despite increasing J. It is due to a higher power in the uplink NOMA. Since the U_F is targeted for improvement in all CNOMA schemes in the literature, the U_{N1} of uplink NOMA has better EC performance than U_{NJ}. It can also be seen the EC performance decreases significantly in the non-linear EH case compared to linear EH, and the performance decreases more in the presence of IQI and ISIC. We observe also the EC performance of both users with linear/non-linear EH increases as J increases in all imperfections cases (ideal/non-ideal IQI and perfect/imperfect SIC). Also, it is seen that the ISIC decreases the EC performance of U_{NJ} with ideal/non-ideal IQI conditions. The ISIC has a more significant impact in the presence of non-linear EH and non-ideal IQI. Furthermore, the EC performance of the ideal IQI outperforms the non-ideal case and the non-ideal decreases the EC performance of U_{NJ} more than U_F. This is due to the different power allocations of each user's signal and SIC process.

In Figure 6.8, we present the EC performance of our considered system with linear and non-linear EH w.r.t τ with ideal/non-ideal and SIC imperfections when SNR=10 dB and IRR=20 dB. We observe that the optimal τ is proportional to the number of U_{NJ} denoted as J with ideal/non-ideal conditions. It can be seen again the ideal IQI is superior to non-ideal conditions. The non-linear EH degrades the performance at high SNR regions compared to linear EH, which reflects the practical transmission. The change of τ values has more effects on the EC performance of the non-ideal IQI, which explains the influence of τ on the RF impairment of our system.

To examine the impact of α_2 on the EC performance of our system, Figure 6.9, presents the EC performance of our considered system with linear and non-linear EH w.r.t α_2 with ideal/non-ideal IQI and SIC imperfections when SNR=20 dB and IRR=20 dB. In both linear and non-linear EH, it is observed that increasing α_2 increases the EC performance of U_{NJ} and decreases the EC performance of U_F with all J values for ideal/non-ideal IQI. Also, the EC performance of the users

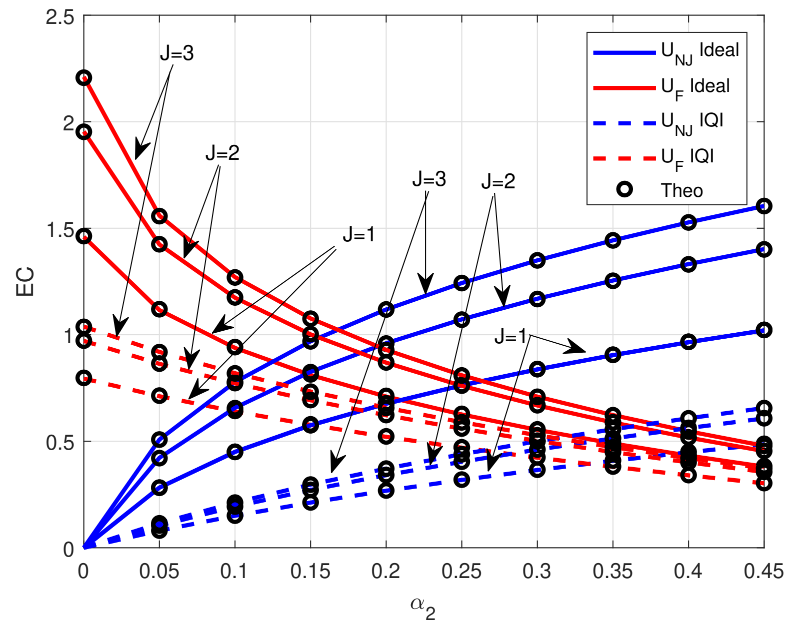

(a) *Linear EH.*

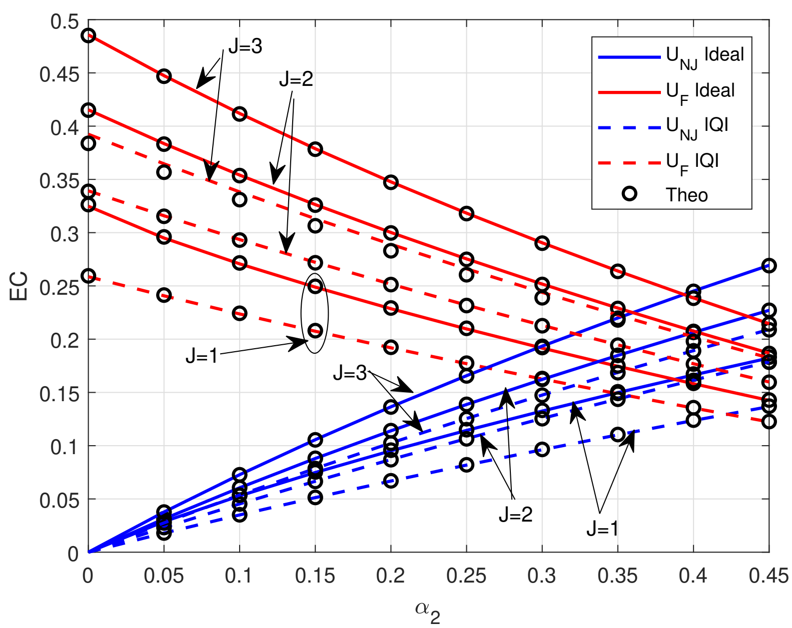

(b) *Non-linear EH.*

Figure 6.9: *EC w.r.t. α_2 for HTC-NOMA-WPCCN with linear and non-linear EH.*

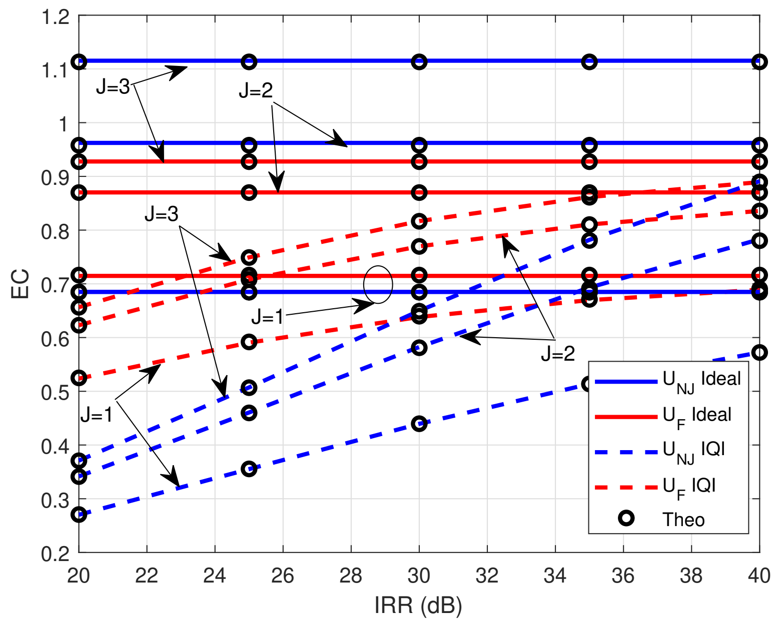

(a) *Linear EH.*

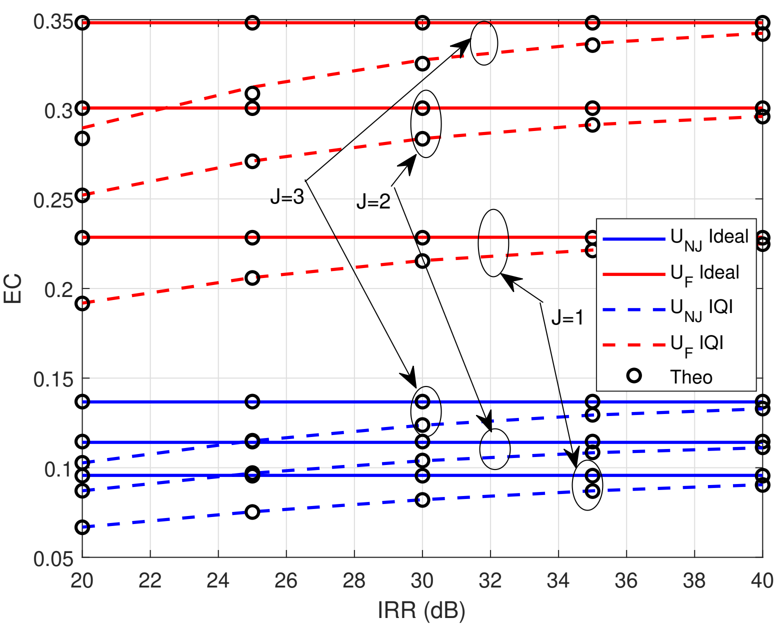

(b) *Non-linear EH.*

Figure 6.10: *EC w.r.t. IRR for HTC-NOMA-WPCCN with linear and non-linear EH.*

with all J values decreases in the presence of non-ideal IQI imperfections compared to the ideal IQI. Moreover, the non-linear EH degrades the EC performance compared to linear EH in all α_2 and the performance is more degraded in the presence of non-ideal IQI. It can be stated that the change in α_2 in the presence of non-ideal IQI conditions and non-linear EH affects the SIC and the detected signals at AP, highlighting the substantial effect of α_2 on RF impairment.

To examine the impact of IRR on the EC performance of our system, Figure 6.10, presents the EC performance of our considered system with linear and non-linear EH w.r.t IRR with ideal/non-ideal IQI and SIC imperfections when SNR=20 dB. In both linear and non-linear EH, it is evident that when IRR increases, the EC performance of the users with all J values rises and closely matches the ideal case (ideal IQI) in the high IRR. Again, the non-linear EH decreases the EC performance compared to linear EH and the performance gets worse in the presence of non-ideal IQI. Besides, increasing J increases the OP of users in the ideal/non-ideal IQI conditions. According to the gaps between the curves depicting perfect IQI matching and the non-ideal IQI, it can be shown that the non-ideal IQI has a range of effects on the EC performance of the users in the considered system which demonstrates the negative effects of IQI on RF impairments.

In Figure 6.11, we present the throughput performance of our considered system with linear and non-linear EH compared to uplink NOMA with ideal/non-ideal IQI and ISIC when Tr_1=0.2, Tr_2=0.3 and IRR=20 dB. It is observed that U_F in the HTC-NOMA-WPCCN with linear and non-linear EH outperforms its counterpart in the uplink NOMA scheme with the ideal/non-ideal IQI while U_{N1} in the uplink NOMA is superior to U_{NJ} in HTC-NOMA-WPCCN with the ideal/non-ideal IQI and linear/non-linear EH. This is due to the different distribution of power allocation levels for users between the uplink NOMA and HTC-NOMA-WPCCN. Also, the non-linear EH limits throughput performance and is affected more by the presence of non-ideal IQI, which more closely matches the practical operation of the transmission. It can also be seen the IQI has more effect on the U_F than U_{N1} in the uplink NOMA. Also, we can observe a big impact of the IQI on all U_{NJ} in HTC-NOMA-WPCCN with linear/non-linear EH compared to U_F. It is due to the SIC process to detect U_F signal in the systems. In this figure, we observe also the throughput performance with linear/non-linear EH increases with the increase of the J values in the ideal/non-ideal IQI and ISIC. The throughput performance of the ideal IQI outperforms the non-ideal condition. Furthermore, the ISIC with ideal/non-ideal IQI conditions decreases the throughput performance with linear/non-linear EH despite the increase in J values.

Figure 6.12 presents the throughput performance with idea/non-ideal IQI and linear and non-linear EH under ISIC w.r.t τ when Tr_1=0.01, Tr_2=0.009, IRR=20 dB and SNR=10 dB. In both linear and non-linear EH, we observe that the increase τ increases the throughput performance of both users with ideal/non-ideal IQI in all J values. Besides, the increasing J improves the throughput performance with ideal/non-ideal IQI conditions. Again, the non-linear EH degrades the performance and is more impacted in the presence of non-ideal IQI conditions. It is observed

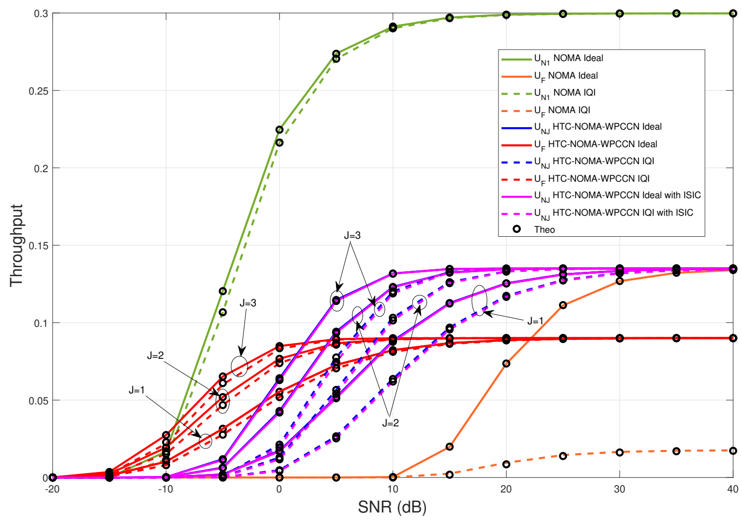

(a) *Linear EH.*

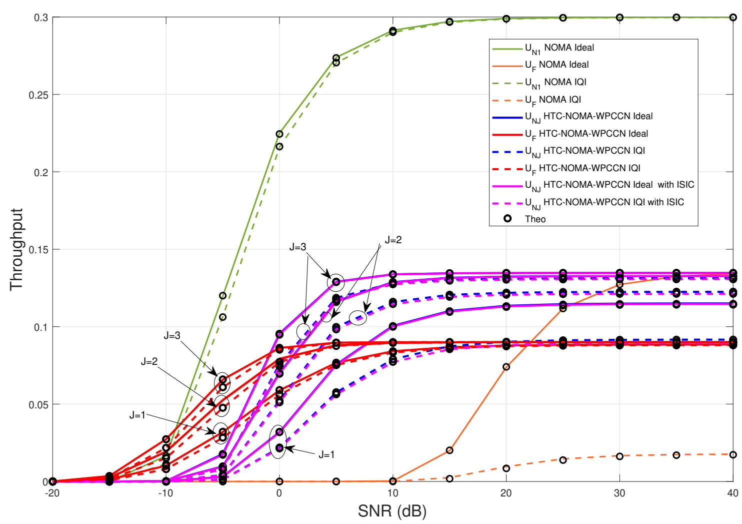

(b) *Non-linear EH.*

Figure 6.11: *Throughput w.r.t. SNR comparison for HTC-NOMA-WPCCN and uplink NOMA with linear and non-linear EH.*

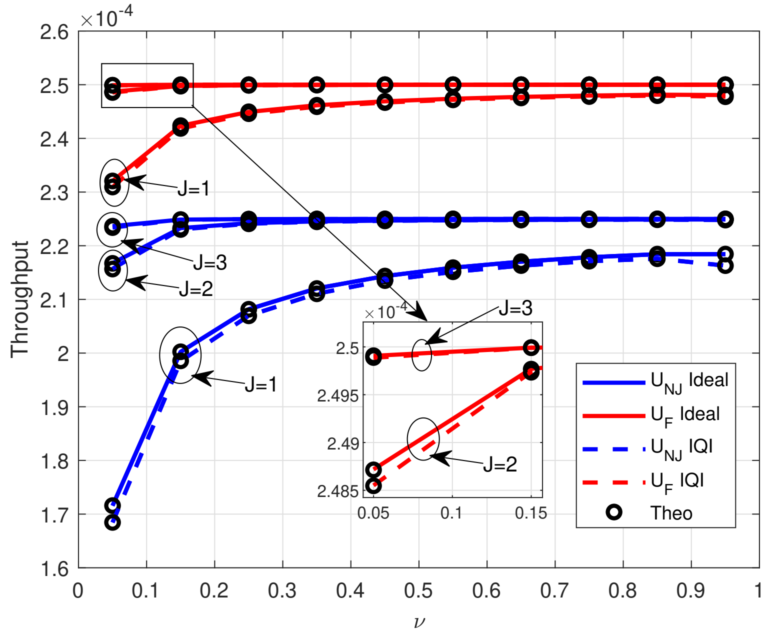

(a) *Linear EH.*

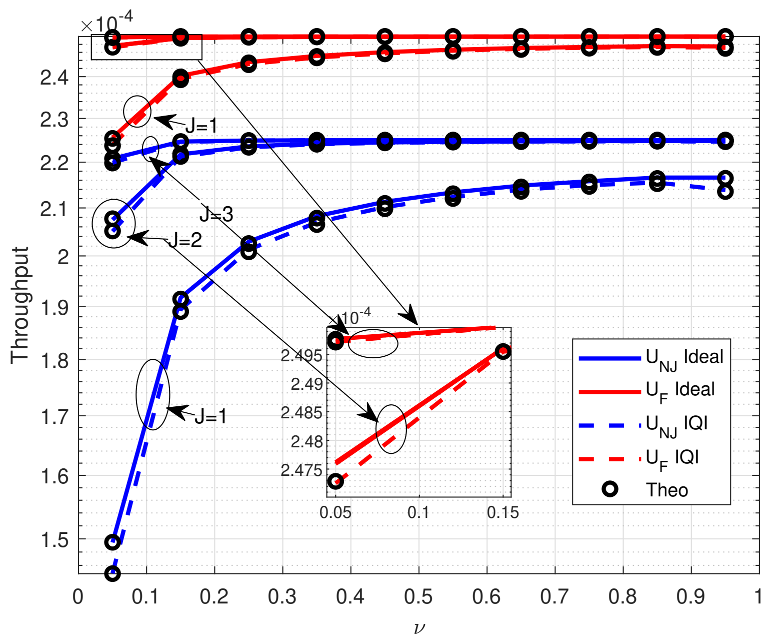

(b) *Non-linear EH.*

Figure 6.12: *Throughput w.r.t. τ for HTC-NOMA-WPCCN with linear and non-linear EH.*

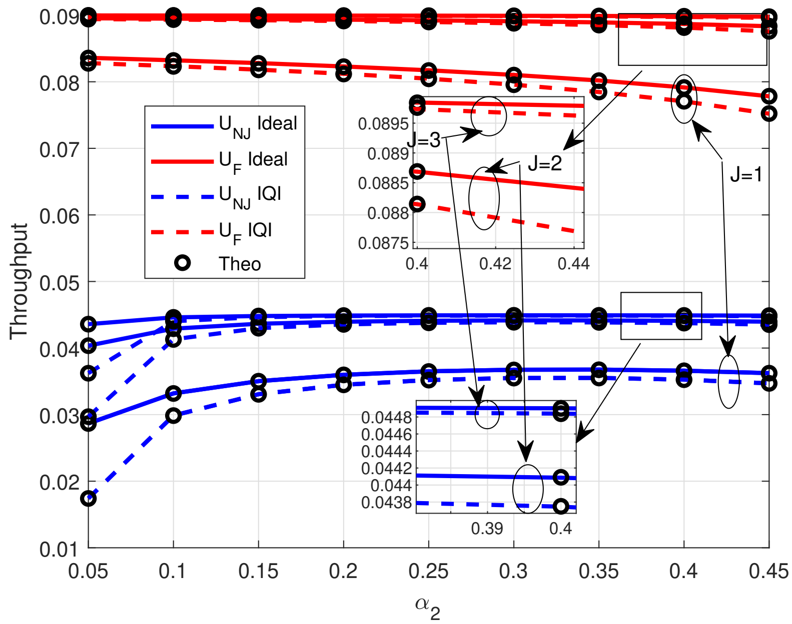

(a) *Linear EH.*

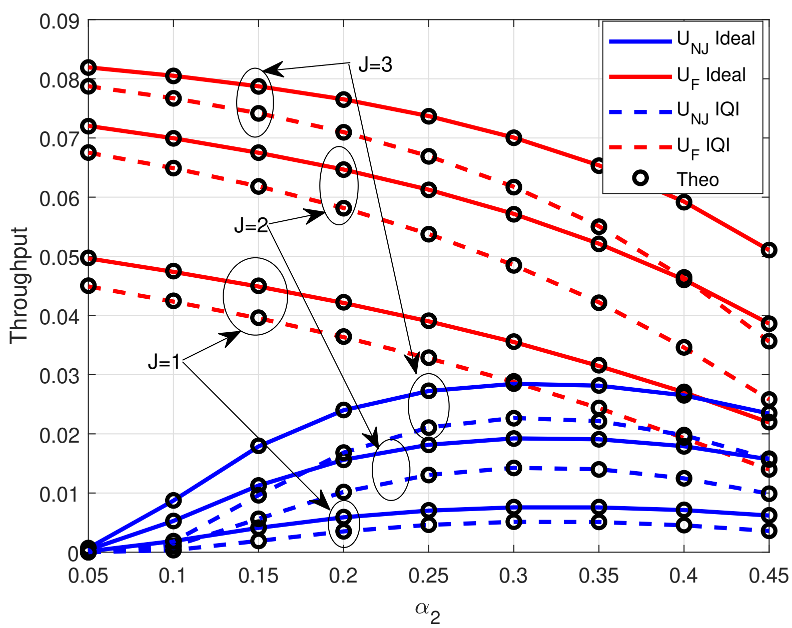

(b) Non-linear EH.

Figure 6.13: Throughput w.r.t. α_2 for HTC-NOMA-WPCCN with linear and non-linear EH.

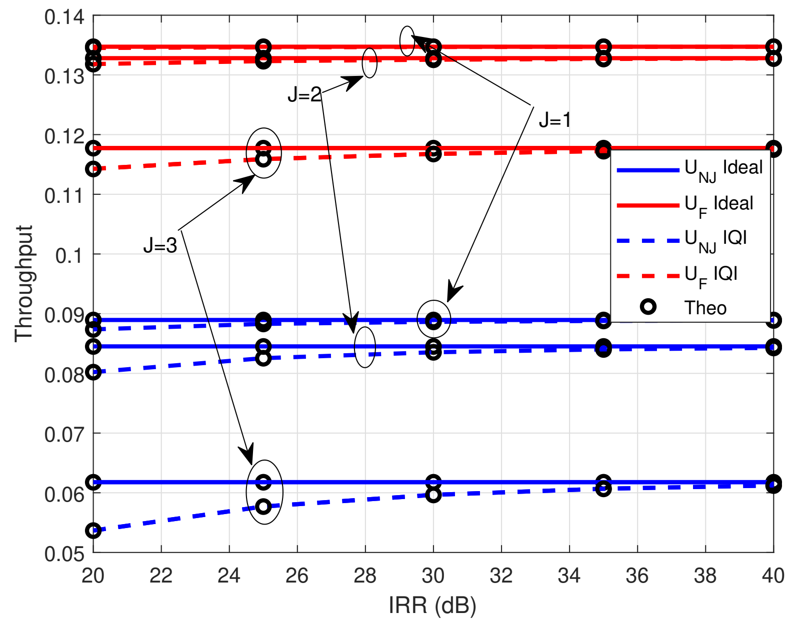

(a) *Linear EH.*

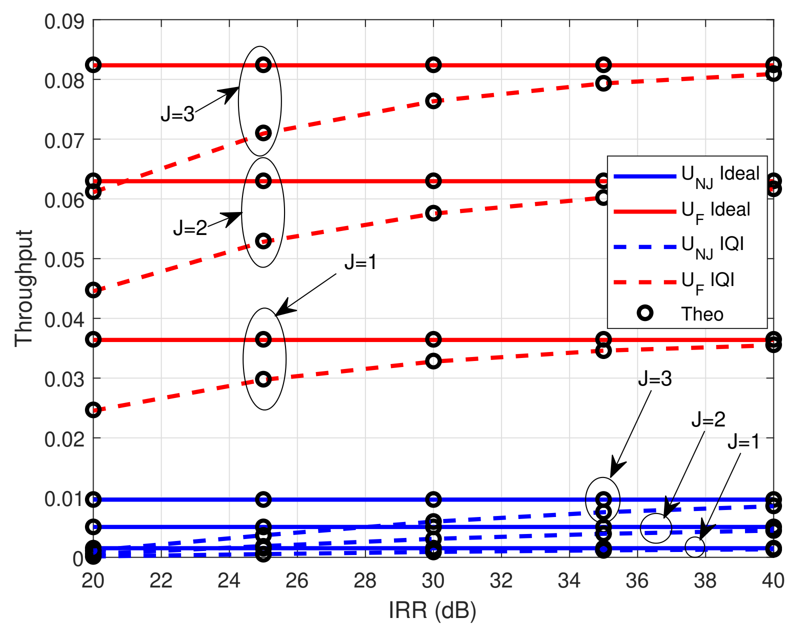

(b) *Non-linear EH.*

Figure 6.14: *Throughput w.r.t. IRR for HTC-NOMA-WPCCN with linear and non-linear EH.*

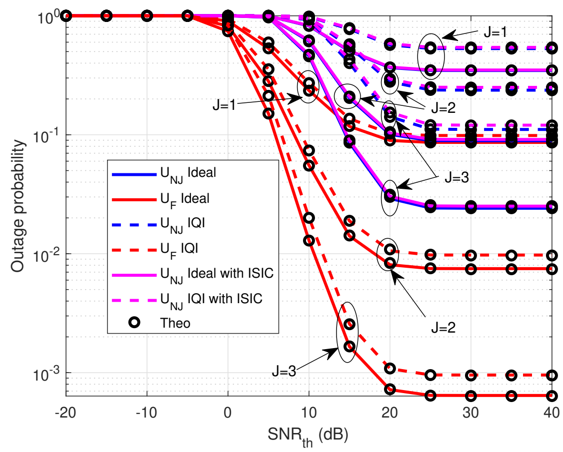

(a) *OP.*

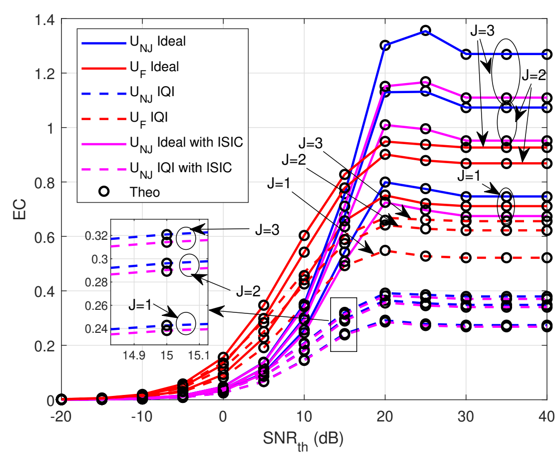

(b) *EC.*

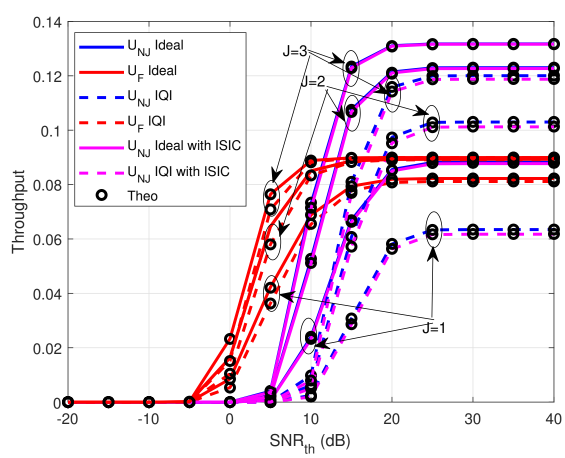

(c) *Throughput.*

Figure 6.15: *HTC-NOMA-WPCCN w.r.t. SNR$_{th}$: OP, EC and Throughput.*

that the choice of optimal τ is fully correlated with the number of J values to improve throughput performance, and this latter is affected by the IQI imperfections.

To examine the impact of α_2 on the throughput performance of our system, in Figure 6.13, we present the throughput performance of our considered system with linear and non-linear EH w.r.t α_2 with ideal/non-ideal IQI and SIC imperfections when Tr_1=0.2, Tr_2=0.1, SNR=20 dB and IRR=20 dB. In both linear and non-linear EH, we observe that the change of α_2 affects the throughput performance of users with all J values for ideal/non-ideal IQI. Again, the non-linear EH degrades the performance of the system, which is more influenced by non-ideal IQI conditions. Also, the throughput performance of the users increases with all J values in the presence of ideal/non-ideal IQI conditions. It can be concluded that the SIC and the detected signals at AP are impacted by the change in α_2 and non-linear EH when the non-ideal IQI condition is available, emphasizing the significant impact of α_2 and non-linear EH on RF impairment.

To evaluate the effect of IRR on our system, Figure 6.14, presents the throughput performance with idea/non-ideal IQI and linear/non-linear EH under ISIC when Tr_1=0.3, Tr_2=0.2 and SNR=20dB. In both linear/non-linear EH, we observe that the increase in the throughput performance is proportional to an increase in J values. Also, throughput performance degrades in the non-linear EH and the impact increases with non-ideal IQI. Besides, the growth of the IRR increases the throughput performance of both users with all J values for linear/non-linear EH and nearly matches the ideal IQI in the high IRR. It is clear that IQI has a negative impact on the RF impairments in our system.

To evaluate the effect of SNR_{th} on our system, Figure 6.15, presents the OP, EC and throughput performance w.r.t. SNR_{th} with idea/non-ideal IQI under ISIC when Tr_1=0.3, Tr_2=0.2 and SNR=20dB. We observe that in the OP, EC and throughput, the system performance improves as SNR_{th} increases and creates an error floor at the high SNR_{th}. Although the curves indicate enhanced performance when SNR_{th} is high, this is impractical. The presence of IQI degrades the system performance of OP, EC and throughput. Again, increases in J values enhance the system performance of users.

6.5 Conclusion

In this chapter, we have examined the performance of the proposed HTC-NOMA-WPCCN with linear/non-linear EH in the presence of IQI and SIC imperfections. The investigation has been extended by considering the multi-helper-user scheme to improve the system's performance. The OP, EC, and throughput expressions of users were analyzed for linear and non-linear EH over the Rayleigh fading channel. The proposed system is compared to the uplink NOMA and single helper user, and its performance is evaluated through different parameters such as parameters of WPCCN, IQI, ISIC, IRR, and power allocation. Our analytical derivations are verified by computer simulations. The results illustrated that our proposed system outperforms uplink NOMA and the single helper user schemes. The multi-helper-user with and without IQI and SIC imperfections increases the system performance. The change in the IRR, WPCN, and power allocation parameters affects the SIC and IQI which reduce the system's performance. The non-linear EH limits system performance in high SNR regions and is significantly impacted by IQI and SIC imperfections. Finally, IQI has a negative impact on RF impairment despite increasing the number of helper users which confirms the need for IQI mitigation to exploit the capabilities of the systems. This chapter presents the effects of the practical implementations of non-linear EH with practical drawbacks, such as ISIC and IQI, which will be useful in future research.

Chapter 7

UAV-Mounted RIS for Cooperative NOMA Systems with Practical Constraints

7.1 Introduction

Due to the unprecedented growth of punctual mobile data traffic and strict QoS requirements, the upcoming next generation of wireless networks is set to provide ultra-reliable and low-latency communication and immersive reality, etc, which will enable a variety of applications, such as multiple access techniques, RIS, low-orbit satellites, and UAV networks [185]. In this regard, NOMA offers high connection and low latency. In NOMA, the superposition-coding signal with different power levels is used for user signals [186]. Besides, UAV communication networks are seen as an exciting option to increase the QoS in crowded areas and extend the coverage of current networks in difficult environments due to their low cost, LoS air-to-ground channel, and flexible deployment [186]. However, the flying duration of UAV is strictly constrained preventing them from meeting the demands of long missions. To resolve this problem, researchers proposed several solutions, such as battery capacity increase, wireless charging, and solar energy. Recently, researchers have advocated the use of RIS in wireless networks to construct smart radio environments for energy-efficient and cost-effective implementations. The structure of RIS is made of a thin and flexible metasurface material that contains passive circuitry. It can intelligently control the propagation of the incident electromagnetic waves and reflect or refract these waves in a desired way, thereby turning the wireless channel into a controllable environment, and enhancing the overall system performance [185, 186].

7.1.1 Related Works

In the existing literature, several papers consider the scenario of RIS with UAV, but the RIS is fixed on the ground (e,g., wall of a tall building) in their assumptions as in [187]. In this regard, a new vision is proposed in [185] in which UAV can be adapted with RIS (referred to as UAV-RIS) and used for wireless communications as a reflective layer between ground base stations and ground devices. This trend has attracted a great deal of research attention in recent studies [186, 188] where the OP and ergodic spectral efficiency are investigated for UAV-RIS to serve NOMA ground devices. The optimal resource allocations of UAV-RIS with zero-forcing beamforming have been developed in [189], where each UAV serves several ground devices in its cluster. In another work [190], the maximization problem of UAV-RIS has been formulated by determining the best power control factors at the ground base station (consisting of a massive antenna) and the phase shifts of several RISs. On the other hand, radio-frequency equipment is a critical component of the massive network of interrelated devices that enables communication between nodes. In practical communication systems, the radio-frequency component experiences a variety of HWI that compromise the overall system performance [191, 64]. In addition, another issue in cellular networks affecting the system performance is inter-cell interference (ICI), where cell-edge devices or nodes are more exposed to signals from neighboring cells [192].

7.1.2 Motivation and Contributions

As we have mentioned above, UAV-RIS has been analyzed for the OP, ergodic spectral efficiency, and throughput in [186, 188, 189, 190]. To the best of the authors' knowledge, the BER of UAV-RIS with/without NOMA has not been investigated. In addition, it is important to take into account practical scenarios for the performance analysis, such as the effect of HWI, ICI, and ISIC. Based on the above discussions, in this chapter, we investigate UAV-RIS for NOMA with a joint impact of HWI, ICI, and imperfect SIC, as being in practical implementations. Thus, the contributions of this chapter are provided as follows:

- We consider the UAV-RIS-aided NOMA network scheme while assuming that the direct link is unavailable due to obstacles, the NOMA ground devices receive signals using UAV-RIS. We consider that the ideal and non-ideal HWI exist at all nodes in our system. In addition, we consider the ground devices suffer from ICI of the other cells (e.g., the signals forwarded from the UAV-RIS of the neighboring cells), which is the first investigation with HWI and ICI jointly in the literature for RIS. The presence of HWI and ICI affects the SIC process to detect the signals of NOMA users. Thus, the imperfect SIC is considered in our investigation.
- We derive the BER of UAV-RIS under HWI, ICI, and imperfect SIC. Also, we obtain the upper bound of our proposed system. Also, the EE for our considered system is obtained.

For the sake of fair comparison, we compare our results with two schemes: UAV without RIS and traditional UAV-RIS OMA and we validate our analysis with Monte-Carlo simulations.

- The results show that the proposed scheme achieves higher performance gain compared to UAVs without RIS. Moreover, it is found that the HWI and ICI have a negative impact on the system performance, which affects the SIC to detect the symbols at the receivers.

7.2 System and Channel Models

In this chapter, we consider that the source (S) communicates with two NOMA users named U_1 and U_2 with the aid of UAV-RIS as illustrated in Figure 7.1. In this scenario, we consider the following assumptions: 1) The users are equipped with a single antenna. In contrast, the UAV is equipped with RIS that has N as a symbol reflecting elements. 2) The HWI exists at S, NOMA users, and the nodes of neighboring cells. 3) The direct communication between S and users is blocked due to large obstacles, and the NOMA users receive the S signal through the reflected link only. 4) The users experience interference from neighboring cells (i.e., UAV-RIS transmissions from other cells), called ICI. Also, in the work, the phase-shift matrix of the RIS is assumed to be discrete, with individual elements signifying phase shifts introduced by reflecting elements. This allows phase shifts to be independently adjusted, giving the RIS more control over the propagation of electromagnetic waves for improved wireless channel efficiency [191]. Usually, the communication link involving S-UAV and UAV-U_i considers the influence of both small-scale and large-scale fading. Large-scale fading is contingent on the distance existing between the transmitter and receiver [32]. In the downlink scenario, we take into account three-dimensional Cartesian coordinates (x, y, z) for positioning UAV and NOMA users as presented in Fig.7.1. We begin by identifying the location of the S, U_1, and U_2 as follows. The position coordinates of the S is $\mathsf{S}(-x_s, 0, 0)$, whereas the position coordinates of ground users U_1 and U_2 are indicated as $\mathsf{U}_1(x_1, 0, -z_1)$ and $\mathsf{U}_2(x_2, 0, z_2)$, respectively. The central position of the UAV's circular trajectory, characterized by a radius r and altitude T_h, can be pinpointed to the coordinates $O'(0, h, 0)$. Supposing that φ is the angle between the position of the UAV on the circle and the x-axis, we can easily indicate the position coordinates of the UAV as $\mathsf{UAV}(r.\cos(\varphi), r.\sin(\varphi), T_h)$. Based on this analysis, we calculate the Euclidean distance between S-UAV, UAV-U_1, and UAV-U_2, respectively, as $d_s = \sqrt{r^2 + T_h^2 + x_s^2 + 2rx_s\cos(\varphi)}$, $d_1 = \sqrt{(r\cos(\varphi) - x_1)^2 + (r\sin(\varphi) + z_1)^2 + T_h^2}$, and $d_2 = \sqrt{(r\cos(\varphi) - x_2)^2 + (r\sin(\varphi) - z_2)^2 + T_h^2}$. Additionally, we assume that small-scale fading between S-UAV and UAV-U_i follows the Rayleigh distribution[1].

[1]We assume that there is no direct link between the BS-UAV and the UAV-U_i because of the presence of tall buildings or other obstructions (i.e., possible obstruction of signals by natural features), which cause reflections, diffractions, and scattering of the signals. This chpter uses Rayleigh fading to model the wireless communication environment for UAVs, providing a statistical representation of signal fluctuations caused by multipath propagation.

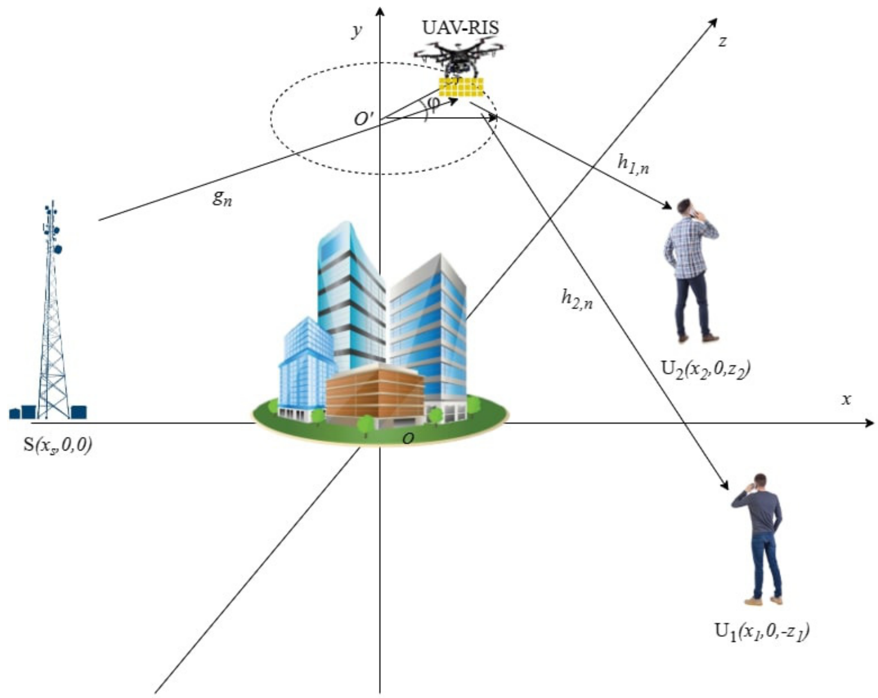

Figure 7.1: *UAV-RIS NOMA system model.*

Based on NOMA, we assume that the users are ordered based on the end-to-end (e2e) channel[2] gains as $|q_1|^2 < |q_2|^2$, where q_1 and q_2 can be given as $q_i = \sum_{n=1}^{N} \sqrt{d_{s,n}^{-\alpha} d_{i,n}^{-\alpha}} g_n \exp{(j\phi_{i,n})} h_{i,n}$, where $g_n = \nu_n \exp{(-j\theta_n)}$, $h_{i,n} = \mu_{i,n} \exp{(-j\psi_{i,n})}$ are Rayleigh fading channels between S-UAV, and UAV-U$_i$, $i = \{1, 2\}$, $\phi_{i,n}$ represents the adjustable phase induced by the n^{th} reflector of the RIS, ν_n and $\mu_{i,n}$ are independently Rayleigh distributed random variables, $d_{s,n}$ and $d_{i,n}$ represent the distances between S and the projection of the n^{th} reflective elements on the ground users, and α is the path-loss exponent, which can be given as [186] $\alpha = \ell_1 Plos(\emptyset) + \alpha_1$, where $Plos(\emptyset)$ is the probability that there will be a LoS component between S-UAV and UAV-users, which is given as [186] $Plos(\emptyset) = [1+\ell_2 \exp -\alpha_2(\emptyset - \ell_2)]^{-1}$, where ℓ_1, ℓ_2, α_1 and α_2 are environment and transmission frequency dependent parameters, and $\emptyset$ is the elevation angle between the S and the RIS reflecting elements and between the RIS reflecting elements and users in radian. Without loss of accuracy, it is given that $d_{s,n} = d_s$ and $d_{i,n} = d_i$. Based on the above assumptions, S transmits a superimposed coding signal to the users through the UAV-RIS, which is given as $X_{SC} = \sqrt{\alpha_1} s_1 + \sqrt{\alpha_2} s_2$, $\alpha_1 > \alpha_2$, in which $\alpha_1 + \alpha_2 = 1$, where α_1 and α_2 are power allocation factors for U$_1$ and U$_2$, s_1 and s_2 are the signals[3] of the U$_1$ and U$_2$. Considering the HWI and ICI, the received signal reflected through

[2] The e2e channel refers to the end-to-end channel between S and users, through the UAV-RIS.

[3] To accurately analyze the performance of the NOMA scheme with varying power allocations, s_1 and s_2 are normalized using the unit average power.

the UAV-RIS at NOMA users can be expressed as

$$y_i = \left(\sqrt{P_s} X_{SC} + \eta_{t,i}\right) q_i + \eta_{r,i} + I_i + w, \quad i = \{1, 2\} \tag{7.1}$$

where I_i is the ICI of transmissions of neighboring cells. Since we assume that the nodes of neighboring suffer from HWI, I_i can be defined as

$$I_i = \sum_{j \neq i}^{L} \left(\left(\sqrt{P_j} X_{SC} + \eta_{t,j} \right) q_j + \eta_{r,j} \right), \tag{7.2}$$

where L represents the number of transmissions of the neighboring cells, $q_j = \sqrt{d_{sj}^{-\alpha} d_j^{-\alpha}} \ \sum_{n=1}^{N} g_{n,j} \ \exp\left(j\phi_{n,j}\right) \ h_{n,j}$, d_{sj} is the distance between S and UAV-RIS of the j^{th} cells, d_j represents the distance between UAV-RIS of the j^{th} cells and U$_i$, $g_{n,j} = \nu_{n,j} \exp\left(-j\theta_{n,j}\right)$ is the Rayleigh fading channel between S-UAV of the j^{th} cells, $h_{n,j} = \mu_{n,j} \exp\left(-j\psi_{n,j}\right)$ is the Rayleigh fading channel between UAV of the j^{th} cells and U_i, $\nu_{n,j}$ and $\mu_{n,j}$ are independently Rayleigh distributed random variables of j^{th} cells, $\phi_{n,j}$ represents the adjustable phase induced by the n^{th} reflector of RIS of the j^{th} cells, $\eta_{t,i} \sim \mathcal{CN}(0, P_s k_{t,i}^2)$ and $\eta_{r,i} \sim \mathcal{CN}(0, P_s k_{r,i}^2 |q_i|^2)$ are distortion noises at the transmitter and receiver of the HWI [4], respectively, $\eta_{t,j} \sim \mathcal{CN}(0, P_j k_{t,j}^2)$ and $\eta_{r,j} \sim \mathcal{CN}(0, P_j k_{r,j}^2 |q_j|^2)$ are distortion noises at the transmitter and receiver of j^{th} cells of the HWI respectively, $k_{t,i}^2$ and $k_{r,i}^2$ are the HWI level at the transceivers, $k_{t,j}^2$ and $k_{r,j}^2$ are the HWI level of j^{th} cells at the transceivers, P_s is the transmit power of S, P_j is the total transmit power of j^{th} cells, and $w \sim \mathcal{CN}(0, \sigma^2)$ is the AWGN.

Consequently, to maximize the SNR using $\phi_{i,n} = \theta_n + \psi_{i,n}$ and $\phi_{n,j} = \theta_{n,j} + \psi_{n,j}$ by adjusting the reflector phases, (7.1) can be rewritten as

$$y_i = \sqrt{d_s^{-\alpha} d_i^{-\alpha}} \ \sqrt{P_s} \ \sum_{n=1}^{N} \ \nu_n \ \mu_{i,n} X_{SC} + W_i, \tag{7.3}$$

where $W_i = z_1 X_{SC} k_{t,i} + z_1 k_{r,i} + \sum_{j \neq i}^{L} (X_{SC} z_2 + z_2(k_{t,j} + k_{r,j})) + w$, $z_1 = \sqrt{d_s^{-\alpha} d_i^{-\alpha}} \sqrt{P_s} \ \sum_{n=1}^{N} \nu_n \mu_{i,n}$, $z_2 = \sqrt{d_{sj}^{-\alpha} d_j^{-\alpha}} \sqrt{P_j} \sum_{n=1}^{N} \mu_{n,j} \nu_{n,j}$, and W_i has zero-mean with the variance $\sigma_{W,i}^2$ of U$_i$.

The MLD of s_1 symbols at the U$_1$ is designed for the RIS scheme by pretending s_2's symbols as noise, and it is given by

$$\tilde{s}_1 = \arg\min_m \{ |y_1 - \sqrt{d_s^{-\alpha} d_1^{-\alpha}} \ \sqrt{P_s} \ \sum_{n=1}^{N} \ \nu_n \ \mu_{1,n} s_{1,m}|^2 \}. \tag{7.4}$$

Likewise, the MLD of s_1 symbols at the U$_2$ is created for the RIS scheme by portraying s_2's symbols as noise, and it is provided by

$$\tilde{s}_1 = \arg\min_m \{ |y_2 - \sqrt{d_s^{-\alpha} d_2^{-\alpha}} \ \sqrt{P_s} \ \sum_{n=1}^{N} \ \nu_n \ \mu_{2,n} s_{1,m}|^2 \}. \tag{7.5}$$

[4] In practical applications, transceivers encounter various HWIs. The impact of these impairments can be effectively verified and analyzed by containing an additive independent distortion noise as in [64, 191].

However, to detect the s_2 at U_2, a SIC should be implemented. The MLD of s_2 symbols at the U_2 for the UAV-RIS NOMA scheme can be given as

$$\tilde{s}_2 = \arg\min_{m}\{|\acute{y}_2 - \sqrt{d_s^{-\alpha} d_2^{-\alpha}}\ \sqrt{P_s}\ \sum_{n=1}^{N}\ \nu_n\ \mu_{2,n} s_{2,m}|^2\}, \tag{7.6}$$

where

$$\acute{y}_2 = y_2 - \sqrt{d_s^{-\alpha} d_1^{-\alpha}}\ \sqrt{P_s}\ \sum_{n=1}^{N}\ \nu_n\ \mu_{1,n} \tilde{s}_{1,m}, \tag{7.7}$$

where $s_{i,m}$ denotes the m^{th} constellation point of U_i.

7.3 Performance Analysis

In this section, we analyze the BER and EE for UAV-RIS NOMA over the Rayleigh fading channel.

7.3.1 Bit Error Rate

In this section, we analyze the error probability of UAV-RIS NOMA considering both the ideal and non-ideal conditions (i.e., with and without HWI and ICI). The presence of HWI and ICI affect the SIC process and the BER performance. Therefore, the imperfect SIC is considered in the proposed system. In particular, the average BER and then the upper bound are obtained.

Since ν_n, $\mu_{i,n}$, $\nu_{n,j}$, and $\mu_{n,j}$ of (7.1) and (7.2) are independently Rayleigh distributed random variables, we put $\mathsf{A}_1 = \nu_n \mu_{i,n}$ and $\mathsf{A}_2 = \nu_{n,j}\mu_{n,j}$. Therefore, $\mathbb{E}[\mathsf{A}_1]$=$\mathbb{E}[A_2]$=$\frac{\pi}{4}$ and $\mathsf{VAR}[\mathsf{A}_1] = \mathsf{VAR}[\mathsf{A}_2]$ $= (1 - \frac{\pi^2}{16})$. For a sufficiently large number of reflecting elements $N >> 1$, according to the central limit theorem, A_1 and A_2 follows Gaussian distribution with parameters, $\mathbb{E}[\mathsf{A}_1]$=$\mathbb{E}[\mathsf{A}_2]$=$N\frac{\pi}{4}$ and $\mathsf{VAR}[\mathsf{A}_1] = \mathsf{VAR}[\mathsf{A}_2] = N(1 - \frac{\pi^2}{16})$ [191, 193]. Assuming the HWI and ICI, the BER of the UAV-RIS for U_1 is obtained by using the decision rule provided in (7.4) as

$$P_1(e) = \frac{1}{2}\sum_{s=1}^{2} \mathrm{Q}\left(\sqrt{\frac{P_s \chi_s \psi_1 \lambda}{\sigma_{W,1}}}\right), \tag{7.8}$$

where $\chi_s = [(\sqrt{\alpha_1} + \sqrt{\alpha_2}), (\sqrt{\alpha_1} - \sqrt{\alpha_2})]$, $\psi_i = d_s^{-\alpha} d_i^{-\alpha}$, and $\lambda = |A_1|^2 = |\sum_{n=1}^{N} \nu_n \mu_{i,n}|^2$. The variance $\sigma_{W,1}$ contains the transmitted superimposed coding symbols, therefore there are two different levels of power in BPSK. Hence, the variance $\sigma_{W,1}$ for U_1 can be formulated as

$$\sigma_{W,1} = \psi_1 \varpi_1 K_a^2 + \zeta_s \aleph K_b^2 + \aleph K_b^2 + \sigma^2, \tag{7.9}$$

where $K_a^2 = k_{t,i}^2 + k_{r,i}^2$, and $K_b^2 = k_{t,j}^2 + k_{r,j}^2$ are the aggregate level of HWI, as described in [64, 193]. Based on the central limit theorem, it can be said that $\mathbb{E}[|\sum_{n=1}^{N}\ \nu_n\ \mu_{i,n}|^2]$ and $\mathbb{E}[|\sum_{n=1}^{N}\ \nu_{n,j}\ \mu_{n,j}|^2]$ of $\sigma_{W,1}$ in (9) follow a zero-mean Gaussian distribution for N number of reflectors of j^{th} cells. We can obtain $\mathbb{E}[|\sum_{n=1}^{N}\ \nu_n\ \mu_{i,n}|^2] = N(1 - \frac{\pi^2}{16})$ and $\mathbb{E}[|\sum_{n=1}^{N}\ \nu_{n,j}\ \mu_{n,j}|^2] = N(1 - \frac{\pi^2}{16})$. We use the

MGF as defined in [191] of A_1, which follows the non-central chi-square distribution, so the average BER for BPSK is given by

$$P_1(e) = \frac{1}{2\pi} \sum_{s=1}^{2} \int_0^{\frac{\pi}{2}} \left(\frac{1}{\varpi_{1,a}}\right)^{\frac{1}{2}} \exp\left(\frac{-\Upsilon_{1,a}}{\varpi_{1,a}}\right) \mathrm{d}\eta. \tag{7.10}$$

Likewise, the analytical BER for U_2 is based on the correct and erroneous SIC. Hence, supposing the HWI and ICI, we obtain the average BER of the UAV-RIS for U_2 by using the decision rules provided in (7.6) and (7.7) as

$$P_2(e) = \frac{1}{2} \sum_{f=1}^{6} \kappa_f \ \mathrm{Q}\left(\sqrt{\frac{P_s \aleph_f \psi_2 \lambda}{\sigma_{W,2}}}\right), \tag{7.11}$$

where $\kappa_f = [1, 1, -1, 1, 1, -1]$ and $\aleph_f = [\alpha_2, \alpha_2, (\sqrt{\alpha_1} + \sqrt{\alpha_2}), (\sqrt{2\alpha_1} + \sqrt{\alpha_2}), (\sqrt{\alpha_1} - \sqrt{\alpha_2}), (2\sqrt{\alpha_1} - \sqrt{\alpha_2})]$. The variance $\sigma_{W,2}$ contains the transmitted superimposed coding symbols, thus there are two different levels of power in BPSK. Hence, the variance $\sigma_{W,2}$ for U_2 can be formulated as

$$\sigma_{W,2} = \psi_2 \varpi_2 K_a^2 + \delta_f \aleph K_b^2 + \aleph K_b^2 + \sigma^2, \tag{7.12}$$

where $\varpi_i = P_s |\sum_{n=1}^{N} \nu_n \mu_{i,n}|^2$, $\aleph = \sum_{j \neq i}^{L} \iota P_j |\sum_{n=1}^{N} \nu_{n,j} \mu_{n,j}|^2$, $\iota = d_{sj}^{-\alpha} d_j^{-\alpha}$, and $\delta_f = [(\sqrt{\alpha_1} - \sqrt{\alpha_2}), (\sqrt{\alpha_1} + \sqrt{\alpha_2}), (\sqrt{\alpha_1} + \sqrt{\alpha_2}), (\sqrt{\alpha_1} + \sqrt{\alpha_2}), (\sqrt{\alpha_1} - \sqrt{\alpha_2}), (\sqrt{\alpha_1} - \sqrt{\alpha_2})]$.

By using the same method for U_1, we calculate the average BER for U_2 for BPSK as follow

$$P_2(e) = \frac{1}{2\pi} \sum_{f=1}^{6} \kappa_f \int_0^{\frac{\pi}{2}} \left(\frac{1}{\varpi_{2,a}}\right)^{\frac{1}{2}} \exp\left(\frac{-\Upsilon_{2,a}}{\varpi_{2,a}}\right) \mathrm{d}\eta, \tag{7.13}$$

where $\varpi_{i,a} = 1 + \alpha_{i,a}\Lambda$, $\Upsilon_{i,a} = \wp_{i,a}\Lambda$, $\alpha_{i,a} = \frac{N(16-\pi^2)P_s\psi_i}{8\sin^2(\eta)\sigma_{W,i}}$, $\wp_{i,a} = \frac{N^2\pi^2 P_s \psi_i}{16\sin^2(\eta)\sigma_{W,i}}$, and Λ is equal to χ_s for BER of U_1 and equal to $\aleph_f$ for BER of U_2.

To acquire insights, we compute the upper bound of (7.10) and (7.13), respectively, by setting $\eta = \pi/2$ as

$$P_i(e) \leq \frac{1}{4} \sum_{r=1}^{\vartheta} \partial \left(\frac{1}{\varpi_{i,b}}\right)^{\frac{1}{2}} \exp\left(\frac{-\Upsilon_{i,b}}{\varpi_{i,b}}\right), \tag{7.14}$$

where $\varpi_{i,b} = 1 + \alpha_{i,b}\Lambda$, $\Upsilon_{i,b} = \wp_{i,b}\Lambda$, $\alpha_{i,b} = \frac{N(16-\pi^2)P_s\psi_i}{8\sigma_{W,i}}$, $\wp_{i,b} = \frac{N^2\pi^2 P_s\psi_i}{16\sigma_{W,i}}$, ϑ is equal to 2 for BER of U_1 and equal to 6 for BER of U_2, and ∂ is equal to 1 for U_1 and equal to κ_f for U_2. This result leads to the following observation. The error performance of UAV-RIS NOMA improves with increasing N. However, it is limited by the imperfection of the non-ideal conditions (i.e., HWI and ICI) that cause an error floor at high SNR regions.

In our considered system, we provide the BER of the system, which is the error probability when the U_1, U_2, or both detect their symbols incorrectly. Hence, the BER of the system for UAV-RIS NOMA with HWI and ICI can be expressed as [64, 193]

$$P_{system}(e) = 1 - (1 - P_1(e))(1 - P_2(e)), \tag{7.15}$$

where $P_1(e)$ and $P_2(e)$ are the BER of U_1 and U_2, respectively.

7.3.2 Energy Efficiency

The capacity of our considered system for both users with HWI and ICI is given by

$$C_{RIS,1} = log_2(1 + \frac{(d_s d_1)^{-\varsigma}\alpha_1 P_s|\sum_{n=1}^{N} \ \nu_n \ \mu_{1,n}|^2}{(d_s d_1)^{-\varsigma}\alpha_2 P_s|\sum_{n=1}^{N} \ \nu_n \ \mu_{1,n}|^2 + (d_s d_1)^{-\varsigma} P_s|\sum_{n=1}^{N} \ \nu_n \ \mu_{1,n}|^2 K_a^2 + \xi_a + \sigma^2}), \tag{7.16}$$

$$C_{RIS,2} = log_2(1 + \frac{(d_s d_2)^{-\varsigma}\alpha_2 P_s|\sum_{n=1}^{N} \ \nu_n \ \mu_{1,n}|^2}{(d_s d_2)^{-\varsigma} P_s|\sum_{n=1}^{N} \ \nu_n \ \mu_{1,n}|^2 K_a^2 + \xi_a + \sigma^2}), \tag{7.17}$$

where $\xi_a = \sum_{j\neq i}^{L}(d_{sj}d_j)^{-\varsigma}P_j|\sum_{n=1}^{N} \ \nu_{n,j} \ \mu_{j,n}|^2 + \sum_{j\neq i}^{L}(d_{sj}d_j)^{-\varsigma}P_j|\sum_{n=1}^{N} \ \nu_{n,j} \ \mu_{j,n}|^2 K_b^2$.

Hence, the sum rate is given by

$$C_{RIS,sumrate} = C_{RIS,1} + C_{RIS,2}. \tag{7.18}$$

In UAV-RIS NOMA, the total power consumption comprises the S transmit power, and the hardware static power dissipation at the S, RIS, and user terminals. The EE can be written as [194] by

$$P_{Total} = Z_e P_s + P_h + P_{RIS} + \sum_{t=1}^{2} P_{UE,i}, \tag{7.19}$$

where P_s is the transmitting power of S, P_h and P_{RIS} are the total hardware static dissipated power at the S and RIS, respectively, in which $P_{RIS} = N \ P_N$, where P_N is the power consumption of each phase shifter of RIS, and Z_e is the efficiency of the transmit power amplifier.

Thus, the EE can be written as in [194] by

$$\eta_{RIS,EE} = \frac{C_{RIS,sumrate}}{P_{Total}}. \tag{7.20}$$

7.4 Numerical Results

In this section, we present the Monte-Carlo simulations to validate the derivations of the previous sections. We discuss the effect of HWI, ICI, and imperfect SIC on the error performance of UAV-RIS NOMA. Without loss of generality, we consider that $k = K_a^2 = K_b^2$, $P = P_s = P_j$, and the total transmit SNR is defined as $\gamma = \frac{P}{\sigma^2}$. The parameters used in all simulations are given by [186] $r = 5$ m, $T_h = 20$ m, $\varphi = \frac{\pi}{4}$, $\mathsf{S}(-5, 0, 0)$, $\mathsf{U}_1(10, 0, -10)$, $\mathsf{U}_2(5, 0, 5)$, $d_{sj} = 100$ m, $d_j = 100$ m, $\ell_1 = -1.5$, $\alpha_1 = 3.5$, $\ell_2 = 2$, $\alpha_2 = 0.16$, $\emptyset = 1.2$, $k = 0, 0.15$, $L = 0, 3$, the computer simulation repeated 10^5 iterations, and $\alpha_2 = 0.1, 0.2$.

In Figure 7.2, we present the BER performance of UAV-RIS for two NOMA users with the impact of HWI and ICI with fixed $k = 0.15$ and $L = 3$. We observe that the analytical results perfectly matched with simulation results. The upper bound is quite strict because the analytical

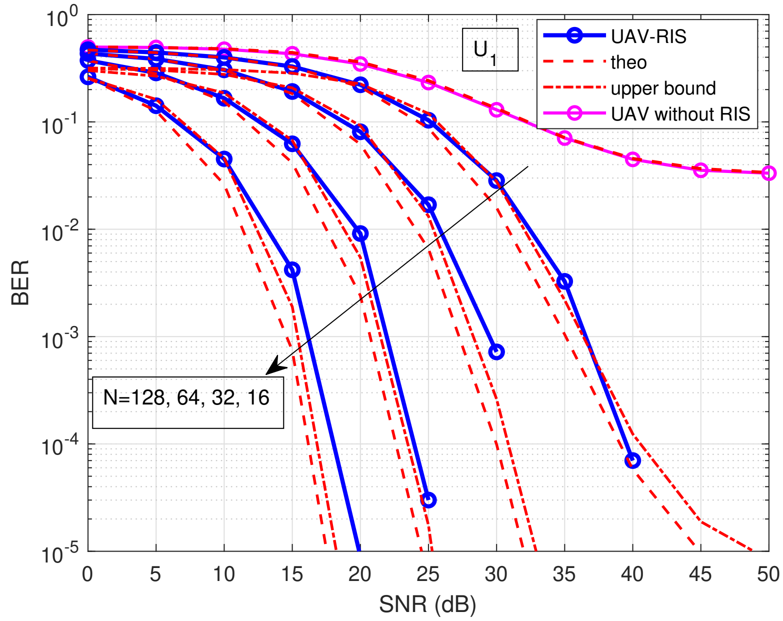

(a)

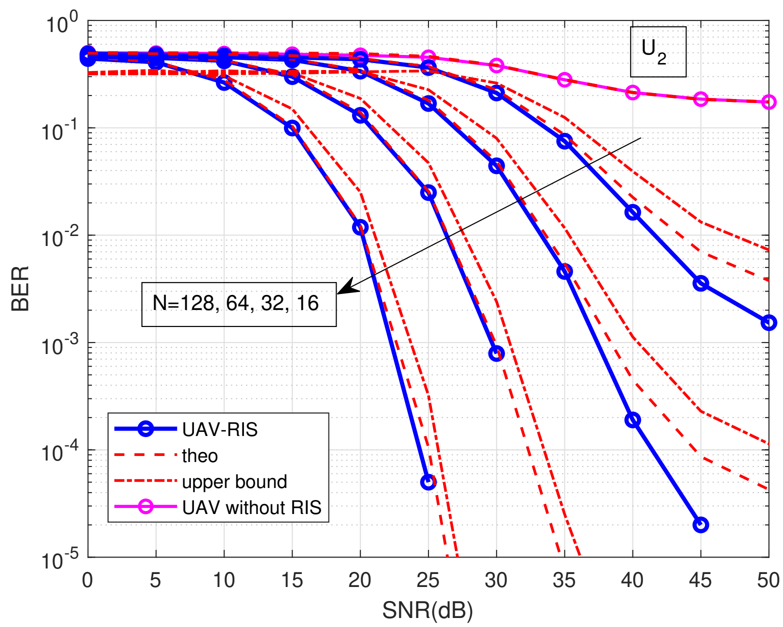

(b)

Figure 7.2: *BER w.r.t. SNR of UAV-RIS NOMA with the fixed value of the effect of HWI and ICI: (a) U_1; (b) U_2.*

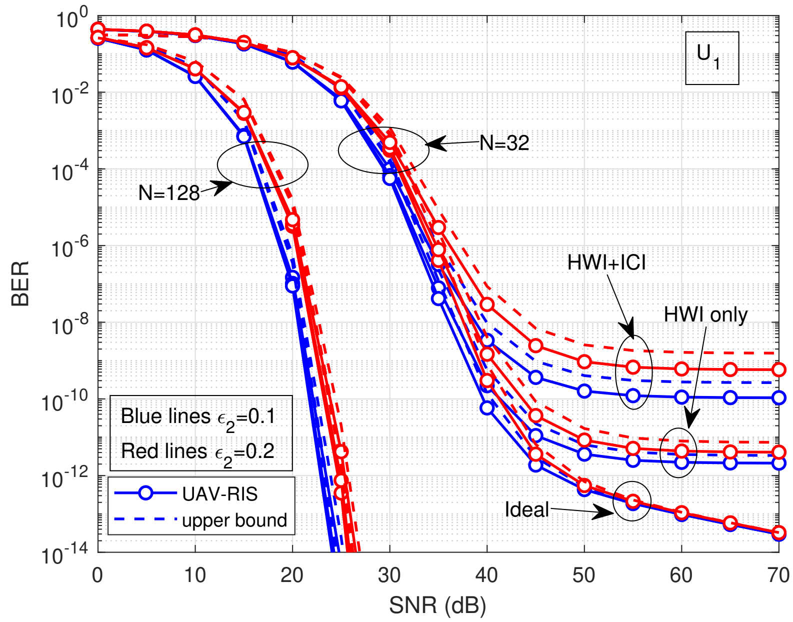

(a)

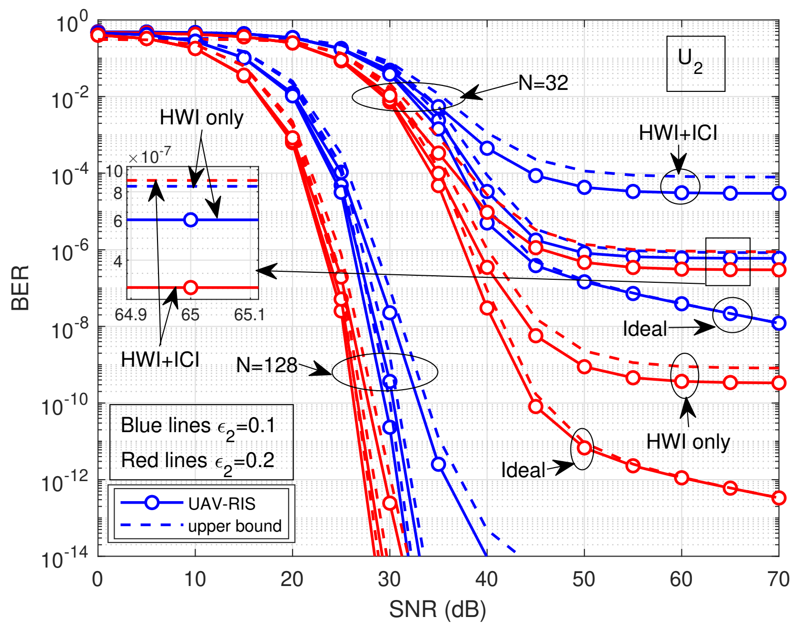

(b)

Figure 7.3: *BER w.r.t. SNR of UAV-RIS NOMA with the effect of HWI and ICI: (a) U_1; (b) U_2.*

and simulation results match for $N \geq 64$. It can be also seen that increasing the number of elements N provides a better BER performance. Clearly, the performance of UAV-RIS is superior to that of UAV without RIS scheme with increasing N and achieves a performance gain of more than 5 dB with less error at lower SNRs. This figure is extended to Fig.7.3 for more investigation into the impact of ideal and non-ideal conditions (i.e., with/without HWI and ICI) using the analytical expressions. It is observed from this figure that the BER curves have a waterfall region and a saturation region in the ideal and non-ideal cases at high SNR values. This observation can be explained as follows. According to (7.14), for the low values of $N\frac{P}{\sigma_{W,i}}$, we achieve an incredibly low BER performance by increasing N due to N^2 in the exponential form. On the other side, for the high values of $N\frac{P}{\sigma_{W,i}}$, the BER performance is saturated due to the $\frac{-1}{2}$ exponent in the high SNR values. Moreover, the presence of HWI and ICI have much impact on the system performance in the high SNR values, especially for U_2 more than U_1 due to the SIC process. It is observed that the BER is nearly the same for both ideal and non-ideal conditions until a particular SNR value. Therefore, there is a trade-off between the number of N and the level of SNR to enable the impacts of the HWI and ICI to be reasonably disregarded. Despite the significant impact of the HWI and ICI which leads to creating an error floor at the higher SNR values, the reached BER at higher values of N is gratifying and sufficient to ignore the influence of HWI and ICI at low SNR values to maintain high EE. Moreover, the change in the power allocation does not improve the performance while it affects one user at the expense of the other. It affects the SIC and the detection of the signals.

To show the role of UAV, in Figure 7.4, we present the BER of system from (7.15) versus $T(m)$ with different LoS probability for UAV-RIS NOMA compared to OMA with the effect of HWI and ICI when SNR=50 dB, N=32, and $Plos(\emptyset) = 0.1, 0.3$. In this figure, it is assumed that the TDMA is implemented for OMA, where each user transmits its signals at different times. It is observed that increasing T values degrades the BER performance of the system. It is due to increasing the Euclidean distance between the S and UAV and between UAV and users. In the lower values of T, when the HWI and ICI have a joint effect, there is more imperfection in the system compared to HWI only and ICI only. The impact of ICI exceeds that of HWI at higher T values. It can be explained as follows. Increasing the altitude of a UAV may increase its proximity to neighboring UAVs, which means increasing the effect of ICI. In higher values of T, the impact of and ICI are relatively matched to the ideal case due to the increasing error to detect the symbols in the higher Euclidean distances. It can also be observed that increasing the LoS component value also means improving direct visibility between the transmitter and the receiver, which reduces path loss and enhances performance. It can be also seen that the OMA has better performance gain compared to NOMA. Combining the users' signals in NOMA makes it suffer from IUI, which complicates the SIC performance to detect the users' signals. Moreover, the presence of and ICI impedes the SIC process and causes more errors in the detection of the users' signals. On the other side, OMA

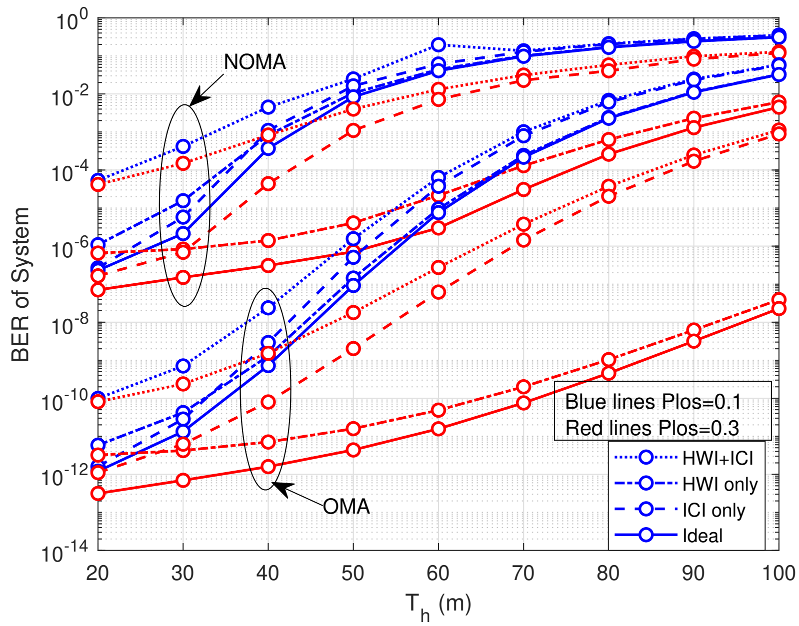

Figure 7.4: *BER of system w.r.t. altitude $T_h(m)$ of UAV-RIS NOMA with the effect of HWI and ICI.*

transmits the signals at different times, therefore it does not suffer from IUI.

Figure 7.5 presents the EE w.r.t. N for UAV-RIS NOMA and UAV-RIS OMA with ideal and non-ideal with different Plos=0.1, 0.3, where SNR= 50 dB, P_s=10 dBm, P_h=4 dBm, P_N=10 dBm, $P_{(UE,i)}$=10 dBm, and Z_e=1.2 as used in [194]. We observe that increasing N improves the EE performance, while the presence of non-ideal conditions degrades the EE performance. It is also observed that increasing the LoS component value improves direct visibility between the transmitter and the receiver, which reduces path loss and enhances EE performance. Through this figure, we can see that in the presence of non-ideal conditions, increasing N does not improve the EE performance. Thus, it becomes evident that, even in the presence of non-ideal conditions, the increase in N does not yield an improvement in EE performance. To further investigate, we illustrate the EE w.r.t. N under HWI and ICI with different SNR values in Figure 7.6. It can be seen that elevating N fails to enhance EE performance at high SNR values because is limited in the higher N values. In contrast, at lower SNR values, the EE increases with the rise in N. Therefore, it is evident that increasing N does not lead to an enhancement in EE performance at high SNR values in the presence of HWI and ICI. However, despite the pronounced influence of HWI and ICI limiting EE performance at higher SNR values, a noteworthy enhancement in EE is achieved by increasing N at lower SNR levels. This improvement is satisfactory and adequate to alleviate and disregard the impact of HWI.

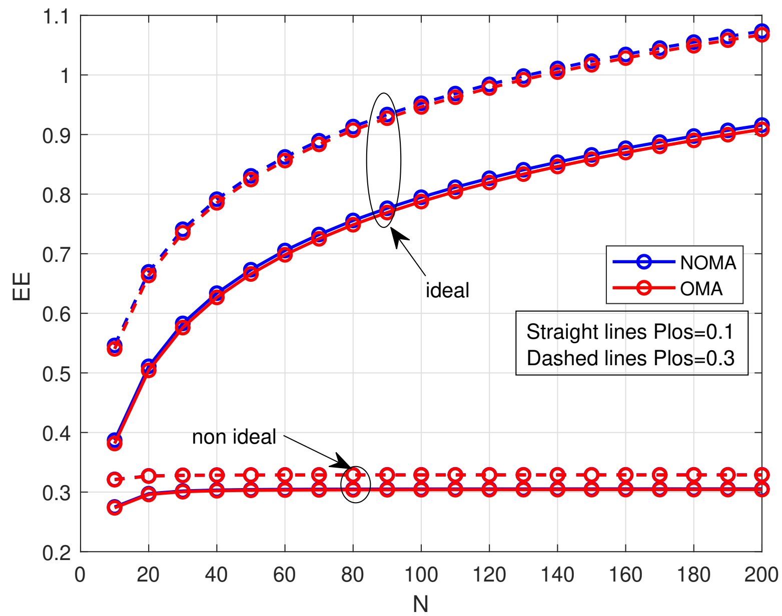

Figure 7.5: *EE w.r.t. N with different Plos for NOMA and OMA with ideal and non-ideal (i.e., with and without HWI and ICI).*

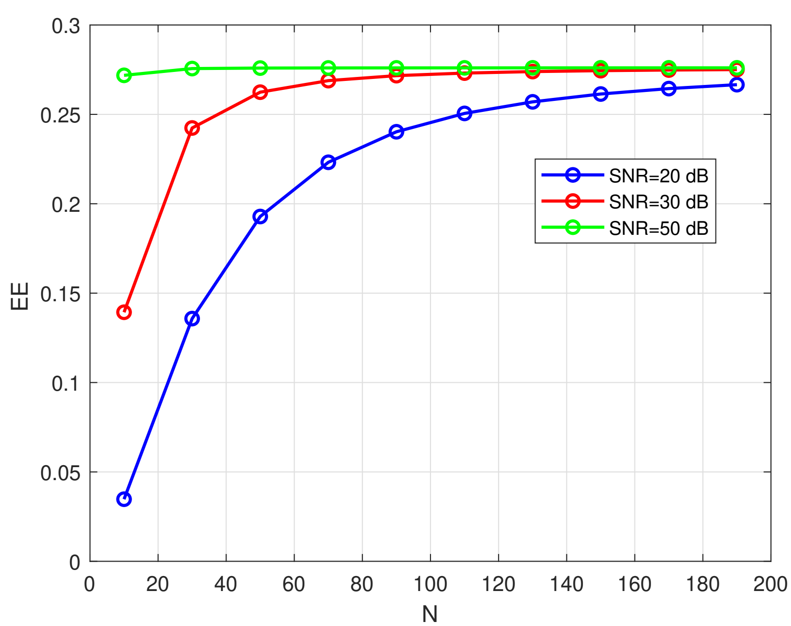

Figure 7.6: *EE w.r.t. N with different SNR.*

7.5 Conclusion

In this chapter, the error probability is analyzed for UAV-RIS NOMA. We consider that practical constraints such as ICI, and imperfect SIC exist in our proposed system. We discussed the effects of these imperfections on the system's performance. The upper bound of the analytical derivation is obtained and the analytical derivations are validated by Monte Carlo simulations. The results show that the non-ideal conditions (HWI, ICI, and imperfect SIC) cause a degradation in the system performance at high SNR regions. However, these degradations can be ignored by increasing the number of reflecting elements at low SNR because it achieves satisfying results, which leads to the preservation of high EE. Moreover, the proposed system has a higher performance gain compared to the UAV without RIS, while OMA has better performance than NOMA because it does not suffer from IUI.

General Conclusion and Future Works

1. General Conclusion:

In recent decades, there has been an increased demand for high data rates, reduced latency, and increased network capacity. The evolution from 1G to 5G had been predicated on the OMA transmission scheme. One advantage of such orthogonal designs was that simple receivers could achieve high system performance. In the past few years, NOMA has drawn a lot of interest as a potential multiple-access technique for 5G and beyond (B5G). In NOMA, several users could share the same radio resources in terms of time, frequency, and/or code. To increase communication coverage, improve performance, and counteract channel drawbacks including fading, path loss, and shadowing, CNOMA was proposed as a promising solution to resolve these issues. In this thesis, we have investigated CNOMA with several technologies to enhance the system performance and efficiency such as cooperation with and without direct links, multiple relays (multi-hop relay), EH, and UAV-mounted RIS. The aims of each system were described as follows:

- Two main schemes were employed in CNOMA: Cooperative WDL and cooperative with DL. The first aimed to improve system performance, and the second aimed to increase the coverage area.
- The multi-hop relay is intended to mitigate channel issues like path loss, fading, and interference that often happen during long-distance communications.
- By utilizing RF energy sources, EH in wireless communication aimed to reduce dependence on conventional power sources, enable self-sufficient operation with low cost, and power devices sustainably.
- UAV-mounted RIS aimed to improve wireless communication to promote effective data transmission and emergency communications. This integration maximizes coverage, minimizes interference, and boosts signal strength.

We have analyzed cooperative NOMA with the mentioned systems for throughput, BER, OP, and EC. The IQI, HWI, ISIC, and ICSI were assessed. The contributions of this thesis were highlighted in each chapter below:

- In Chapter 1, the fundamental concepts of wireless communication networks, NOMA, and CNOMA were defined. Besides, EH technology was reviewed as a promising solution to resolve the problem of limited or damaged batteries. RIS and UAV technology were also reviewed as promising solutions to achieve the requirements of 6G wireless networks.
- In Chapter 2, the CNOMA WDL was considered to extend the coverage area. Since the far user could not receive its signal, the near user worked as an assistance user to help the far user to receive its signal. The closed-form EC, OP, and BER over the Rayleigh fading channel were derived and validated with simulations. The impact of the power allocation and helper user distance was discussed. The outcomes of our simulation indicated that the helper user's position significantly influenced the performance improvement for the far user, where the best position of the helper user is in the middle. The power allocation impacted performance, and alterations to it affected the performance of one user at the expense of another.
- In Chapter 3, CNOMA with DL was considered to improve the performance of far users when direct and indirect links were available. The closed-form OP and BER with ISIC and ICSI over the Rayleigh fading channel were derived. The asymptotic analysis of OP at high SNR regions was performed to reveal the insights of the system performance. Our derivations were validated with simulations. As a benchmark, we compared our results with traditional NOMA. The change in power allocation and the helper user distance affected the performance of the system, which affected the SIC process. The ICSI degraded the system performance at high SNR and influenced the SIC to detect the users' signals.
- In Chapter 4, we have proposed the MH-DF-CNOMA system with two schemes under practical scenarios i.e., the ICSI and ISIC were taken into account. The first scheme, MH-DF-CNOMA WDL, was used to extend the coverage area when the group of multiple intermediate relay nodes delivered the signal to the users in shadowed areas or places outside of the cell range. We obtained the e2e OP and BER expressions under ICSI and ISIC. The second scheme, MH-DF-CNOMA with DL, was used to improve the QoS and system performance. When a direct and indirect link was available using the group of multiple intermediate relay nodes to deliver the signal to the far users to improve the received signal quality. It was presumed that the MRC was implemented to combine the received signals because the distant user received two copies of its signals. The e2e OP and BER expressions for the considered systems under ICSI and ISIC were derived. The influence of power allocation, the number of relays, ICSI, and SIC on the performance of the system was discussed. We validated our derivations of both systems through simulations. According to the results, both of the MH-DF-CNOMA schemes

decreased the OP and BER when the number of relays increased. Our scheme achieved higher performance gains compared to the single relay scheme. Furthermore, the SIC process was impacted by changes in the power allocation because they had an impact on system performance. Signal detection and the SIC process at nodes were impacted in the presence of the ICSI.

- In Chapter 5, two CNOMA with RF EH schemes were investigated. The first one, CNOMA with TS and PS protocols with ICSI, ISIC, and ICI were analyzed in terms of BER over the Rayleigh fading channel. The second one is CNOMA with a HEH protocol. The OP and BER were obtained over the Nakagami-m fading channel. The HEH protocol was compared with no-EH and the conventional EH protocols (PS and TS protocols). The impact of power allocation, ICSI, ICI, and EH parameters on the system performance was examined for both schemes. Monte Carlo simulations validated the analytical derivations. The findings indicated that, at high SNR, the SIC process was impacted by the ICSI and ICI variables. In comparison to no-EH and conventional EH protocols, the HEH protocol achieved greater performance gains. More precisely, the hybrid scheme could achieve 1-3 dB and 0.5-1.5 dB better BER and OP performances, respectively, than other schemes, depending on the channel characteristics. Finally, the HEH protocol could maximize system performance by ten times (e.g., $10^4 \rightarrow 10^5$).
- Chapter 6 investigated the proposed HTC-NOMA-WPCCN system with both linear and non-linear EH in the presence of IQI and SIC imperfections. The study considered a multi-helper-user scheme to enhance system performance. We analyzed the OP, EC, and throughput expressions for users under linear and non-linear EH. The proposed system was compared to uplink NOMA and single helper user schemes across various parameters such as WPCCN, IQI, ISIC, IRR, and power allocation. Results indicated the superiority of the proposed system over uplink NOMA and single helper user schemes. The SIC and IQI were affected by the changes in IRR, WPCN, and power allocation impacting system performance. Non-linear EH limited performance in high SNR regions, exacerbated by SIC imperfections and IQI. Finally, IQI had a detrimental impact on RF impairment even when the number of helper users rose, proving that IQI mitigation was required to fully utilize the capabilities of the systems.
- In Chapter 7, we investigated the UAV-RIS for the NOMA system under real-world constraints like ICI and ISIC. We analyzed the BER of the considered system and derived its upper bound analytically. Also, we have evaluated the EE of our system and compared it with two other schemes: UAV without RIS and traditional UAV-RIS OMA. Our findings revealed that practical factors such as HWI, ICI, and ISIC deteriorated system performance at high SNR levels. However, at low SNR levels, increasing the number

of reflective elements could mitigate these effects and maintain high EE. Finally, our proposed system outperformed the UAV without RIS, although OMA exhibited better performance compared to NOMA.

2. Future Works:

The research community has begun to discuss use cases, requirements, and technologies that will enable 6G systems. Among other issues, existing networks are unable to adequately cover rural and disaster areas. Densifying cellular cells is one way to improve network resilience; however, this requires high-capacity backhaul connections and prohibitive deployment and operating costs for network operators. To resolve these problems, current 6G research is concentrated on creating non-terrestrial networks (NTN) that will enable high-capacity global connectivity ubiquitously. In contrast to the conventional design of earlier wireless generation networks, which aimed to connect a quasi-dimensional space, 6G envisages a three-dimensional heterogeneous architecture where non-terrestrial stations such as satellites, UAV, and HAPS are incorporated into terrestrial infrastructures.

The integration of CNOMA and NTN has the potential to improve spectral efficiency, provide more connectivity in remote areas, and ensure reliable communication in challenging environments by leveraging NOMA's efficient resource allocation and NTN's extensive coverage. We're exploring a new paradigm: integrating NTN with EH for NOMA to enhance EE. This novel approach harnesses NTN's expansive coverage and EH capabilities, aiming to optimize resource usage and extend the network lifetime. Furthermore, RIS receives much attention in the literature by installing it on aerial platform stations to increase the system's efficiency. Integrating RIS with NOMA and NTN poses a major challenge in wireless communication. Addressing this demands creative solutions to optimize resources, manage interference, and capitalize on their combined potential. Success here could revolutionize network efficiency, coverage, and reliability. On the other hand, the devices suffer from hardware defects (i.e., HWI and IQI) that affect the system's performance. Therefore, solutions should be considered to mitigate these effects and improve system performance. Within the realm of NTN, it's imperative to address hardware defects like HWI and IQI that limit system performance. Implementing solutions to mitigate these issues is essential for optimizing NTN-enabled communication systems and ensuring reliable and efficient connectivity. Moreover, massive MIMO systems with a large number of antennas (up to hundreds) at the BS or access point are a natural extension of the conventional small-scale MIMO technology that has garnered significant attention due to its potential to increase spectral efficiency and improve system performance. The integration of massive MIMO with NTN and NOMA will provide an unprecedented opportunity that could lead to significant performance improvements in the future. Furthermore, the integration of deep learning and NTN NOMA technology is poised to revolutionize 6G communication networks. Through this integration, we can maximize network throughput, reduce interference, and improve signal quality.

Bibliography

[1] Muhammad Zeeshan Asghar, Shafique Ahmed Memon, and Jyri Hämäläinen. Evolution of wireless communication to 6g: Potential applications and research directions. *Sustainability*, 14(10):6356, 2022.

[2] 6G: The next hyper-connected experience for All. *Samsung 6G Vision*, 2020.

[3] Partha Pratim Ray. A perspective on 6G: Requirement, technology, enablers, challenges and future road map. *Journal of Systems Architecture*, 118:102180, 2021.

[4] Faical Khennoufa, Khelil Abdellatif, Halim Yanikomeroglu, Metin Ozturk, Taissir Elganimi, and Ferdi Kara. Multi-Layer network formation through HAPS base station and transmissive RIS-equipped UAV. *arXiv preprint arXiv:2405.01692*, 2024.

[5] Mojtaba Vaezi, Zhiguo Ding, and H Vincent Poor. *Multiple access techniques for 5G wireless networks and beyond*, volume 159. Springer, 2019.

[6] Afif Osseiran, Jose F Monserrat, and Patrick Marsch. *5G mobile and wireless communications technology.* Cambridge University Press, 2016.

[7] Safia Beddiaf, Abdellatif Khelil, Faical Khennoufa, Ferdi Kara, Khaled Rabie, Xingwang Li, Hakan Kaya, Ahmet Emir, and Halim Yanikomeroglu. Impact of hardware impairment on the uplink SIMO Cooperative NOMA with selection relay under imperfect CSI. *IEEE Access*, 2023.

[8] Yuya Saito, Yoshihisa Kishiyama, Anass Benjebbour, Takehiro Nakamura, Anxin Li, and Kenichi Higuchi. Non-orthogonal multiple access (NOMA) for cellular future radio access. In *IEEE 77th vehicular technology conference (VTC Spring)*, pages 1–5, 2013.

[9] Zhiyong Chen, Zhiguo Ding, Xuchu Dai, and Rui Zhang. An optimization perspective of the superiority of NOMA compared to conventional OMA. *IEEE Transactions on Signal Processing*, 65(19):5191–5202, 2017.

[10] Babu AV et al. Non-orthogonal multiple access in full-duplex-based coordinated direct and relay transmission (CDRT) system: Performance analysis and optimization. *EURASIP Journal on Wireless Communications and Networking*, 2020(1):1–27, 2020.

[11] Ferdi Kara and Hakan Kaya. BER performances of downlink and uplink NOMA in the presence of SIC errors over fading channels. *IET Communications*, 12(15):1834–1844, 2018.

[12] Faical Khennoufa, Khelil Abdellatif, and Ferdi Kara. Bit error rate and outage probability analysis for multi-hop decode-and-forward relay-aided NOMA with imperfect SIC and imperfect CSI. *AEU-International Journal of Electronics and Communications*, 147:154124, 2022.

[13] Faical Khennoufa and Abdellatif Khelil. Exact bit error rate of cooperative NOMA without diversity combining. In *IEEE International Conference on Artificial Intelligence for Cyber Security Systems and Privacy (AI-CSP)*, pages 1–5, 2021.

[14] Faical Khennoufa and Abdellatif Khelil. Capacity performance comparison of cooperative NOMA and OMA systems in DF and AF. *Electrical Engineering*, 2:1, 2021.

[15] Hassan Sajjad and Muhammad Jamil. Error rate performance of multi-hop communication systems over Nakagami-m fading channel, 2012.

[16] Mahmoud Aldababsa. *Analysis of hybrid antenna diversity techniques in non-orthogonal multiple access systems with practical impairments for 5g*. PhD thesis, Gebee technical University, 2020.

[17] Marvin K Simon and Mohamed-Slim Alouini. *Digital communication over fading channels*. New York: Wiley, 2001.

[18] Jinlong Zhao, Xinwei Yue, Shaoli Kang, and Wanwei Tang. Joint effects of imperfect CSI and SIC on NOMA based satellite-terrestrial systems. *IEEE Access*, 9:12545–12554, 2021.

[19] Y-W Peter Hong, Wan-Jen Huang, and C-C Jay Kuo. *Cooperative communications and networking: technologies and system design*. Springer Science & Business Media, 2010.

[20] Ezio Biglieri, Robert Calderbank, Anthony Constantinides, Andrea Goldsmith, Arogyaswami Paulraj, and H Vincent Poor. *MIMO wireless communications*. Cambridge university press, 2007.

[21] Andrea Sabrina Marcano Fani. *Capacity dimensioning for 5G mobile heterogeneous networks*. PhD thesis, Technical University of Denmark, 2018.

[22] Wonjae Shin, Mojtaba Vaezi, Byungju Lee, David J Love, Jungwoo Lee, and H Vincent Poor. Non-orthogonal multiple access in multi-cell networks: Theory, performance, and practical challenges. *IEEE Communications Magazine*, 55(10):176–183, 2017.

[23] Mojtaba Vaezi, Robert Schober, Zhiguo Ding, and H Vincent Poor. Non-orthogonal multiple access: Common myths and critical questions. *IEEE Wireless Communications*, 26(5):174–180, 2019.

[24] Ming Zeng, Wanming Hao, Octavia A Dobre, and Zhiguo Ding. Cooperative NOMA: State of the art, key techniques, and open challenges. *IEEE Network*, 34(5):205–211, 2020.

[25] Dusit Niyato, Dong In Kim, Zhu Han, and Marco Maso. Wireless powered communication networks: Architectures, protocol designs, and standardization. *IEEE Wireless Communications*, 23(2):8–9, 2016.

[26] Mojtaba Vaezi, Gayan Amarasuriya Aruma Baduge, Yuanwei Liu, Ahmed Arafa, Fang Fang, and Zhiguo Ding. Interplay between NOMA and other emerging technologies: A survey. *IEEE Transactions on Cognitive Communications and Networking*, 5(4):900–919, 2019.

[27] Yunfei Chen. *Energy harvesting communications: principles and theories.* John Wiley & Sons, 2019.

[28] Tharindu D Ponnimbaduge Perera, Dushantha Nalin K Jayakody, Shree Krishna Sharma, Symeon Chatzinotas, and Jun Li. Simultaneous wireless information and power transfer (SWIPT): Recent advances and future challenges. *IEEE Communications Surveys & Tutorials*, 20(1):264–302, 2017.

[29] Zhiqiang Wei, Xianghao Yu, Derrick Wing Kwan Ng, and Robert Schober. Resource Allocation for Simultaneous Wireless Information and Power Transfer Systems: A Tutorial Overview. *Proceedings of the IEEE*, 2021.

[30] Muntadher Alsabah, Marwah Abdulrazzaq Naser, Basheera M Mahmmod, Sadiq H Abdulhussain, Mohammad R Eissa, Ahmed Al-Baidhani, Nor K Noordin, Sadiq M Sait, Khaled A Al-Utaibi, and Fazirul Hashim. 6G wireless communications networks: A comprehensive survey. *Ieee Access*, 9:148191–148243, 2021.

[31] Syed Agha Hassnain Mohsan, Nawaf Qasem Hamood Othman, Yanlong Li, Mohammed H Alsharif, and Muhammad Asghar Khan. Unmanned aerial vehicles (UAVs): Practical aspects, applications, open challenges, security issues, and future trends. *Int. Service Rob.*, pages 1–29, 2023.

[32] Sandeep Kumar Singh, Kamal Agrawal, Keshav Singh, Chih-Peng Li, and Mohamed-Slim Alouini. NOMA enhanced UAV-assisted communication system with nonlinear energy harvesting. *IEEE Open Journal of the Communications Society*, 3:936–957, 2022.

[33] Hongliang Zhang, Boya Di, Lingyang Song, and Zhu Han. *Reconfigurable intelligent surface-empowered 6G.* Springer, 2021.

[34] Shuhao Zeng, Hongliang Zhang, Boya Di, Yunhua Tan, Zhu Han, H Vincent Poor, and Lingyang Song. Reconfigurable intelligent surfaces in 6G: Reflective, transmissive, or both? *IEEE Commun. Lett.*, 25(6):2063–2067, 2021.

[35] Omar Maraqa, Aditya S Rajasekaran, Saad Al-Ahmadi, Halim Yanikomeroglu, and Sadiq M Sait. A survey of rate-optimal power domain NOMA with enabling technologies of future wireless networks. *IEEE Communications Surveys & Tutorials*, 22(4):2192–2235, 2020.

[36] Zhiguo Ding, Xianfu Lei, George K Karagiannidis, Robert Schober, Jinhong Yuan, and Vijay K Bhargava. A survey on non-orthogonal multiple access for 5G networks: Research challenges and future trends. *IEEE Journal on Selected Areas in Communications*, 35(10):2181–2195, 2017.

[37] Juhi Garg, Priyanka Mehta, and Kapil Gupta. A review on cooperative communication protocols in wireless world. *International Journal of Wireless & Mobile Networks*, 5(2):107, 2013.

[38] Monika Jain, Sandhya Soni, Nikhil Sharma, and Divyang Rawal. Performance analysis at far and near user in NOMA based system in presence of SIC error. *AEU-International Journal of Electronics and Communications*, 114:152993, 2020.

[39] Xiaodong Liu, Zezong Chen, Yuhao Wang, Fuhui Zhou, Yusang Luo, and Rose Qingyang Hu. BER analysis of NOMA-enabled visible light communication systems with different modulations. *IEEE Transactions on Vehicular Technology*, 68(11):10807–10821, 2019.

[40] Ferdi Kara and Hakan Kaya. The error performance analysis of the decode-forward relay-aided-NOMA systems and a power allocation scheme for user fairness. *J. Fac. Eng. Archit. Gazi Univ*, 35(1):97–108, 2020.

[41] Ferdi Kara and Hakan Kaya. Error analysis of decode-forward cooperative relaying NOMA schemes over Nakagami-m fading channels. In *IEEE 28th Signal Processing and Communications Applications Conference (SIU)*, pages 1–4, 2020.

[42] Sandhya Soni, Monika Jain, Divyang Rawal, Nikhil Sharma, and Ranjith Liyanapathirana. Performance analysis of DF cooperative-NOMA system with QPSK-BPSK scheme in the presence of SIC errors. In *IEEE International Conference on Electrical Engineering Research & Practice (ICEERP)*, pages 1–6, 2019.

[43] KARA Ferdi and KAYA Hakan. Improved error performance in NOMA-based diamond relaying. In *2020 IEEE Microwave Theory and Techniques in Wireless Communications (MTTW)*, volume 1, pages 151–156. IEEE, 2020.

[44] M Sashiganth, SJ Thiruvengadam, and D Sriram Kumar. BER analysis of full duplex NOMA downlink and uplink co-operative user relaying systems over Nakagami-m fading environment. *Physical Communication*, 38:100963, 2020.

[45] Ferdi Kara and Hakan Kaya. Improved user fairness in decode-forward relaying non-orthogonal multiple access schemes with imperfect SIC and CSI. *IEEE Access*, 8:97540–97556, 2020.

[46] S Ross. A First Course in Probability, vol. 56, no. 3, 1988.

[47] Izrail Solomonovich Gradshteyn and Iosif Moiseevich Ryzhik. *Table of integrals, series, and products*. Academic press, 2014.

[48] Galymzhan Nauryzbayev, Sultangali Arzykulov, Theodoros A Tsiftsis, and Mohamed Abdallah. Performance of cooperative underlay CR-NOMA networks over Nakagami-m channels. In *IEEE International Conference on Communications Workshops (ICC Workshops)*, pages 1–6, 2018.

[49] Zhiguo Ding, Mugen Peng, and H Vincent Poor. Cooperative non-orthogonal multiple access in 5G systems. *IEEE Communications Letters*, 19(8):1462–1465, 2015.

[50] Hongwu Liu, Zhiguo Ding, Kyeong Jin Kim, Kyung Sup Kwak, and H Vincent Poor. Decode-and-forward relaying for cooperative NOMA systems with direct links. *IEEE Transactions on Wireless Communications*, 17(12):8077–8093, 2018.

[51] Xuesong Liang, Yongpeng Wu, Derrick Wing Kwan Ng, Yiping Zuo, Shi Jin, and Hongbo Zhu. Outage performance for cooperative NOMA transmission with an AF relay. *IEEE Communications Letters*, 21(11):2428–2431, 2017.

[52] Mengqi Yang, Jian Chen, Long Yang, Lu Lv, Bingtao He, and Boyang Liu. Design and performance analysis of cooperative NOMA with coordinated direct and relay transmission. *IEEE Access*, 7:73306–73323, 2019.

[53] Peng Xu, Yunwu Wang, Gaojie Chen, Gaofeng Pan, and Zhiguo Ding. Design and evaluation of buffer-aided cooperative NOMA with direct transmission in IoT. *IEEE Internet of Things Journal*, 8(10):8145–8158, 2020.

[54] Hongwu Liu, Nikolaos I Miridakis, Theodoros A Tsiftsis, Kyeong Jin Kim, and Kyung Sup Kwak. Coordinated uplink transmission for cooperative NOMA systems. In *IEEE Global Communications Conference (GLOBECOM)*, pages 1–6, 2018.

[55] Guoxin Li and Deepak Mishra. Cooperative NOMA networks: User cooperation or relay cooperation? In *IEEE international conference on communications (ICC)*, pages 1–6, 2020.

[56] Md Fazlul Kader, SM Riazul Islam, and Octavia A Dobre. Device-to-device aided cooperative NOMA transmission exploiting overheard signal. *IEEE Transactions on Wireless Communications*, 21(2):1304–1318, 2021.

[57] Sandeep Joshi and Ranjan K Mallik. Cooperative NOMA with AF Relaying over Nakagami-m Fading in a D2D Network. In *IEEE 89th Vehicular Technology Conference (VTC2019-Spring)*, pages 1–6, 2019.

[58] Jiazhen Zhang, Xiaofeng Tao, Huici Wu, and Xuefei Zhang. Performance analysis of user pairing in cooperative NOMA networks. *IEEE Access*, 6:74288–74302, 2018.

[59] Xianli Gong, Xinwei Yue, and Feng Liu. Performance analysis of cooperative NOMA networks with imperfect CSI over Nakagami-m fading channels. *Sensors*, 20(2):424, 2020.

[60] Guoxin Li, Deepak Mishra, and Hai Jiang. Cooperative NOMA with incremental relaying: Performance analysis and optimization. *IEEE Transactions on Vehicular Technology*, 67(11):11291–11295, 2018.

[61] Yingying Zhang, Zhen Yang, Youhong Feng, and Shihao Yan. Performance analysis of a novel uplink cooperative NOMA system with full-duplex relaying. *IET Communications*, 12(19):2408–2417, 2018.

[62] Ferdi Kara and Hakan Kaya. Threshold-based selective cooperative NOMA: Capacity/outage analysis and a joint power allocation-threshold selection optimization. *IEEE Communications Letters*, 24(9):1929–1933, 2020.

[63] Safia Beddiaf, Abdellatif Khelil, Faical Khennoufa, and Khaled Rabie. On the impact of IQI on cooperative NOMA with direct links in the presence of imperfect CSI. *Physical Communication*, 56:101952, 2023.

[64] Safia Beddiaf, Abdellatif Khelil, Faical Khennoufa, Ferdi Kara, Hakan Kaya, Xingwang Li, Khaled Rabie, and Halim Yanikomeroglu. A Unified Performance Analysis of Cooperative NOMA With Practical Constraints: Hardware Impairment, Imperfect SIC and CSI. *IEEE Access*, 10:132931–132948, 2022.

[65] Anis Amazigh Hamza, Iyad Dayoub, Ihsen Alouani, and Abderrahmane Amrouche. On the error rate performance of full-duplex cooperative NOMA in wireless networks. *IEEE Transactions on Communications*, 70(3):1742–1758, 2021.

[66] Ferdi Kara and Hakan Kaya. On the error performance of cooperative-NOMA with statistical CSIT. *IEEE Communications Letters*, 23(1):128–131, 2018.

[67] Ferdi Kara and Hakan Kaya. Threshold-based selective cooperative-NOMA. *IEEE Communications Letters*, 23(7):1263–1266, 2019.

[68] Stefan Valentin, Dereje H Woldegebreal, Tobias Volkhausen, and Holger Karl. Combining for cooperative WLANs-a reality check based on prototype measurements. In *IEEE International Conference on Communications Workshops*, pages 1–5, 2009.

[69] SM Riazul Islam, Nurilla Avazov, Octavia A Dobre, and Kyung-Sup Kwak. Power-domain non-orthogonal multiple access (NOMA) in 5G systems: Potentials and challenges. *IEEE Communications Surveys & Tutorials*, 19(2):721–742, 2016.

[70] Fa-Long Luo and Charlie Jianzhong Zhang. *Signal processing for 5G: algorithms and implementations*. John Wiley & Sons, 2016.

[71] Aria Nosratinia, Todd E Hunter, and Ahmadreza Hedayat. Cooperative communication in wireless networks. *IEEE communications Magazine*, 42(10):74–80, 2004.

[72] Caijun Zhong and Zhaoyang Zhang. Non-orthogonal multiple access with cooperative full-duplex relaying. *IEEE Communications Letters*, 20(12):2478–2481, 2016.

[73] Xianbin Xie, Jinhua Liu, Jiawen Huang, and Shiwei Zhao. Ergodic capacity and outage performance analysis of uplink full-duplex cooperative NOMA system. *IEEE Access*, 8:164786–164794, 2020.

[74] Mohammed Belal Uddin, Md Fazlul Kader, and Soo Young Shin. Exploiting NOMA in D2D assisted full-duplex cooperative relaying. *Physical Communication*, 38:100914, 2020.

[75] V Aswathi and AV Babu. Full/half duplex cooperative NOMA under imperfect successive interference cancellation and channel state estimation errors. *IEEE Access*, 7:179961–179984, 2019.

[76] Min Xu, Fei Ji, Miaowen Wen, and Wei Duan. Novel receiver design for the cooperative relaying system with non-orthogonal multiple access. *IEEE Communications Letters*, 20(8):1679–1682, 2016.

[77] Baha Eddine Youcef Belmekki, Abdelkrim Hamza, and Benoît Escrig. Outage analysis of cooperative noma using maximum ratio combining at intersections. In *IEEE International Conference on Wireless and Mobile Computing, Networking and Communications (WiMob)*, pages 1–6, 2019.

[78] Dan Deng, Lisheng Fan, Xianfu Lei, Weiqiang Tan, and Dongqing Xie. Joint user and relay selection for cooperative NOMA networks. *IEEE Access*, 5:20220–20227, 2017.

[79] Yangyang Zhang, Jianhua Ge, Erchin Serpedin, Redha M Radaydeh, and Yifan Hu. On cooperative NOMA relay selection under Nakagami-m fading and imperfect channel estimation. *Transactions on Emerging Telecommunications Technologies*, 29(12):e3535, 2018.

[80] Jinjuan Ju, Wei Duan, Qiang Sun, Shangce Gao, and Guoan Zhang. Performance analysis for cooperative NOMA with opportunistic relay selection. *IEEE Access*, 7:131488–131500, 2019.

[81] Tasneem Assaf, Arafat Al-Dweik, Mohamed El Moursi, and Hatem Zeineldin. Exact BER performance analysis for downlink NOMA systems over Nakagami-m fading channels. *IEEE Access*, 7:134539–134555, 2019.

[82] Hamad Yahya, Emad Alsusa, and Arafat Al-Dweik. Exact BER analysis of NOMA with arbitrary number of users and modulation orders. *IEEE Transactions on Communications*, 69(9):6330–6344, 2021.

[83] KARA Ferdi and KAYA Hakan. A true power allocation constraint for non-orthogonal multiple access with M-QAM signalling. In *IEEE Microwave Theory and Techniques in Wireless Communications (MTTW)*, volume 1, pages 7–12. IEEE, 2020.

[84] Gang Shen, Jimin Liu, Dongyao Wang, Jikang Wang, and Shan Jin. Multi-hop relay for next-generation wireless access networks. *Bell Labs Technical Journal*, 13(4):175–193, 2009.

[85] Mazen Omar Hasna and M-S Alouini. Outage probability of multihop transmission over Nakagami fading channels. *IEEE Communications Letters*, 7(5):216–218, 2003.

[86] Norman C Beaulieu and Samy S Soliman. Exact analytical solution for end-to-end SNR of multihop AF relaying systems. In *2011 IEEE GLOBECOM Workshops (GC Wkshps)*, pages 580–585. IEEE, 2011.

[87] Hafiz Yasar Lateef, Mounir Ghogho, and Desmond C McLernon. Performance analysis of multi-hop cooperative relay networks over generalized-K fading channels. In *2011 Australian Communications Theory Workshop*, pages 71–76. IEEE, 2011.

[88] Tran Tin Phu, Trung Duy Tran, Miroslav Voznak, et al. Security-reliability analysis of NOMA-based multi-hop relay networks in presence of an active eavesdropper with imperfect eavesdropping CSI. *Advances in Electrical and Electronic Engineering*, 15(4):591–597, 2017.

[89] Tran Thanh-Na and journal=Electronics pages=8–167 year=2019 publisher=MDPI Miroslav, Vo. Multi-Points Cooperative Relay in NOMA System with N-1 DF Relaying Nodes in HD/FD Mode for N User Equipments with Energy Harvesting.

[90] Eduardo Morgado, Inmaculada Mora-Jimenez, Juan J Vinagre, Javier Ramos, and Antonio J Caamano. End-to-end average BER in multihop wireless networks over fading channels. *IEEE transactions on wireless communications*, 9(8):2478–2487, 2010.

[91] Faical Khennoufa, Abdellatif Khelil, and Elhadi Kenane. BER and outage performance for multi-hop user-relays NOMA with imperfect SIC and CSI. In *IEEE International Conference of Advanced Technology in Electronic and Electrical Engineering (ICATEEE)*, pages 1–6, 2022.

[92] Ferdi Kara and Hakan Kaya. On the error performance of cooperative-NOMA with statistical CSIT. *IEEE Communications Letters*, 23(1):128–131, 2018.

[93] Yue Qi, Xinliang Zhang, and Mojtaba Vaezi. Over-the-air implementation of NOMA: New experiments and future directions. *IEEE Access*, 9:135828–135844, 2021.

[94] Ziad Qais Al-Abbasi, Khaled M Rabie, and Daniel KC So. EE optimization for downlink NOMA-based multi-tier CRANs. *IEEE Transactions on Vehicular Technology*, 70(6):5880–5891, 2021.

[95] Dinh-Thuan Do, Tu-Trinh Thi Nguyen, Chi-Bao Le, Miroslav Voznak, Zeeshan Kaleem, and Khaled M Rabie. UAV relaying enabled NOMA network with hybrid duplexing and multiple antennas. *IEEE Access*, 8:186993–187007, 2020.

[96] Ishan Budhiraja, Neeraj Kumar, Sudhanshu Tyagi, Sudeep Tanwar, Zhu Han, Md Jalil Piran, and Doug Young Suh. A systematic review on NOMA variants for 5G and beyond. *IEEE Access*, 9:85573–85644, 2021.

[97] Nausheen Ashraf, Shahzad Amin Sheikh, Sajjad Ahmad Khan, Ibraheem Shayea, and Marium Jalal. Simultaneous wireless information and power transfer with cooperative relaying for next-generation wireless networks: A review. *IEEE Access*, 9:71482–71504, 2021.

[98] Shijun Lin, Huixin Tang, Baoshan Lu, and Jianghong Shi. Energy minimization for NOMA cellular networks with two-dimensional resource allocation. *IEEE Transactions on Green Communications and Networking*, 7(1):42–56, 2022.

[99] Hyun-Ho Choi and Kisong Lee. Cooperative wireless power transfer for lifetime maximization in wireless multihop networks. *IEEE Transactions on Vehicular Technology*, 70(4):3984–3989, 2021.

[100] Mohammad Reza Ghavidel Aghdam, Behzad Mozaffari Tazehkand, and Reza Abdolee. Joint optimal power allocation and beamforming for MIMO-NOMA in mmWave communications. *IEEE Wireless Communications Letters*, 11(5):938–941, 2022.

[101] Priyank Sharma, Atul Kumar, and Matadeen Bansal. Performance analysis of downlink NOMA over η–μ and κ–μ fading channels. *IET Communications*, 14(3):522–531, 2020.

[102] Zheng Shi, Hong Wang, Yaru Fu, Guanghua Yang, Shaodan Ma, and Xinrong Ye. Outage performance and optimal design of MIMO-NOMA enhanced small cell networks with imperfect channel-state information. *China Communications*, 18(10):107–128, 2021.

[103] Zhiguo Ding, Zheng Yang, Pingzhi Fan, and H Vincent Poor. On the performance of non-orthogonal multiple access in 5G systems with randomly deployed users. *IEEE signal processing letters*, 21(12):1501–1505, 2014.

[104] Yanshi Sun, Zhiguo Ding, and Xuchu Dai. A new design of hybrid SIC for improving transmission robustness in uplink NOMA. *IEEE Transactions on Vehicular Technology*, 70(5):5083–5087, 2021.

[105] Xingwang Li, Mengle Zhao, Changsen Zhang, Wali Ullah Khan, Jun Wu, Khaled M Rabie, and Rupak Kharel. Security analysis of multi-antenna NOMA networks under I/Q imbalance. *Electronics*, 8(11):1327, 2019.

[106] Xinyue Pei, Hua Yu, Miaowen Wen, Shahid Mumtaz, Sattam Al Otaibi, and Mohsen Guizani. NOMA-based coordinated direct and relay transmission with a half-

duplex/full-duplex relay. *IEEE Transactions on communications*, 68(11):6750–6760, 2020.

[107] Xingwang Li, Jingjing Li, Yuanwei Liu, Zhiguo Ding, and Arumugam Nallanathan. Residual transceiver hardware impairments on cooperative NOMA networks. *IEEE Transactions on Wireless Communications*, 19(1):680–695, 2019.

[108] Long Ma, Enyu Li, Qianqian Yang, Xinjie Wang, and Chuanwang Song. Performance analysis and optimization in two-way cooperative NOMA under two-phase transmission protocol. *IEEE Systems Journal*, 16(3):3566–3577, 2022.

[109] Hongwu Liu, Zhiquan Bai, Hongjiang Lei, Gaofeng Pan, Kyeong Jin Kim, and Theodoros A Tsiftsis. A new rate splitting strategy for uplink CR-NOMA systems. *IEEE Transactions on Vehicular Technology*, 71(7):7947–7951, 2022.

[110] Dinh-Thuan Do, Thanh-Luan Nguyen, Khaled M Rabie, Xingwang Li, and Byung Moo Lee. Throughput analysis of multipair two-way replaying networks with NOMA and imperfect CSI. *IEEE Access*, 8:128942–128953, 2020.

[111] Xingwang Li, Meng Liu, Chao Deng, Di Zhang, Xiang-Chuan Gao, Khaled M Rabie, and Rupak Kharel. Joint effects of residual hardware impairments and channel estimation errors on SWIPT assisted cooperative NOMA networks. *IEEE Access*, 7:135499–135513, 2019.

[112] Zheng Yang, Zhiguo Ding, Yi Wu, and Pingzhi Fan. Novel relay selection strategies for cooperative NOMA. *IEEE Transactions on Vehicular Technology*, 66(11):10114–10123, 2017.

[113] Ferdi Kara and Hakan Kaya. Error probability analysis of NOMA-based diamond relaying network. *IEEE Transactions on Vehicular Technology*, 69(2):2280–2285, 2019.

[114] Meng Shen, Zihao Huang, Xianfu Lei, and Lisheng Fan. BER analysis of NOMA with max-min relay selection. *China Communications*, 18(7):172–182, 2021.

[115] Lina Bariah, Sami Muhaidat, and Arafat Al-Dweik. Error probability analysis of NOMA-based relay networks with SWIPT. *IEEE Communications Letters*, 23(7):1223–1226, 2019.

[116] Dinh-Thuan Do and Chi-Bao Le. Impact of fixed power allocation in wireless energy harvesting NOMA networks. *International Journal of Communication Systems*, 32(14):e4016, 2019.

[117] V Narasimha Nayak and Kiran Kumar Gurrala. A novel resource allocation for SWIPT-NOMA enabled AF relay based cooperative network. *Wireless Personal Communications*, 118:2699–2716, 2021.

[118] Justin Jose, Anirudh Agarwal, Ondrej Krejcar, and Vimal Bhatia. Power controlled outage-aware optimal protocol for NOMA-assisted underlay D2D networks. *AEU-International Journal of Electronics and Communications*, 157:154418, 2022.

[119] Chengpeng Liu, Lin Zhang, Zhi Chen, and Shaoqian Li. Outage probability analysis in downlink SWIPT-assisted cooperative NOMA systems. *Journal of Communications and Information Networks*, 7(1):72–87, 2022.

[120] Yuehao Yu, Zheng Yang, Yi Wu, Jamal Ahmed Hussein, Wen-Kang Jia, and Zhicheng Dong. Outage performance of NOMA in cooperative cognitive radio networks with SWIPT. *IEEE Access*, 7:117308–117317, 2019.

[121] Dac-Binh Ha and Sang Quang Nguyen. Outage performance of energy harvesting DF relaying NOMA networks. *Mobile Networks and Applications*, 23:1572–1585, 2018.

[122] Shubham Bisen, Parvez Shaik, and Vimal Bhatia. On performance of energy harvested cooperative NOMA under imperfect CSI and imperfect SIC. *IEEE Transactions on Vehicular Technology*, 70(9):8993–9005, 2021.

[123] V Aswathi and Anchare V Babu. Outage and throughput analysis of full-duplex cooperative NOMA system with energy harvesting. *IEEE Transactions on Vehicular Technology*, 70(11):11648–11664, 2021.

[124] Md Fazlul Kader, Mohammed Belal Uddin, Anik Islam, and Soo Young Shin. Cooperative non-orthogonal multiple access with SWIPT over Nakagami-m fading channels. *Transactions on Emerging Telecommunications Technologies*, 30(5):e3571, 2019.

[125] Ferdi Kara. On the outage performance of SWIPT-NOMA-CRS with imperfect SIC and CSI. *Turkish Journal of Electrical Engineering and Computer Sciences*, 29(2):1139–1156, 2021.

[126] MB Shirazi and MR Zahabi. A novel full-duplex relay selection and resource management in cooperative SWIPT NOMA networks. *Journal of Electrical and Computer Engineering Innovations (JECEI)*, 11(1):161–172, 2023.

[127] Minh-Tuong Nguyen, Thai-Hoc Vu, and Sunghwan Kim. Performance analysis of wireless powered cooperative NOMA-based CDRT IoT networks. *IEEE Systems Journal*, 16(4):6501–6512, 2022.

[128] Laleh Eslami and Ghasem Mirjalily. Fairness-aware resource allocation for D2D-enabled IoT in NOMA-based cellular networks with mutual successive interference cancellation. *Physical Communication*, 55:101901, 2022.

[129] Noushin Khosravi Largani and Bahareh Akhbari. Enhancing secrecy performance of energy harvesting NOMA systems using IoT user scheduling under untrusted users. *IET Communications*, 16(18):2208–2218, 2022.

[130] Toi Le-Thanh and Khuong Ho-Van. Overlay networks with nonlinear energy scavenging and noma-assisted decoding: security performance analysis. *Arabian Journal for Science and Engineering*, 47(11):14789–14807, 2022.

[131] Saman Atapattu and Jamie Evans. Optimal energy harvesting protocols for wireless relay networks. *IEEE Transactions on Wireless Communications*, 15(8):5789–5803, 2016.

[132] Guoxin Li, Deepak Mishra, Yulin Hu, and Saman Atapattu. Optimal designs for relay-assisted NOMA networks with hybrid SWIPT scheme. *IEEE Transactions on Communications*, 68(6):3588–3601, 2020.

[133] AA Amin, Mohammed Belal Uddin, and Soo Young Shin. Performance enhancement of hybrid SWIPT protocol for cooperative NOMA downlink transmission. *arXiv preprint arXiv:1906.09159*, 2019.

[134] Ahmed Al Amin and Soo Young Shin. Performance evaluation of cooperative NOMA-based improved hybrid SWIPT protocol. *arXiv preprint arXiv:2106.10799*, 2021.

[135] Suyue Li, Lina Bariah, Sami Muhaidat, Paschalis Sofotasios, Jie Liang, and Anhong Wang. Error analysis of NOMA-based user cooperation with SWIPT. In *IEEE 15th International Conference on Distributed Computing in Sensor Systems (DCOSS)*, pages 507–513, 2019.

[136] Suyue Li, Lina Bariah, Sami Muhaidat, Paschalis C Sofotasios, Jie Liang, and Anhong Wang. SWIPT-enabled cooperative NOMA with mth best relay selection. *IEEE Open Journal of the Communications Society*, 1:1798–1807, 2020.

[137] Faical Khennoufa, Khelil Abdellatif, and Ferdi Kara. Bit error rate evaluation of relay-aided cooperative NOMA with energy harvesting under imperfect SIC and CSI. *Physical Communication*, 52:101630, 2022.

[138] Lina Mohjazi, Sami Muhaidat, and Mehrdad Dianati. Performance analysis of differential modulation in SWIPT cooperative networks. *IEEE Signal Processing Letters*, 23(5):620–624, 2016.

[139] Xun Zhou, Rui Zhang, and Chin Keong Ho. Wireless information and power transfer: Architecture design and rate-energy tradeoff. *IEEE Transactions on communications*, 61(11):4754–4767, 2013.

[140] Yan Gao, Yunfei Chen, and Aiqun Hu. Throughput and BER of wireless powered DF relaying in Nakagami-m fading. *Science China Information Sciences*, 60:1–13, 2017.

[141] Peng Liu, Saeed Gazor, Il-Min Kim, and Dong In Kim. Energy harvesting noncoherent cooperative communications. *IEEE Transactions on Wireless Communications*, 14(12):6722–6737, 2015.

[142] Roberto Bosisio and Umberto Spagnolini. Collision model for the bit error rate analysis of multicell multiantenna OFDMA systems. In *IEEE International Conference on Communications*, pages 5732–5737, 2007.

[143] Roberto Bosisio and Umberto Spagnolini. Interference coordination vs. interference randomization in multicell 3GPP LTE system. In *IEEE Wireless Communications and Networking Conference*, pages 824–829, 2008.

[144] Faical Khennoufa and Khelil Abdellatif. BER performance of co-operative relay NOMA-assisted PS protocol with imperfect SIC and CSI. *International Journal of Sensors Wireless Communications and Control*, 13(2):99–107, 2023.

[145] Mohammadreza Babaei, Ümit Aygölü, and Ertugrul Basar. BER analysis of dual-hop relaying with energy harvesting in nakagami-m fading channel. *IEEE Transactions on Wireless Communications*, 17(7):4352–4361, 2018.

[146] Alok Kumar Shukla, Vibhum Singh, Prabhat K Upadhyay, Abhinav Kumar, and Jules M Moualeu. Performance analysis of energy harvesting-assisted overlay cognitive NOMA systems with incremental relaying. *IEEE Open Journal of the Communications Society*, 2:1558–1576, 2021.

[147] Faical Khennoufa, Abdellatif Khelil, Khaled Rabie, Hakan Kaya, and Xingwang Li. An efficient hybrid energy harvesting protocol for cooperative NOMA systems: Error and outage performance. *Physical Communication*, 58:102061, 2023.

[148] Yuanwei Liu, Wenqiang Yi, Zhiguo Ding, Xiao Liu, Octavia A Dobre, and Naofal Al-Dhahir. Developing NOMA to next generation multiple access: Future vision and research opportunities. *IEEE Wireless Communications*, 29(6):120–127, 2022.

[149] Anthony Ngozichukwuka Uwaechia and Nor Muzlifah Mahyuddin. A comprehensive survey on millimeter wave communications for fifth-generation wireless networks: Feasibility and challenges. *IEEE Access*, 8:62367–62414, 2020.

[150] Huu Q Tran, Ca V Phan, and Quoc-Tuan Vien. Performance analysis of power-splitting relaying protocol in SWIPT based cooperative NOMA systems. *EURASIP Journal on Wireless Communications and Networking*, 2021(1):1–26, 2021.

[151] Mengru Wu, Qingyang Song, Lei Guo, and Abbas Jamalipour. Joint user pairing and resource allocation in a SWIPT-enabled cooperative NOMA system. *IEEE Transactions on Vehicular Technology*, 70(7):6826–6840, 2021.

[152] Radhika R Kurup and AV Babu. Power adaptation for improving the performance of time switching SWIPT-based full-duplex cooperative NOMA network. *IEEE Communications Letters*, 24(12):2956–2960, 2020.

[153] Ashish Rauniyar, Paal E Engelstad, and Olav N Østerbø. On the performance of bidirectional NOMA-SWIPT enabled IoT relay networks. *IEEE Sensors Journal*, 21(2):2299–2315, 2020.

[154] Faical Khennoufa, Abdellatif Khelil, Khaled Rabie, Hakan Kaya, and Xingwang Li. An efficient hybrid energy harvesting protocol for cooperative NOMA systems: Error and outage performance. *Physical Communication*, page 102061, 2023.

[155] Ba Cao Nguyen, Tran Manh Hoang, Phuong T Tran, and Tan N Nguyen. Outage probability of NOMA system with wireless power transfer at source and full-duplex relay. *AEU-international Journal of Electronics and Communications*, 116:152957, 2020.

[156] Runzhou Li, Peilin Hong, Kaiping Xue, Ming Zhang, and Te Yang. Resource allocation for uplink NOMA-based D2D communication in energy harvesting scenario: A two-stage game approach. *IEEE Transactions on Wireless Communications*, 21(2):976–990, 2021.

[157] Shufeng Li, Zelin Wan, and Libiao Jin. Joint rate maximization of downlink and uplink in NOMA SWIPT systems. *Physical Communication*, 46:101324, 2021.

[158] Kunrui Cao, Buhong Wang, Haiyang Ding, Lu Lv, Runze Dong, Tianhao Cheng, and Fengkui Gong. Improving physical layer security of uplink NOMA via energy harvesting jammers. *IEEE Transactions on Information Forensics and Security*, 16:786–799, 2020.

[159] Chaozhu Zhang and Xinghua Jia. Joint beamforming optimization for NOMA-based wireless powered multi-pair two-way AF and DF relaying networks. *IET Communications*, 13(4):387–395, 2019.

[160] Ishan Budhiraja, Neeraj Kumar, Sudhanshu Tyagi, Sudeep Tanwar, and Zhu Han. An energy efficient scheme for WPCN-NOMA based device-to-device communication. *IEEE Transactions on Vehicular Technology*, 70(11):11935–11948, 2021.

[161] Dongyeong Song, Wonjae Shin, Jungwoo Lee, and H Vincent Poor. Sum-throughput maximization in NOMA-based WPCN: A cluster-specific beamforming approach. *IEEE Internet of Things Journal*, 8(13):10543–10556, 2021.

[162] Liang Huang, Runkai Nan, Kaikai Chi, Qiaozhi Hua, Keping Yu, Neeraj Kumar, and Mohsen Guizani. Throughput guarantees for multi-cell wireless powered communication networks with non-orthogonal multiple access. *IEEE Transactions on Vehicular Technology*, 71(11):12104–12116, 2022.

[163] Bin Lyu, Parisa Ramezani, Dinh Thai Hoang, and Abbas Jamalipour. IRS-Assisted downlink and uplink NOMA in wireless powered communication networks. *IEEE Transactions on Vehicular Technology*, 71(1):1083–1088, 2021.

[164] Piao Zeng, Qingqing Wu, and Deli Qiao. Energy minimization for IRS-aided WPCNs with non-linear energy harvesting model. *IEEE Wireless Communications Letters*, 10(11):2592–2596, 2021.

[165] Yingting Liu, Yinghui Ye, Haiyang Ding, Feng Gao, and Hongwu Yang. Outage performance analysis for SWIPT-based incremental cooperative NOMA networks with non-linear harvester. *IEEE Communications Letters*, 24(2):287–291, 2019.

[166] Long Ma, Enyu Li, and Qianqian Yang. On the performance of full-duplex cooperative NOMA with non-linear EH. *IEEE Access*, 9:145968–145976, 2021.

[167] Azar Hakimi, Mohammadali Mohammadi, Zahra Mobini, and Zhiguo Ding. Full-duplex non-orthogonal multiple access cooperative spectrum-sharing networks with non-linear energy harvesting. *IEEE Transactions on Vehicular Technology*, 69(10):10925–10936, 2020.

[168] Quang Nhat Le, Animesh Yadav, Nam-Phong Nguyen, Octavia A Dobre, and Ruiqin Zhao. Full-duplex non-orthogonal multiple access cooperative overlay spectrum-sharing networks with SWIPT. *IEEE Transactions on Green Communications and Networking*, 5(1):322–334, 2020.

[169] Kamal Agrawal, Mark F Flanagan, and Shankar Prakriya. NOMA with battery-assisted energy harvesting full-duplex relay. *IEEE Transactions on Vehicular Technology*, 69(11):13952–13957, 2020.

[170] Dinh-Thuan Do and Minh-Sang Van Nguyen. Device-to-device transmission modes in NOMA network with and without Wireless Power Transfer. *Computer Communications*, 139:67–77, 2019.

[171] Yafang Zhang, Suili Feng, and Weijun Tang. Performance analysis and optimization for power beacon-assisted wireless powered cooperative NOMA systems. *IEEE Access*, 8:198436–198450, 2020.

[172] Xingwang Li, Meng Liu, Chao Deng, P Takis Mathiopoulos, Zhiguo Ding, and Yuanwei Liu. Full-duplex cooperative NOMA relaying systems with I/Q imbalance and imperfect SIC. *IEEE Wireless Communications Letters*, 9(1):17–20, 2019.

[173] Anh Tuyen Le, Xiaojing Huang, Y Jay Guo, et al. On the impacts of i/Q imbalance in analog least mean square adaptive filter for self-interference cancellation in full-duplex radios. *IEEE Transactions on Vehicular Technology*, 71(10):10683–10693, 2022.

[174] Lutfi Samara, Ridha Hamila, and Naofal Al-Dhahir. Secrecy performance of full-duplex jamming and reception under I/Q imbalance. *IEEE Transactions on Vehicular Technology*, 70(9):9560–9565, 2021.

[175] Malek M Alsmadi, Najah Abu Ali, Mohammed Hayajneh, and Salama S Ikki. Downlink NOMA networks in the presence of IQI and imperfect SIC: Receiver design and performance analysis. *IEEE Transactions on Vehicular Technology*, 69(6):6793–6797, 2020.

[176] Bassant Selim, Sami Muhaidat, Paschalis C Sofotasios, Bayan S Sharif, Thanos Stouraitis, George K Karagiannidis, and Naofal Al-Dhahir. Outage probability of multi-carrier NOMA systems under joint I/Q imbalance. In *IEEE International Conference on Advanced Communication Technologies and Networking (CommNet)*, pages 1–7, 2018.

[177] Xingwang Li, Yike Zheng, Mohammad Dahman Alshehri, Linpeng Hai, Venki Balasubramanian, Ming Zeng, and Gaofeng Nie. Cognitive AmBC-NOMA IoV-MTS networks with IQI: Reliability and security analysis. *IEEE Transactions on Intelligent Transportation Systems*, 2021.

[178] Xingwang Li, Mengyan Huang, Yuanwei Liu, Varun G Menon, Anand Paul, and Zhiguo Ding. I/Q imbalance aware nonlinear wireless-powered relaying of B5G networks: Security and reliability analysis. *IEEE Transactions on Network Science and Engineering*, 8(4):2995–3008, 2020.

[179] Xingwang Li, Meng Liu, Dan Deng, Jingjing Li, Chao Deng, and Qingping Yu. Power beacon assisted wireless power cooperative relaying using NOMA with hardware impairments and imperfect CSI. *AEU-International Journal of Electronics and Communications*, 108:275–286, 2019.

[180] Faical Khennoufa, Abdellatif Khelil, Safia Beddiaf, Ferdi Kara, Khaled Rabie, Hakan Kaya, Ahmet Emir, Salama Ikki, and Halim Yanikomeroglu. Wireless powered cooperative communication network for dual-hop uplink NOMA with IQI and SIC imperfections. *IEEE Access*, 2023.

[181] Daniel Zwillinger and Alan Jeffrey. *Table of integrals, series, and products*. Elsevier, 2007.

[182] Xingwang Li, Jingjing Li, and Lihua Li. Performance analysis of impaired SWIPT NOMA relaying networks over imperfect Weibull channels. *IEEE Systems Journal*, 14(1):669–672, 2019.

[183] Ferdi Kara and Hakan Kaya. On the error performance of cooperative-NOMA with statistical CSIT. *IEEE Communications Letters*, 23(1):128–131, 2018.

[184] Ferdi Kara. Error performance of cooperative relaying systems empowered by SWIPT and NOMA. *Physical Communication*, 49:101450, 2021.

[185] Safwan Alfattani, Wael Jaafar, Yassine Hmamouche, Halim Yanikomeroglu, Abbas Yongaçoglu, Ngoc Dũng Đào, and Peiying Zhu. Aerial platforms with reconfigurable smart surfaces for 5G and beyond. *IEEE Communications Magazine*, 59(1):96–102, 2021.

[186] Lina Bariah, Fouzi Boukhalfa, Wael Jaafar, Sami Muhaidat, and Halim Yanikomeroglu. On the Performance of RIS-enabled NOMA for Aerial Networks. In *IEEE Wireless Communications and Networking Conference (WCNC)*, pages 1–6, 2023.

[187] Neelima Agrawal, Ankur Bansal, Keshav Singh, and Chih-Peng Li. Performance evaluation of RIS-assisted UAV-enabled vehicular communication system with multiple non-identical interferers. *IEEE Transactions on Intelligent Transportation Systems*, 23(7):9883–9894, 2021.

[188] Sourabh Solanki, Junhee Park, and Inkyu Lee. On the performance of IRS-aided UAV networks with NOMA. *IEEE Transactions on Vehicular Technology*, 71(8):9038–9043, 2022.

[189] Yijiu Li, Cheng Yin, Tan Do-Duy, Antonino Masaracchia, and Trung Q Duong. Aerial reconfigurable intelligent surface-enabled URLLC UAV systems. *IEEE Access*, 9:140248–140257, 2021.

[190] Minh-Hien T Nguyen, Emiliano Garcia-Palacios, Tan Do-Duy, Octavia A Dobre, and Trung Q Duong. UAV-aided aerial reconfigurable intelligent surface communications with massive MIMO system. *IEEE Transactions on Cognitive Communications and Networking*, 8(4):1828–1838, 2022.

[191] Ayse E Canbilen, Ertugrul Basar, and Salama S Ikki. On the performance of RIS-assisted space shift keying: ideal and Non-Ideal transceivers. *IEEE Transactions on Communications*, 70(9):5799–5810, 2022.

[192] Momiao Zhou, Yimeng Li, Yanshi Sun, and Zhizhong Ding. Outage Performance of RIS-Assisted V2I Communications with Inter-Cell Interference. *IEEE Wireless Communications Letters*, 2023.

[193] Faical Khennoufa, Khelil Abdellatif, Ferdi Kara, Halim Yanikomeroglu, Khaled Rabie, Taissir Y Elganimi, and Safia Beddiaf. Error performance analysis of UAV-mounted RIS for NOMA systems with practical constraints. *IEEE Communications Letters*, 2024.

[194] Xinwei Yue and Yuanwei Liu. Performance analysis of intelligent reflecting surface assisted NOMA networks. *IEEE Transactions on Wireless Communications*, 21(4):2623–2636, 2021.

[195] John G Proakis. *Digital communications*. McGraw-Hill, Higher Education, 2008.

[196] Neha Jain and Vivek Ashok Bohara. Energy harvesting and spectrum sharing protocol for wireless sensor networks. *IEEE Wireless Communications Letters*, 4(6):697–700, 2015.

[197] George K Karagiannidis, Theodoros A Tsiftsis, and Ranjan K Mallik. Bounds for multihop relayed communications in Nakagami-m fading. *IEEE Transactions on communications*, 54(1):18–22, 2006.

[198] The wolfram functions site, 2001.

[199] VS Adamchik and OI Marichev. The algorithm for calculating integrals of hypergeometric type functions and its realization in REDUCE system. In *PISSAC*, pages 212–224, 1990.

Appendix A

Appendix A: Proof of (2.20) and (2.21)

The ABER at the U_1 can be presented as in [17]

$$P_1 = \frac{1}{2}\Big[\sum_{i=1}^{2}\Big(\int_0^\infty Q(\Gamma_i) f_{\Gamma_i}(\Gamma_i) d_{\Gamma_i}\Big)\Big], \tag{A.1}$$

where $f_{\Gamma_i}(\Gamma_i)$ is the Rayleigh distributed probability density function which is given as

$$f_{\Gamma_i}(\Gamma_i) = \frac{1}{\bar{\Gamma}_i} \exp\left(\frac{-\Gamma_i}{\bar{\Gamma}_i}\right). \tag{A.2}$$

An alternative representation of the Q-function as defined by Craig's formulation as in [195].

$$Q(x) = \frac{1}{\pi}\int_0^{\frac{\pi}{2}} \exp\left(\frac{-x^2}{2sin^2(\theta)}\right). \tag{A.3}$$

Furthermore, the MGF is provided as follows

$$MGF_\Gamma(x) = \int_0^\infty \exp(x\Gamma) f_\Gamma(\Gamma) d_\Gamma. \tag{A.4}$$

Then, the ABER can be given as

$$P_1 = \frac{1}{2}\Big[\sum_{i=1}^{2}\left(\frac{1}{\pi}\int_0^{\frac{\pi}{2}} MGF_{\Gamma_i}\left(\frac{-1}{2sin^2(\theta)}\right) d\theta\right)\Big], \tag{A.5}$$

with

$$MGF_{\Gamma_i}(x) = (1 - x\bar{\Gamma}_i)^{-1}. \tag{A.6}$$

Replacing (A.6) into (A.5), it becomes

$$P_1 = \frac{1}{2}\Big[\sum_{i=1}^{2}\left(\frac{1}{\pi}\int_0^{\frac{\pi}{2}} \left(1 + \frac{\bar{\Gamma}_i}{2sin^2(\theta)}\right)^{-1}\right)\Big]. \tag{A.7}$$

However, according to [17], the term of (A.7) can be presented as

$$\frac{1}{\pi}\int_{0}^{\frac{\pi}{2}}\left(1+\frac{\bar{\Gamma}_i}{2sin^2(\theta)}\right)^{-1}d\theta=\frac{1}{2}\left[1-\sqrt{\frac{\frac{\bar{\Gamma}_i}{2}}{1+\frac{\bar{\Gamma}_i}{2}}}\right]. \tag{A.8}$$

The proof is completed.

Appendix B

Appendix B: Proof of (2.22) and (2.23)

U_2 implements the SIC to detect its symbols. The detection of s_2 at U_2 is based on the detection of s_1 symbols correct or not. Thus, the BER of s_2 at U_2 is based on the sum of the following cases: Case one: U_2 detects the s_1 symbols correctly, then it is removed from the received signal. Thereafter, the U_2 implements the MLD process on the remaining s_2 symbols with AWGN, the error occurs if $P(\sqrt{P_t}\sqrt{\alpha_2}h_2 < (\sqrt{\alpha_1} - \sqrt{\alpha_2})e + n)$. Case two: U_2 detects the s_1 symbols wrongly, and it is subtracted from the received signal. Thereafter, when the MLD process is implemented, the error occurs if $P(\sqrt{P_t}(2\sqrt{\alpha_2}+\sqrt{\alpha_2})h_2 < (\sqrt{\alpha_1}+\sqrt{\alpha_2})e+n)$. Therefore, the BER of U_2 is given by

$$P_{BS2,s_2}(e) = P_{BS2,s_1}(correct) + P_{BS2,s_1}(error), \tag{B.1}$$

where $P_{BS2,s_1}(correct)$ and $P_{BS2,s_1}(error)$ the probabilities if s_1 symbols are detected correctly or erroneously, respectively.

Each term of (B.1), can be expressed by

$$\begin{aligned} P_{BS2,s_1}(correct) = \frac{1}{2}[P(\sqrt{P_t}\sqrt{\alpha_2}h_2 < (\sqrt{\alpha_1} - \sqrt{\alpha_2})e + n) \\ + P(\sqrt{P_t}\sqrt{\alpha_2}h_2 < (\sqrt{\alpha_1} + \sqrt{\alpha_2})e + n < \sqrt{P_t}(\sqrt{\alpha_1} + \sqrt{\alpha_2})h_2)], \end{aligned} \tag{B.2}$$

$$\begin{aligned} P_{BS2,s_1}(error) = \frac{1}{2}[P(\sqrt{P_t}(2\sqrt{\alpha_1} + \sqrt{\alpha_2})h_2 < (\sqrt{\alpha_1} + \sqrt{\alpha_2})e + n) \\ + P(\sqrt{P_t}(\sqrt{\alpha_1} - \sqrt{\alpha_2})h_2 < (\sqrt{\alpha_1} - \sqrt{\alpha_2})e + n < \sqrt{P_t}(2\sqrt{\alpha_1} - \sqrt{\alpha_2})h_2)]. \end{aligned} \tag{B.3}$$

In the case of ICSI, e is not zero i.e., $e \neq 0$. However, in scenario when the CSI is considered perfect, e is equal to zero,i.e., $e = 0$. By substituting (B.2) and (B.3) into (B.1), the BER of s_2 at U_2 can be expressed as

$$P_{BS2,s_2}(e) = \frac{1}{2}\sum_{v=1}^{6}\kappa_v Q\left(\sqrt{P_t\gamma\aleph_v|h_2|^2}\right). \tag{B.4}$$

By exploiting the alternative form of the Q(.)function and MGF as in [195], the BER of s_2 at U_2 is given by

$$P_{BS2,s_2}(e) = \frac{1}{4}\sum_{v=1}^{6}\kappa_v\left(\sqrt{\frac{P_t\gamma\aleph_v E[|h_2|^2]}{2 + P_t\gamma\aleph_v E[|h_2|^2]}}\right). \tag{B.5}$$

The proof is completed.

Appendix C

Appendix C: Proof of (3.30)

After the received signals from BS and U_2 are summed at the U_1 by using MRC. We consider that the BS sent a symbol (+1) for U_1. During the SIC at U_2, the symbol of U_1 is detected erroneously as (-1) and forwarded to U_1 (this is called error propagation). Hence, the MRC is implemented to combine the received signal in the case of error propagation. Thus, the total of the received signals at the U_1 by MRC is given by

$$y_{Prop,s1} = y_1|\hat{h}_1^*|^2 + y_{12}|\hat{h}_{21}^*|^2 = \gamma_{BS1,s1,j} - \gamma_{21,s1} + \check{n}_a, \tag{C.1}$$

where $\check{n}_a$ is the effective noise with $\check{n}_a \sim \mathcal{CN}\left(0, \frac{1}{2}\left[(\daleth_j + 1)\gamma\sigma_e^2 + 2\right]\right)$. Through the MLD decision rule at the U_1 s_1=+1 is declared if $y_{Coop,s1} \geq 0$. Thus, the BER of the error propagation for the U_1 symbols is defined as

$$P_{Prop,s1} = P(\gamma_{BS1,s1,j} - \gamma_{21,s1} \geq \check{n}_a) = Q\left(\frac{\gamma_{BS1,s1,j} - \gamma_{21,s1}}{\sigma_{\check{n}_a}^2}\right). \tag{C.2}$$

From (C.2), if the relay forwards an incorrect symbol, this has a significant impact instead of noise on the decision variable MLD. Accordingly, we approximate the BER as $\gamma_{BS1,s1,j} - \gamma_{21,s1} < 0$. The average error probability under error propagation is calculated as

$$\begin{aligned} &P_{Prop,s1} = P(\gamma_{BS2,s1,j} - \gamma_{21,s1} \geq 0) \\ &= \int_{\gamma_{BS1,s1,j}}^{\infty} \int_0^{\gamma_{21,s1}} \frac{1}{\overline{\gamma}_{BS1,s1,j}\overline{\gamma}_{21,s1}} \exp\left(-\frac{\gamma_{BS1,s1,j}}{\overline{\gamma}_{BS1,s1,j}}\right) \exp\left(-\frac{\gamma_{21,s1}}{\overline{\gamma}_{21,s1}}\right) d\gamma_{BS1,s1,j} d\gamma_{21,s1} \\ &= \frac{\overline{\gamma}_{21,s1}}{\overline{\gamma}_{21,s1} + \overline{\gamma}_{BS1,s1,j}}. \end{aligned} \tag{C.3}$$

The proof is completed.

Appendix D

Appendix D: Proof of (5.38)

The OP of U_1 depends on phases one and two, so the OP of U_1 happens if the minimum SINR of the two phases is less than the threshold θ_1. Hence, the e2e OP of U_1 is expressed as

$$P_{\text{e2e},U_1}(\text{out}) = 1 - P\left(\min(\gamma_{BSR,s_1}, \gamma_{U_1,s_1}) \geq \theta_1\right). \tag{D.1}$$

We rewrite (D.1) as

$$P_{\text{e2e},U_1}(out) = 1 - P\left(\gamma_{BSR,s_1} \geq \theta_1\right) P\left(\gamma_{U_1,s_1} \geq \theta_1\right). \tag{D.2}$$

The dedicated Nakagami-m channel is defined in [146, Eq. (19) and Eq. (20)]. Thus, by utilizing the PDF and the CDF, the terms of (D.2) can be determined, respectively, as

$$P\left(\gamma_{BSR,s_1} \geq \theta_1\right) = 1 - e^{-\frac{m_r}{\Omega_r}\ell_1} \sum_{t=0}^{m_r-1} \frac{1}{t!}\left(\frac{m_r}{\Omega_r}\ell_1\right)^t, \tag{D.3}$$

and

$$P\left(\gamma_{U_1,s_1} \geq \theta_1\right) = P\left(|h_r|^2|h_1|^2 \geq \flat_1\right), \tag{D.4}$$

The (16) contains the multiplying of two random variables (RVs). The OP of the product of two RVs over the Nakagami-m fading is given in [196]. Hence, the OP of (D.4) can be determined as

$$\begin{aligned} P\left(|h_r|^2|h_1|^2 \geq \flat_1\right) &= 1 - \int_0^\infty f_{|h_r|^2}(x) P\left(|h_1|^2 \geq \flat_1/x\right) dx \\ &= 1 - \frac{1}{\Gamma(m_r)\Gamma(m_1)(\frac{\Omega_r}{m_r})^{m_r}} \times \\ &\int_0^\infty x^{m_r-1} e^{-\frac{m_r x}{\Omega_r}} \Gamma(m_1, \flat_1 m_1/x\Omega_1)\, dx, \end{aligned} \tag{D.5}$$

where $f_{|h_r|^2}(x)$ is the PDF of the dedicated Nakagami-m channel as defined in [146, Eq. (19)]. The integral of (D.5) is presented in [197, Eq. (7)] by

$$P\left(|h_r|^2|h_1|^2 \leq \lambda_1\right) = 1 - \frac{G_{1\,3}^{2\,1}\left({}_{m_r,m_1,0}^{\quad 1}\middle|\frac{\flat_1}{\Omega_r\Omega_1}\right)}{\Gamma(m_r)\Gamma(m_1)}. \tag{D.6}$$

We find the OP of U_1 for EH CNOMA by substituting (D.3) and (D.6) into (D.2) as given in (5.28). To calculate the OP of U_2, we follow the same steps.

The proof is completed.

Appendix E

Appendix E: Proof of (5.39)

The relay uses the harvested power (i.e., PS, TS, and hybrid) to forward the SC information to the users. Since the U_1 detects its symbols without SIC, the BER at U_1 in the second phase can be represented by

$$P_{II,s_1}(e) = \frac{1}{2}\sum_{j=1}^{2} \mathrm{Q}(\sqrt{\gamma \daleth_j \Psi |h_1|^2 |h_r|^2}). \tag{E.1}$$

As shown in (E.1), the BER contains two random variables that are multiplied which are related to the first and second phases' link quality. Since the BER of (E.1) defines the BER of phase two, however, it contains $|h_r|^2$ of phase one in the transmit power of the relay. Thus, the ABER of (E.1) cannot be easily acquired by averaging Gamma distribution of Nakagami-m. It is necessary to derive the joint PDF of $Y = |h_1|^2|h_r|^2$. Thus, the ABER of Y is given in [145] as

$$P_{II,s_1}(e) = \frac{1}{2}\sum_{i=1}^{2} \int_0^{\infty} \mathrm{Q}(\sqrt{\gamma \daleth_j \Psi Y}) f_Y(Y) dY, \tag{E.2}$$

where $f_Y(Y)$ is the PDF of Y, which can be acquired by the PDF of the product of two chi-square distributions and can be defined after simplification using [47, 3.478,4] as

$$f_Y(Y) = 2\left(\frac{m_1 \Omega_r}{\Omega_1 m_r}\right)^{\frac{u_1}{2}} \Delta_1 Y^{u_2 - 1} \mathrm{K}_{u_1}\left(\sqrt{2\frac{m_1 m_r}{\Omega_r \Omega_1} Y}\right), \tag{E.3}$$

where $\mathrm{K}_v(.)$ is the modified Bessel function of the second kind and is given in [47, Eq. (8.446)]. By using $\mathrm{Q}(\sqrt{2x}) = 0.5\ \mathrm{erfc}(\sqrt{x})$ and the Meijer-G function [47, Eq. (9.3)] conversions as in [198, Eq.(06.27.26.0006.01)] and [47, Eq.(9.34.3)] and we substitute these conversions into (E.2) with algebraic manipulations and by using [47, Eq. (9.311)] and [199, Eq. (14)], the closed-form ABER of U_1 in the second phase is expressed as

$$P_1(e) = \frac{1}{4\sqrt{\pi}} \sum_{i=1}^{2} \Delta_1 G_{4\,5}^{3\,3} \left({}^{0,1-u_2,0.5-u_2,1-u_2}_{0.5u_1,-0.5u_1,1-u_2,u_2,0} \middle| \frac{\Delta_3}{4} \right). \tag{E.4}$$

We use the same method, to obtain the ABER of U_2 in the second phase.

The proof is completed.